UNCLASSIFIED

AD NUMBER

AD832042

NEW LIMITATION CHANGE

TO

Approved for public release, distribution unlimited

FROM

Distribution authorized to U.S. Gov't. agencies and their contractors; Critical Technology; MAY 1968. Other requests shall be referred to Air Force Materials Lab., AFSC, Wright-Patterson AFB, OH 45433.

AUTHORITY

AFML ltr, 18 Apr 1973
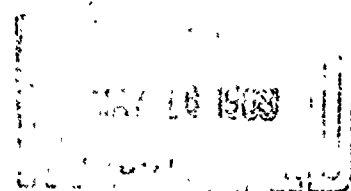
THIS PAGE IS UNCLASSIFIED

AFML-TR-68-32

THE APPLICABILITY OF A
FRACTURE MECHANICS-NONDESTRUCTIVE TESTING DESIGN CRITERION

P. F. Packman, H. S. Pearson,
J. S. Owens, and G. B. Marchese

Lockheed-Georgia Company

TECHNICAL REPORT AFML-TR-68-32

May 1968

AIR FORCE MATERIALS LABORATORY
AIR FORCE SYSTEMS COMMAND
WRIGHT-PATTERSON AIR FORCE BASE, OHIO

ABSTRACT

This report describes the work conducted on a program designed to investigate the potential applicability of a combined Fracture Mechanics–Nondestructive Inspection procedure as a design approach for aircraft structures. The program consisted of three phases, conducted simultaneously: (1) a literature survey to determine if sufficient fracture toughness information exists to determine a statistically valid value of K_{Ic}; (2) a test program to determine the minimum size of a crack, that can be detected by each of four NDT methods: X-ray, magnetic-particle, penetrant, and ultrasonics; and (3) a test program to determine if fracture mechanics, when combined with flaw size as determined by NDT, can accurately predict the failure load of selected structures.

The results show that the sensitivity of the present NDT techniques needs improvement, particularly for small surface cracks. All NDT methods showed high accuracies in crack location, but not crack length. Ultrasonics and magnetic particle inspection appeared to be superior to penetrant and X-ray inspection.

The available test information on K_{Ic} for most materials is at best marginal for use in the design of critical components. The scatter in K_{Ic} is large and the 90% lower bound confidence values of K_{Ic} based on the standard deviation are so low as to render the design impractical.

The fracture mechanics–nondestructive testing failure load predictions generally agree with the actual failure loads to within 10%. Except for the small crack lengths the FM/NDT failure predictions were better than those predictions made using standard design.

Failure load predictions for test cylinders containing both one inch diameter bored hole and a small crack near the hole are in excellent agreement with the actual failure load. The average error was 9.7% for the 7075-T6511 Aluminum specimens and 5.2% for the 4330V Modified Steel.

THE APPLICABILITY OF

FRACTURE MECHANICS-NONDESTRUCTIVE TESTING DESIGN CRITERION

P. F. Packman, H. S. Pearson, J. S. Owens, and

G. B. Marchese

FOREWORD

This report was submitted by the authors in January 1968

This Technical Report has been reviewed and is approved.

Albert Olevitch

Albert Olevitch
Chief, Materials Engineering Branch
Materials Applications Division
AF Materials Laboratory

ii

TABLE OF CONTENTS

TABLE OF CONTENTS (Cont'd)

TABLE OF CONTENTS (Cont'd)

LIST OF FIGURES

LIST OF FIGURES (Cont'd)

LIST OF FIGURES (Cont'd)

x

LIST OF FIGURES (Cont'd)

xi

LIST OF FIGURES (Cont'd)

LIST OF FIGURES (Cont'd)

LIST OF FIGURES (Cont'd)

xiv

LIST OF FIGURES (Cont'd)

xv

LIST OF FIGURES (Cont'd)

LIST OF TABLES

LIST OF TABLES (Cont'd)

SECTION I

INTRODUCTION

A statistical dependence is implied in the design concept of a structural component for an aerospace vehicle using standard mechanical properties such as ultimate tensile stress and tensile yield stress. It is assumed by the designer that the material of which the component is to be made will have mechanical properties that conform to the design values. These design values are usually obtained from handbooks or from selected tests conducted on a similar material.

Design specifications generally recognize the statistical nature of the material properties in an indirect way. These procedures have been satisfactory for past performance, and they may be satisfactory for future design procedures. However, the development of advanced aerospace systems such as high-supersonic and hypersonic atmospheric vehicles, together with the need for long extraterrestrial flights and the greater use of ultra-high-strength materials on conventional aircraft, have increased the need for greater structural efficiency. The problem for the designer is made more complex by the use of new materials, the increased uncertainty of operational loads, and the introduction of unknown environments.

Thus, it is evident that there is a need for the development of a different conceptual design method. This method should be aimed at future material requirements such as extremely high strength and elevated temperature durability with both static and dynamic loading conditions. The new analysis should establish reliable design techniques that will result in a component of the least possible weight with a satisfactory probability of survival under the operating conditions. The tradeoff in weight as opposed to the probability of survival should be calculable, and the economics involved in maintaining the degree of structural integrity should be known.

A design philosophy for high-strength materials that uses the theory of linear elastic fracture mechanics is a most promising replacement for the present design philosophy. Researchers in the field of fracture mechanics have developed an extensive background and experience in determining when a material containing a small defect under an external load will fail. This fracture concept, when coupled with a nondestructive inspection technique to determine accurately the size of the flaw in the part, appears to have some validity as a design criterion.

This report summarizes the efforts directed towards establishing a procedure for the use of a fracture mechanics-nondestructive testing (FM/NDT) criterion in the design of aerospace structural components.

Basic Aspects of Structural Reliability

In its simplest form, structural reliability is used to determine whether or not a material under load will fail (1). This implies that there is an exact definition of failure. In actual components, the concept of failure is quite complex and may not be applicable to all components. For the purposes of this preliminary analysis failure is defined to be "The total loss in load-carrying ability of the part when subjected to a monotonically increasing tensile load." Thus, structural reliability can be quantitatively defined as the probability of survival of a part under a given load. The survival concept implies that the material will withstand the load, while the failure approach states that the material will exhibit a catastrophic failure. The probability of survival is determined by a relationship between the applied load and the particular strength of the component.

1

In the strict sense, both load and strength are probabilistic in nature and can vary continuously throughout the lifetime of the structure. The design philosophy should then take into account not only the applied load spectrum but also the environment and structural changes that occur during the planned lifetime of the structure.

The present design methodology uses material specifications that are statistical in a limited sense. The philosophy used in material property specifications is outlined briefly in the following paragraphs.

Consider a simple test specimen pulled in tension until failure. The ultimate tensile strength σ_{tu} is measured. This process is repeated on a large number of similar specimens made from different heats of material. Each value of σ_{tu} is recorded, and a plot of the number of specimens that fail at a stress interval $\Delta\sigma_{tu}$ is plotted as shown in Figure 1a. If this process is repeated for a large number of specimens, the value of $\Delta\sigma_{tu}$ may be made as small as possible and a continuous curve drawn as shown in Figure 1b. The mean value of σ_{tu} can be determined and the results plotted in terms of a probability density function versus the percent mean value of the ultimate tensile strength (see Figure 2). This defines the probability of the strength of the material lying between two values of σ_{tu} as a function of σ_{tu}.

Because the scatter in the strength of the material is well known or can be determined from a series of tests, the average or mean value of σ_{tu} can be known with a high degree of confidence. The average σ_{tu} is not used in design practice, however. The design strength is that value of the σ_{tu} which "most" of the material will exceed. In Military Handbook 5, for example, aluminum alloy strengths are given as either "A" or "B" values. The values of the strength given in the "A" column are those values which the material producer has indicated to be the minimum expected for a given material. That is, at least 99% of the material will meet or exceed this value of $\sigma_{tu}(A)$.

Values appearing in the "B" column are strength properties which the producer has indicated will be met or exceeded by 90% of the material supplied by them. Both the "A" and "B" strength values are given at a 95% confidence level. (The confidence level refers to the probability of reaching a correct inference, i.e., being correct in 95 out of 100 trials.)

The two levels, $\sigma_{tu}(A)$ and $\sigma_{tu}(B)$ are shown in Figure 3. For the material tested to failure, 1% of the specimens would fail at $\sigma_{tu}(A)$ or less, and 99% of the material would survive to fail at values higher than $\sigma_{tu}(A)$. For the "B" level, 10% of the specimens would fail at $\sigma_{tu}(B)$ or less, and 90% would survive. It is obvious that the "B" value is larger than the "A" value.

The material allowables $\sigma_{tu}(A)$ and $\sigma_{tu}(B)$ do not guarantee the satisfactory performance of the structure. If the allowable ultimate load were calculated using the "A" value, the probability of the structure failing at this load would be 10^{-2}. However, if the maximum working load were such that the working stresses are less than $_{tu}(A)$, the structure would have
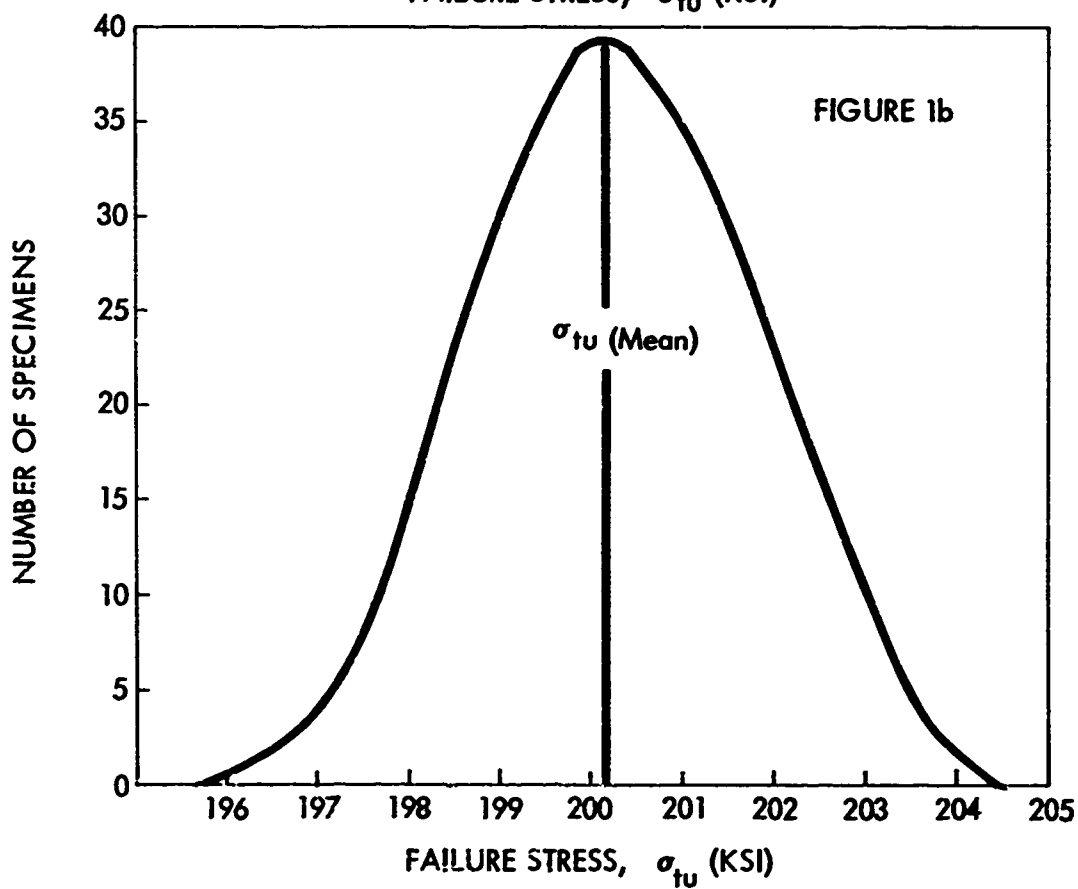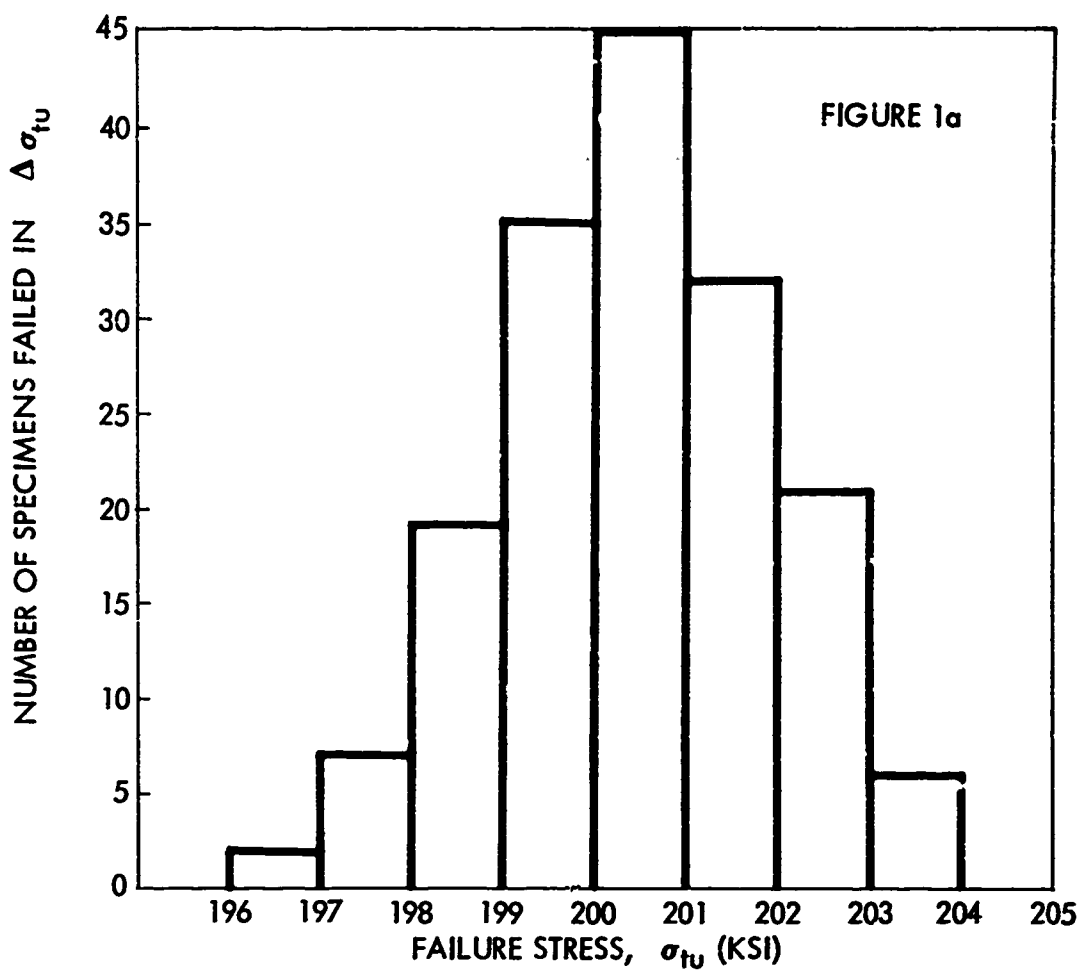
FIGURE 1a

FIGURE 1b

FIGURE 1 - CONSTRUCTION OF DISTRIBUTION FUNCTION FOR FAILURE STRESS
OF TENSILE TEST MEMBER
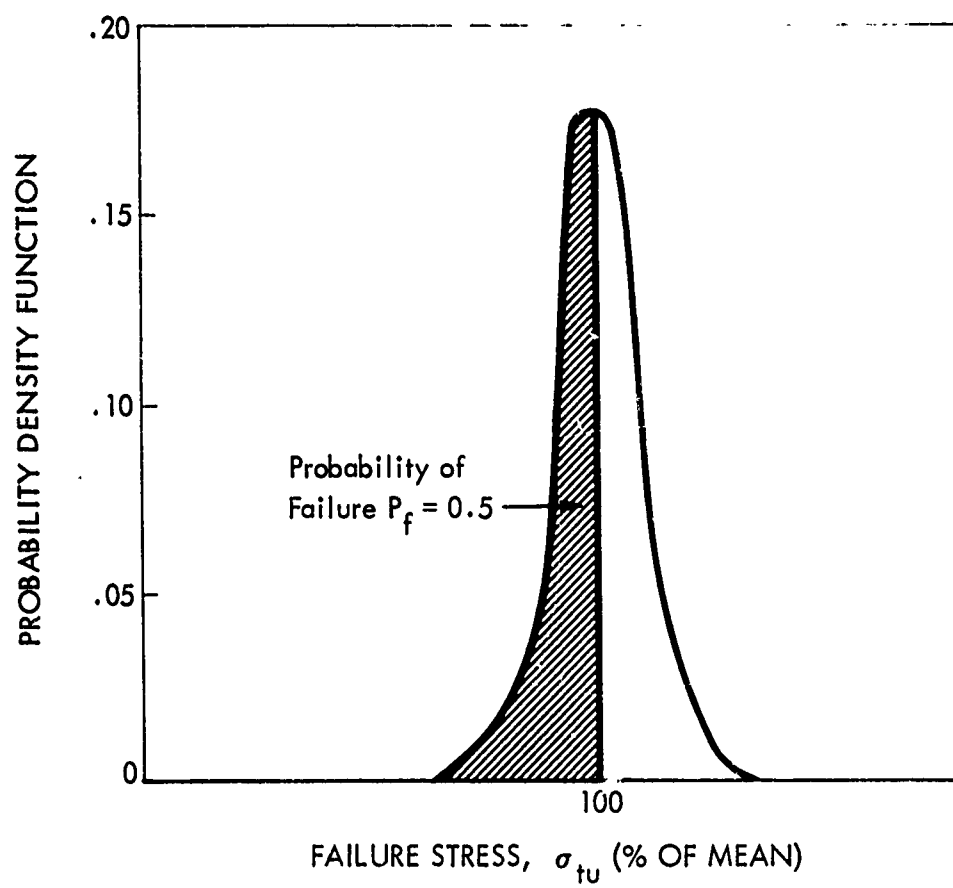
FIGURE 2 – PROBABILITY DENSITY FUNCTION VERSUS FAILURE STRESS
FOR TENSILE TEST

4
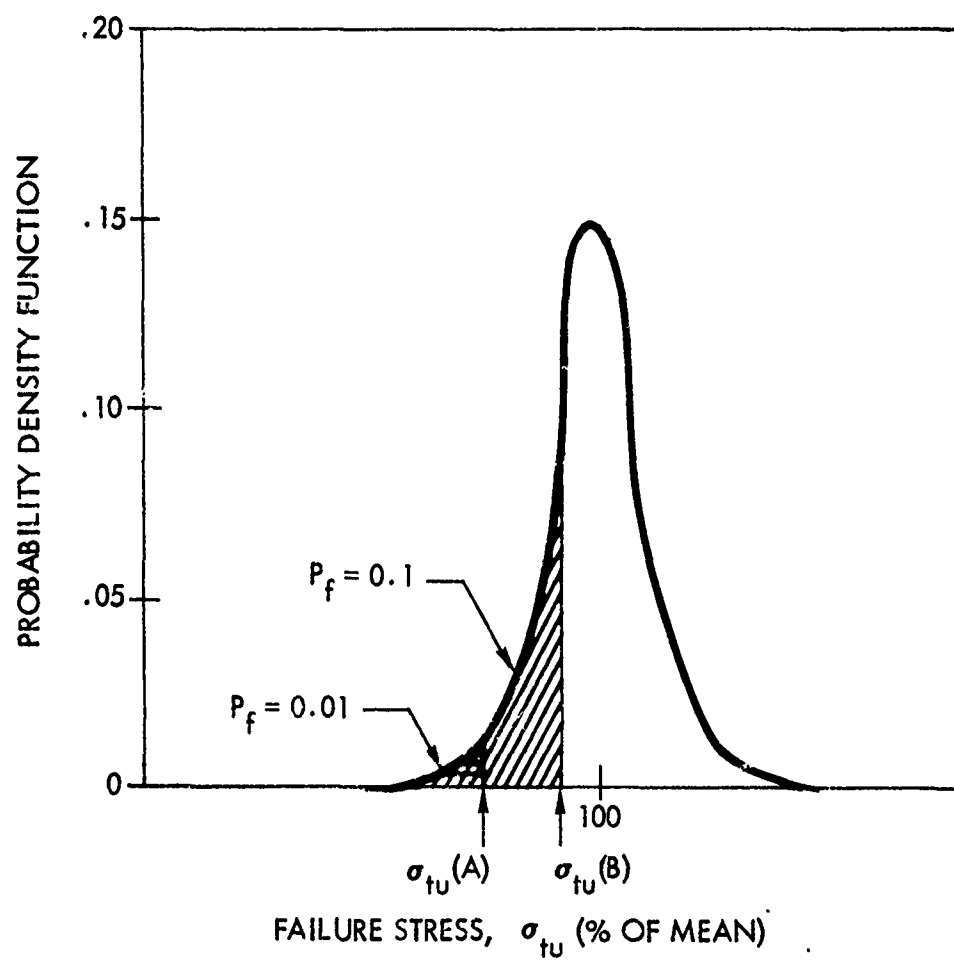
FIGURE 3 – LOCATION OF $\sigma_{tu}(A)$ AND $\sigma_{tu}(B)$ VALUES FOR
FAILURE STRESS OF TENSILE TEST

corresponding decrease in probability of failure. The working stress (σ_w) can be defined with a factor of safety (FS) such that:

$$FS \ \sigma_w \ = \ \sigma_{tu}(\text{mean}) \tag{1}$$

A working stress with FS = 1.5 is shown on a probability density plot in Figure 4. The introduction of a 1.5 factor of safety decreases the probability of failure from 10^{-2} to 10^{-50}, and hence, the structure has a high level of reliability.

To ensure the high reliability of the structural component, particularly when the component is to be loaded to high stresses, an additional factor is used. The mean ultimate strength is divided by a factor "k" greater than 1.0, which is determined by considering the uncertainties involved in the material, the processing uncertainties, and the unknowns involved due to fluctuating loads The resulting "reduced tensile ultimate" is then assumed to have a distribution function for the strength identical to that for the actual tensile ultimate. The $\sigma_{tu}(A)$ is then obtained for the reduced tensile ultimate and the working stress defined by an equation similar to Equation (1) with $\sigma_{tu}(\text{mean})$ replaced by $\sigma_{tu}(\text{reduced mean})$.

Two assumptions have been made in this simple analysis: the scatter in strength values is not large, and the strength properties of the actual component conform to the statistical strength properties of the material.

The scatter in strength values about the mean strength is given by the coefficient of variation (γ). This is a measure of the standard deviation as a fraction of the mean, where the standard deviation is the square root of the arithmetic mean of the square of the deviations from the mean. A large γ indicates that the curve tends to spread out about the mean. (This is shown in Figure 5a.) If the coefficient of variation in Figure 4 were 0.025, the probability of failure at the working stress $\sigma_w = \sigma_{tu}(\text{reduced mean})/1.5$ would be 10^{-50}.

If, however, the coefficient of variation were increased to 0.25 as shown in Figure 5a, the probability of failure at the same working stress $\sigma_w = \sigma_{tu}(\text{reduced mean})/1.5$ would now be about 10^{-3}. This is several orders of magnitude higher and would occur at the same working stress as in Figure 4, even though the reduced mean strength $\sigma_{tu}(\text{reduced mean})$ were the same.

If the working stress were calculated using the $\sigma_{tu}(A)$ value rather than the reduced mean, the situation depicted in Figure 5b would then occur. Here, the mean strength is the same, but the coefficient of variation is 0.025 for the first curve and 0.25 for the second. The value of $\sigma_{tu}(A)$ for the first curve is much higher than the value of $\sigma_{tu}(A)'$ for the second curve. Thus, to obtain the same probability of failure, the working stresses would have to be much lower for the material with a larger coefficient of variation.

If the strength properties of the component did not conform to those used in obtaining the $\sigma_{tu}(A)$ value, there would be no method of knowing the mean σ_{tu} of the material used in the component. To determine this σ_{tu}, a series of tensile coupons would have to be made from the component. If these values did not agree with the original distribution function, the probability of failure could be different than that assumed. For example, in Figure 6, the distribution function for the material would indicate that the probability of failure was 10^{-50}. The distribution function for test coupons taken from the actual component show that the actual probability of failure is only 10^{-5}.
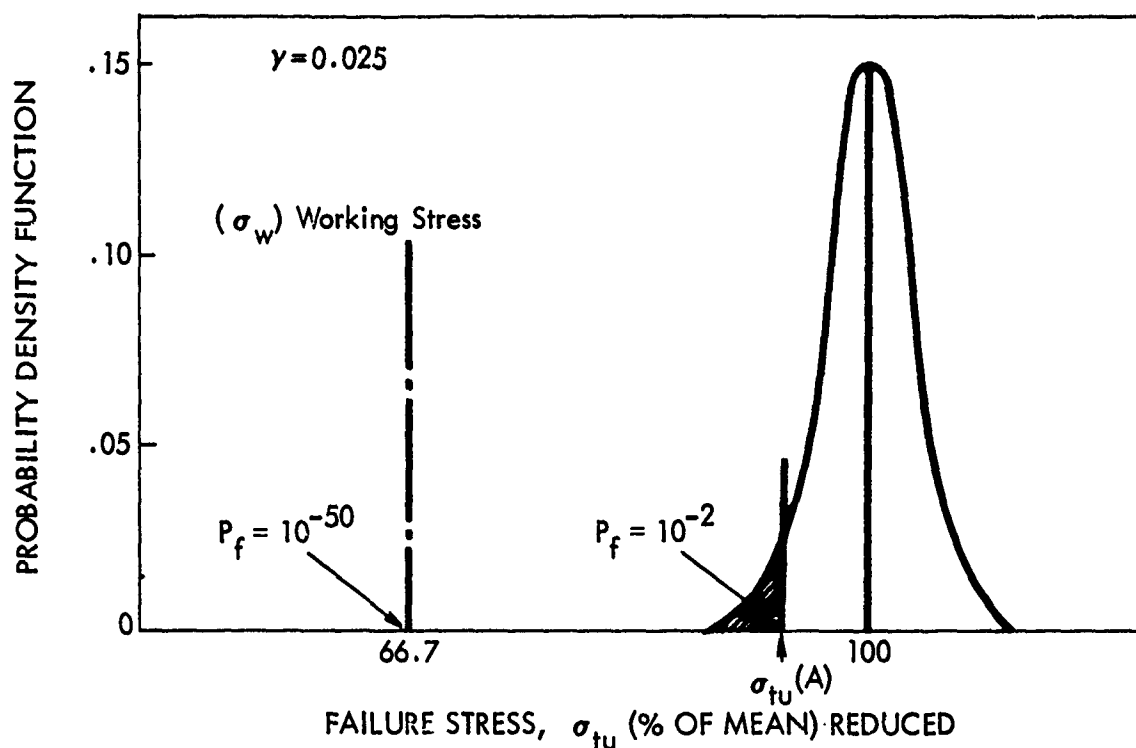
FIGURE 4 – LOCATION OF WORKING STRESS AS % OF MEAN σ_{tu} (COEFFICIENT OF VARIATION, $\gamma = 0.025$)
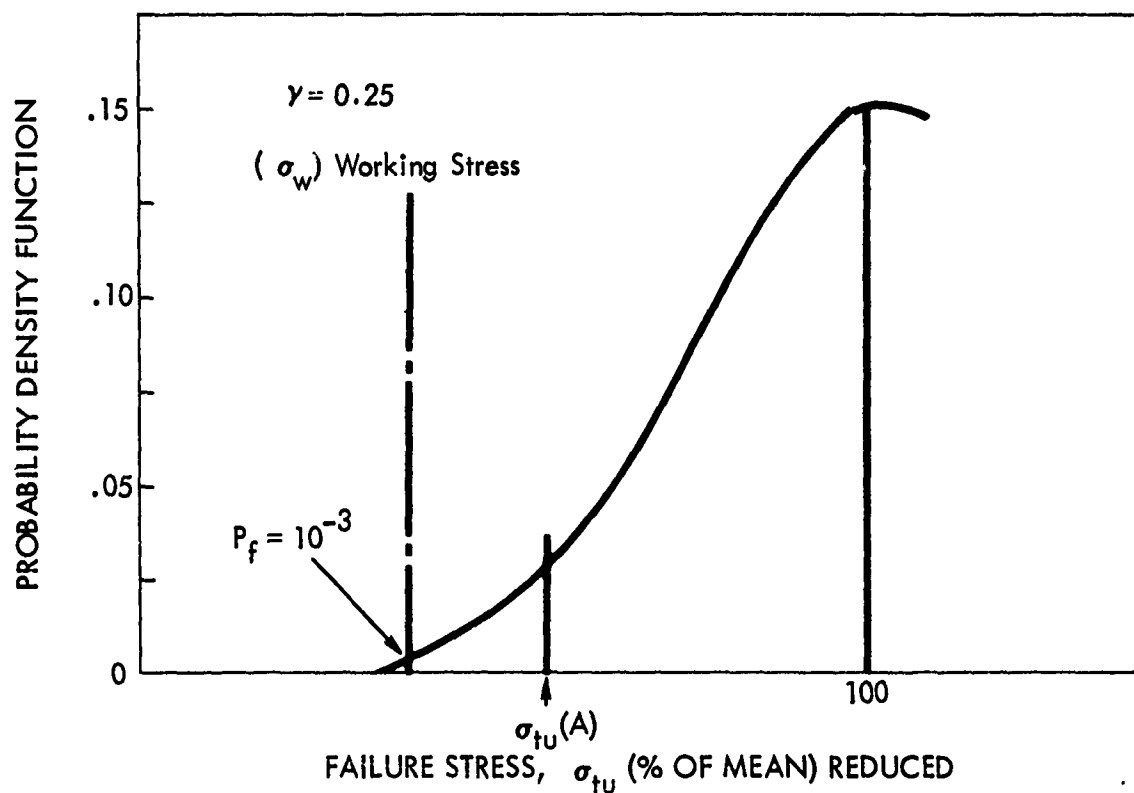
FIGURE 5a – EFFECT OF LARGE COEFFICIENT OF VARIATION ON THE PROBABILITY OF FAILURE AT THE WORKING STRESS
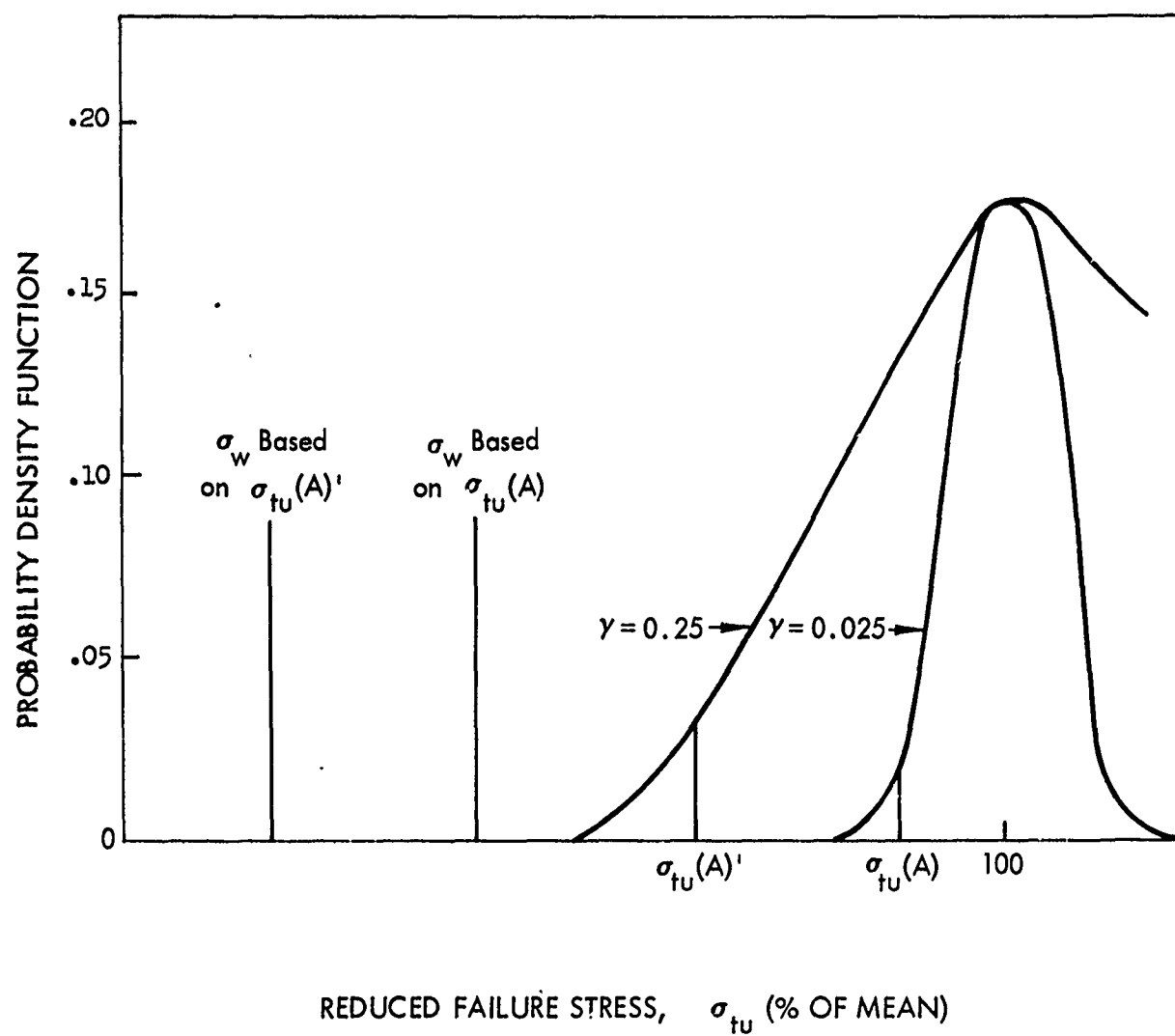
FIGURE 5b – EFFECT OF COEFFICIENT OF VARIATION ON THE WORKING
STRESS BASED ON $\sigma_{tu}(A)$
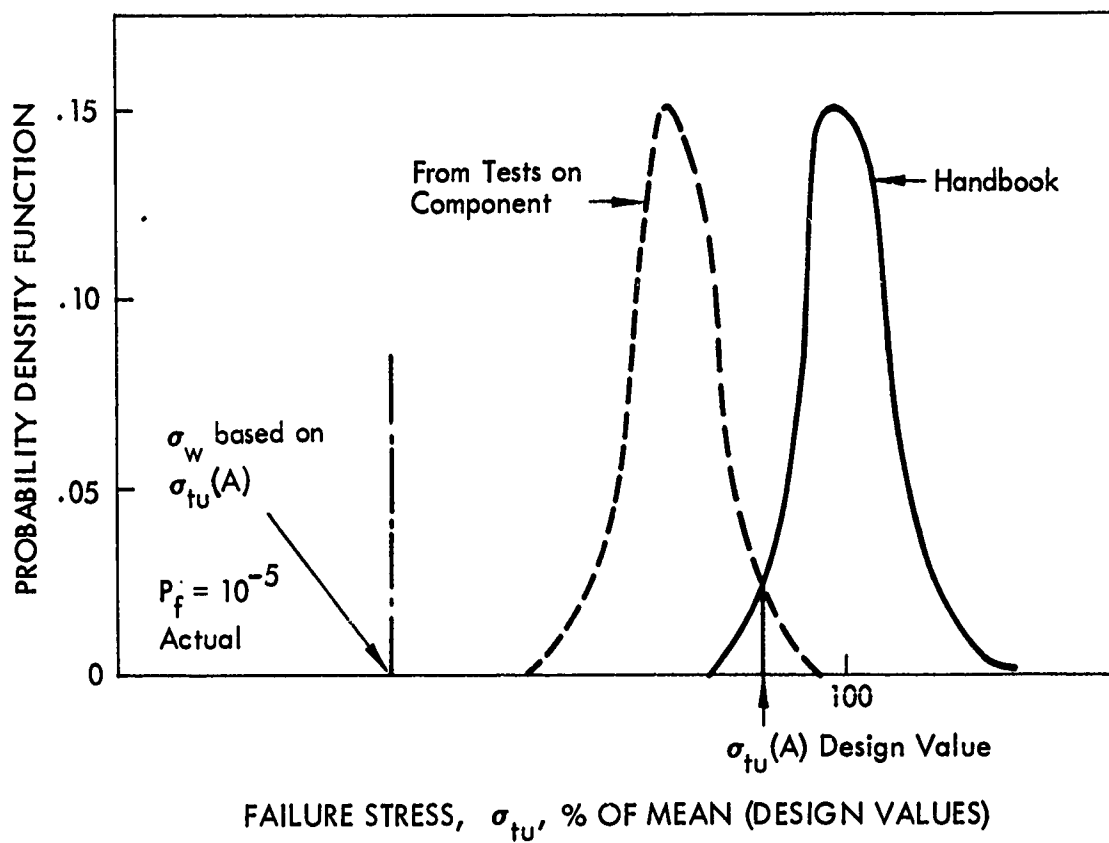
FIGURE 6 – EFFECT OF NONCONFORMITY OF COMPONENT PROPERTIES
ON PROBABILITY OF FAILURE

The effect of the second assumption on the strength of the component is normally minimized by giving different values of $\sigma_{tu}(A)$ for sheet, plate, and forging, and specifying the thickness range over which the $\sigma_{tu}(A)$ is to be applied.

There is, however, another factor that must be considered in using the strength values. This is the assumption that all of the materials used in the manufacture of the component do not contain defects. It is known that any actual manufacturing process introduces some form of defect into the material. This defect may be in the form of delaminations produced by forging, lack-of-fusion cracks in the welding process, or small scratches that occur during final machining and subsequent machining. Each of these defects may have a detrimental effect on the final load-carrying capacity of the component.

The effect of small defects on the strength of a material is the basis for the formulation of the present theories of linear elastic fracture mechanics. Thus, it is reasonable to examine the potential of using linear elastic fracture mechanics as a basis for formulating a design criterion.

Fracture Mechanics Design Concept

Although it is assumed that the concepts of linear elastic fracture mechanics are understood by the reader, many excellent references are available for a brief review of fracture mechanics and background in this field (2,3,4,5).

Fracture mechanics postulates that there exists a small flaw in the material under investigation. The relationship between the failure stress (σ_f) of the part and the flaw size (2c) is given as

$$\sigma_f = \text{Constant} \quad K_{Ic} \ c^{-1/2} \qquad (2)$$

where K_{Ic} is the plane strain stress intensity factor and 2c is the crack length. The value of K_{Ic} of the particular material is also assumed to have a probabilistic nature. Hence, curves such as those in Figures 1, 2, and 3 can be constructed for K_{Ic}. A schematic sketch of a probable distribution of K_{Ic} is shown in Figure 7. As was outlined previously, a minimum value of K_{Ic} is determined. This is defined as $K_{Ic}(A)$, and 99% of the material would be expected to have a value greater than $K_{Ic}(A)$. In a similar manner, a "B" value for the K_{Ic} can also be established.

There would also be a distribution function for the values of the flaw sizes. This is plausable, since given a material with a particular processing history, a normal distribution of flaw sizes typical of the processing could be expected. This is shown schematically in Figure 8. In contrast to the choice of the minimum expected value of K_{Ic}, the value of 2c that is chosen must be a maximum value. This is because of the inverse-square-root relationship between crack size and strength. Hence, for the crack length, the upper bound 99% confidence limit of 2c would be used. Here, 99% of the material would be expected to have a crack size smaller than this value. The location of c(A) is shown in Figure 8.
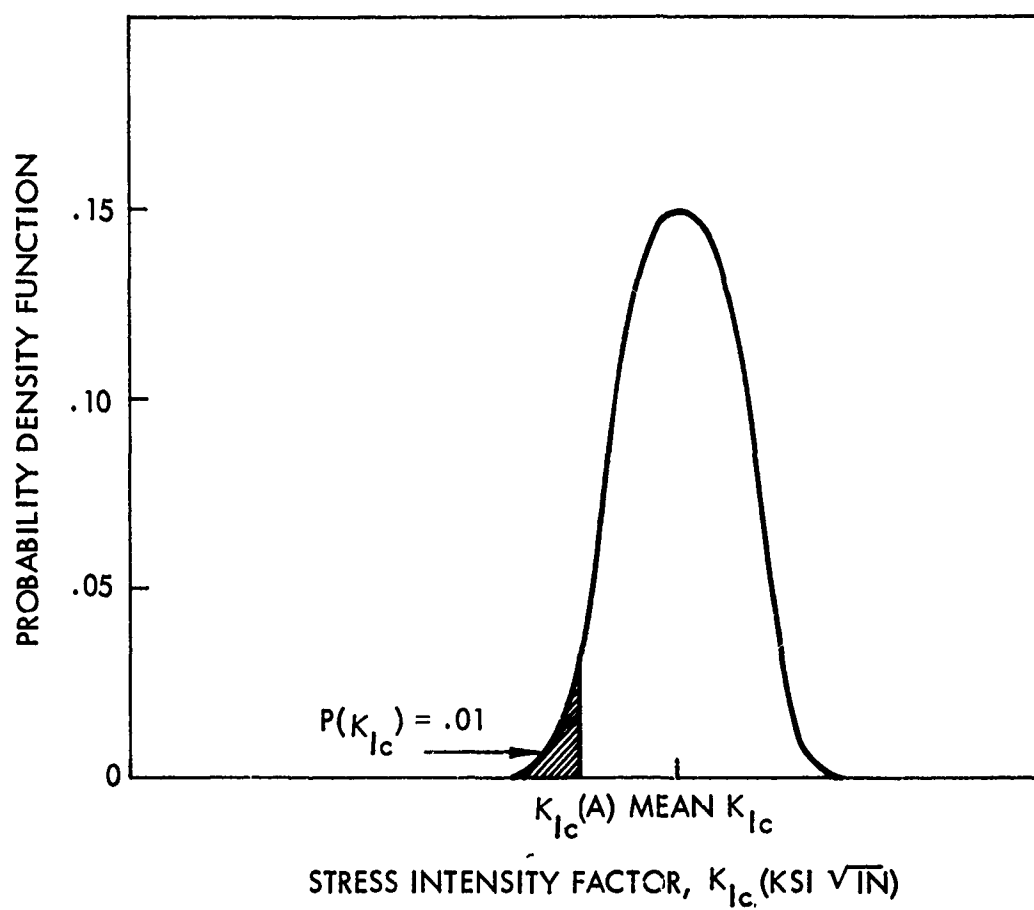
FIGURE 7 – DISTRIBUTION FUNCTION FOR K_{Ic}
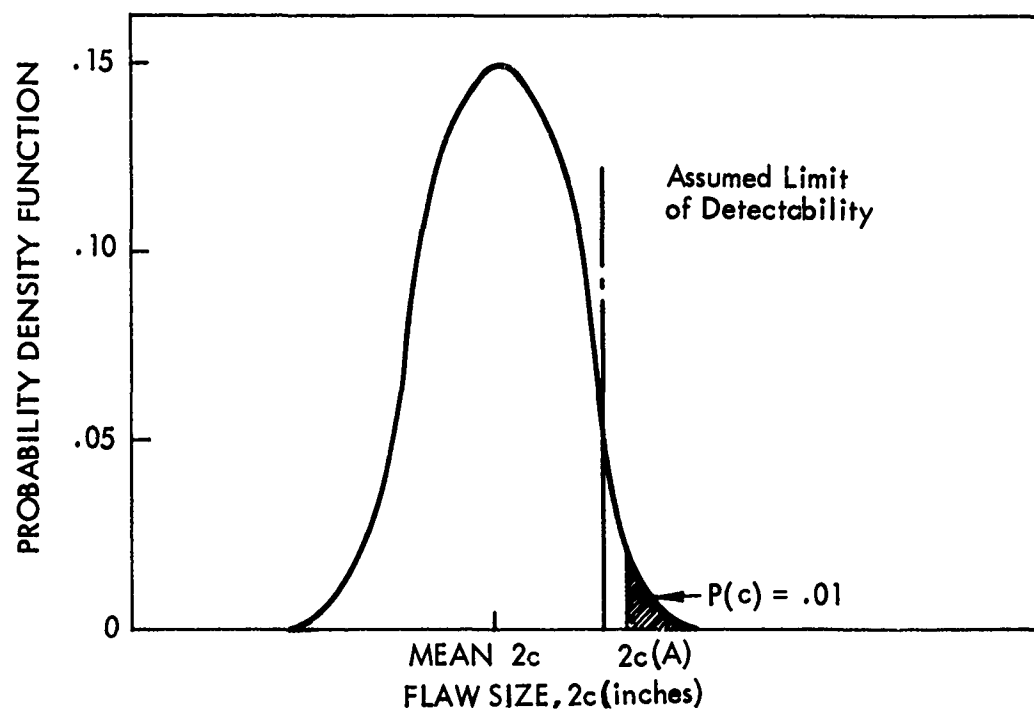
FIGURE 8 – ASSUMED DISTRIBUTION OF FLAW SIZE

11

A combination of the K_{Ic} distribution and the 2c distribution would result in a distribution function for the fracture stress. This is shown in Figure 9. In a manner similar to Equation 1, a working stress σ_w can now be defined as FS $\sigma_w = \sigma_f$.

The potential of a fracture mechanics-nondestructive testing design analysis is shown in Figure 10. The working stress σ_w has been calculated using the reduced ultimate stress. The probability of failure at this working stress is 10^{-4}. However, if the distribution function for the actual fracture stresses were used the probability of failure at the same working stress σ_w would be 10^{-7}. Thus, depending on the magnitude of the reduction of the tensile ultimate, an increase in the reliability of the structure can be obtained using the true fracture stress distribution. By using the true fracture stress rather than the reduced ultimate stress as a design philosophy, the working stress can be increased to σ_w', where the probability of failure is now 10^{-6}. Thus, if the confidence in the two design philosophies were equal, the actual working stress in the component could be increased with no loss in safety.

The validity of the fracture mechanics design procedure depends on the ability to determine the flaw distribution function "2c". Since the a priori assumption is that the material contains flaws, some reliable method must be used to detect these flaws in the component prior to failure. The use of nondestructive testing to detect flaws in materials is well known (6,7,8,9,10). In the curve shown in Figure 8, most of the flaw sizes may be below the limit of detectability of the NDT procedure. Thus, it is mandatory to know the reliability of the NDT method for each flaw size. For example, if the minimum size of flaw that could be detected by the NDT procedure were greater than the upper bound 99% confidence limit for the crack size 2c(A) chosen for the particular design, there would be no way of determining if the actual component contained flaws of this magnitude. Upon loading of the component, these flaws could grow and cause catastrophic failure. An ideal situation is shown in Figure 11, where the minimum detectable flaw size by the NDT technique is well below the mean flaw size of the material.

Two assumptions used in the analysis should be discussed. First, it is assumed that there are sufficient data available to obtain a satisfactory distribution function for the K_{Ic} values shown schematically in Figure 7. It is assumed further that this function has a small coefficient of variation so that a 99% probability limit for $K_{Ic}(A)$ can be determined that is not too different from the mean K_{Ic}. If this were not true, the difficulties outlined in Figures 4 and 5 would reduce the reliability to unsatisfactory levels. Second, it is assumed that the fracture mechanics formulation can account for the complexity of the actual component. This would determine a magnitude for the constant in Equation (2), relating the flaw size 2c, the critical stress intensity factor, K_{Ic}, and the actual component failure stress.

Program Objectives

Figure 12 shows the general plan followed by the two design methods. The standard design procedure using handbook data such as σ_{tu} and σ_{ty} is shown at the left, the FM/NDT procedure on the right. The objective in both analyses is to predict the true fracture stress of a component. In both analyses the stress analysis of the component based on loading conditions and component configuration must be determined. However, in contrast to the standard procedures, additional data must be available to use the FM/NDT procedure.

12
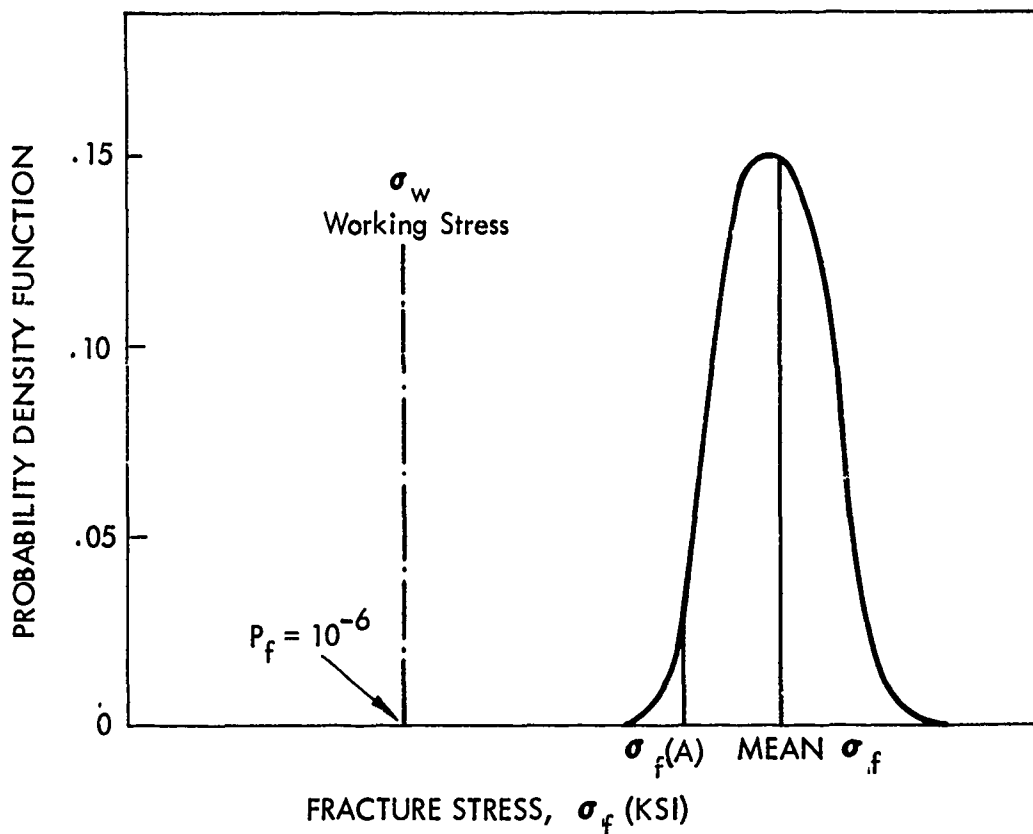
FIGURE 9 – DISTRIBUTION FUNCTION FOR FRACTURE STRESS
USING FRACTURE MECHANICS
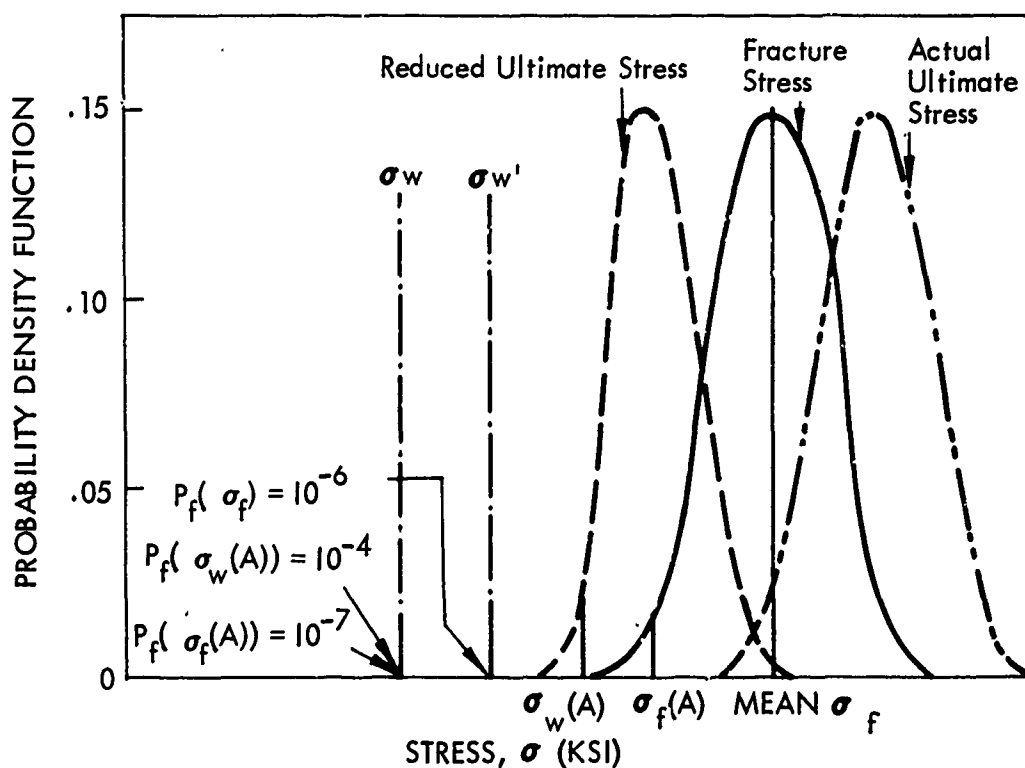
FIGURE 10 – PROBABILITY OF FAILURE AT WORKING STRESS COMPARED
USING σ_f DISTRIBUTION AND σ_{tu} DISTRIBUTION

13
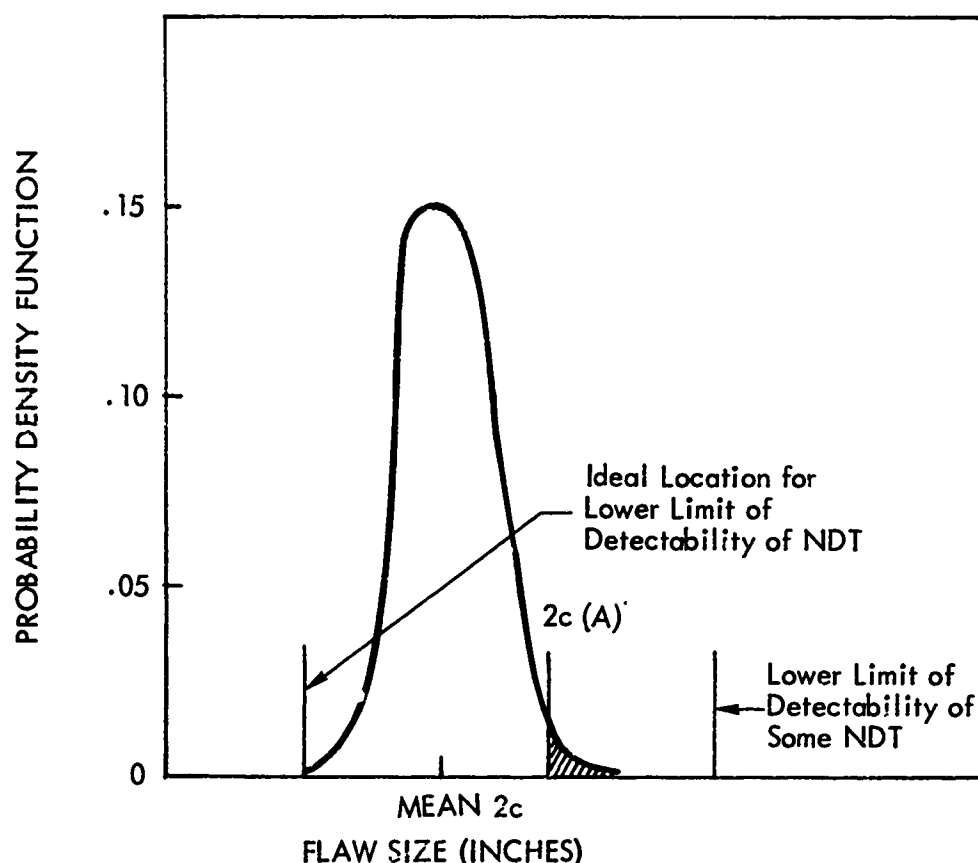
FIGURE 11 - LOCATION OF 2c(A) AND LOWER LIMIT OF NDT DETECTABILITY

C-130 HERCULES

TRUE FRACTURE STRESS

PREDICTED
FRACTURE STRESS
(STANDARD PROCEDURE)

PREDICTED
FRACTURE STRESS
(FRACTURE MECHANICS/NDT)

STRESS ANALYSIS OF COMPONENT
BASED ON LOADING CONDITIONS
AND COMPONENT CONFIGURATION

NO FLAW

MIL HDBK 5
DATA

FLAW GEOMETRY
(NDT DATA)
SEE FIG. 13

MATHEMATICAL MODEL
(FRACTURE MECHANICS
FORMULATION)

FRACTURE PARAMETERS
$K_c(B)$, K_{Ic} DATA

SEE FIG. 14

FIGURE 12 - CALCULATION OF LIMITING STRESS BY STANDARD DESIGN
PROCEDURES (LEFT) AND BY FRACTURE MECHANICS/NDT PROCESS (RIGHT)

These include the K_{Ic} and the flaw size. The general plan for the determination of these parameters is shown in Figure 13 and 14.

The general objective of the research program reported here is to provide a basis for which the validity of the combined FM/NDT design procedure can be determined. Thus, there are several short-range objectives:

o   To determine the minimum flaw sizes that can be detected reliably by standard NDT procedures, the sensitivity of the NDT procedure, the accuracy of the resulting flaw size prediction, and the accuracy of the flaw size location. Four NDT techniques have been chosen: X-ray, penetrant, magnetic particle, and ultrasonics.

o   To determine a distribution function for K_{Ic} for the selected materials: 7075-T6511 and 4330V Modified steel. These materials correspond to the materials used in actual C-5A components.

o   To determine the accuracy of a combined FM/NDT design analysis in predicting the failure load of a simple structure, and the failure load of several selected C-5A components.

This report summarizes the experimental program and the results, conclusions, and recommendations obtained.

The remainder of the report is divided as follows:

Section II - Materials and Specimen Preparation

The materials used in the program and the sequence used in obtaining fatigue cracks in the simple test cylinders are presented.

Section III - Nondestructive Testing

The available literature is examined to determine what the predicted accuracies and sensitivities of the four chosen NDT methods would be. The methods and procedures used in nondestructive examination of the test cylinders are outlined. Finally, the results of the nondestructive tests on the precracked test cylinders are presented.

Section IV - Test Program

The testing procedures used for the test cylinders and techniques used in testing the round precracked fracture toughness specimens are presented.

Section V - Fracture Analysis

The results contained in Sections III and IV are combined to predict the fracture stress of the test cylinders. The accuracy and reliability of the proposed FM/NDT method are discussed.

Section VI - Applications

The application of an FM/NDT design is evaluated. The predictions of failure load using the FM/NDT procedure are compared to the actual test results on the C-5A components. Finally, several applications of the method to fatigue environmental loading are discussed.

Section VII - Summary
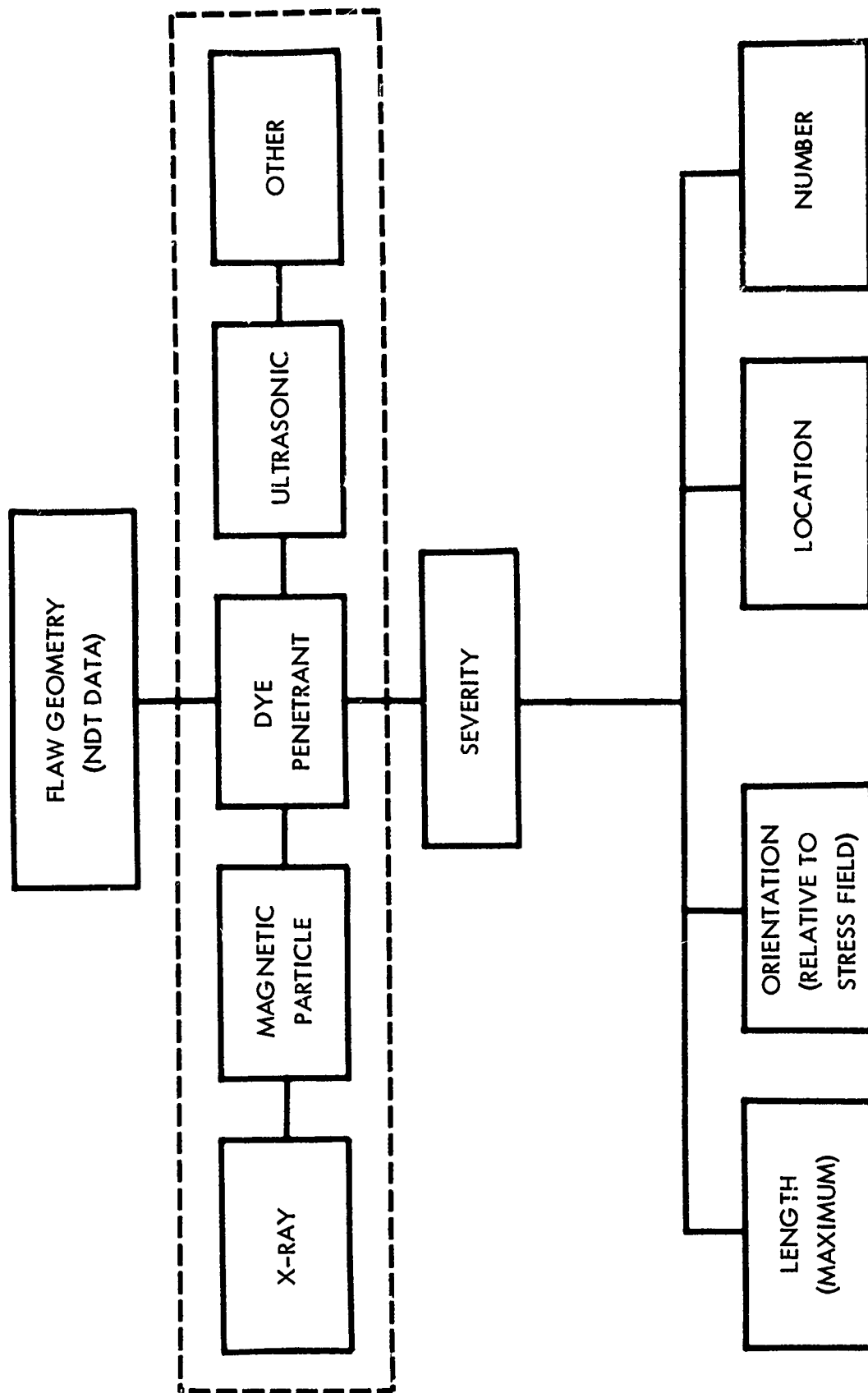
FIGURE 13 – DETERMINATION OF FLAW MORPHOLOGY BY NDT
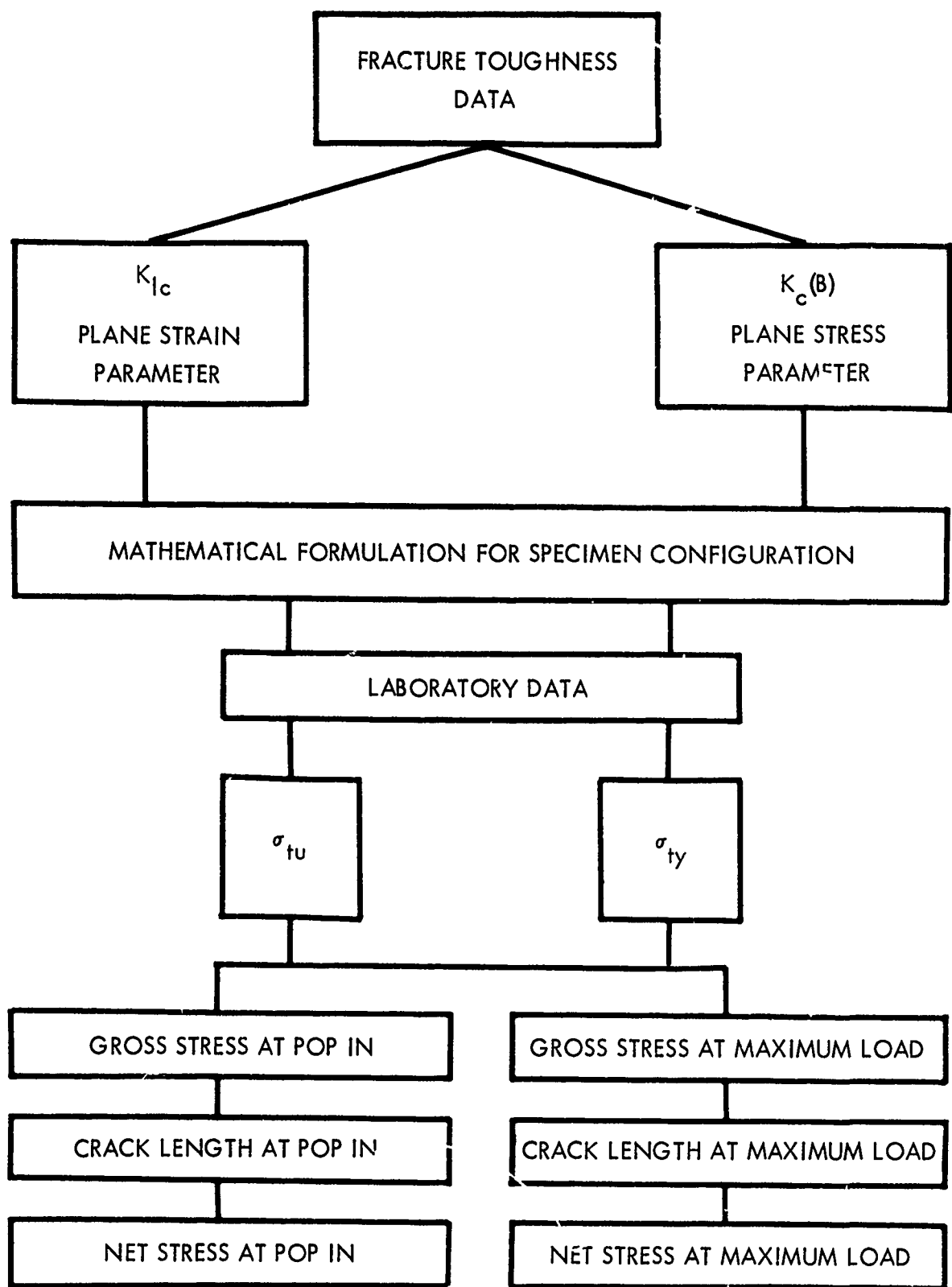
FIGURE 14 – CALCULATIONS FOR FRACTURE TOUGHNESS PARAMETERS

SECTION II

MATERIALS AND SPECIMEN PREPARATION

Materials

The materials used in this investigation were 4330V Modified steel and 7075-T6511 Aluminum. A billet of 4330V Modified steel was purchased and machined into round, circumferentially notched and fatigue-precracked fracture toughness specimens. These were used to determine K_{Ic} for the 4330V Modified steel. The chemical analysis of the steel is given in Table 1. Typical photomicrographs of the 4330V Modified structure are shown in Figures 15 and 16. The structure exhibits some selective banding in the longitudinal direction. The alloy phases consist of primary alpha iron (white) with partially spherodized pearlite (dark gray) and extremely fine-grain pearlite (light gray). Several complex sulfide inclusions were found, the average diameter of the inclusions was about 0.005 inch.

Photographs of the microstructure of the 7075-T6511 alloy are shown in Figures 17 and 18. The structure is typical of extruded precipitation-hardened aluminum alloys. It consists of elongated grains of alpha aluminum with precipitated inclusions in the grain boundaries. The longitudinal section (Figure 18) shows the extreme elongation of the grains with gray Al_2Zn and possible Al_2CuMg precipitates. The precipitated phases $Al_{12}Mg_2Cu$ and $MgZn_2$ assumed to be responsible for the high strength of the aluminum alloys cannot be resolved in the optical microscope.

Seamless 4330V Modified steel cold-drawn tubing with composition following AMS 6427 and extruded 7075-T6511 Aluminum tubing were used for the test cylinders.

TABLE I

CHEMICAL ANALYSIS OF 4330V MODIFIED STEEL FOR DETERMINATION OF K_{Ic}

Element	Percent
Carbon	0.306
Molybdenum	0.35
Nickel	1.79
Manganese	0.83
Chromium	0.87
Silicon	0.34
Vanadium	0.08
Iron	Balance

Specimen Preparation

General

The 7075-T6511 Aluminum and 4330V Modified steel test cylinders are three inches in diameter, 1/4 inch thick, and 32 inches long. They were precracked in fatigue to produce a small surface "thumbnail" crack. The steel specimens were then heat-treated to the desired strength level. Both the aluminum and steel specimens were inspected by NDT to determine

FIGURE 15 4330V MODIFIED STEEL. MAGNIFICATION 100X.
LONGITUDINAL SECTION
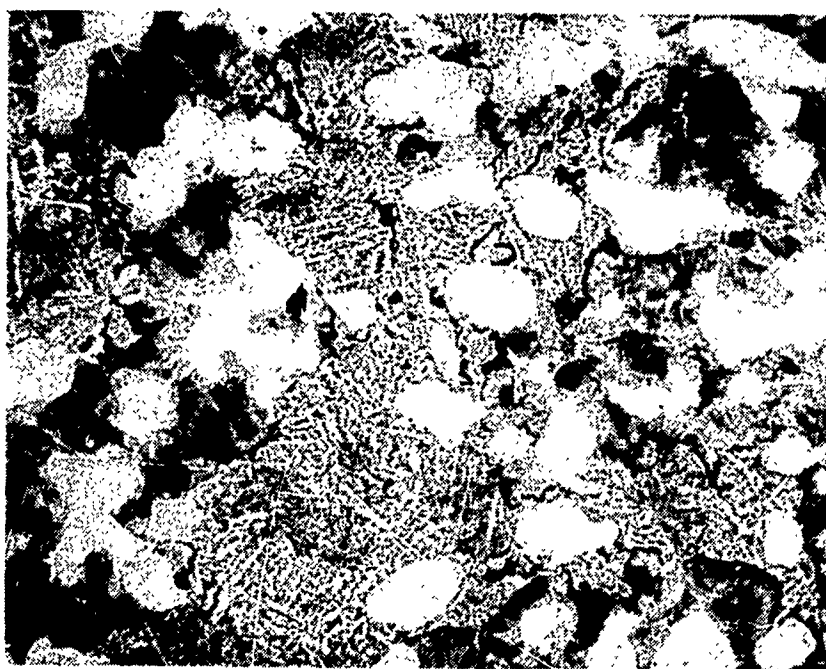
FIGURE 16 4330V MODIFIED STEEL. MAGNIFICATION 100X.
TRANSVERSE SECTION

FIGURE 17 7075-T6511 ALUMINUM EXTRUSION.
TRANSVERSE SECTION. MAGNIFICATION
250X.
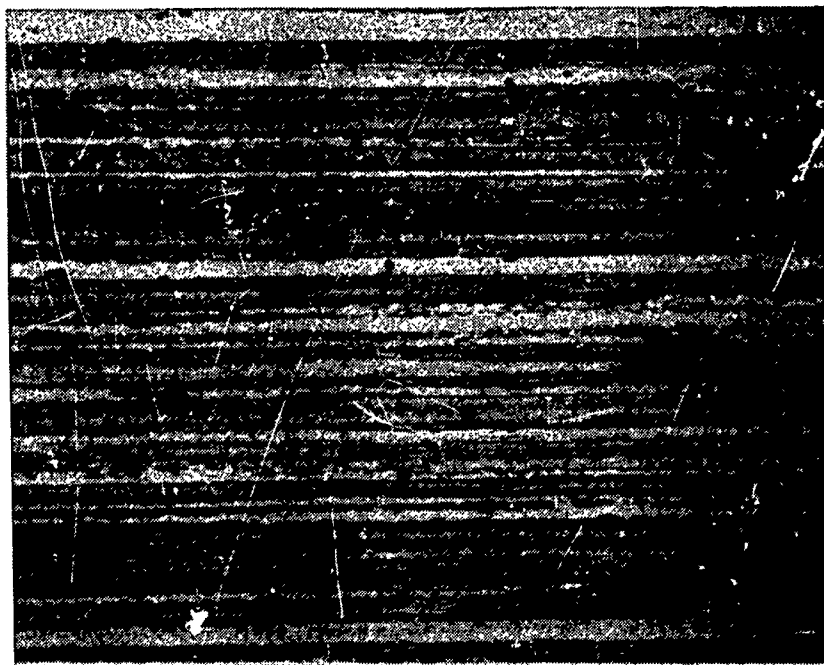
FIGURE 18 7075-T6511 ALUMINUM EXTRUSION.
LONGITUDINAL SECTION.
MAGNIFICATION 250X.

the size and location of flaws, then tested to failure in a uniaxial tension test. The failed surfaces were examined to determine the actual sizes of the flaws. Figure 19 shows the significant steps in the program.

The tubes were inspected by laboratory facilities, and by production facilities as time permitted, prior to failure-testing.

Techniques and Procedures

Cracks were initiated in the aluminum and steel cylinders by fatigue-cycling in a Riehle-Ametek closed-loop fatigue machine capable of fatigue loads ± 50,000 pounds. The test cylinders were mounted horizontally in a bending fixture shown schematically in Figure 20.

The baseplate of the fixture is attached to the hydraulic cylinder of the machine, and the pressure block is attached to the load cell. The specimen is placed on bearing blocks attached to the baseplate with Teflon shims used to protect the surface of the specimen. A mirror system mounted under the specimen was used in conjunction with a telephotometer to view the surface of the specimen. Figure 21 depicts the fatigue setup, and Figures 22, 23, and 24 show details of the jig.

To determine the stress on the cylinders, one steel and one aluminum cylinder (Figure 25) were used as calibration specimens. Strain-gage rosettes were installed on both specimens as shown in Figure 26. The calibration specimens were loaded statically, und calibration curves obtained by varying the load and incrementally recording load versus strain. Applied load was measured on both the Riehle-Ametek percent-of-range meter and a Mosley X-Y recorder equipped with a strain-gage preamplification system calibrated to indicate load from the SR-4 load cell.

The aluminum calibration specimen and the first two test specimens were installed in the fixture with their ends fixed by the upper sections of the bearing blocks. The calibration was performed, and one specimen was precracked successfully. The second specimen, however, developed severe cracks originating from the pinholes at both ends. Even though this specimen did develop a suitable crack in the center, both ends had to be removed. To prevent cracking at the ends, it was decided to simply support the ends. This setup was found to be successful, and all other specimens were tested in this manner, i.e., with the pin and upper blocks removed. Calibration curves (Figures 27 and 28) were subsequently obtained for the modified test setup (simply supported ends) using aluminum and steel cylinder calibration specimens.

To determine how the stress varied with location throughout the surface under the pressure block, a series of calibrations was made. The simply supported cylinder was moved along the longitudinal centerline, effectively relocating the strain gage. The results of these calibrations are shown in Figures 29 and 30. In each case, the relationship between stress and applied load was linear. The rosette strain data were analyzed, and the stress in the axial leg was found to be the maximum tensile principal stress, indicating that the gage was properly oriented.

Because of the large number of cylinders to be prepared, several crack initiation procedures were investigated. Briefly, these are as follows:

Method 1: a. Cycle cylinder 10,000 cycles.
            b. Remove and polish.
            c. If no crack is visible, recycle and examine continuously until crack is observed.
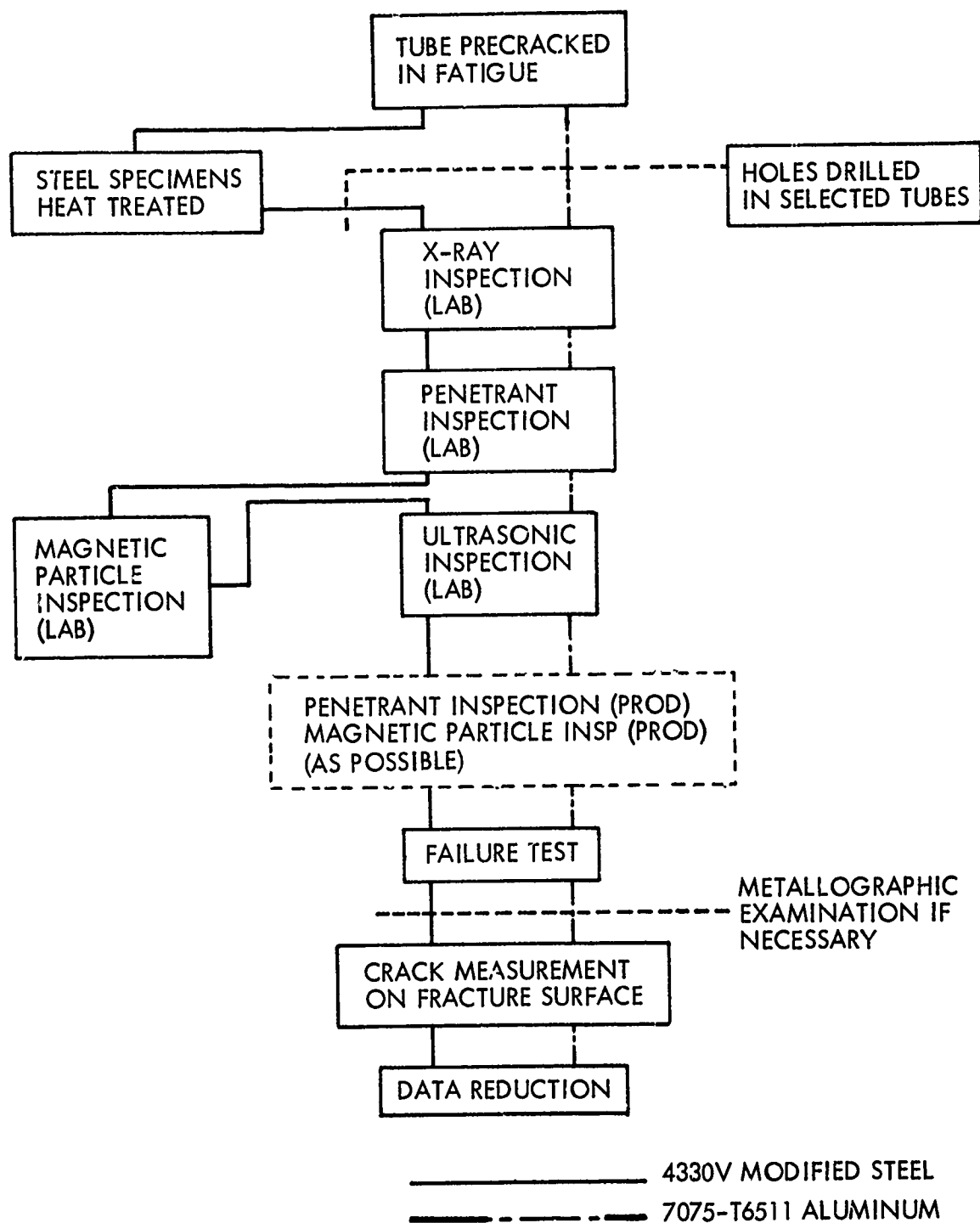
FIGURE 19 FLOW CHART SHOWING MILESTONES IN SPECIMEN PREPARATION

Hold Down Bolts

Twist Resisting Pins

Load

Specimen

Torque Pull Down Bolts

Table Attachment Stud
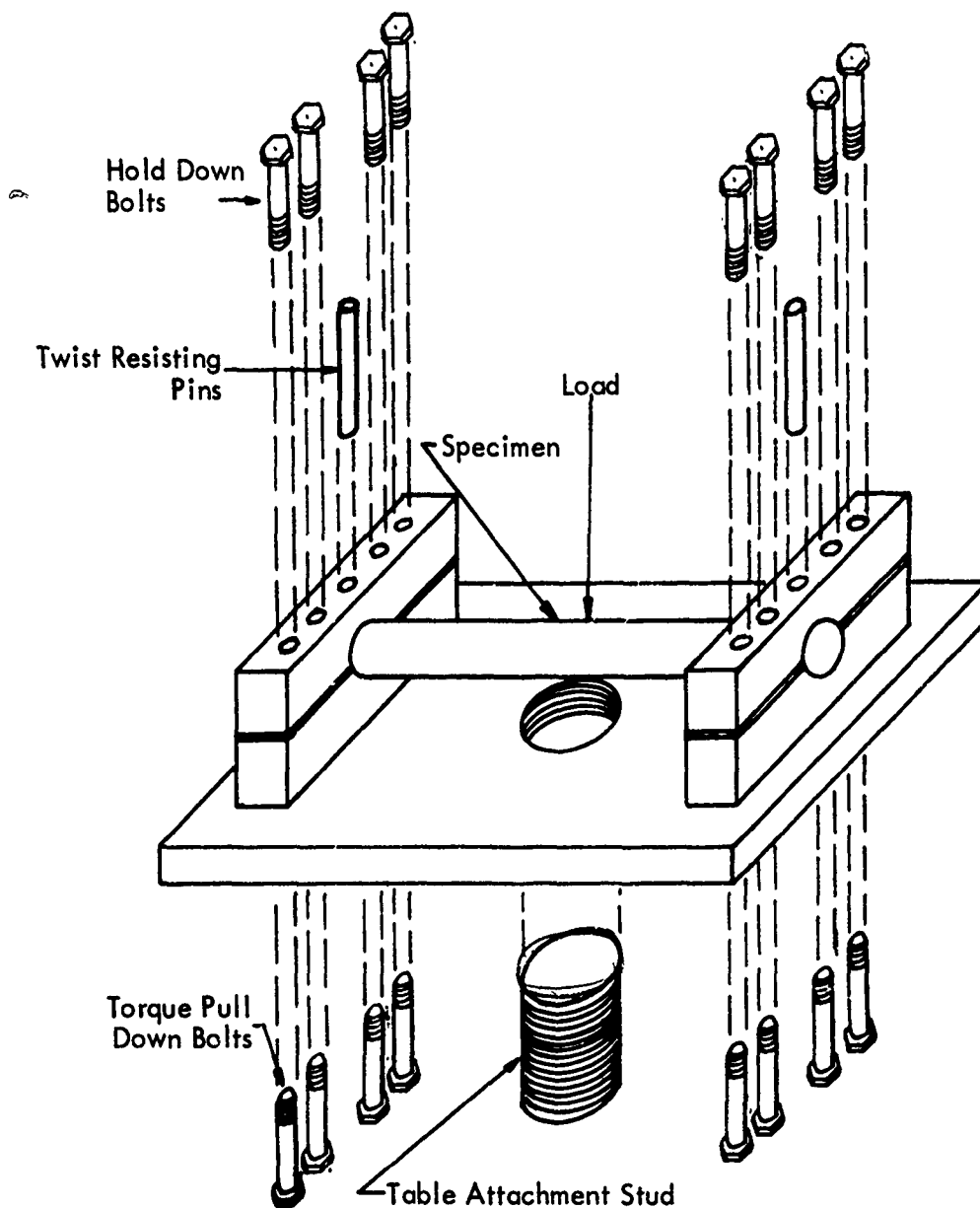
FIGURE 20 SCHEMATIC SKETCH OF LOADING FIXTURE FOR FATIGUE CRACKING OF TEST CYLINDERS

CONTROL CONSOLE

LOAD   POSITION

CYCLES

LOAD CELL

SPECIMEN

PRESSURE BLOCK

TELEPHOTOMETER

BENDING
FIXTURE

HYDRAULIC CYLINDER
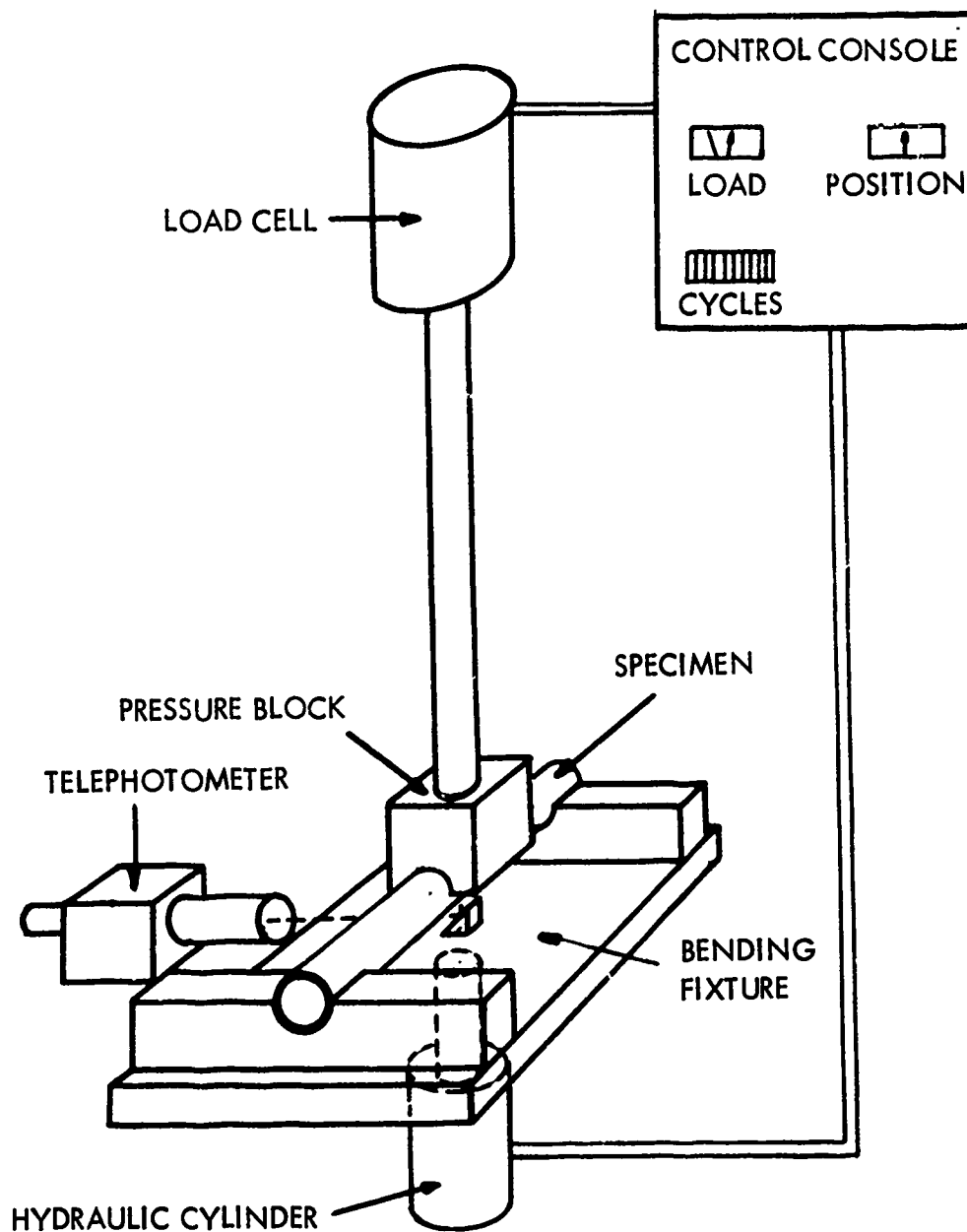
FIGURE 21 SCHEMATIC SKETCH OF TEST EQUIPMENT USED FOR
FATIGUE CRACKING OF TEST CYLINDERS

25
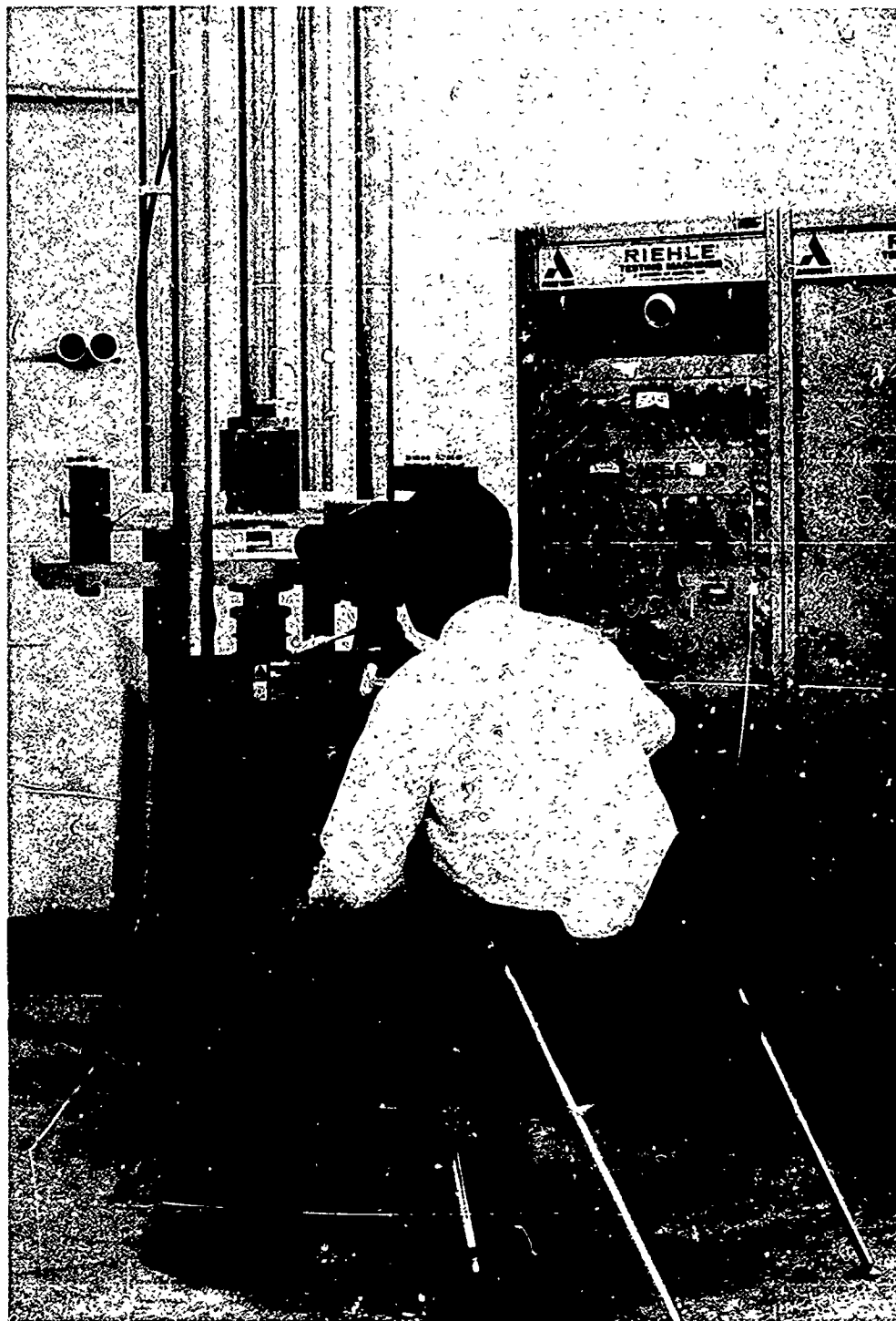
FIGURE 22 TEST EQUIPMENT USED FOR FATIGUE CRACKING THE
TEST CYLINDERS
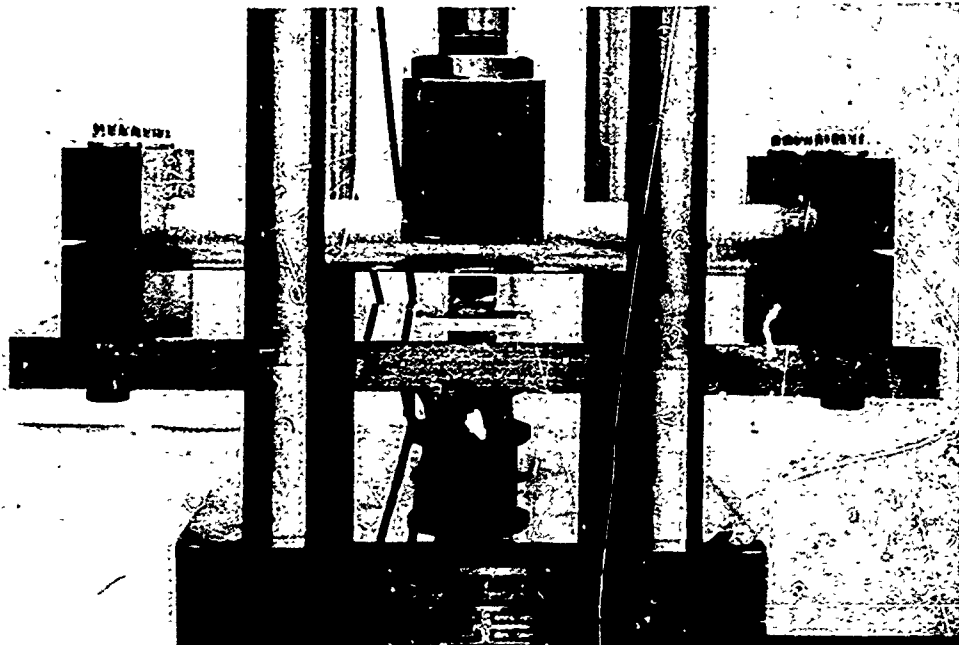
FIGURE 23 SIDE VIEW OF BENDING FATIGUE JIG USED FOR PRECRACKING
TEST CYLINDERS
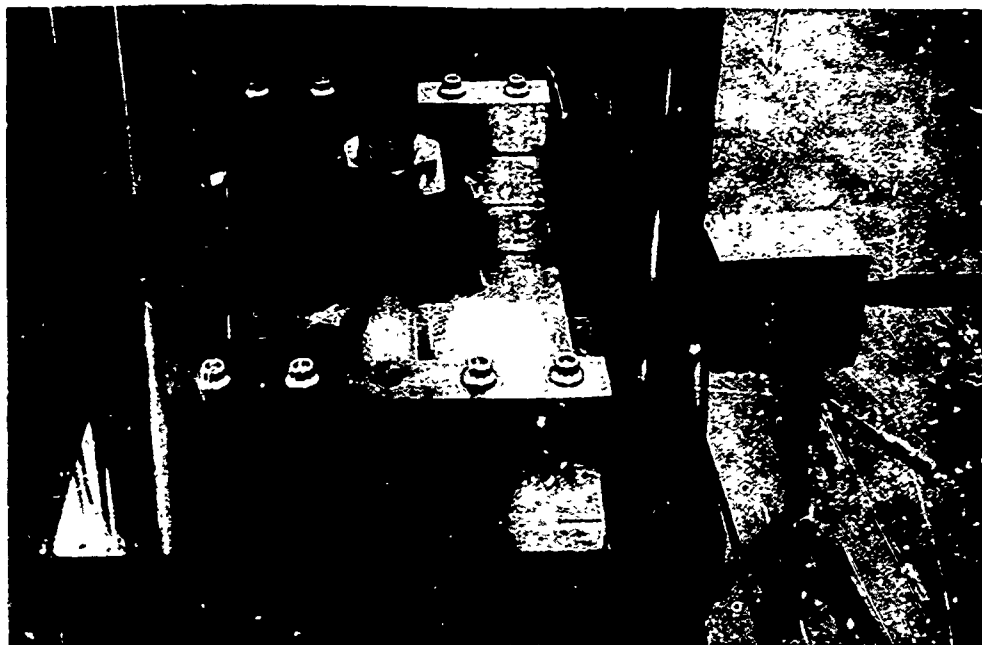
FIGURE 24 END VIEW OF BENDING FATIGUE JIG USED FOR PRECRACKING
TEST CYLINDERS. TELEPHOTOMETER FOR VIEWING TENSION
SURFACE IS AT RIGHT
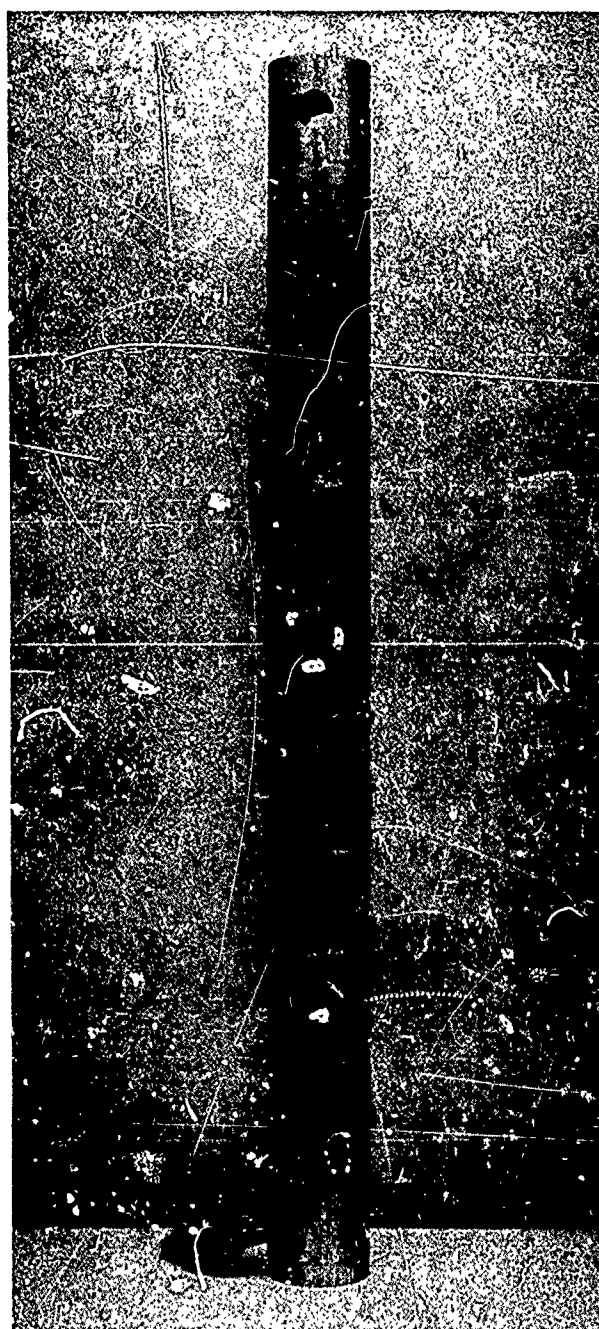
FIGURE 25 7075-T6511 ALUMINUM TEST CYLINDER WITH STRAIN
ROSETTE FOR CALIBRATION OF BENDING FATIGUE JIG
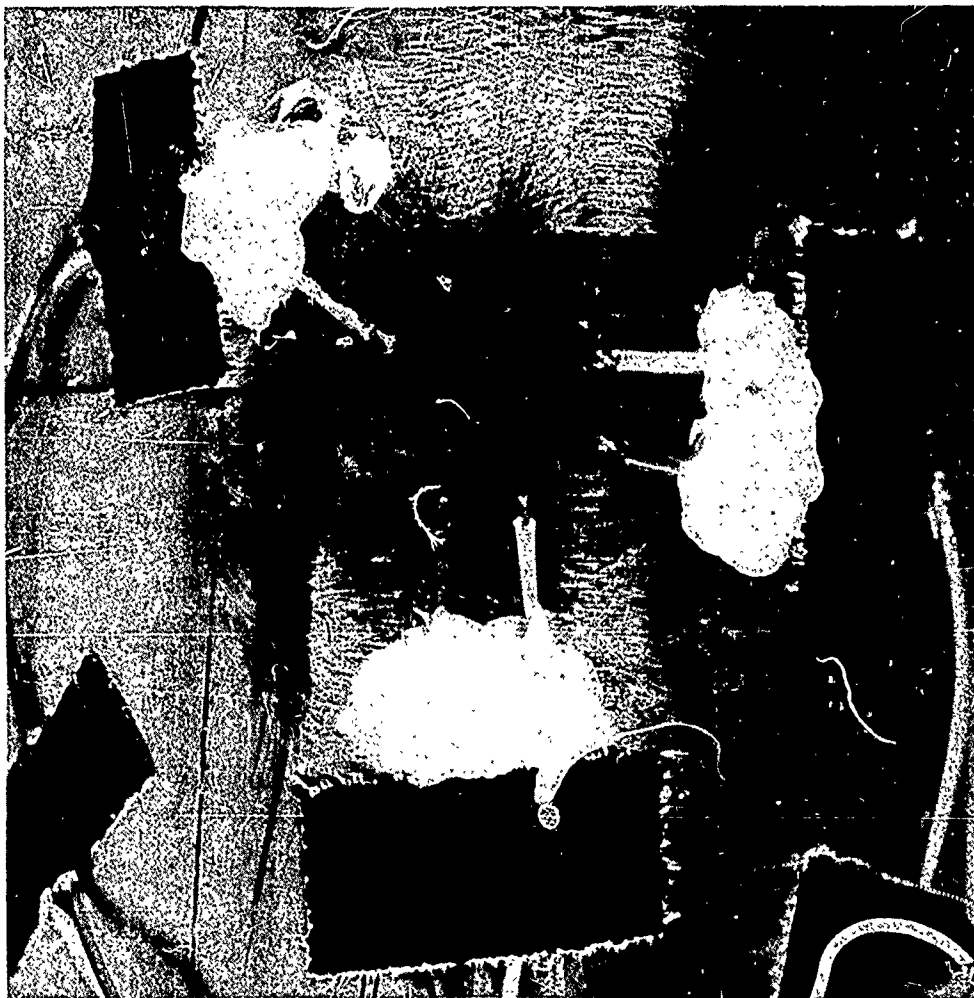
FIGURE 26 STRAIN ROSETTE ON 7075-T6511 ALUMINUM TEST
CYLINDER
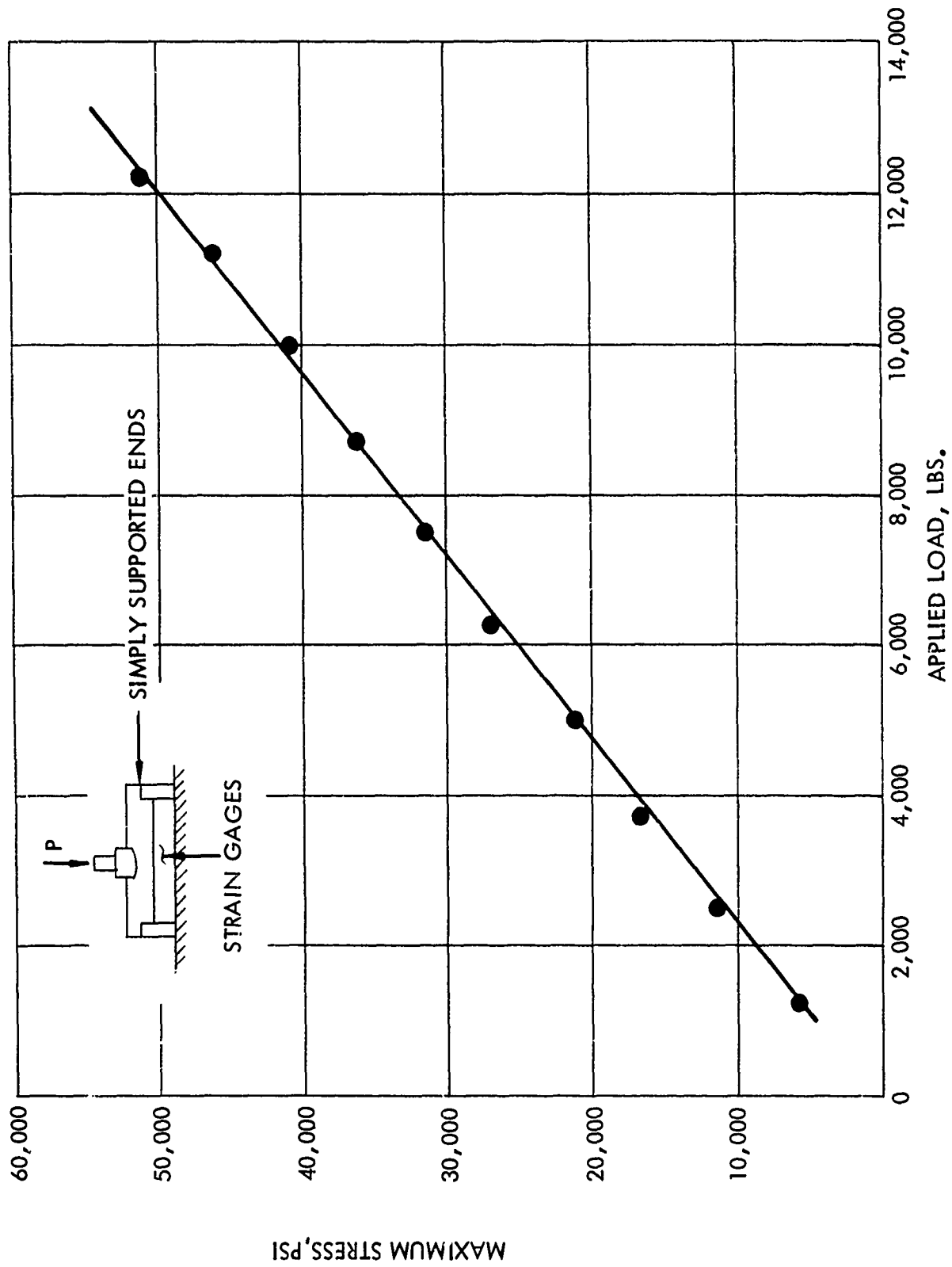
FIGURE 27   CALIBRATION CURVE MAXIMUM STRESS VS. APPLIED LOAD, SIMPLY SUPPORTED ENDS, 7075–T6511 ALUMINUM SPECIMEN (3" DIA., 1/4" WALL)

30
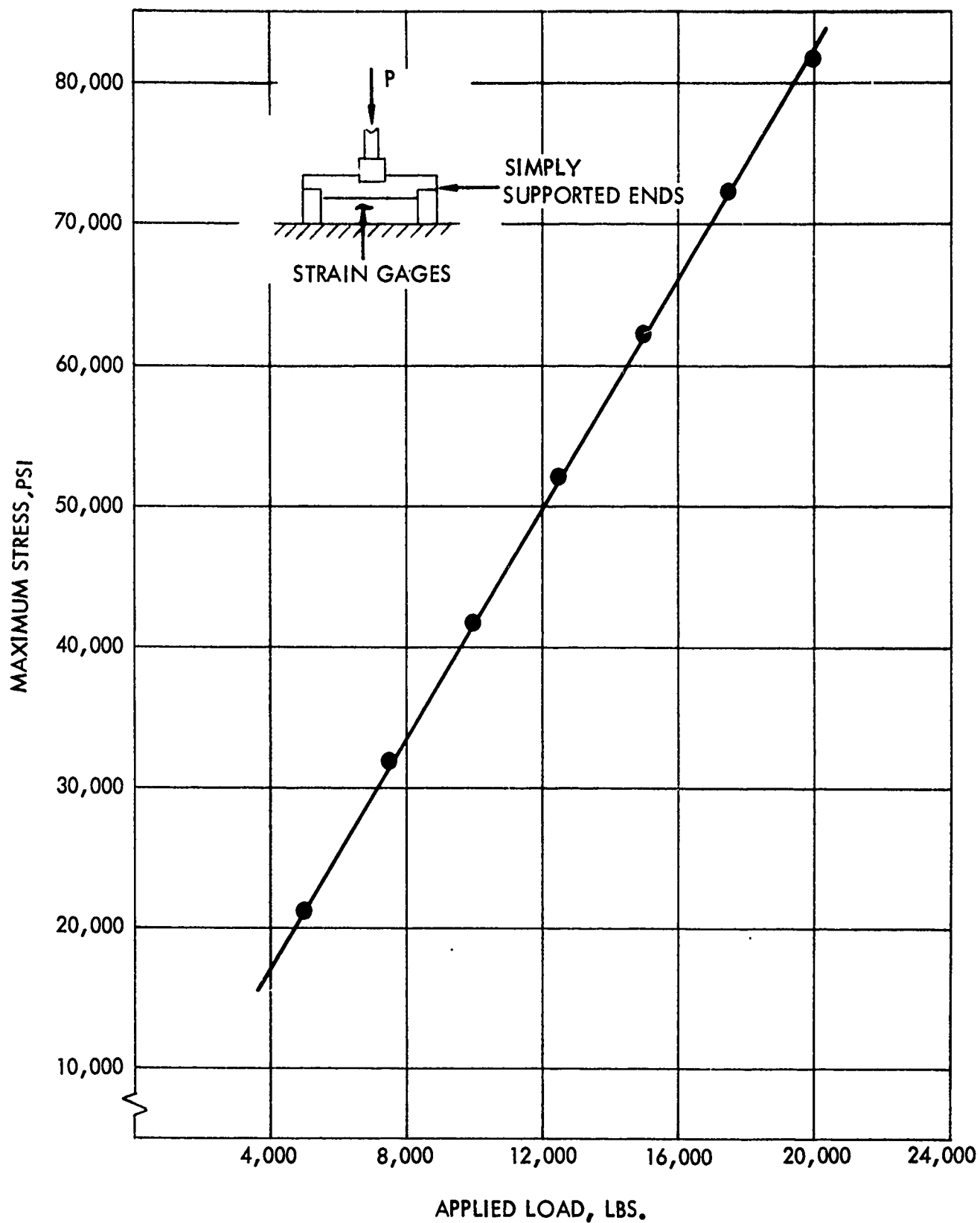
FIGURE 28 CALIBRATION CURVE, MAXIMUM STRESS VS. APPLIED LOAD,
SIMPLY SUPPORTED ENDS, 4330V MODIFIED STEEL SPECIMEN
(3" DIA., 1/4" WALL)
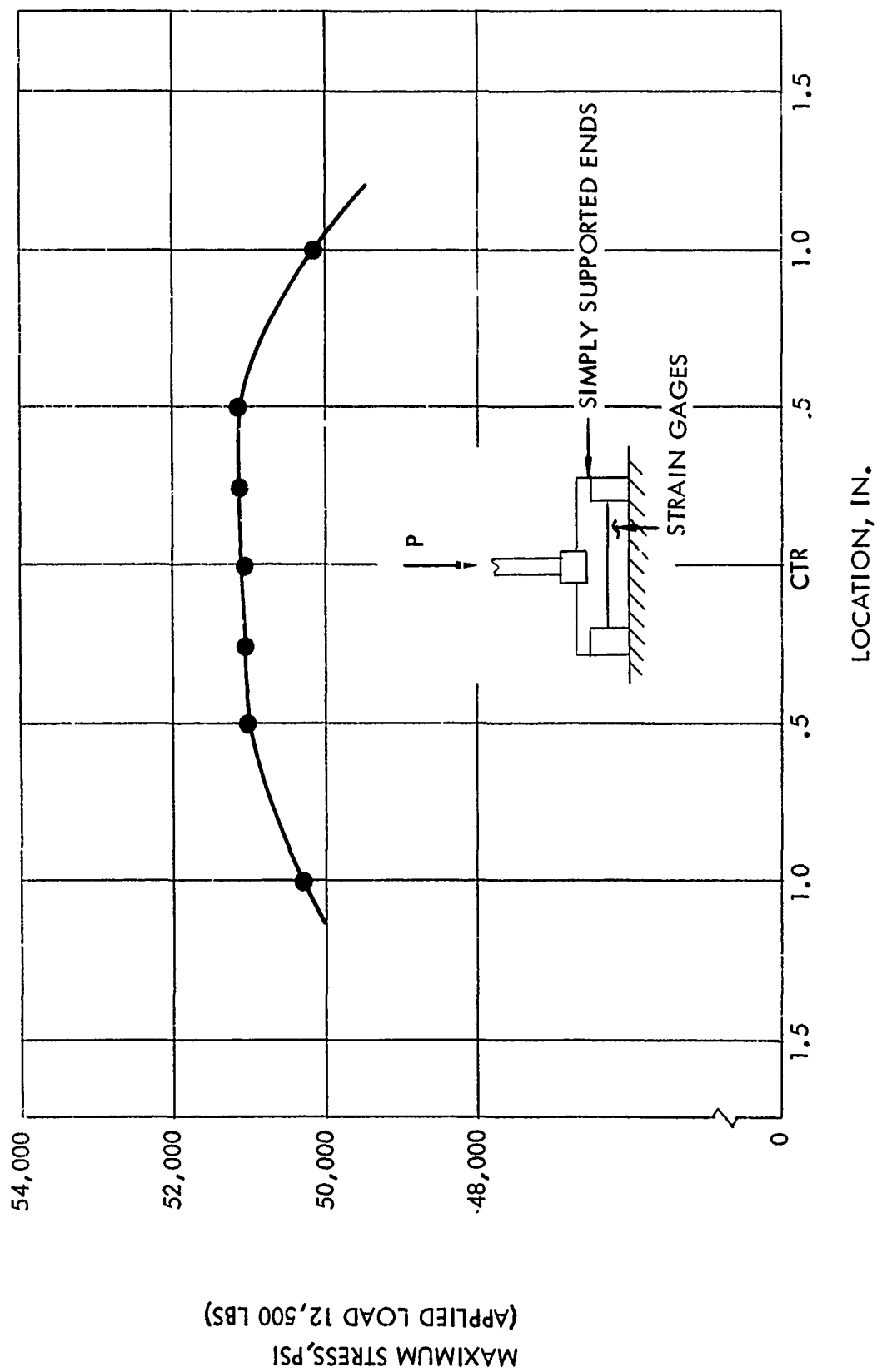
FIGURE 29 DISTRIBUTION OF STRESS VS. STRAIN GAGE LOCATION.
7075–T6511 ALUMINUM CALIBRATION SPECIMEN

32
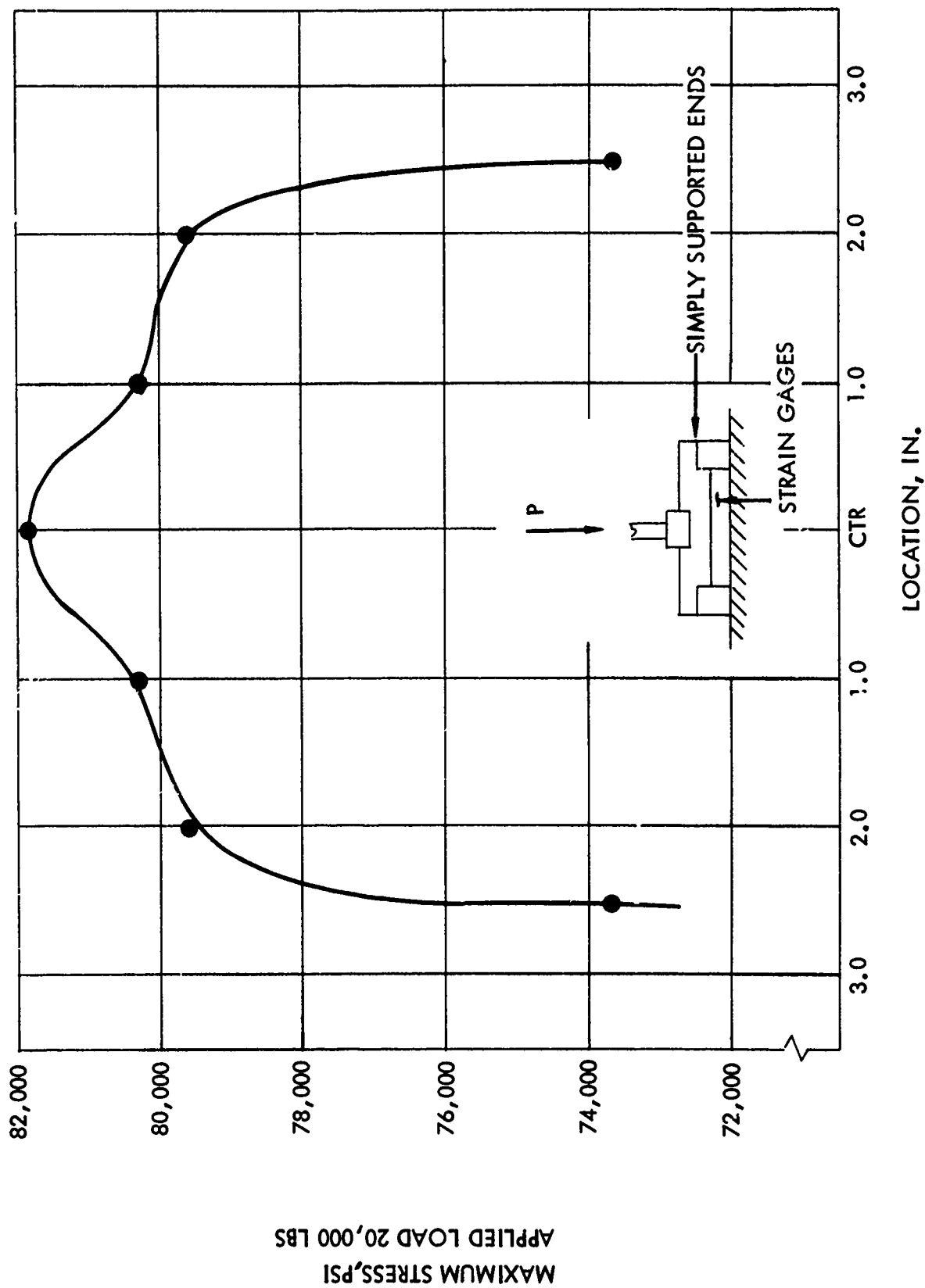
FIGURE 30 DISTRIBUTION OF STRESS VS. STRAIN GAGE LOCATION.
4330V MODIFIED STEEL CALIBRATION SPECIMEN (3" DIA., 1/4" WALL)

33

Method 2: a. Cycle cylinder 10,000 cycles.
b. Remove and polish.
c. Recycle for a predetermined number of cycles.

Method 3: a. Place small indentation mark on tensile face.
b. Cycle and examine continuously until small crack is observed.

Method 4: a. Place micro-weld spot in tensile surface.
b. Polish surface to remove evidence of weld mark.
c. Cycle with continued examination until small crack is observed.

The following loading sequence was used to precrack the aluminum cylinders:
After the specimen was positioned, the mean load was increased until a load of 6,700 pounds corresponding to a tensile stress of 28,000 psi was reached. The amplitude control was increased to the approximate setting, and the cyclic control was turned on. Using both means of load measurement, the amplitude control was varied until a maximum of 11,000 pounds (46,000 psi) and a minimum of 2,500 pounds (10,000 psi) were attained. The cyclic rate was 2.5 cps.

The loading sequence for the steel cylinders followed the same procedure as was used for the aluminum. The mean load on the steel cylinders was 12,000 pounds (51,000 psi), the maximum load was 20,000 pounds (82,000 psi), and the minimum load was 5,000 pounds (20,000 psi). The cyclic rate was 3 cps.

In the aluminum cylinders for crack lengths less than 0.05 inch, Method 2 was found to give the most satisfactory results. Specimens were cycled for 10,000, 12,000, and 15,000 cycles and then inspected. Small fatigue cracks were found on some of the fracture surfaces. For crack lengths greater than 0.05 inch, Method 4 was found to give the most consistent results. The small micro-weld spot was less than 0.030 inch in diameter and about 0.020 inch deep. Numerous cooling cracks were present in the fusion zone of the micro-weld. When the specimen was fatigued, one of these cracks grew beyond the heat-affected zone. The fatigue cycling was stopped when the crack had grown to a predetermined length. Crack lengths ranging from 0.10 to 0.3 inch were produced in approximately 20,000 cycles by this process. The method is not suitable for small cracks, since a crack less than 0.05 inch would lie in metal that is affected by the thermal cycling due to welding. Since the aluminum tubes were not heat-treated prior to the failure testing, this could affect the critical fracture stress.

Method 3 was tried on several aluminum specimens and met with varying degrees of success. Small punch marks produced what appeared to be tensile over-stressed regions near the surface from which the fatigue crack originated. Initially, small indentations were placed on the tensile surface of the test cylinders using a tungsten-carbide punch. This type of stress concentrator was discarded when it became evident that cracks often initiated at small surface scratches rather than at the indentation mark. All subsequent cracks in the aluminum cylinders were obtained using Methods 2 and 4.

There was some question regarding the procedure to follow for the fatigue cracking of the 4330V Modified steel tubes. Two approaches were possible: (1) to produce fatigue cracks in the specimen prior to the heat-treatment or (2) to fatigue the specimens after the heat-treatment. It was decided to use the weld spot to produce all of the cracks in the 4330V Modified steel, and all specimens were fatigued in the annealed condition. There are several reasons for this decision:

1. As the weld spot in the steel could be made very small (0.03 inch), cracks ranging in length from 0.050 inch could be produced.

34

2. The detrimental effects of the micro-weld spot and heat-affected areas due to the weld cycle would be minimized because of the subsequent heat-treatment.

3. Crack growth rates in the heat-treated specimens were much faster than those in the annealed condition, and crack length could not be controlled as accurately.

4. The heat-treatment resulted in "staining" of the crack faces, making initial crack sizes easy to measure on the failed specimens.

Several attempts were made to produce suitable inclined cracks in the 7075-T6511 aluminum tubes, but none were satisfactory. The extruded aluminum has a definite texture and anisotropy. Hence, the inclined crack growth was intermittent and consisted of a series of small cracks and tears, resulting in a "staircase" effect. The overall visible appearance of the crack shows it at an incline to the axis of the tube. However, at about 500x, the tip of the crack is in a plane normal to the axis of the tube, i.e., identical to the 0° specimens. Thus, all cracks used in the program were normal to the longitudinal axis.

Two distinct types of specimen were prepared. The first type of specimen contained only the fatigue precrack. The second had a 1-inch-diameter hole bored in the cylinder wall at a predetermined location. The analysis of each of these specimens is presented in Section V. Tables II and III present the surface crack size schedule for the 7075-T6511 Aluminum and 4330V Modified steel cylinders.

TABLE II

SURFACE CRACK SIZE SCHEDULE – 7075-T6511 ALUMINUM CYLINDERS

Surface 2c Crack Size (inches)	No. of Specimens	No. of Specimens (1" Dia. Bored Hole)
0-.05	10	
.05-.10	10	3
.10-.15	10	3
.15-.20	10	3
.20-.25	10	3
.25-.30	10	
.30-.35	5	3
.35-.40	5	
.40-.45	5	3
.45-.50	5	
Total	80	18

35

TABLE III

SURFACE CRACK SIZE SCHEDULE – 4330V MODIFIED STEEL CYLINDERS

Surface 2c Crack Size (inches)	No. of Specimens	No. of Specimens (1" Dia. Bored Hole)
0-.05	10	3
.05-.10	10	
.10-.15	10	3
.15-.20	10	3
.20-.25	10	3
.25-.30	10	
.30-.35	5	3
.35-.40	5	
.40-.45	5	3
.45-.50	5	
Total	80	18

SECTION III

NONDESTRUCTIVE TESTING

Review of NDT

Background

Nondestructive testing (NDT) is of vital importance in the inspection, production, and testing of military aircraft and aerospace components. Aircraft reliability depends on the use and development of nondestructive testing techniques. Nondestructive testing will assume even greater importance with the development of more advanced weapons systems and more stringent and less conservative design criteria.

Considerable written information exists on NDT, although it is a relatively new field. Unfortunately, obtaining detailed data requires a lengthy search through technical journals, contractors reports, and advertising literature. The reports that are published in the literature deal primarily with instrumentation procedures and the feasibility of new NDT methods. Significant NDT data are scarce and relative, partly due to the qualitative manner in which NDT is currently used. This situation gives rise to frequent duplication of effort in the solution to NDT problems.

The interpretation of NDT data requires experience and ability on the part of the inspector. Each inspection technique has its own particular sources of error, and each specimen geometry presents a different problem. In many cases, the operator must know what he is looking for to eliminate extraneous information and estimate correctly the severity of the flaw.

The need to increase the effectiveness of all existing NDT methods requires that programs in the following areas be initiated (11).

1. Determination of the capabilities and limitations of each NDT method, and the variables which influence test method effectiveness (Tables IV and V).

2. Automation techniques that will reduce inspection time and eliminate human factors.

3. Development of standards for each test method.

This section presents a discussion of the four NDT inspection methods used in the experimental portion of this program:

1. X-ray
2. penetrant
3. magnetic particle
4. ultrasonics

Approximately 1,000 publications on the subject matter were examined as well as the abstracts in the Report Guides published by the Army Materials Research Agency (7,8,9,10)

Specifically, answers to the following questions were sought:

1. What are the sensitivity limits of each of the four NDT methods?
   (Flaw size, shape, location, etc.)

2. What types of defects can be found with a high degree of reliability?
   (Cracks, porosity, inclusions, etc.)

3. What are the limiting factors in finding the flaws?
   (Thickness, materials, shape, cost, etc.)

TABLE IV
NDT PRIORITY

Location	Type	Material	Specification	Selection* Priority		
Surface	Crack Machine flaws Porosity	Magnetic	Defect Size	1.MP	2.P	3.UT
		Non-Magnetic	Defect Size	1.P	2.UT	
	Crack	Magnetic	Size	1.MP	2.UT	3.XR
			Depth	1.UT	2.XR	3.MP
Subsurface	Inclusion	Non-Magnetic	Size	1.UT	2.XR	
	Porosity		Depth	1.UT	2.XR	
	Grain Size	All	Size	1.UT	2.XR	
			Depth	1.UT	2.XR	
Internal Defect I	Crack	All	Size	1.UT	2.XR	
			Depth	1.UT	2.XR	
	Inclusion	All	Size	1.UT	2.XR	
			Depth	1.UT	2.XR	
	Porosity	All	Size	1.XR	2.UT	
			Depth	1.UT	2.XR	
Internal Defect II	Delamination	All	Size	1.UT	2.XR	
			Depth	1.UT	2.XR	
Thickness	Not Applicable	All	Not Applicable	1.UT	2.XR	

*MP-Magnetic Particle   P-Penetrant-Zyglo   UT-Ultrasonic   XR-X-Ray

TABLE V

OPERATIONS CHART FOR FOUR NDT METHODS

Method	Magnetic Particle	Penetrant	Ultrasonic	X-Ray
Equipment	Magnaflux	Zyglo	Sperry Reflectoscope Model UCD and Transducers	Gelac Production X-ray Equipment
When to use	Surface or subsurface flaws, cracks, porosity or nonmetallic inclusions.	Surface cracks, porosity, laps, cold shut and fatigue and grinding cracks.	Internal defects, cracks, laminations, inclusions, porosity, grain structure and thickness gaging, also surface cracks.	Internal flaws, cracks, seams, porosity, holes, inclusion and thickness variations.
Where to use	Ferromagnetic material tubing any shape, size, or composition and in-service testing for fatigue cracks.	Metals, glass, ceramics, castings, forgings machined parts, and cutting tools.	Metals and hard non-metallic materials. Sheets, tube, rod, forging, castings, in-service part testing.	Forgings, castings, tubing, formed metal parts, and corrosion surveys.
Why to use	1. Simple 2. Easy 3. Portable 4. Fast 5. Positive	1. Simple 2. Accurate 3. Fast 4. Economical 5. Easy to interpret results	1. Fast and dependable. 2. Easy to operate. 3. Easily Automated. 4. Immediate test results. 5. Portable. 6. Highly accurate. 7. High sensitivity. 8. Permanent record on chart paper.	1. Record on film. 2. High sensitivity on thin sections. 3. Adjustable energy level. 4. Fluoroscopy techniques available.
Limitations	1. Parts must be magnetic. 2. Power source. 3. Demagnetize tested parts. 4. Parts must be clean.	1. Only surface defects. 2. Surface cleanliness required.	1. Requires contact or immersion of part. 2. Training required for interpretation of results.	1. High initial cost. 2. Power source. 3. Radiation hazard. 4. Trained technician required.

4. What is the size and shape of the minimum detectable flaw in the unit test cylinder by each of the NDT methods?

X-ray

X-ray inspection is best suited to examination for distributed defects such as porosity, shrink-age, and chemical heterogeneity. The efficiency of X-ray inspection in detecting cracks is strongly dependent upon knowledge of the probable location and orientation of such cracks (2). The extent to which X-ray inspection can be utilized in NDT, is largely dependent on several factors including:

1. Intensity of X-rays
2. Part configuration and material
3. X-ray wavelength
4. Dimensions of source
5. Duration of emmissions
6. Method and sensitivity of detection

Increasing the voltage of an X-ray tube produces radiation of higher intensity and shorter minimum wavelength. The shorter wavelengths penetrate the part more easily, and thus lower the contrast in the image of the part. If, however, very low voltages are used, the contrast between parts of non-uniform thickness may be too great for satisfactory viewing. Separate exposures may be used to examine sections of different thicknesses within a part with the obvious penalty of increased time and cost.

The contrast with which a given defect is revealed by X-ray inspection depends on a) the wavelength of the radiation used, b) the contrast capability of the film or fluorescent screen used as a viewing surface, and c) the amount of background and scattered radiation.

The largest effective dimension of the actual source of radiation is called the focal spot. The diagonal of the focal spot is taken as the operating dimension. Since this dimension will be imaged on the film, the X-ray method cannot resolve anything smaller than

$$p = \frac{fd}{D}$$

where p is the penumbral width, D the focus to object distance, d the object to film distance and f the diagonal of the focal spot. The maximum value of p is usually taken as 0.01 inch, but if the film is to be examined under high magnification, a value of p may be 0.005 inch. This simple calculation is used to determine the optimum focus to object distance D. Typical values of the focal spot dimensions are: 0.5 to 1.5 mm dia. for machines with operating vol-tages up to 300 KV, 1.5-5 mm dia. for machines in the 300-1000 KV range and up to 10 mm dia. for a 2 million KV machine.

X-radiation originates at the focal spot of the tube, and proceeds in straight lines to the visualizing surface. Since the focal spot has a finite size, the resolution of features of the part on the visual presentation is a geometric problem. The nomograph shown in Figure 31 presents the expected performance. For example, given a part of thickness t = 0.25 inch, a tube with a focal spot of 1 mm in diameter and a 30 inch distance from the X-ray tube to the specimen, one would not expect to resolve any flaw less than 0.007 mm in length. In actual practice, a spot this size would be overlooked on the X-ray film.
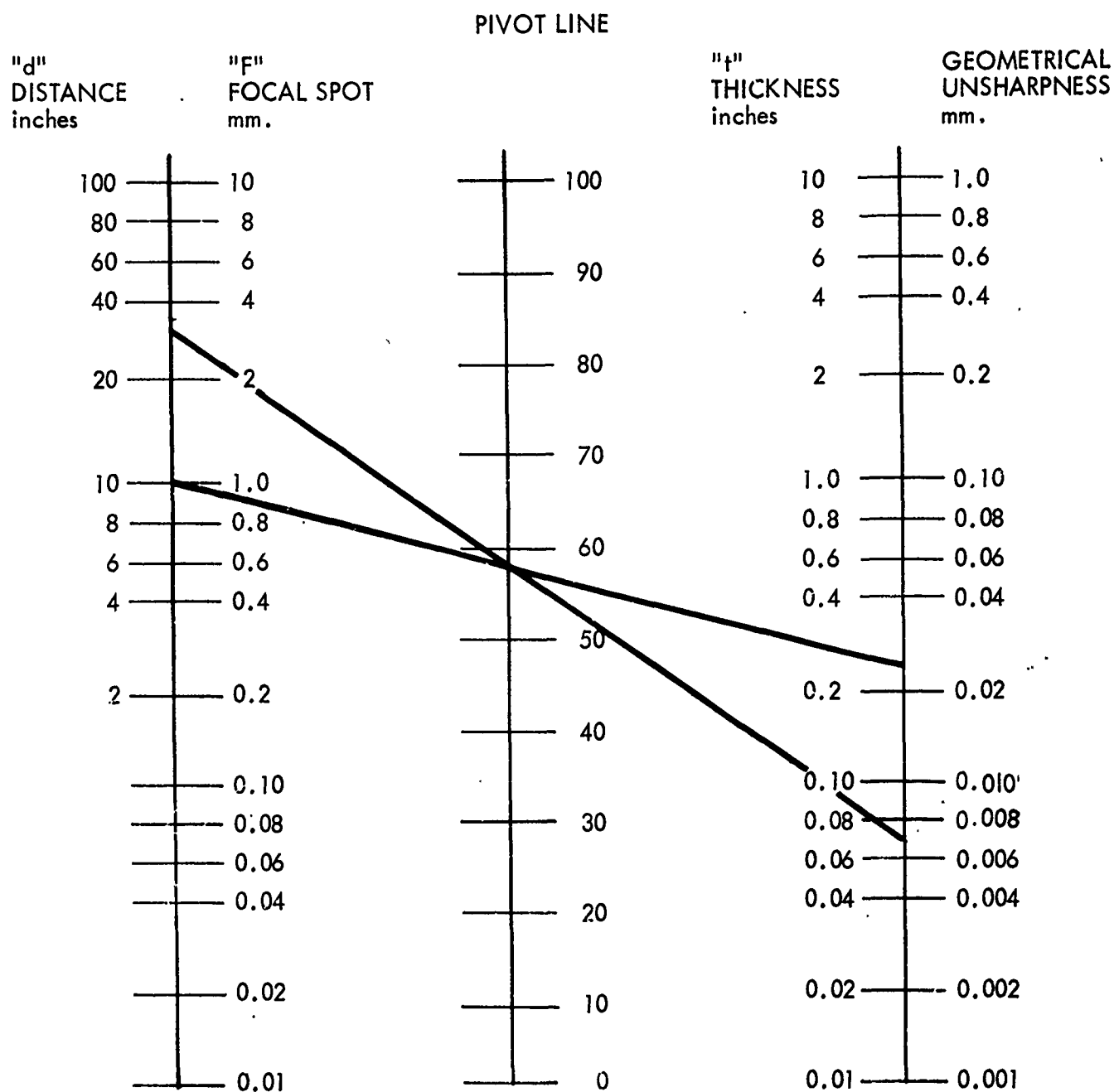
FIGURE 31 NOMOGRAPH FOR DETERMINING GEOMETRICAL
UNSHARPNESS, Ft/d

The milliamperage, voltage, and total time that the X-ray generating tube is energized, determine the amount of radiation emitted by the X-ray tube. Changes in the current, when all other factors are held constant, cause a change in radiation intensity, but not in penetrating power since the wavelengths are not changed. The voltage affects the quality and the intensity of the X-ray beam. The increase in voltage causes a change in wavelength. Shorter wavelength offers more penetrating power.

Two methods of X-ray inspection are used: radiography and fluoroscopy. Radiography is characterized by a permanent record of results, greater sensitivity, and the possibility of detailed analysis of the film to give the location of a defect within the thickness of a part; but, it is the more expensive and lengthier of the two techniques. Fluoroscopy is a more flexible method especially when the orientation of the part can be changed during examination (6).

Both radiography and fluoroscopy depend upon the production of shadows by the defects in the part being inspected. Therefore, the resolution of the shadows and the contrast with which they are shown on the viewing surface (film or fluorescent screen) are critical parameters in determining sensitivity. Control of resolution is amenable to analysis, but control of contrast is largely a result of cut-and-try methods. Resolution of flaws cannot be clearly defined on a part prior to examination of the finished film, and therefore, X-ray inspection is very largely an art (13). The resolution of a fluoroscopic examination is limited by the fluorescent compound used for the screen and will generally be of the order of 0.5 to 1 mm (12).

The sensitivity of X-ray inspection is determined with a penetrameter. This device is usually a flat strip made of a material similar to that of the part, and of a thickness approximately equal to 2 percent of the part thickness. Small circular holes of specified diameters are drilled into the penetrameter, and the penetrameter is placed on the specimen to be tested. The visibility of the penetrameter and drilled holes on the exposed and finished photographic plate is a measure of the X-ray sensitivity. The graininess, unsharpness, and lack of contrast of the flaw image on the developed plate determine the size of the minimum detectable defect. With some specifications, e.g., those using British Standards, it is sufficient to be able to distinguish the outline of the steps. In other specifications, it is necessary to distinguish the images of the holes. It is claimed that the latter standard gives a higher number, i.e., gives poorer sensitivity. The sensitivity is expressed as a percentage, given by 100 times the ratio between the thickness of the thinnest penetrameter step visible in the radiograph and the maximum thickness of the specimen. A sensitivity of better than 2 percent is usually claimed for commercial equipment. Penetrameters may be used to give an indication of the resolution of a radiograph, but they should not be depended upon to show precisely the size of the minimum defect that is detectable using X-rays (6).

One problem in examination of a part by X-rays is the secondary scattering produced. This is characterized by an increase in wavelength of the radiation and a loss of the directionality of the incident radiation. Scattered radiation tends to degrade the image produced by the incident radiation that is transmitted without change. Two means are used to reduce the effect of secondary scattering: screening the film and filtering the radiation at the tube.

Lead foils placed on both sides of the film will reduce the effect of scattered radiation, since the soft scattered radiation is absorbed more easily than is the harder transmitted radiation. Another benefit derived from the use of lead foil screens is that their fluorescence may reduce exposure time. Image sharpness is not reduced so long as the screens are in intimate contact with the film.

Filtration of the radiation produced by the tube reduces the proportion of long wavelengths in the incident beam thus improving the quality of the image as longer wavelengths produce more scattered radiation than shorter wavelengths. The depth of a defect within the part may best be found by the double-exposure method, Figure 32. When the images of markers M_1 and M_2 are superimposed and suitable measurements made on the films, the distance of the defect above the film plane, d, is calculated from:

$$d = \frac{\vartheta SF}{\psi + \vartheta} \tag{3}$$

where ψ, ϑ, and SF are determined as shown in Figure 32.

Penetrant

This inspection method uses a penetrating liquid for locating discontinuities open to the surface. It is applicable to any non-porous solid material which will not be harmed by the solution. Basically, the penetrant inspection process involves the following (14).

1. A penetrating liquid is applied to the surface of the test article. This can be accomplished by dipping, brushing, or spraying.

2. A period of time is allowed for the liquid to penetrate any cracks, pores, etc., by capillary action.

3. The residual surface penetrant is removed by washing with water, using a specified solvent, or by other accepted methods which do not appreciably remove the solution from surface openings.

4. The part is then subjected to a developing operation in which a porous material is used to draw a portion of the penetrant in the defect to the surface and to magnify the indication.

5. The part is then examined.

Penetrants can be of a type which are viewed with the unaided eye as in color contrast systems or of the fluorescent type in which examination is by black light.

Penetrants are primarily used on non-ferromagnetic materials, although they are readily adaptable to all non-porous solid materials (Table IV). The primary restriction with the use of penetrants is that the defect must be open to the surface of the part (Table V). The detectability of defects with penetrants is basically a function of:

1. The geometry of the opening.
2. The cleanliness of the opening.
3. The physical size of the opening.

Several classifications of penetrants are available. Table VI shows the classification that corresponds to Military Specifications (15).

All penetrants fall into three broad classifications:

1. Water-washable oil-base penetrants. These penetrants give a bright yellow fluorescent indication. They are available in several levels of color intensity and flaw sensitivity. Typical Magnaflux Zyglo penetrants in this class are (16):

    ZL-1C   not recommended for broad shallow defects
    ZL-17A   high sensitivity, not used for rough or porous surfaces
    ZL-18A   extreme sensitivity, limited to smooth surfaces
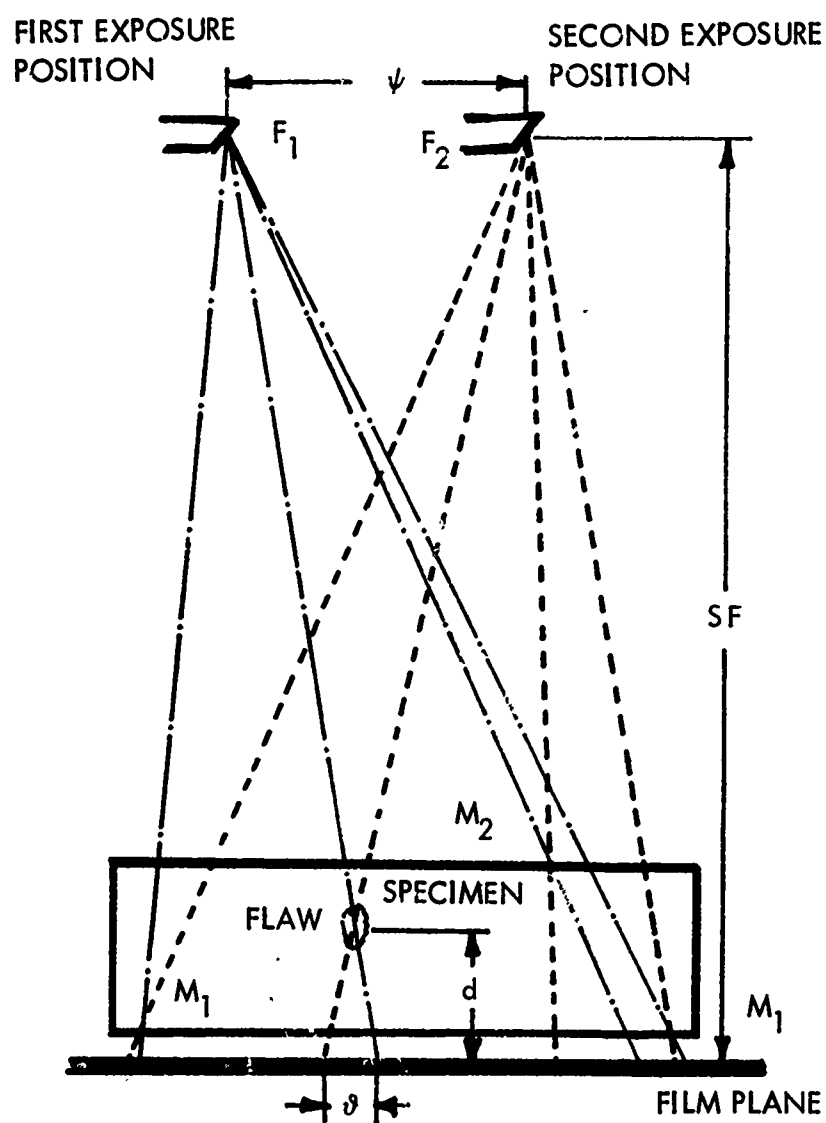
FIGURE 32 PARALLAX (DOUBLE EXPOSURE) TECHNIQUE FOR
DETERMINING DEFECT LOCATION

44

TABLE VI

MIL SPECIFICATIONS FOR PENETRANTS

MIL SPEC	TYPE
MA 2	Fluorescent penetrant, water washable
MA 3	Fluorescent penetrant, post-emulsifier
MA 5	Fluorescent penetrant, high sensitivity post-emulsifier
MA 6	Visible dye penetrant, solvent removable
MA 7	Visible dye, water washable
MB 3	Emulsifier, fluorescent
MB 5	Emulsifier, visible dye
MC 4	Non-aqueous wet developing
MC 5	Wet Developer
MC 6	Dry Developer

2. Water-washable water-base penetrants. These penetrants can be regulated by the strength of the solution. They are used on products that can be harmed by oils. Typical Magnaflux products in this class are (16):

   ZL-3A   red color, does not conform to Military Specification
   ZL-4B   high sensitivity, high cost

3. Post-emulsifier penetrants. These materials use a separate emulsifier for increasing the sensitivity in testing. This penetrant type includes low chlorine type and low sulphur types. Typical Magnaflux products include (16):

   ZL-2   normal sensitivity
   ZL-22   high sensitivity, not recommended for titanium alloys
   ZL-221   high sensitivity high detail
   ZL-30A   ultra high sensitivity, used for fine cracks.

Two types of developers are used commercially: dry and wet. The developer is used to increase the sensitivity of the penetrant. The developer acts as a capillary system to draw the penetrant out of the defect, exposing more penetrant to the surface. In this manner, the indication of the penetrant is enhanced over that of the undeveloped system.

Both the width and the intrinsic brightness of the resulting line determine the ease with which the human eye with no magnification can detect crack indication (17). This is particularly true when the lines have widths below the limit of resolution of the human eye, which is about 0.1 mm. Penetrant systems are an excellent method of revealing fine surface discontinuities a fraction of a micron in width. Typical crack indications in a rejected steel part are shown in Figure 33 for an example.

A number of general factors are involved in the selection of a particular type of penetrant:

1. The surface condition of the part being inspected.
2. The expected surface condition of the defect.
3. The expected shape of the defect.
4. The expected size of the defect.
5. The capillarity of the penetrant.
6. The wetting ability of the penetrant.

Items 1, 2, 3, and 4 are normally estimated, based on a knowledge of the part being examined. Items 5 and 6 are calculable.

Capillarity is the ability of a liquid to rise in a capillary tube. It is normally determined by laboratory tests but can also be calculated by determining the penetration pressure:

$$P = \frac{2S \, Cos\Phi}{W} \tag{4}$$

where
   P = Capillary pressure
   S = Surface tension of the penetrant
   Φ = Equilibrium contact angle of the liquid and the surface of the crack
   W = Width of the crack

The driving force for the penetration of cracks by a liquid is proportional to a static penetration factor (18). This factor is related to the surface tension of the liquid penetrant-air interface, the contact angle between the liquid-air interface and liquid-solid interface in the crack, and the viscosity of the liquid penetrant. Movement of liquid into a crack will

FIGURE 33 REJECTED STEEL PART SHOWING EXAMPLES OF INDICATIONS
OBTAINED USING PENETRANT INSPECTION METHOD

occur spontaneously when the contact angle is less than 90°. For all the common penetrants used, the contact angle is on the order of 10°. With these angles, there is no question concerning the potential of the penetrants to enter cracks in the solid. The rate at which the penetrant enters the crack, and hence, the total volume of material in the crack, is a more difficult theoretical problem. The ability of the human eye to see the penetrant depends on the contrast ratio of the penetrater-developer system, the viewing illumination, the luminous emission coefficient of the penetrant, and the size of the indication. Theoretical values for these parameters and experimental results on several commercial penetrant-developer systems have been obtained by Houck and McCauley (18), Harris (19), and McCauley and Van Winkle (20).

Harris also studies the ability of several commercial penetrants and developers to detect small cracks. His results can be summarized in Table VII.

The sensitivity panels consisted of brass sheet specimens with a nickel-chrome plating. The specimens were bent over a radial or cantilever bending die to produce an array of fine cracks on the tensile surface. All specimens were examined under similar lighting conditions without optical magnification.

None of the plates prepared had one crack size exclusively; in general a variety of crack sizes were present. Therefore, the systems were designated by go, no-go parameters. The conclusions were: (1) the fluidized dry developers are superior to unfluidized developers; (2) a spray-can developer was next in effectiveness; and (3) water-dispersed developers were the least effective in revealing cracks.

The developer sensitivity claimed by Magnaflux Corporation (16) is given in Table VIII .

There appears to be no doubt, on the part of the manufacturers, that any surface flaw wider than 0.5 mil can be detected by standard penetrant inspection techniques. However, this does not assure the accurate determination of surface crack length. Consider a crack whose surface shape is an elongated ellipse, as shown in Figure 34. The tips of the crack, however, are narrower than this minimum size. Hence, the penetrant system will indicate an apparent crack length $2c'$ less than the actual crack length $2c$; the error depends on the a/c eccentricity of the ellipse. Since the crack length is the important geometric parameter in fracture, this error could be serious.

If the material is ductile, resulting in a relaxation of stresses at the tip of the crack, the problem is less critical, since the crack will open up more due to plastic deformation at its extremities. In this case, c/a will decrease. However, with brittle materials, the sharpness of the crack could result in large errors in crack length.

A measure of the capability of penetrants to detect flaws and correctly indicate their size is provided by the crack opening displacement (COD). The value of COD for specimens subjected to uniaxial loading (21) is given by:

$$\text{COD} = \frac{4G_{Ic}}{\pi \sigma_{ty}} \tag{5}$$

where G_{Ic} is the critical strain energy release rate, and σ_{ty} is the tensile yield strength of the material.

48

TABLE VII

EXPERIMENTAL SENSITIVITY OF PENETRANT SYSTEMS

$\left[\text{REFERENCE } 19\right]$

Penetrant (MIL Specs See Table III)	Developer (*) MIL Specs (Magnaflux)	Sensitivity crack width (Mils)		
		Fine	Medium	Coarse
		0.019 To 0.117	0.09 To 0.13	0.500
MA2	D2 Dilute (ZP-5)	-	+	+
	D2 Conc	--	-	+
	D7 Not Fluidized (ZP-4A)	-	-+	+
	D1 Spray (ZP-9)	-	-+	+
	D1 Spray (ZP-9)	-	+	+
MA3	D2 Dilute	-	+	+
	D7 Fluidized	-	+	+
	D1 Spray	-	+	+
MA5	D2 Dilute	-	+	+
	D7 Fluidized	-	+	+

*A (+) indicated a strong indication, a (-+) a moderate indication, and (-) little or no indication of the crack.

TABLE VIII

MAGNAFLUX DEVELOPER SENSITIVITY
[REFERENCE 16]

Penetrant	Developer	Sensitivity		
		Fine	Medium	Coarse
		0.2	0.8	2.0
		0.5	1.2	4.0
		(Crack width in microns)		
ZL-2 (Post-Emulsifier)	SP-4 (dry powder)	none	weak	strong
	ZP-5 (water soluble)	none	weak	strong
	ZP-11 (high sensitivity water soluble)	some	strong	strong
	ZP-9 (non-aqueous suspension)	some	strong	strong
ZL-22 (High Resolution Post-Emulsifier)	ZP-4	none	weak	strong
	ZP-5	none	weak	strong
	ZP-11	weak	strong	strong
	ZP-9	weak	strong	strong
ZL-30A	ZP-4	weak	strong	strong
	ZP-5	weak	strong	strong
	ZP-11	strong	strong	strong
	ZP-9	strong	strong	strong
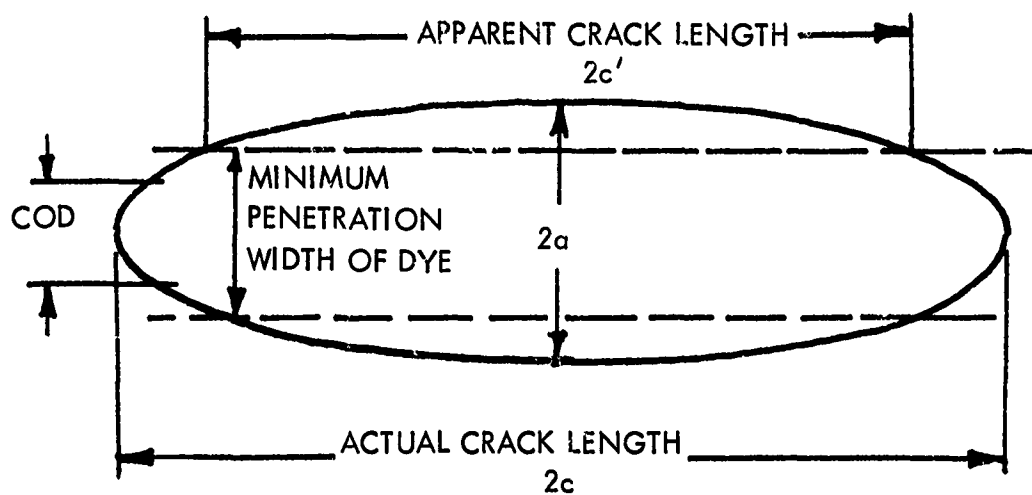
FIGURE 34 ERROR IN CRACK LENGTH PRODUCED BY INSUFFICIENT PENETRATION OF DYE INDICATOR INTO CRACK

Hence, if the COD is greater than the minimum penetrable crack width (0.0005"), the penetrant will detect the entire surface length of the crack.

The Lockheed Georgia Research Laboratory has the capability of performing penetrant inspections with a wide range of penetrants of various sensitivities. This versatility is required since considerable developmental activities are conducted. One such system being used by this laboratory is a penetrant identified as Magnaflux Hy-Rez. Although this is a color-contrast method and not a fluorescent type, it does offer a high degree of sensitivity and contrast. The Hy-Rez method involves the following steps:

1. Spraying of the penetrant, which dries after entrance into the defect.
2. Removal of excess penetrant.
3. Application of a developer to bring out indications and provide background contrast.
4. Applications of a fixer which prevents any bleed-out of nondried solution.

Fluorescent penetrants were used to a great extent in this program due to the high sensitivity which can be obtained with this method. Records of indications are made using this technique by the application of celophane tape to the inspected surface. In addition to its high sensitivity, one of the prime advantages of this method is that the bleed-out is minimal; thus problems generated by large cracks are reduced.

The Lockheed-Georgia production penetrant inspection system uses a post-emulsifiable fluorescent method. The penetrant is Magnaflux ZL-2, which is not water-soluble.

The Magnaflux ZE-3 emulsifier is applied after penetration to enable the following water wash to remove the excess penetrant. A ZP-5 wet developer is used. The accuracy of the laboratory process is slightly enhanced due to the use of ZP-4 developer in dry form.

A penetrant inspection system has the following advantages:

1. A large number of small parts can be inspected more efficiently than by other methods.
2. There are no limitations with respect to size or shape of a part.
3. The process is essentially simple compared with other techniques.

Magnetic-Particle Inspection

Magnetic-particle inspection requires the generation of a magnetic field within the part to be examined. If the part does not contain any inhomogeneities, the strength of the magnetic field on the surface varies smoothly from place to place. On the other hand, in the vicinity of a flaw, the magnetic field is disturbed. The interaction of the applied magnetic field and the flaw creates pseudo-poles within the part in the vicinity of the flaws. When magnetic particles are flowed over the part, they accumulate in the vicinity of these poles and indicate the location and extent of the flaw.

The magnetic particles may be used either wet or dry. A dry technique is used for the inspection of large forgings and castings (6). The dry technique is preferred when the defect is located beneath the surface or when the part to be inspected has a rough surface. The wet-particle technique is used for production and maintenance inspection since it can be washed off easily.

The wet technique with fluorescent magnetic particles to be examined under U.V. light is a trademarked process of the Magnaflux Corporation called "Magnaglo." This combines the advantages of flaw identification with fluorescent particles and the speed of magnetic-particle inspection. Both Magnaflux and Magnaglo are trademarked magnetic-particle inspection techniques (22). A number of factors must be considered during the per-

formance of a magnetic-particle inspection. The prime factor is the selection of the method of magnetization. This method selection is a function of five basic factors:

1. Alloy, shape, and condition of part.
2. Type of magnetizing current.
3. Direction of the magnetic field.
4. Sequence of operations.
5. Value of flux density.

The alloy, shape, and condition of a part are of importance since these factors affect the permeability of the part; i.e., the ease with which it can be magnetized.

The type of magnetizing current (AC, DC, etc.) is a function of the availability of a particular unit as well as the type of defect being sought.

Of the five factors involved in selecting a method, the direction of magnetic field is the most critical.

The sensitivity of magnetic-particle inspection techniques to flaws depends on the orientation of the flaw with respect to the magnetic field. For surface cracks, the best indications are found if the flaw is located at right angles to the magnetizing field. This is due to the strength of the poles created by the magnetic field, and is given in terms of (a) the length of the flaw, (b) the strength of the magnetic field, and (c) the line of the angle between the field and the flaw (23). When the direction of the defects is not known, the part must be magnetized in more than one direction.

The sequence of operations must be considered during a magnetic-particle inspection to obtain the greatest sensitivity for a particular part. Two basic sequential methods are used, depending on the shape, alloy, and type of part:

1. The continuous-field method inspection consists of applying the particles during the magnetizing cycle. This method offers the greatest sensitivity and may be used reliably with steels having both high and low retentivity.

2. The residual-field method of inspection consists of a long magnetizing cycle, after which the particles are applied. This method is used in special applications such as confirming the presence of subsurface defects or where lower sensitivity is tolerable.

The flux density, which is the strength of the induced magnetic field, must be controlled so that the induced field is of sufficient magnitude to be interrupted adequately by the defect yet not so large that the defect area is bridged. Since flux density is controlled by the amount of current, a relationship between the current setting and the size, shape, and material of the part must be determined. A "rule of thumb" which has been used for a number of years is approximately 600 to 800 amperes per linear inch of section thickness or diameter when using a circular field (magnetizing current flowing through the part being inspected) with direct current.

If the flaw is open to the surface and located at right angles to the magnetic field, the sensitivity of the process is comparable to that of dye penetrants; crack width should be on the order of 0.0005". Incipient fatigue cracks having a depth of about 0.001" should be readily located by either the wet or dry method (24). However, the actual depth of the crack has little effect on the ease of detection, except that the deeper the crack the greater the magnetic particle buildup over it. This results from the increase in leakage flux due to the increased size of the flaw and the larger width of the crack. On the other hand, if the faces of the crack are pressed together, the magnetic flux leakage is reduced almost to the average field strength throughout the body of the material. In this case, the magnetic particles do not produce an indication.

Over 50 varieties of standard magnetic-particle test machines are available for industrial use (25). These vary as to: (1) the type of magnetizing current used: AC, DC, mixed or permanent magnet type; (2) nature of the instrument: portable, experimental, or production; and (3) the type of test materials used: wet or dry.

Magnetic-particle indications fall into three broad classes (26):

1. Surface discontinuities
2. Subsurface discontinuities
3. Nonrelevant magnetic disturbances

Surface discontinuities produce sharp, distinct patterns which are usually limited to the immediate areas surrounding the discontinuity. Subsurface discontinuities are usually less distinct, and the magnetic particle indications become broader and fuzzier if the discontinuity causing them lies deeper beneath the surface. In either case, the higher the current density, the more distinct the indication.

Extraneous indications, in most cases, are caused by leakage fields at sharp edges or at the ends of the part and particle adherence due to local poles. Local areas of cold-working may reduce the magnetic permeability of the material and cause nonrelevant disturbances (27).

In contrast to the dye penetrants, magnetic-particle inspection can be used to detect cracks lying completely below the surface. Since the magnetic-particle indication is due primarily to the field strength of the pseudo-poles generated by the interaction of the flaw and the magnetic field, a subsurface flaw can be detected by an accumulation of magnetic particles on the surface.

The sensitivity of magnetic particle inspection to subsurface flaws is determined as follows. A solid, hardened-tool-steel ring with a series of holes 0.07" in diameter drilled parallel to the ring axis at varying depths is used (Figure 35). Tests on this ring are conducted using a threshold indication method to compare the ability of wet or dry magnetic powders in detecting these subsurface flaws (26). A threshold indication is the minimum magnetic field required to produce a noticeable pattern on the surface of the ring. Figure 36 shows a comparison of two types of magnetic field (AC and DC) and wet and dry powders. It is evident that the combination of half-wave DC power and dry powder can detect a flaw 0.72" below the surface with an operating amperage of approximately 60 Amps. The dry-powder methods are more apt to determine the subsurface flaws than the wet-powder methods, and DC power is superior to AC (24).

It is claimed that magnetic-particle techniques can be used to detect flaws as deep as 2" below the surface (28). As the defect-to-surface distance increases, it becomes difficult to detect the length of flaws. However, using a dry-powder technique, it does appear feasible to detect flaws lying at 0.24" below the surface in a thick plate, if the flaw is larger than 0.07" in diameter. To detect flaws of smaller diameter, they should lie closer to the surface. The depth of the defect must be considered in relation to the overall cross section of the part. It is easier to locate a defect of given size and shape 1/2" below the surface in a section 4" thick than it would be if the same defect were located 1/2" below the surface in a section 1-1/2" thick (26).

Subsurface inspection requires a high degree of skill on the part of the magnetic-particle inspector. He must know what operating currents to use to detect the flaw, and whether it is advisable to use dry powder or wet powder. Thus, it is expected that production-inspection personnel would not detect subsurface flaws by this method as well as a carefully trained technician.
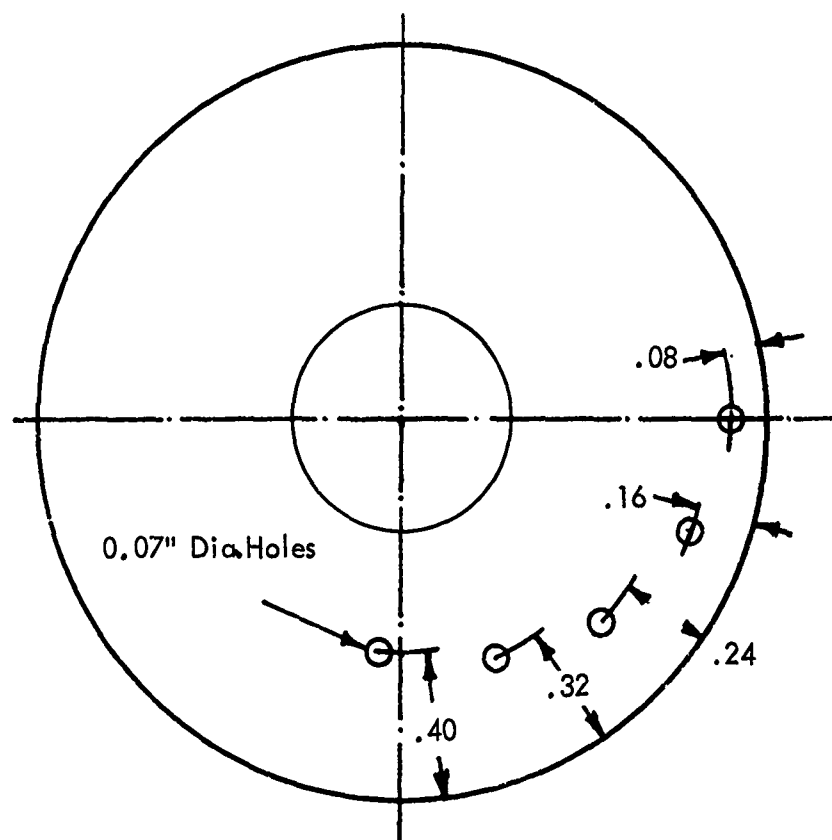
FIGURE 35 SCHEMATIC SKETCH OF SUBSURFACE FLAW SENSITIVITY
RING FOR MAGNETIC PARTICLE NDT

Text labels within figure: 0.07" Dia. Holes, .08, .16, .24, .32, .40
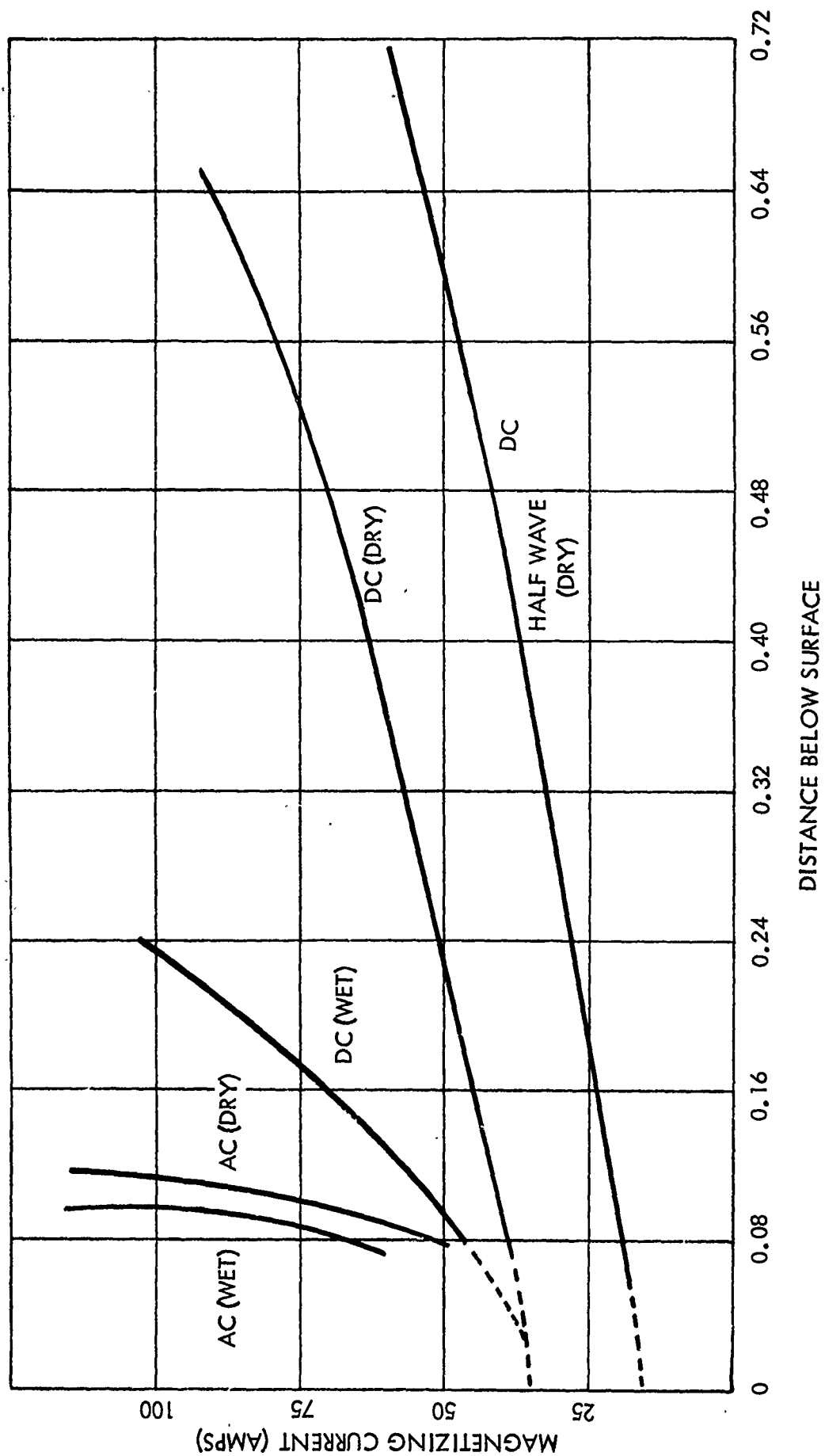
FIGURE 36 COMPARISON OF WET AND DRY, AC AND DC SENSITIVITY OF
MAGNETIC PARTICLE INSPECTION METHODS FOR LOCATING
ARTIFICIAL FLAW (0.07" DIA. HOLE)

56

Magnetic-particle inspection has noted advantages over the penetrant inspection:

1. Both surface and near-to-surface discontinuities are detectable.
2. Defects are detectable under thin films of paint and plating.
3. In general, the method is faster for ferromagnetic parts.

Two noted disadvantages of magnetic particle inspection are:

1. Only ferromagnetic materials can be inspected.
2. The part must be demagnitized after inspection, a time-consuming step (see Table V).

The sensitivity of the magnetic-particle suspension is primarily controlled by the size of particle and the bath concentration. Smaller particles show greater sensitivity when inspecting for small defects as they are attracted more easily by weak fields. The bath concentration must be high enough to provide adequate coverage of the part but must not be so high as to provide unnecessary background.

Ultrasonic Inspection

The ultrasonic methods of NDT are perhaps the most sophisticated and potentially the most informative method for detection of flaws. The use of ultrasound varies from routine laboratory control inspections to determination of basic properties of materials. The instrumentation is basically electronic, with indications being obtained almost instantaneously. Rapid scanning of parts with automatic positioning, plotting, and alarm systems can be used with this technique (29, 30, 31).

Ultrasonic inspection uses a power source which activates and monitors a transducer. The transducer vibrates at a defined frequency on the application of an electrical charge from the power supply. This vibration is transferred to the part in the form of ultrasound and travels through the part in the same manner as audible sound. The presence of a void, crack, or material acoustically different from the part material will reflect or echo the ultrasound. The reflected ultrasound travels back to the transducer. This transducer is then vibrated by the returning energy, which produces an electrical charge. This electrical charge is then received by the power supply and converted to a signal on an oscilloscope screen.

The main types of ultrasonic flaw detection instruments are essentially electronic time-measuring devices. The instruments display the information, either transmitted or reflected intensities, on a timeline basis of a cathode-ray tube. This information can be interpreted directly from the tube (known as "A" scan presentation) or can be presented in a cross-sectional view ("B" scan) or a plan view with respect to the surface ("C" scan).

Two broad categories of ultrasonic instruments are available: continuous-wave systems and pulsed systems. The continuous-wave systems can be further broken into the following categories (32):

(a) Resonance type. Used primarily to measure thickness but can be used to detect flaws in some restricted test geometries.

(b) Transmission type. Measures the transmitted intensity of sound through the specimen, using separate transmitter and receiver probes. The method has the disadvantage of low sensitivity due to the development of standing waves and interference effects.

(c) Reflection type. Measures the pulse reflected from the back of the specimen. Continuous-wave reflection has the same limitations as continuous-wave transmission types.

Pulsed systems are divided into transmission and reflection types. Pulse-transmission or pulse-reflection techniques are those most frequently used for flaw detection.

The most often used ultrasonic techniques for inspection are longitudinal wave techniques and shear wave technique. Since both of these techniques were utilized in this program, both will be discussed.

Longitudinal Wave Techniques - The echo is a reflection of the ultrasonic wave from a free surface. The free surface may be the end of the specimen, an internal crack, or an inclusion. Pulse-echo flaw detection by back-reflection from an internal flaw is shown in Figure 37. The portion of the wave reflected from an internal surface travels a shorter distance, thus returning to the crystal before the echo from the end of the specimen. Hence, by knowing the length of the specimen, the distance from the surface to the flaw can be determined. This process is known as "A" scan on the oscilloscope. Aerojet General (33) established the following tolerances on flaw location measurements.

Depth (inches)	Tolerances (inches)
less than 0.5	± 0.0625
0.5 thru 1.0	± 0.125
greater than 1.0	± 0.25

Minimum flaw sizes for aluminum as recommended by the Society for NDT (34) are given in Table IX.

Since the amplitude of the response is a measure of the flaw size, it is worthwhile to consider the sensitivity of the response system to standard test blocks. The standard ultrasonics test block consists of a cylinder of the material to be tested with flat faces. A small flat-bottom hole is drilled into one end. This flat-bottom hole is used as a standard to estimate the flaw size and the flaw depth. A flaw which gives a stronger reflected signal than a 1/64" diameter is therefore larger. In addition to the 1/64" diameter hole, there are 3/64", 5/64", and 8/64" diameter standards. These holes are available at varying depths. This permits an accurate estimate of the metal through which the ultrasound travels to reach the flaw. Flaws at defined depths are compared to standard holes at the same depth for a more accurate evaluation of defect size. Standard calibration blocks are available from Automation Industries, Inc., Danbury, Connecticut.

Sperry Products gives the following response data for their UM 700 instrument. A hole 8/64" diameter at a distance of 3" from the transducer will yield a 2.8" amplitude on the oscilloscope. At the same distance, a hole 1/64" in diameter will yield a response amplitude of 0.1" on the oscilloscope. The transducer-test block arrangement is such that the response amplitude decreases when the flaw-to-transducer distance is changed from 3".

The experimental results obtained by Morgan (35) on stainless steels are tabulated in Table X.

The size of the flaw is estimated by the height of the echo signal on the screen of the oscilloscope (36). The height (h) of the echo signal from a small flaw under ideal conditions is proportional to the reflected voltage (U_f) from the ultrasonic probe (37).
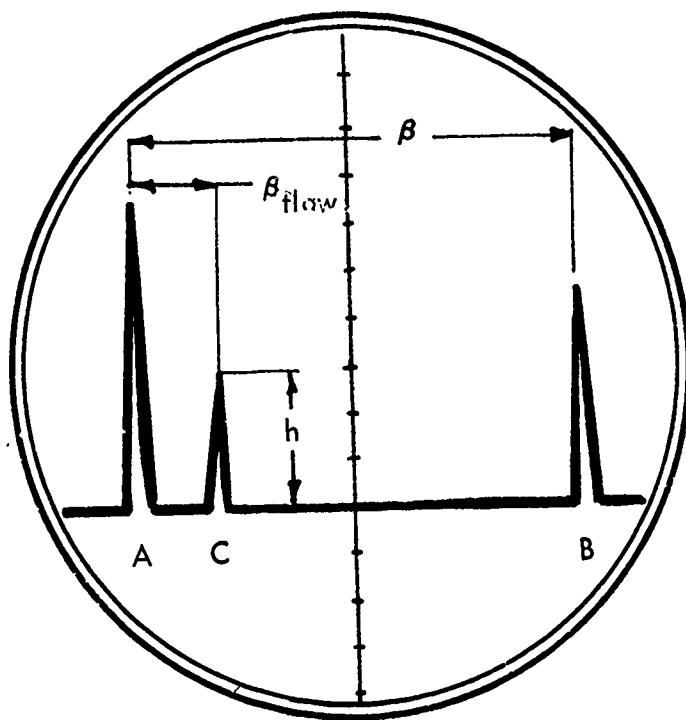
β = Thickness

β_{flaw} = distance to flaw

FIGURE 37 SCHEMATIC SKETCH OF RESPONSE CURVE FROM PULSE ECHO FLAW DETECTION UNIT. (A) FRONT SURFACE (B) BACK SURFACE (C) REFLECTION FROM FLAW. HEIGHT OF INDICATION FROM FLAW IS (h)

TABLE IX

RECOMMENDED ULTRASONIC ACCEPTANCE STANDARDS FOR
AIRFRAME ALUMINUM ALLOY PLATE, FORGINGS, AND EXTRUSIONS

(REFERENCE 34)

Product	Alloy	Thickness (inches)	Discontinuity Class
Die Forgings	2014 7075 7079	.375 and over	B
Hand Forged	2014 7075 7079	All	A
Plate	2014 2024 7075 7079 7178	.250-1.499 1.500-3.00 3.-4.5	B A B
Extrusion	2014 2024 7075 7079 7178	.375 & over 1.5 & over	B A

Discontinuity Class A

Response from 5/64" Dia. Flat-Bottom Hole
Multiple Indications from 3/64" Dia. holes located closer than 1" center-to-center distance

Discontinuity Class B

Response from 8/64" Dia. Flat-Bottom Hole
Multiple indications from 5/64" Dia. holes located closer than 1" center-to-center distance

TABLE X

ULTRASONIC ATTENUATION IN STAINLESS STEEL

(REFERENCE 35)

| Type of Steel | Distance from Defect* | | |
	6 Inches	3 Inches	1 Inch
	Height of Indication (Inch)		
304 Stainless	3/16	3/8	1/4
304 Annealed Stainless	1/8	1/4	1/8
403 Stainless	1/8	1/4	1/16
430 Stainless	9/16	3/4	3/8
A286 Stainless	1/4	3/8	1/4

* The defect in all cases was a 1/8" diameter flat bottom hole 3/4" deep.

$$h \propto U_f = U_c K A_m \left[\pi \frac{D_v}{D} \frac{\beta_o}{\beta} \right]^2 e^{-2 \varkappa \beta}$$

(6)

where U_c = the peak pulse voltage applied to the transducer

K = coefficient of electro-acoustic conversion

D = diameter of the transducer

D_v = diameter of the flaw

A_m = coefficient of amplification

β = depth of flaw

β_o = length of specimen normal to field

$\varkappa$ = damping coefficient

By scanning over the whole sheet, it is possible to plot the locus of all back-reflected projections of the flaws on the inspected surface. With a frequency of 2 mHz and manual control, it is possible to detect flaws of a diameter of 2mm (0.08") to a depth of 300mm (12"), and a diameter of 3mm (0.12") to a depth of 500mm (20") in low alloy steels. At 600mm (24") from a 3mm flaw, the accuracy is ± 25% (37).

Tests conducted by Botsco (38) using a high-resolution ultrasonic instrument with 0.25" thick aluminum plate are given in Table XI.

Hence, it could be concluded that in 0.25" thick aluminum the minimum flaw size that can be detected is 3/64" in diameter by 0.04" deep.

Shear Wave Techniques – When the ultrasonic transducer is tilted at an angle with the normal to the test part, a mode conversion process takes place at the point of incidence into the part. Two or more modes can result; but normally only longitudinal and shear modes are significant. With a proper angle, the longitudinal wave will be totally reflected allowing only the shear wave to enter the part. The chief differences between longitudinal and shear waves are that shear waves travel at about half the velocity of the longitudinal waves and the shear oscillations are normal to the direction of travel whereas longitudinal oscillations are parallel to the direction of travel. The reduced velocity of the shear wave results in a smaller wave length than a longitudinal wave. Hence, better resolution can be obtained with shear waves.

The specific technique used in this investigation will be discussed in detail in the NDT Experimental Program, page 76, and the reader is referred to Reference (6) for additional general information.

The crack detection ability discussed for longitudinal wave techniques is presumed to apply generally to shear wave techniques.

TABLE XI

ULTRASONIC SENSITIVITIES IN 0.25" ALUMINUM PLATE

(REFERENCE 38)

Hole Diameter Inch	Hole Depth Inch	Indication
1/8	0.1-0.015	All indicated (0.020 and 0.015" depth indicated by second and third reflections)
5/64	0.1-0.015	All indicated (0.020 and 0.015" depth indicated by second and third reflections)
3/64	0.1, 0.75, 0.050 0.040	All indicated
	0.030, 0.020, 0.015	None indicated
1/64	0.1-0.015	None indicated

The sensitivity limits of ultrasonic inspection depend upon several additional factors. Surface roughness has an adverse effect on the sensitivity. The frequency of the ultra-sound is important, since higher frequencies are more apt to be reflected by smaller flaws. This is due to the shorter wavelengths of the high frequencies. There is a limit, since at the higher frequencies, more interference is encountered by the grain boundaries in the material.

NDT Experimental Program

The nondestructive testing conducted as a part of this program is divided into three categories:

- o Inspection of test cylinders
- o Inspection of aircraft components
- o Inspection to determine cracking of round fracture toughness specimens.

For continuity, the NDT utilized in inspection of the test cylinders is discussed in this section. The inspection of aircraft components is deferred until Section VI. The inspection to determine cracking of round fracture toughness specimens is discussed in Section V.

The major difference in these three areas of inspection was the ultrasonic techniques utilized. A shear wave technique was used on the test cylinders, longitudinal wave techniques were used on the aircraft components, and a submerged longitudinal wave technique was used for the fracture toughness specimens.

A specially designed fixture was used in inspection of the test cylinders. This was neces-sary since the exact location of the cracks had to be recorded. The fixture is shown in Figures 38 and 39. It consists of a 12-inch-long plug that fits into the inside of the tube. A notched flange on one end of the plug is aligned with a fiducial mark on the end of the tube. An arm with a steel scale swings on a pivot on the flanged end. The angular displacement of the crack on the tube surface is measured by lining up the steel scale with the crack indication. The steel scale is mounted parallel to the axis of the tube. Thus, the location of the ends of the crack from the reference end of the tube and the length of the crack can be measured. Figure 40 is a schematic sketch of the reference dimensions.

Measurements of crack length and crack location are made using each NDT method for each tube. After the specimen is tested to failure in tension, the crack length and location are measured on the failed surface.

X-Ray Inspection

X-ray inspection of the test cylinders is performed using the experimental setup shown sche-matically in Figure 41. Three photographs are taken of each tube. The specimens are ro-tated 120° between each exposure to obtain complete coverage.

The 7075-T6511 Aluminum cylinders are inspected using a Norelco MG-150 X-ray source. This has a beryllium window with two focal spots of 2.5 mm and 0.7 mm. The 0.7 mm focal spot was used with an initial operating voltage of 110 KVC at 5 milliamps. The film-to-focal-plane distance was 36 inches. A 2-minute exposure was used with a D-4 medium-resolution X-ray film.
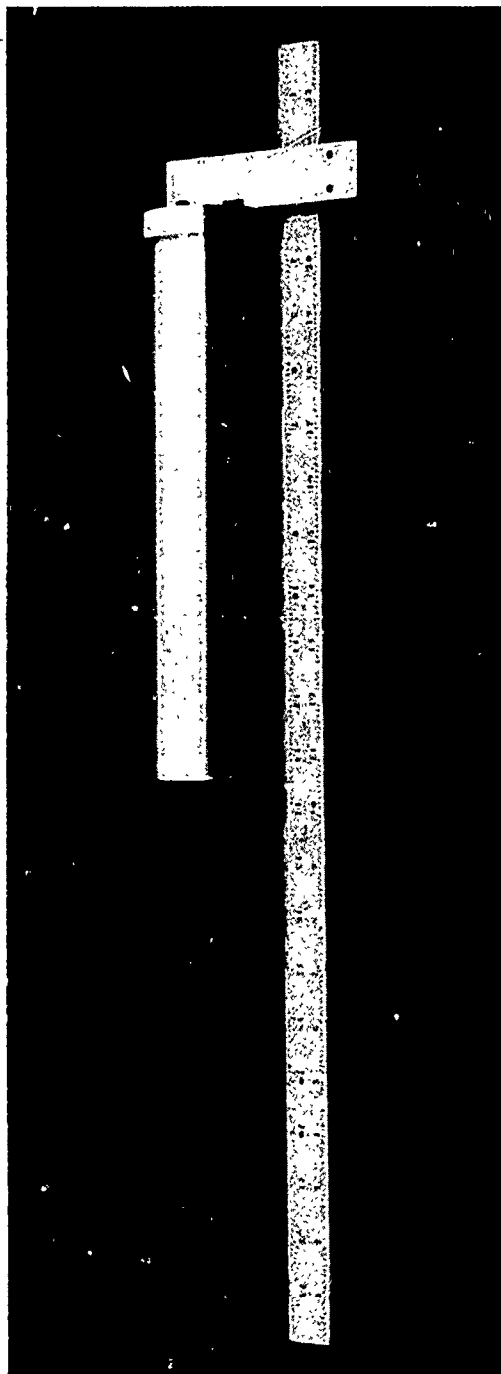
FIGURE 38   FIXTURE USED ON TEST CYLINDERS TO DETERMINE
CRACK LOCATION AND CRACK LENGTH
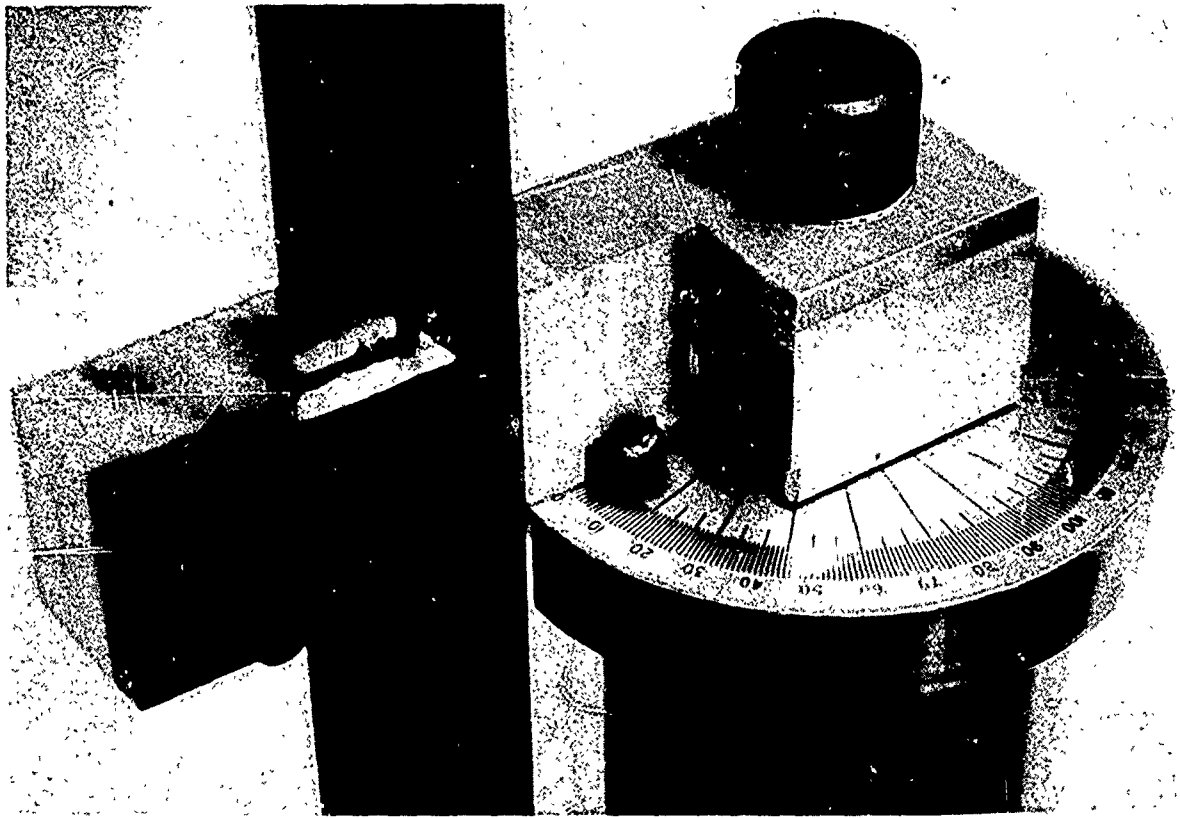
FIGURE 39   DETAIL SHOWING FLANGED END OF FIXTURE FOR
DETERMINING CRACK LOCATION AND CRACK LENGTH
ON TEST CYLINDERS
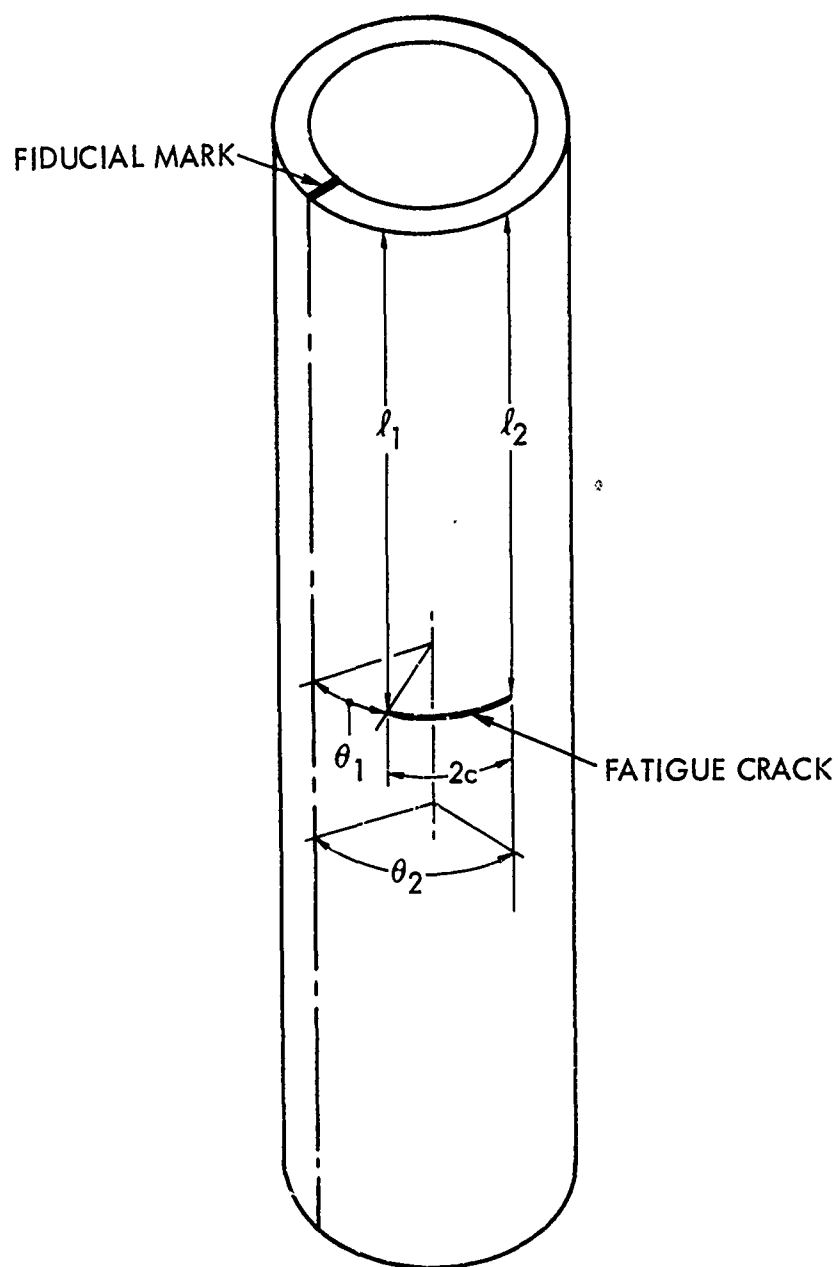
FIGURE 40   SCHEMATIC SHOWING REFERENCE AXES FOR DETERMINATION OF
CRACK LOCATION AND SIZE BY NDT
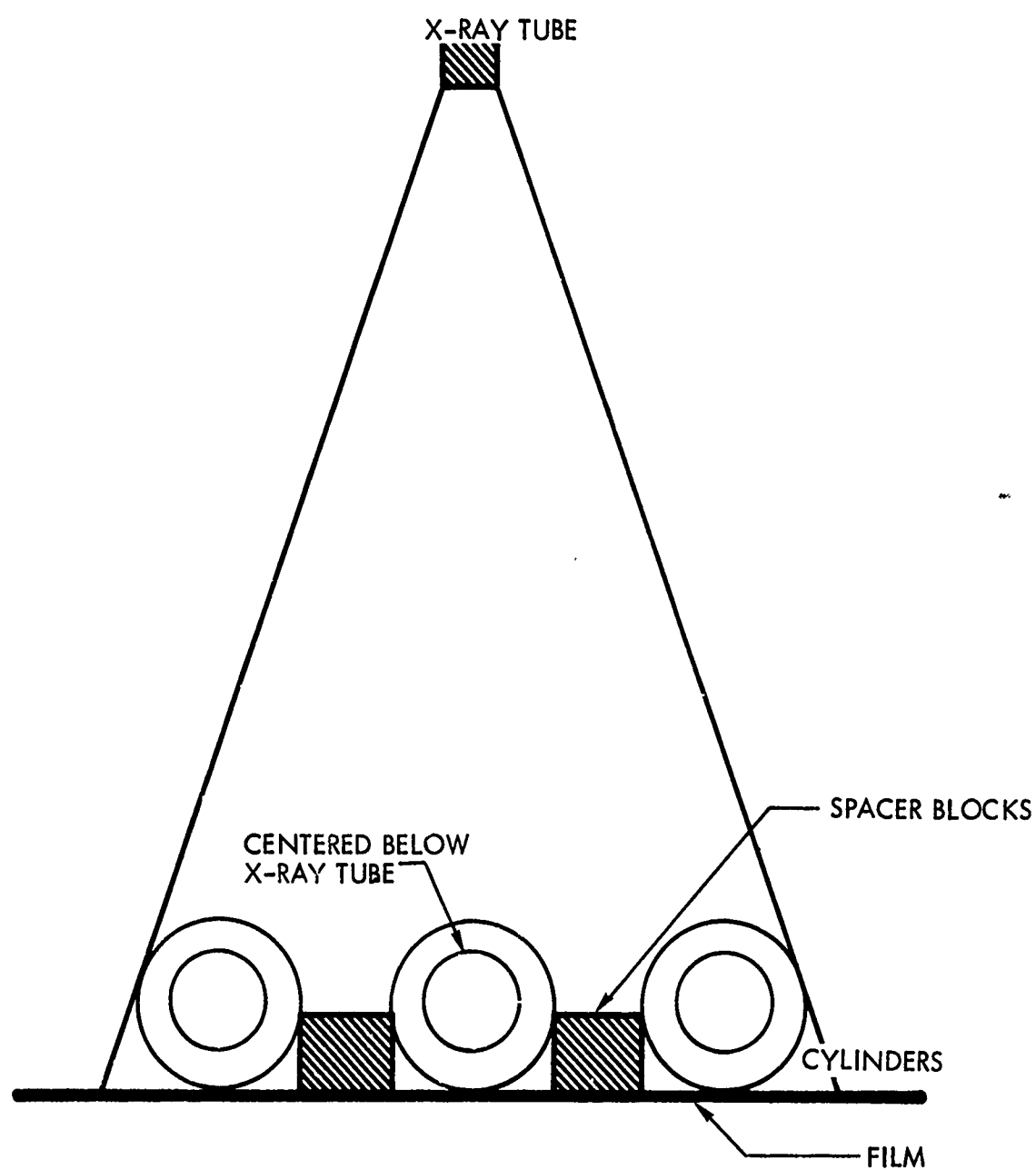
FIGURE 41   SCHEMATIC SKETCH SHOWING X-RAY METHOD USED TO INSPECT
TEST CYLINDERS

To increase resolution and identify smaller flaws, the voltage was increased to 165 KVC volts at 5 milliamps. Using a 36-inch film-to-focal-plane distance, a 3-minute exposure was used on Ansco HD D-2 film (high-resolution X-ray emulsion). No screen was used with the aluminum tubes. These radiography procedures follow Military Standard 453.

For the 4330V Modified steel cylinders, a Norelco MG-300 X-ray source was used. The focal spot sizes for this tube are 4 mm and 1.5 mm. The 4 mm focal spot was used at an operating voltage of 190 KV at 5 milliamps. A lead screen 0.005 inch thick was used as a filter. The film-to-focal-plane distance was 36 inches. Using the medium-resolution D-4 film, the exposure time was 2 minutes.

A typical crack indication appears as a dark line on the X-ray film. Figure 42 shows an enlarged portion of a typical X-ray crack indication found on the 7075-T6511 Aluminum cylinders. The film is medium-resolution D-4. Figure 43 shows an enlarged portion of an X-ray crack indication found in 4330V Modified steel cylinders.

Two problems exist in measuring the size and location of a crack by X-ray inspection. The X-ray focal spot is essentially a point source, and the beam diverges. A defect in the part located some unknown distance above the film may exist anywhere along the line that joins the source and the indication on the film. In some cases, the double-exposure technique may be used to locate the defect; however, this is not practical for many parts.

A complete solution to determine the defect size and location can be obtained for the simple geometric shape used in this investigation. It is assumed that the defect is located in the outer surface of the cylinder or at a known distance below the surface. The position of the defect with respect to the fiducial mark and the length of the defect can be determined directly from the X-ray film.

Using the geometric configuration shown in Figure 44, the distance from the centerline of the tube axis ($\mathcal{C}$) to the defect can be found as follows:

$$\mathcal{C} \, F' = \frac{SF \, (R' \sin \emptyset + \mathcal{C} \, F')}{SF - R + R' \cos \emptyset} \tag{7}$$

where $\mathcal{C} \, F'$ is the distance from the inspected cylinder axis projection on the film to the extremities of the defect.

SF is the source-to-film distance (36 inches)

R' is the distance from the axis of the cylinders to the defect

R is the outer radius of the cylinder

$\emptyset$ is the angle from $\mathcal{C}$ to the defect, measured with the cylinder axis as a center.

For a surface flaw R' = R. If the cylinder is located off center as shown in Figure 44, the equation is given as

$$\mathcal{C} \, F' = \left[\frac{SF \, (R' \sin \emptyset + \mathcal{C} \, F)}{SF - R + R' \cos \emptyset} \right] - \mathcal{C} \, B \tag{8}$$

where $\mathcal{C} \, B$ is the distance from the normal to the film surface to the centerline of the tube.
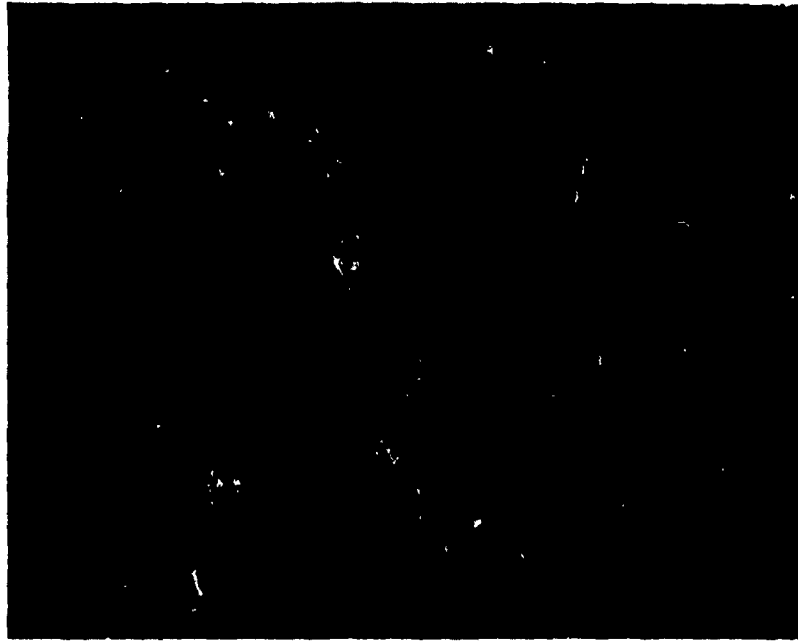
FIGURE 42 TYPICAL INDICATION OF CRACK IN
ALUMINUM,11.6X

FIGURE 43 TYPICAL INDICATION OF CRACK IN 4330V
MODIFIED STEEL,11.6X
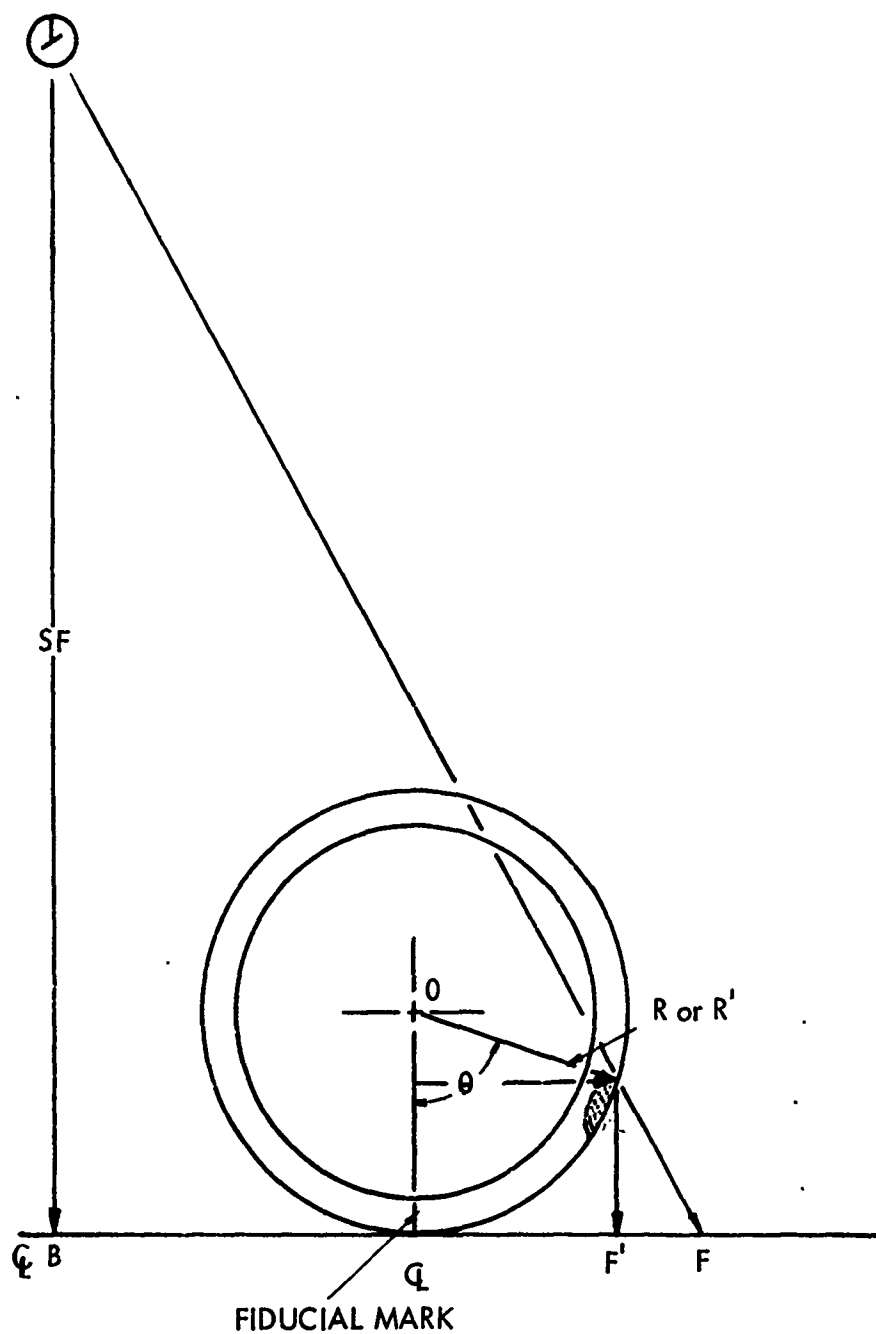
FIGURE 44   SCHEMATIC SHOWING GEOMETRIC CONSTRUCTION USED TO
DETERMINE DEFECT SIZE AND LOCATION ON X-RAY FILM

A computer program was set up to solve these two equations. A graph of centerline to defect on film vs. circumferential distance on the tube is shown in Figure 45. The solid line is for a tube located directly in the path of the X-rays, and the dotted line is for a tube located 3 1/2 inches away.

Penetrant Inspection

The penetrant inspection of both the aluminum and steel cylinders used Magnaflux ZL-2, a commercial post-emulsifier penetrant. This fluorescent material was viewed on the test cylinders after the developing process by irradiation with ultraviolet light. The unaided eye was used to inspect the cylinders for cracks under ultraviolet light. The procedure followed normal production penetrant-inspection techniques (6).

The emulsifier, Magnaflux ZE-3, was applied in a separate step immediately after application of the ZL-2. This allowed the penetrant solution to be removed from the surface of the test part but did not affect the penetrant which had entered cracks and small surface defects. The developer used to enhance crack detection was Magnaflux ZP-4 in dry form.

The penetrant inspection area consisted of six stations: the cleaning and degreasing tank, penetrant tank, emulsifier tank, drying rack, developer tank, and the inspection booth. The cylinders were prepared for penetrant inspection first by being thoroughly cleaned and degreased by scrubbing with a cloth saturated with acetone. The cylinders were then immersed in the penetrant (ZL-2) for at least 15 minutes. After removal from the penetrant tank (shown in Figure 46) and draining off the excess penetrant solution, the test parts were immersed in the emulsifier for 2 minutes. The residual emulsion solution was then washed off with tap water. A period of drying at room temperature followed, and forced-heated air was applied when drying was near completion. When the parts were thoroughly dry, they were submerged in the dry developer compound for 45 minutes.

After removal from the developer tank, the cylinders were carried to the inspection booth, where ultraviolet light was used to detect the penetrant-filled cracks. The end points of the cracks were carefully marked so that the crack could be located and measured when the ultraviolet light was removed. The position of the crack was measured with the fixture shown in Figures 38 and 39.

Surface defects such as cracks, scratches, nicks, and pits could be detected during inspection, as the fluorescent-penetrant provided a color and brightness which contrasted sharply with the cylinder material while exposed to the ultraviolet radiation.

Magnetic-Particle Inspection

This method is suitable only for materials which can be intensely magnetized, such as ferromagnetic materials. For this reason, the aluminum cylinders, which are non-ferromagnetic, were not inspected by this method. However, all the steel cylinders were inspected by the magnetic-particle method in the laboratory.

The procedure for inspection of the 4330V Modified steel cylinders uses a continuous-field technique in which the magnetic particles were applied in a water carrier during the magnetizing cycle. The magnetic particles were attracted to the pseudo-poles caused by discontinuities which interrupted or disturbed the magnetic field in the material. Magnetization was retained in the steel cylinders for considerable time after the magnetizing force was removed, thus necessitating a demagnetization cycle after inspection was complete. The particles trapped at a discontinuity caused the discontinuity to be clearly discernible when the particles were irradiated with ultraviolet light.
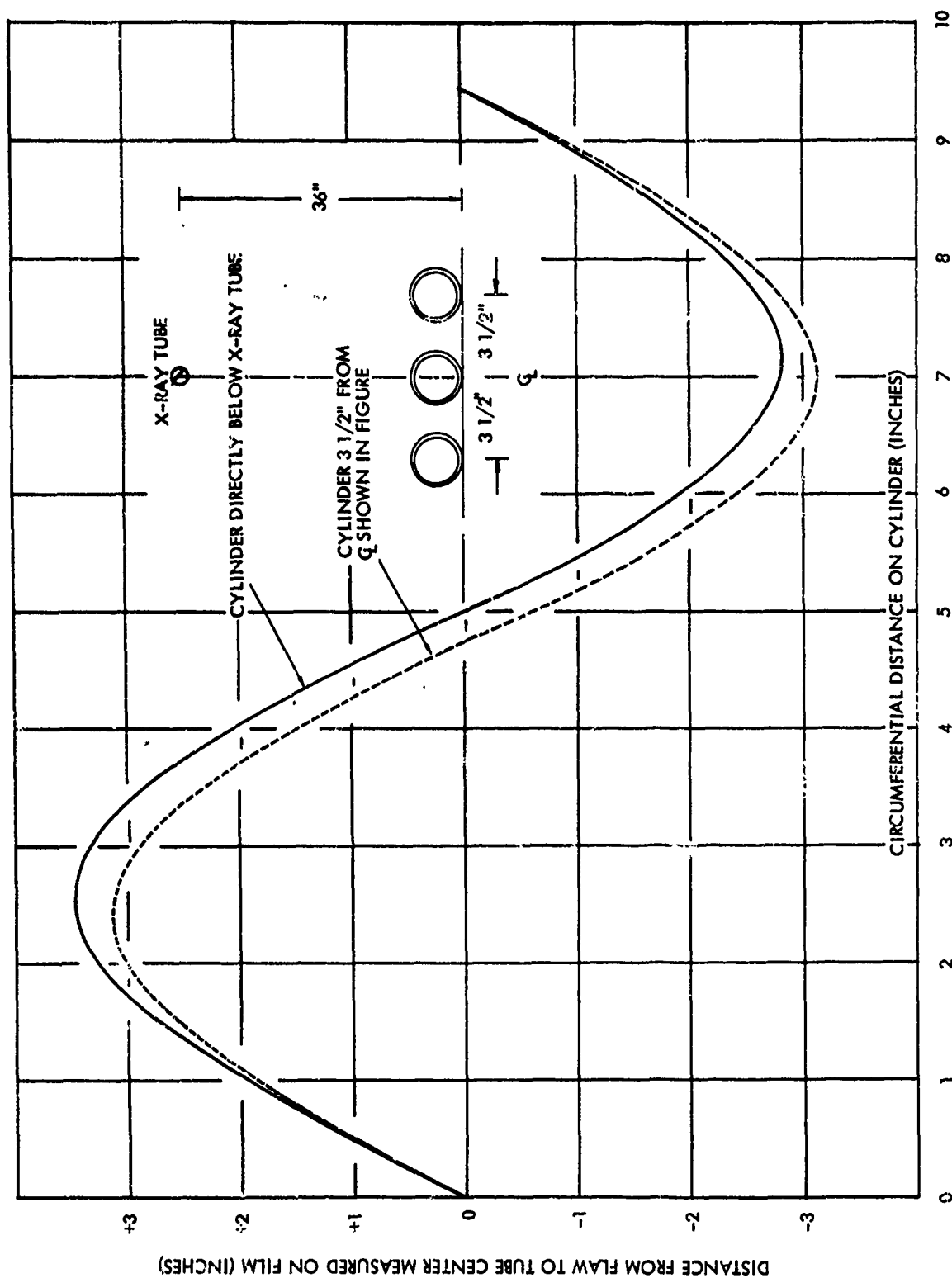
FIGURE 45   GRAPH OF DEFECT LOCATION VERSUS FILM LOCATION FOR
3" DIA. TUBES

74

FIGURE 46 4330V MODIFIED STEEL CYLINDERS BEING REMOVED FROM PENETRANT TANK

The cylinders were magnetized by placing each within a large magnetizing coil so that the longitudinal axis of the cylinder was parallel to the axis of the magnetic field. When they were so placed, the fatigue cracks were oriented at right angles to the magnetic flux lines, thus yielding optimum results. Figure 47 shows a typical tube in the magnetizing coil.

The cylinders were subjected to several short magnetization cycles using 20,000 ampere-turns DC in a unit capable of generating 6000 amperes DC. During the magnetization cycles fluorescent magnetic particles, Magnaflux type 20A, in a water suspension were applied to the cylinder surface. The particle concentration in the solution was 0.22 ml in a 100 ml sample measured by gravitational settling in an ASTM graduated centrifuge tube. The cylinder was then removed from the coil and inspected with an ultraviolet lamp. The end points of the cracks were marked, and the position of the cracks were measured with the locating fixture. When inspection was complete, the steel cylinders were demagnetized and washed to remove particle residue. Figure 47 shows a typical crack indication obtained using this technique on the 4330V Modified steel tubes.

Equipment used by the Lockheed-Georgia production inspection personnel is similar with respect to power rating; however, they utilize an oil-type suspension for the magnetic particles (Magnaflux type 10A). Oil suspension is used primarily in a production shop where evaporational losses are of concern. This problem does not exist in the laboratory, and the water suspension system is used, which reduces fire hazards as well as fumes.

Ultrasonic Inspection

Of the four NDT methods used in this program, the ultrasonic method has the greatest potential for detecting and determining the extent of internal cracks. Since many variations in technique and test parameters are possible, this method also requires the most developmental effort. The decision to use a particular ultrasonic techniques was made after considering many factors, such as shape of test part, type of material, shape and size of suspected flaws, location of flaws, and others. These factors determined test parameters such as mode of testing (immersion or contact), frequency and diameter of transducer crystal, sensitivity required, type of ultrasonic wave to be used, test fixtures to be constructed, and test standards to be used.

Three ultrasonic techniques were considered:

o Immersion, angle beam, pulse-echo shear wave.
o Contact, normal incidence, pulse-echo longitudinal wave.
o Contact, angle beam, pulse-echo, shear-wave.

In the first technique, the test cylinder would be immersed in a tank of water and scanned with an ultrasonic beam which is inclined to the normal at the cylinder surface. The angle of incidence would lie in a plane which includes the axis of the cylinder. Scanning of the test part could be done longitudinally or circumferentially. A holding fixture for precisely positioning and indexing the cylinder would be necessary for repeatability and reliability of data. This technique can readily be automated and affixed with a C-scan printout for complete part coverage. While not used in this program, this technique would be recommended for production testing of this type of part because of its fast-scan capability and potential accuracy.

The normal incidence contact method would involve placing the transducer on the rim of the cylinder and directing the beam longitudinally down the cylinder (a non-contact immersion technique could also be used). The amplitude of the signal reflected by a crack

(CRACK IS LOCATED AT THE TOP ON A LINE WITH THE
CENTER OF THE HOLE.)
TYPICAL CRACK INDICATION

FIGURE 47   NONDESTRUCTIVE TESTING OF 4330V MODIFIED STEEL CYLINDER
BY MAGNETIC PARTICLE METHOD

would depend on crack size, orientation, and distance from the transducer. Multiple reflections between the tubing walls would effectively increase the distance to the crack. Cutout holes in the cylinders could hinder detection of cracks and provide extraneous signals. Costly machining of the cylinder end surfaces would be necessary to provide a smooth and normal contact surface for the transducer.

The angle-beam contact method is similar to the angle-beam immersion method. A major difference is that, in the former, a light oil is used for a couplant rather than water, and the transducer-to-test-part distance is determined by use of a lucite shoe. In both these techniques, the discontinuity is always observed at the same distance, thus eliminating distance as a variable in affecting the echo amplitude. The ultrasonic beam enters the test cylinder at a fixed angle, is reflected from the inner wall, and continues to propagate along the cylinder by periodically reflecting from inner and outer walls, causing nodes and antinodes along the surfaces. The investigator can then observe discontinuities which propagate from the outer surface at any antinode he chooses. The first antinode reflection will usually provide the least confusion and the most accuracy.

This third method was chosen as the technique to be used for crack detection and characterization in the steel and aluminum cylinders in this program. A 5.0-megacycle, SFZ-type transducer with a 0.250-inch-diameter lithium-sulphate crystal was selected because of its sufficient sensitivity and beam size for crack detection and measurement.

Some of the cylinders were also inspected using a 10.0-megacycle, SFZ-type transducer to determine the frequency for which the most accurate results might be expected.

A lucite shoe constructed to hold the transducer while scanning the test cylinders is shown in Figure 48. The shoe provides three functions: 1) a fixed incident angle for the beam impinging on the cylinder, 2) a fixed transducer-to-cylinder distance, and 3) a larger contact surface between transducer and test part. The shoe contains a flat-bottom hole into which the transducer was inserted along with a few drops of oil to assure transfer of energy into the lucite. The lucite surface on which contact with the cylinder is to be made was rounded to be compatible with the outer cylinder radius of curvature. Oil is used as a couplant between the lucite and cylinder surfaces.

The lucite shoe provides a 30-degree (from normal) incident angle for the ultrasonic energy impinging on the surface of the cylinder. At the interface between the lucite/metal media, the beam is split into two components: a longitudinal wave and a shear wave. The angle of incidence is sufficiently high for the longitudinal wave to be totally reflected at the interface, so that only the shear wave enters the test material. The shear wave enters at an angle from the normal of 35 degrees 29 min. for the aluminum cylinders and 37 degrees three min. for the steel cylinders (these angles are computed using Snell's law of reflection and refraction). When a surface discontinuity is detected, an echo is obtained when the discontinuity is 0.356 inch from the point of beam incidence on the surface. Index marks on the side of the shoe were used to locate the position of the crack when an echo was obtained. Index marks on the front of the shoe were also used to determine location and the end points of the crack. The shoe is shown being applied to a test cylinder in Figures 48 and 49.

The ultrasonic generating and detecting equipment used in this program has consisted of two separate units: The Sperry UM/700 and the UM/715 Reflectoscopes. The latter came into use when the former equipment was repaired. Essentially no difference in the results was obtained for either piece of equipment, but separate calibration curves were needed for each. Figure 49 is a photograph of the UM/715 Reflectoscope and test configuration used in this program.

78

FIGURE 48   LUCITE TRANSDUCER SHOE IN PLACE ON ALUMINUM
TEST CYLINDERS
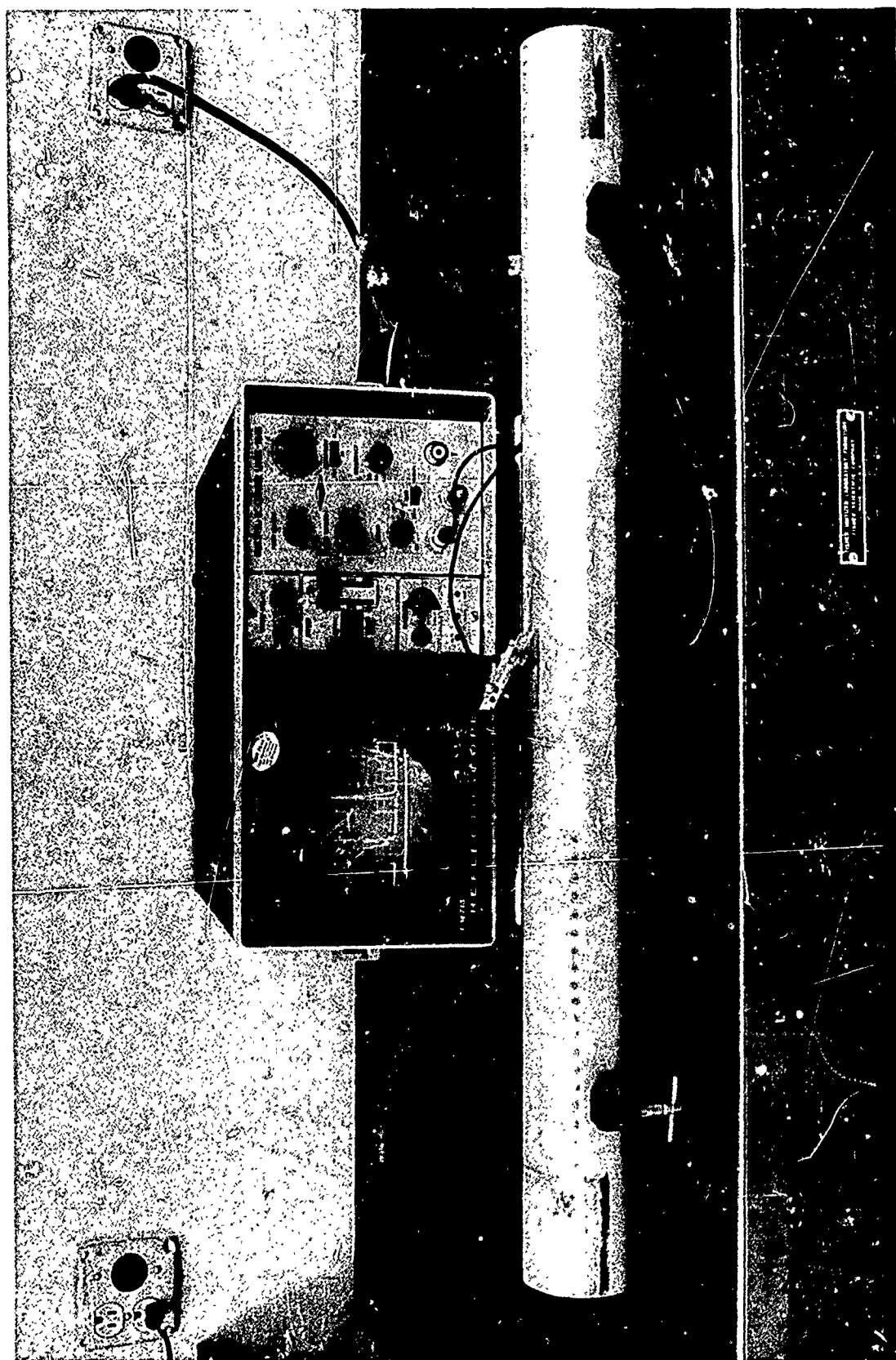
FIGURE 49   SPERRY UM/715 REFLECTOSCOPE USED TO DETECT CRACKS
IN TEST CYLINDERS

The transducer shoe can be used to obtain reflections at a number of locations along the cylinder, depending on its distance from the crack. In making the measurements, the shoe was positioned at one of two locations, designated Position A and Position B, at specific distances from the crack. These are shown in Figure 50. The first reflection, indicates the intersection of the crack and the outer cylinder surface after reflecting off the inner surface of the cylinder. The second reflection is measured at Position B and is obtained when the beam grazes the bottom edge of the crack or is reflected from the intersection of a deep crack and the inner cylinder surface. (The definitions of first and second reflection are arbitrary and were chosen because the first indication, or reflection from the crack is obtained at Postion A).

The procedure used in detecting and measuring cracks was as follows: After warm-up of equipment, the Reflectoscope response was calibrated. The standards used for calibration were sections of test cylinders which had saw-cuts made to various depths to simulate cracks. The cuts were made using a 0.750-inch-radius sawblade 0.05 inch thick. The amplitude information was obtained by placing the transducer near the saw cut and positioning so that a maximum amplitude reflection was obtained. The UM/715 response was adjusted so that a saw cut 0.075 inch deep yielded a 2.5-inch deflection on the Reflectoscope. The deflection heights from shallower saw cuts were then obtained and plotted to obtain a calibration curve. Typical Reflectoscope presentations are shown in Figure 51 for the first reflection and Figure 52 for the second reflection. The position of all knobs on the Reflectoscope were noted and were kept in that position.

Typical calibration curves for the first and second reflections are shown in Figures 53 and 54 for the aluminum cylinders and in Figures 55 and 56 for the steel cylinders.

The calibration curves are nonlinear, largely due to the nonlinear distribution of energy in the ultrasonic beam. Using the two calibration curves, the best measurement accuracy is obtained for cracks which are less than 0.070 inch and greater than 0.100 inch in depth. The use of a large-diameter crystal did not appreciably affect the upper and lower limits of the curves. Sensitivity in detection of very small cracks was reduced by using the larger transducer. For these reasons, the 0.250-inch-diameter crystal was used.

The cylinders were then inspected ultrasonically for discontinuities. To enhance detection, the pulse length of the beam was increased and the transducer was moved longitudinally back and forth over the suspected area. When a discontinuity was detected, the pulse-length was decreased to its former calibration position. The maximum echo amplitude resulting from the discontinuity was measured on the Reflectoscope and compared to the calibration curve. By using the index marks on the transducer shoe, the position of the discontinuity and its end points were marked. The locating fixture was then used to obtain distance and azimuth information from the marks.

Measurement of Fracture Surface

After the cylinder had been tested to failure, the fracture surface was examined. The failed section of the cylinder was placed on two vee blocks, one of which had an index mark. The fiducial mark on the cylinder was aligned with the index mark, and angular displacement of the crack was measured. The location of the ends of the crack was measured with a scale.

In almost all cases, the location and size of the fatigue crack was easy to identify. The fatigue cracks in the 7075-T6511 Aluminum tubes are bright and shiny in contrast to the dull surface typical of the tensile overload area. Typical photographs of fracture surfaces from the failed 7075-T6511 Aluminum tubes are shown in Figures 57 through 60. In all cases, a typical "thumbnail" or "clamshell" shape is observed. The crack lengths measured on the failure surfaces vary from 0.05 to 0.34 inch. The crack depths vary from 0.02 to 0.16 inch.

81
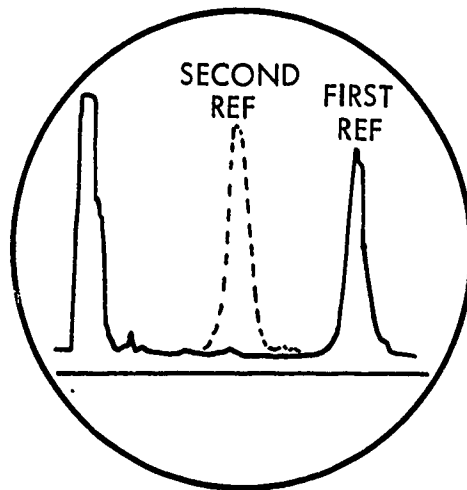
(A) SCHEMATIC SKETCH OF SCOPE DISPLAY
SHOWING FIRST & SECOND REFLECTIONS
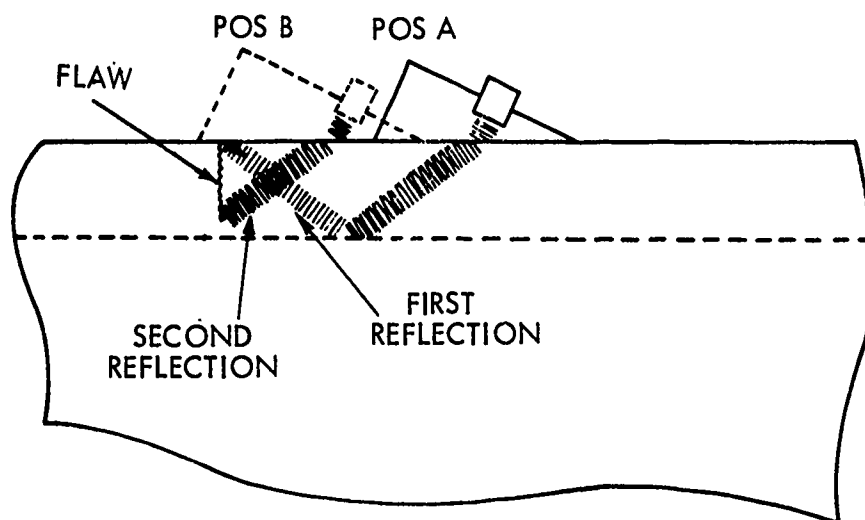
(B) SKETCH SHOWING POSITION OF LUCITE SHOE FOR
FIRST & SECOND REFLECTIONS

FIGURE 50   POSITIONS OF FIRST AND SECOND REFLECTIONS DUE TO
CRACK INDICATIONS (A) ON SCOPE (B) LOCATION OF
LUCITE SHOE

82

(A) 1ST REFLECTION 0.075" DEEP

FIGURE 51

REFLECTOSCOPE PRESENTATIONS
OF DEFECT INDICATION FROM
CALIBRATED SPECIMENS
(7075-T6511 ALUMINUM)
1ST REFLECTION
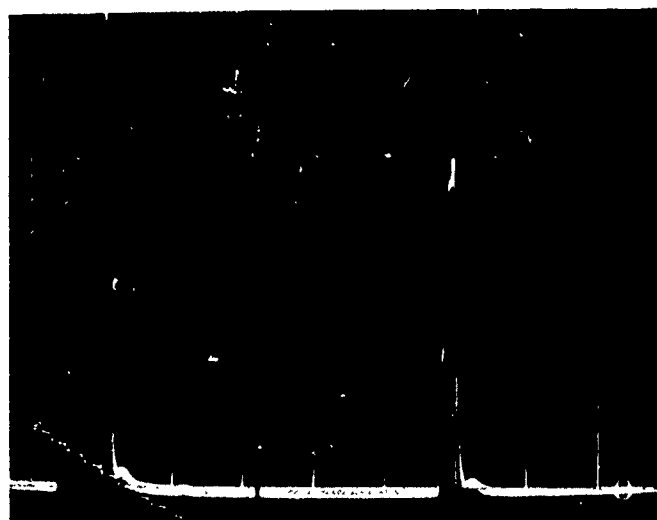
(B) 1ST REFLECTION 0.030" DEEP
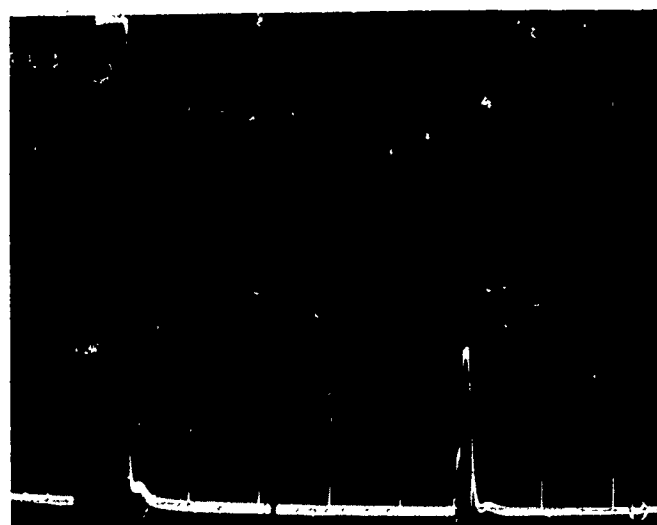
(C) 1ST REFLECTION 0.012" DEEP

83
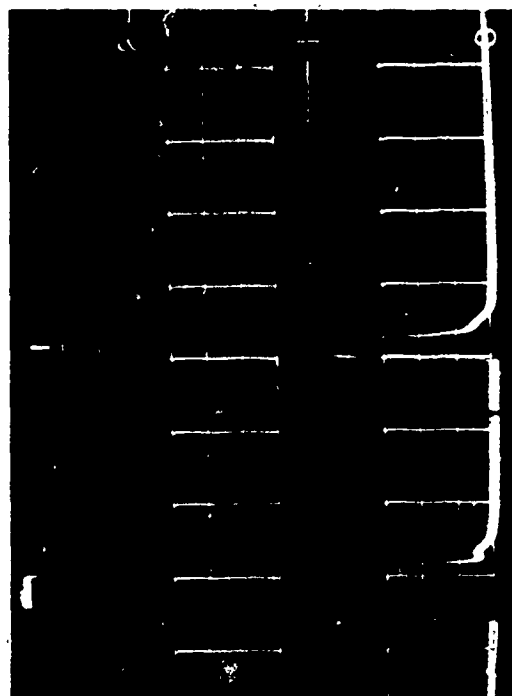
(A) 2ND REFLECTION 0.250" DEEP
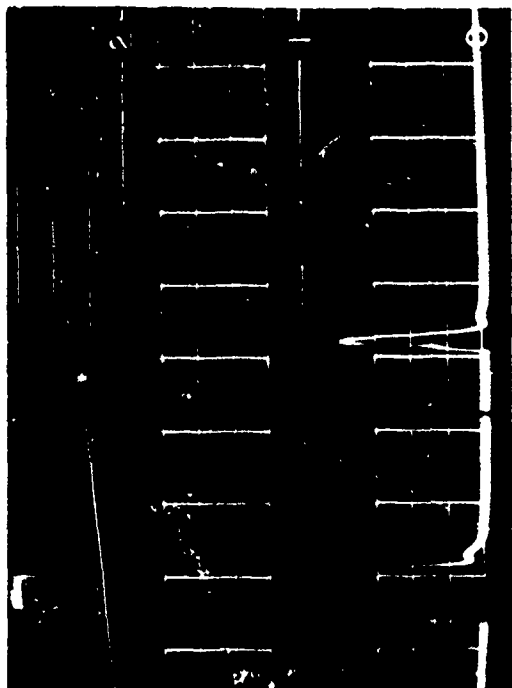
(B) 2ND REFLECTION 0.20" DEEP
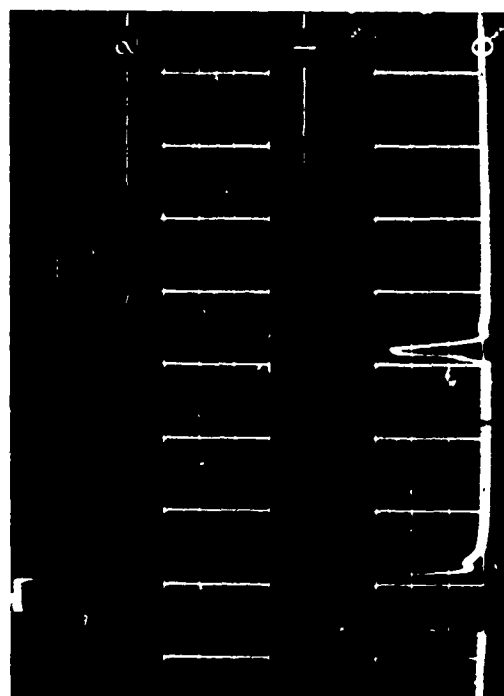
(C) 2ND REFLECTION 0.15" DEEP
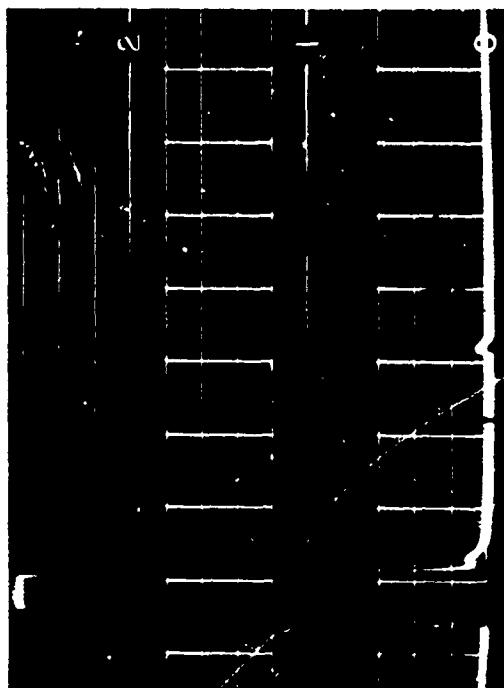
(D) 2ND REFLECTION 0.10" DEEP

FIGURE 52   REFLECTOSCOPE PRESENTATIONS OF DEFECT INDICATIONS
FROM CALIBRATED SPECIMENS (7075-T6511 ALUMINUM)
2ND REFLECTION

84
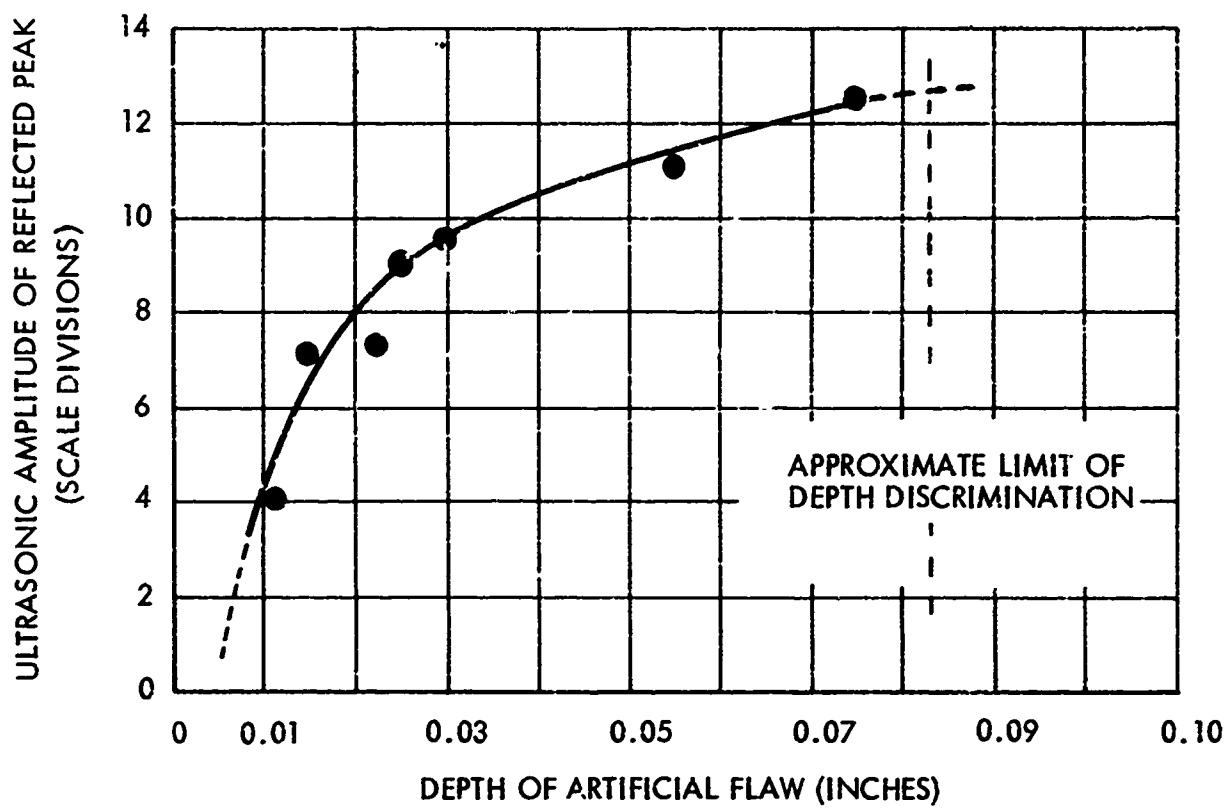
FIGURE 53   CALIBRATION CURVE FOR FIRST REFLECTION FROM
ARTIFICIAL FLAWS. 7075-T6511 ALUMINUM CYLINDERS
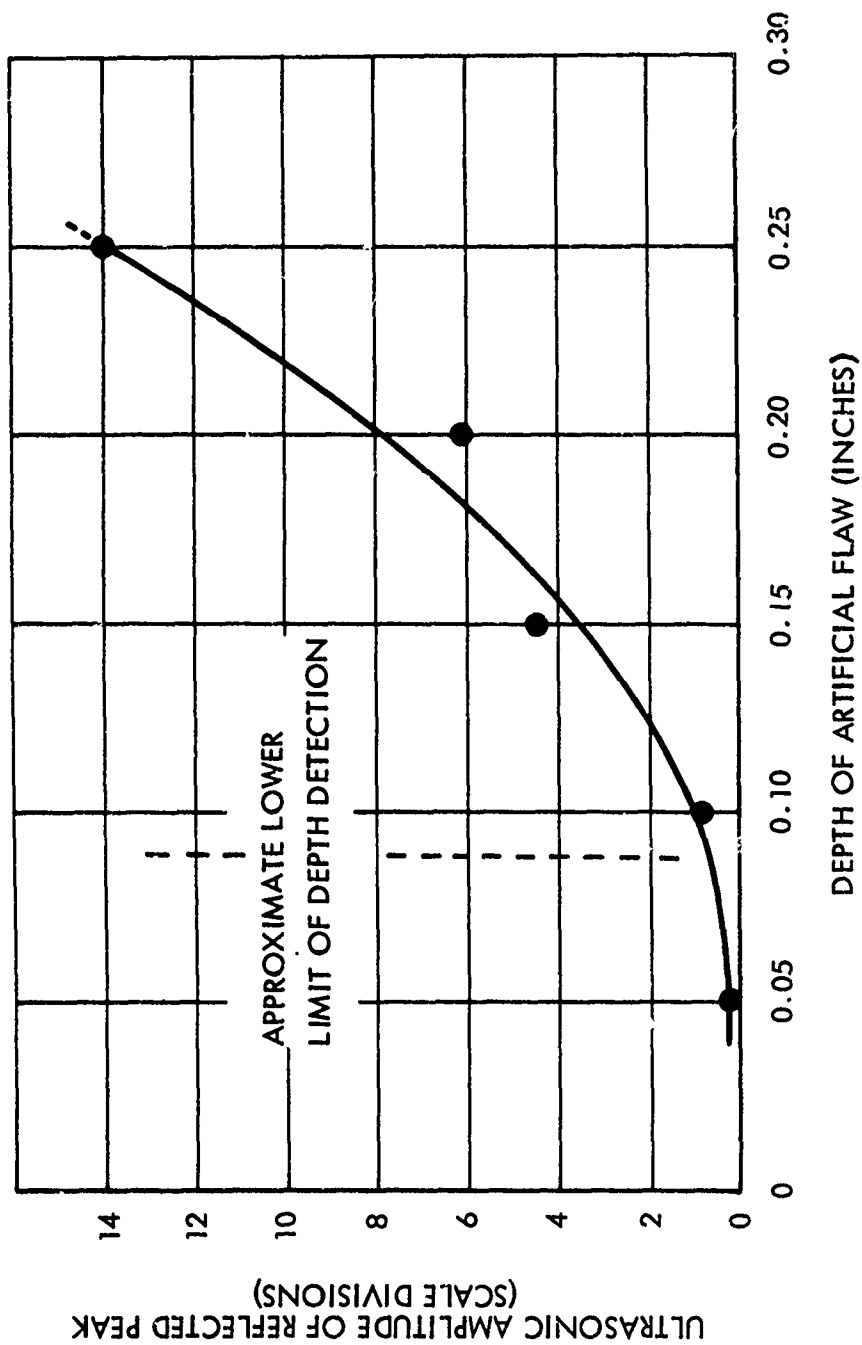
FIGURE 54   CALIBRATION CURVE FOR SECOND REFLECTION FROM ARTIFICIAL FLAWS
7075-T6511 ALUMINUM CYLINDERS
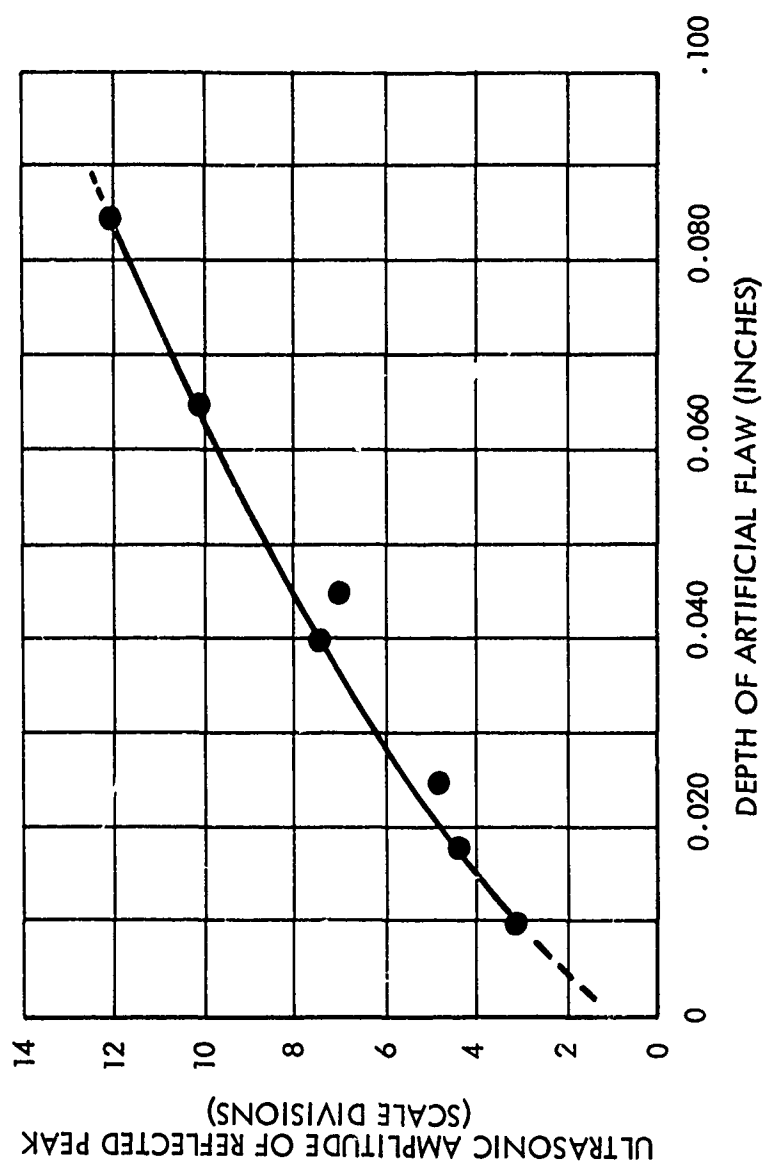
FIGURE 55   CALIBRATION CURVE FOR FIRST REFLECTION FROM ARTIFICIAL FLAWS
4330V MODIFIED STEEL CYLINDERS (220–240 KSI HEAT TREAT CONDITION)
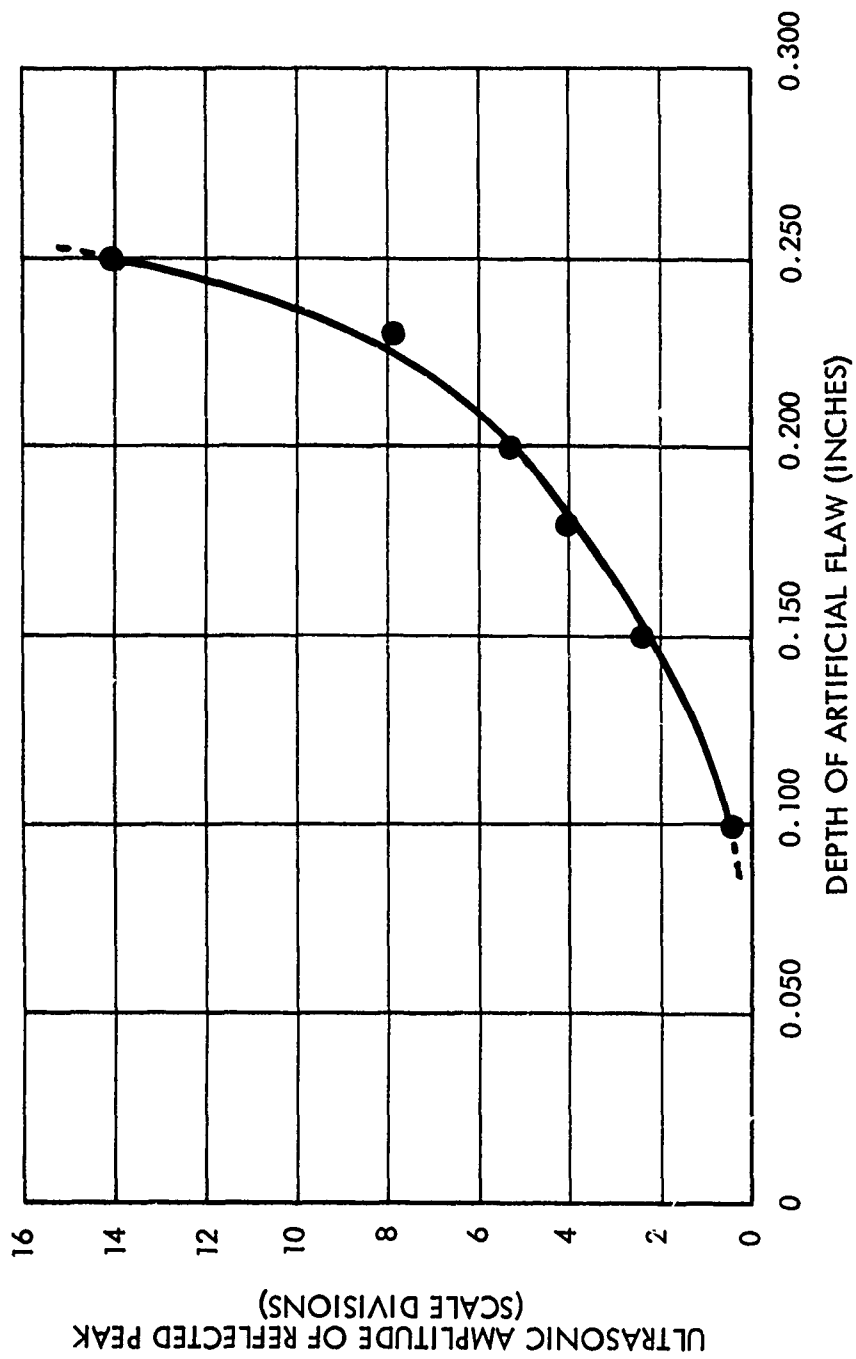
FIGURE 56   CALIBRATION CURVE FOR SECOND REFLECTION FROM ARTIFICIAL FLAWS
IN 4330V MODIFIED STEEL CYLINDERS (220–240 KSI HEAT TREAT CONDITION)

88

FIGURE 57   FRACTURE SURFACE OF FAILED 7075-T6511 ALUMINUM
            TEST CYLINDER. FATIGUE CRACK IS .05 INCHES LONG,
            .024 INCHES DEEP

FIGURE 58   FRACTURE SURFACE OF FAILED 7075-T6511 ALUMINUM
            TEST CYLINDER.   FATIGUE CRACK IS 0.088 INCHES LONG,
            .044 INCHES DEEP
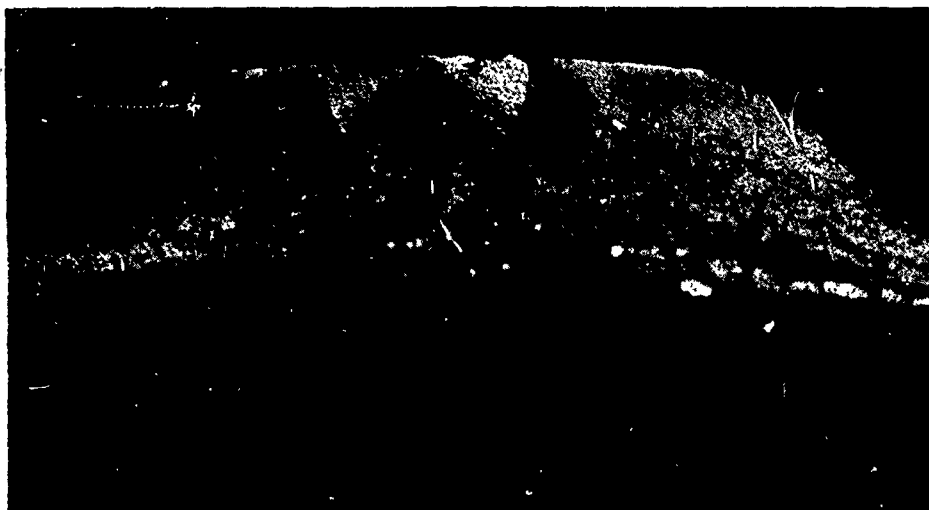
FIGURE 59   FRACTURE SURFACE OF FAILED 7075-T6511 ALUMINUM TEST
CYLINDER.   FATIGUE CRACK IS 0.155 INCHES LONG,
0.085 INCHES DEEP

FIGURE 60   FRACTURE SURFACE OF FAILED 7075-T6511 ALUMINUM TEST
CYLINDER.   FATIGUE CRACK IS 0.34 INCHES LONG, 0.165
INCHES DEEP

Examination of the fracture surfaces of the heat-treated 4330V Modified steel tubes shows two distinctly different crack surfaces. Figure 61 shows a typical fracture surface for a fatigue crack produced in the specimen prior to heat-treating. The following four distinct areas can be seen and identified:

1. The cracking in the micro-weld solidification area. This is a small (0.030 inch diameter) semicircular section showing a rough surface with several short peninsulas of solidified metal extending outward from the center of the solidification area. The surfaces have been stained by oxidation during the heat-treatment.

2. The fatigue-cracked areas extends in a semicircular area from the micro-weld cracked area. This area was also stained during the heat-treatment.

3. The flat fracture area starts from the fatigue crack area. This is shown in Figure 61 by a dull area lighter in color than the fatigue-precracked surface.

4. The shear areas are on the inner and outer surfaces of the tube.

In contrast to the specimens fatigue-precracked prior to heat-treatment, the specimens fatigued-precracked after heat-treatment do not show a sharply defined fatigue area. Figure 62 shows the typical fracture surface obtained from a specimen tested to failure with precracking after heat-treatment. The micro-weld cracking is seen as the inner section. The fatigue-cracked area is concentric with the weld-cracked area. There appears to be a small "ridged" area separating the fatigue crack from the tensile overload fracture surface. (This has been accented by the lighting in the photograph).

The fracture surfaces of tubes tested to failure without prior fatigue precracking were also examined. These specimens were used to determine the ultimate tensile strength and yield strength of the cylinders.

Figure 63 shows the fracture surface of a 4330V Modified steel cylinder that was assumed to be free of defects. The photograph shows staining and a thumbnail crack. The shape of the natural crack in 4330V Modified steel is much flatter than those produced by fatiguing (Figures 61 through 69). Several features of the natural crack are similar to the fatigue-initiated cracks. In particular, there was a stained area indicating that the cracking occurred before heat-treating or during the heat-treat cycle. The staining was not as marked as in the fatigue cracks, indicating that the natural crack is tighter than those produced by fatigue. The cracking occurred on the outer surface and was the site from which the tensile failure initiated.

Typical photographs of fracture surfaces from the failed 4330V Modified steel cylinders are shown in Figures 64 through 69.

Experimental Results, Non-Destructive Testing

Introduction

For each of the 200 specimens used in the test program, the crack length, location and orientation were measured . Using Figure 40 as a guide, measurements of the crack location from the indexed end of the tube were taken and called ℓ_1 and ℓ_2. The orientation of the crack with respect to the fiducial mark were also taken, and were called θ_1 and θ_2. The crack length could be calculated from these measurements as follows:

91
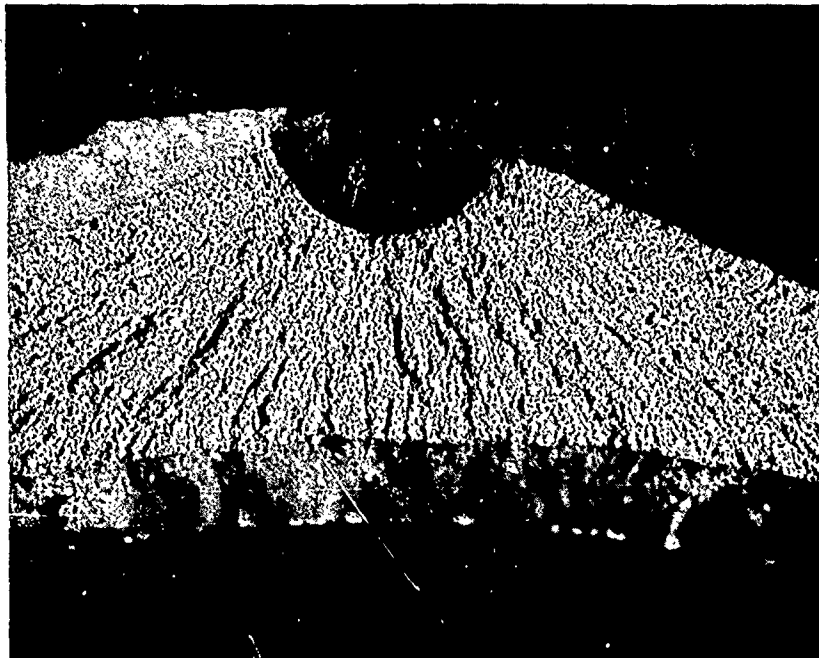
FIGURE 61 FRACTURE SURFACE OF FAILED 4330V MODIFIED STEEL CYLINDER
FATIGUE CRACKED PRIOR TO HEAT TREATMENT
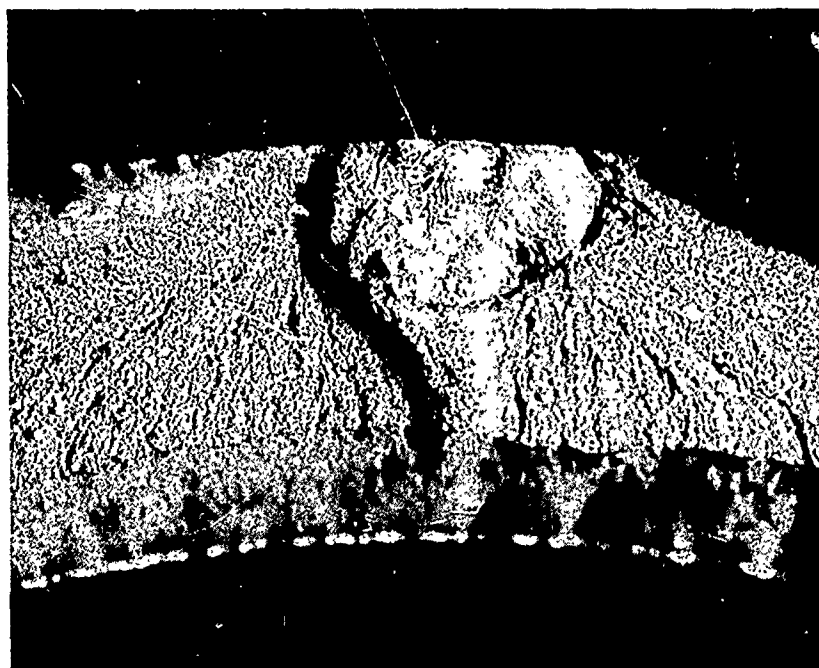
FIGURE 62 FRACTURE SURFACE OF FAILED 4330V MODIFIED STEEL CYLINDER
FATIGUE CRACKED AFTER HEAT TREATMENT
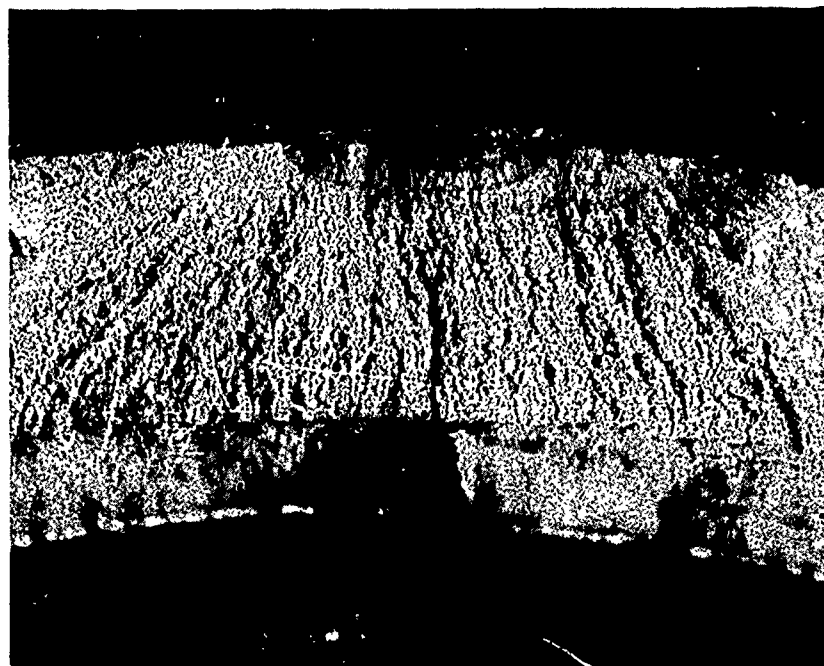
FIGURE 63 FRACTURE SURFACE OF 4330V MODIFIED STEEL TUBE. NO PRIOR
FATIGUE PRECRACKING. AREA SHOWS NATURAL CRACK.
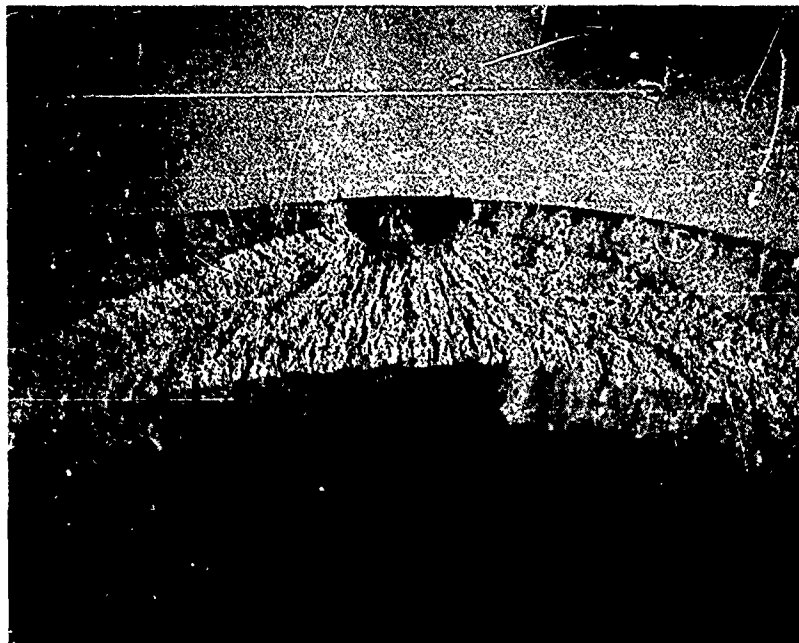
FIGURE 64   FAILURE ORIGIN OF 4330V MODIFIED STEEL
CYLINDER NUMBER S-43 (7X)

FIGURE 65 FAILURE ORIGIN OF 4330V MODIFIED STEEL
CYLINDER NUMBER S-48 (7X)
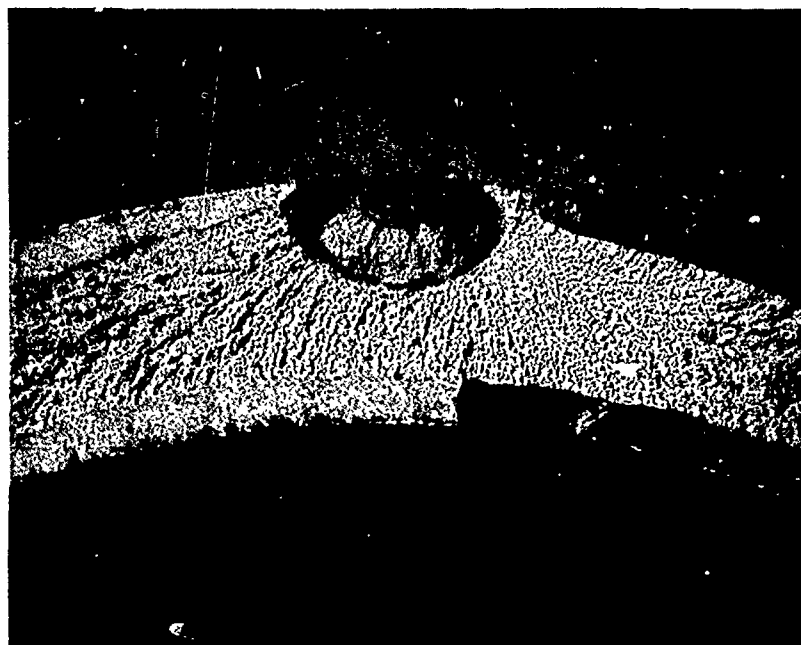
FIGURE 66   FAILURE ORIGIN OF 4330V MODIFIED STEEL
CYLINDER NUMBER S-33 (7X)
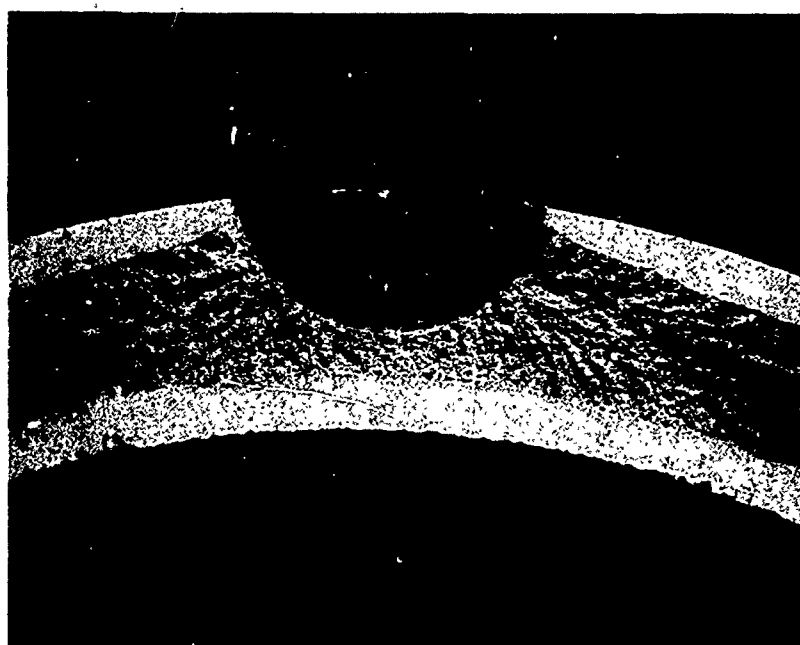
FIGURE 67   FAILURE ORIGIN OF 4330V MODIFIED STEEL
CYLINDER NUMBER S-55 (7X)
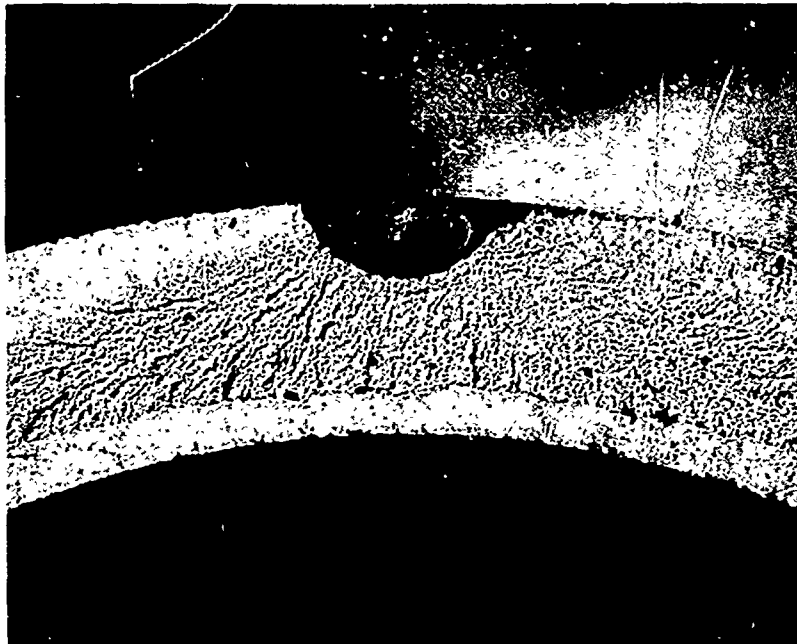
FIGURE 68 FAILURE ORIGIN OF 4330V MODIFIED STEEL
CYLINDER NUMBER S-42 (7X)
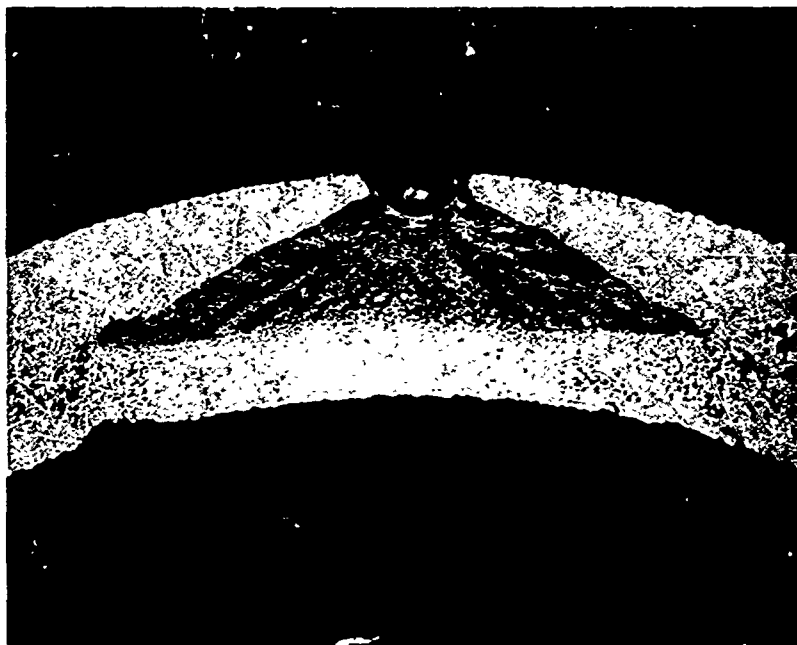
FIGURE 69 FAILURE ORIGIN OF 4330V MODIFIED STEEL
CYLINDER NUMBER S-68 (7X)

$$\hat{2c} \text{ (NDT)} = \sqrt{(r\, \theta_1 - r\, \theta_2)^2 + (\ell_1 - \ell_2)^2} \qquad (9)$$

where r is the outside radius of the cylinder.

The location of the ends of the cracks ℓ_1, ℓ_2 and θ_1, θ_2 are measured directly, as

$$\hat{\ell}_1 \text{ (NDT)}, \ \hat{\ell}_2 \text{(NDT)}, \ \hat{\theta}_1 \text{(NDT)}, \ \hat{\theta}_2 \text{(NDT)} \quad .$$

The (NDT) refers to each of the particular methods used to inspect the cylinders, i.e., X-ray, penetrant, magnetic-particle, ultrasonics.

The sensitivity or capability to detect flaws S(NDT) for each method is calculated according to the following equation

$$S(\text{NDT}) = \frac{N_f \text{ (NDT)}}{N} \qquad (10)$$

where

1. N_f(NDT) is the number of flaws detected on the test cylinders by the specified method.
2. N is the number of flaws detected on the failed cylinders.

This can be expressed as the percent of flaws that were found.

The accuracy of each method, A_{NDT}, to determine the size, 2c, of flaws in each of the two materials is calculated according to the following equation:

$$A_{NDT}(2c) = \frac{1}{N_f \text{ (NDT)}} \sum_{i=1}^{i = N_f \text{ (NDT)}} \left[1 - \frac{\left| \hat{2c}_{NDT} - 2c \right|}{2c} \right]_i \qquad (11)$$

where

1. $\hat{2c}$ is the NDT estimate of the flaw size.
2. 2c is the true value of the flaw size measured on the failed specimens.
3. N_f(NDT) is the total number of flaws detected by the method in the test cylinders.

Similarly, the accuracy of each method in determining the (ℓ) and (θ) of flaws will be calculated according to the following equations, respectively

$$A_{NDT}(\ell) = \frac{1}{N_f(\text{NDT})} \sum_{i=1}^{i = N_f(\text{NDT})} \left[1 - \frac{\left| \hat{\ell}_{NDT} - \ell \right|}{\ell} \right]_i \text{ and,} \qquad (12)$$

$$A_{NDT}(\theta) = \frac{1}{N_f \text{ (NDT)}} \sum_{i=1}^{i = N_f(\text{NDT})} \left[1 - \frac{\left| \hat{\theta}_{NDT} - \theta \right|}{\theta} \right]_i \qquad (13)$$

where

1. $\hat{\theta}_{NDT}$, $\hat{\ell}_{NDT}$ are NDT estimates of the flaw location and orientation.
2. θ, ℓ are the true values of the flaw location measured on the fracture surface of the cylinders.
3. $N_f(NDT)$ is the total number of flaws detected in the cylinders by the method.

I- addition, the overall reliability index of each NDT method R(NDT) will be calculated according to the following equation for each material:

$$R(NDT) = \left[A_{NDT}(c) \right] \left[A_{NDT}(\ell) \right] \left[A_{NDT}(\theta) \right] \left[S(NDT) \right] \text{ where:} \qquad (14)$$

S(NDT) is the method's sensitivity

$A_{NDT}(c)$ is the method's accuracy to determine crack size

$\left. \begin{array}{l} A_{NDT}(\ell) \\ \\ A_{NDT}(\theta) \end{array} \right\}$ are the method's accuracy to determine crack location.

Reliability or reliability index should not be construed to mean reliability in its usual   strict mathematical definition.

Accuracy and reliability are expressed as a dimensionless quantity between 0 and 1.

Grouping within ranges of crack sizes (2c) was chosen as the most appropriate means of data analysis. Eleven sets of crack ranges were chosen (Tables XII and XIII. These start with specimens containing no crack and increase in 0.050-inch increments as follows:

No Crack, 0.001-0.050, 0.051-0.100, 0.101-0.150, 0.151-0.200, etc.

NDT Results - 7075-T6511 Aluminum Cylinders

The experimental results of the NDT inspection of the 7075-T6511 Aluminum cylinders are shown in Figures 70 through 81 and are summarized in Table XII. Figure 70 shows the sensitivity of the X-ray inspection. The results indicate that this method is extremely poor in detecting cracks in the cylinders until the crack size is over 0.45 inch long. About 83% of the cracks could be detected at that crack size. It is interesting to note that X-ray inspection gave some spurious information regarding the existance of cracks in specimens that did not show any cracks on the fracture surface. Approximately 7% of the specimens were identified as having cracks when no cracks could be found on the failed surface.

Figure 71 shows the sensitivity of the penetrant system. The sensitivity is greater than that found for the same cylinders inspected by X-ray and show that, for crack sizes above 0.25 inch, 100% of the cracks present should be detected. The sensitivity drops to below 40% for cracks less than 0.15 inch long, and the method cannot detect cracks below 0.05 inch long.

Figure 72 shows the sensitivity obtained on the ultrasonic tests. Again   ne can expect to detect all of the cracks that are over 0.25 inches long. In contrast to . , penetrant and X-ray results, the sensitivity of the ultrasonic method does not decrease as rapidly in the small crack sizes. Over 60% of the cracks in the 0.10 to 0.15-inch range wer- detected by this method.

99

TABLE XII

RELIABILITY INDICES FOR NDT INSPECTION OF ALUMINUM CYLINDERS

Actual crack (2c) range (inch)	Accuracy by dye penetrant			Accuracy by ultrasonics			Sensitivity			Reliability index		
	Crack length	Crack location		Crack length	Crack location		Dye penetrant	Ultrasonics	X-ray	Dye penetrant	Ultrasonics	X-ray
No crack	---	---	---	---	---	---	0.9333	0.8667	0.9333	0.9333	0.8667	0.9333
0.000-0.050	0.0000	0.0000	0.0000	0.0000	0.0000	0.0000	0.0667	0.1333	0.0667	---	---	---
0.051-0.100	0.265	0.9527	0.9986	0.7272	0.9737	0.9961	0.1538	0.4615	0.0000	0.0387	0.3255	0.0000
0.101-0.150	0.8528	0.9817	0.9968	0.6918	0.9860	0.9961	0.2917	0.6250	0.0417	0.2434	0.4247	0.0417
0.151-0.200	0.7033	0.9674	0.9968	0.7598	0.9639	0.9978	0.3636	0.5000	0.0000	0.2466	0.3654	0.0000
0.201-0.250	0.8157	0.9350	0.9981	0.7131	0.9669	0.9970	0.8571	0.8571	0.0000	0.6525	0.5893	0.0000
0.251-0.300	0.8954	0.9742	0.9985	0.6390	0.9879	0.9533	1.0000	1.0000	0.0000	0.8710	0.6018	0.0000
0.301-0.350	0.8406	0.9418	0.9829	0.7475	0.9527	0.9835	1.0000	1.0000	0.1111	0.7781	0.7004	0.1111
0.351-0.400	0.7871	0.9682	0.9969	0.7292	0.9882	0.9959	1.0000	1.0000	0.0000	0.7597	0.7176	0.0000
0.401-0.450	0.9038	0.9700	0.9979	0.7702	0.9719	0.9965	1.0000	1.0000	0.2500	0.8748	0.7459	0.2500
0.451-0.500	0.9395	0.9233	0.9863	0.6383	0.9240	0.9845	1.0000	1.0000	0.8333	0.8555	0.5806	0.8333
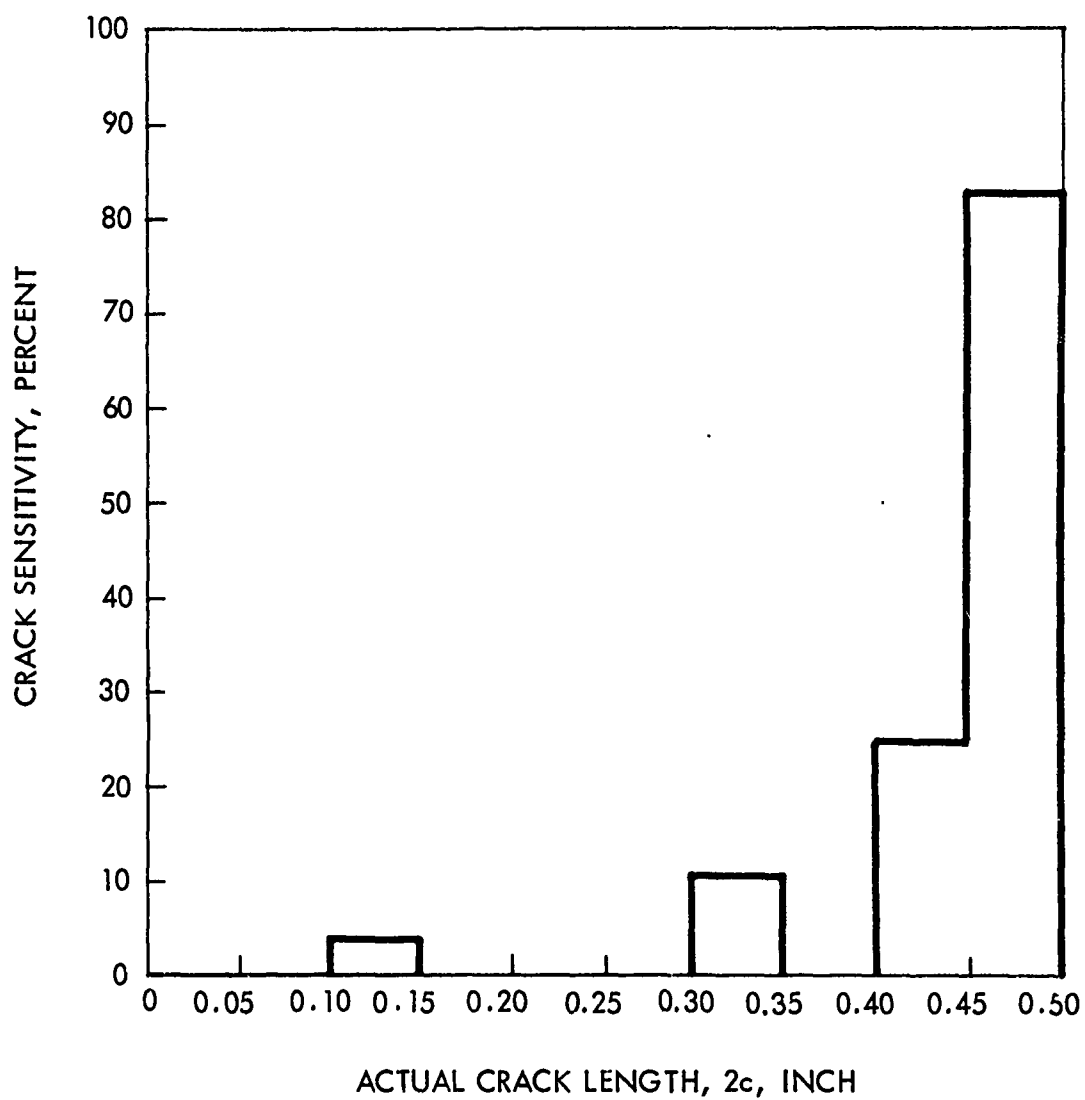
FIGURE 70 – SENSITIVITY OF X–RAY – ALUMINUM CYLINDERS
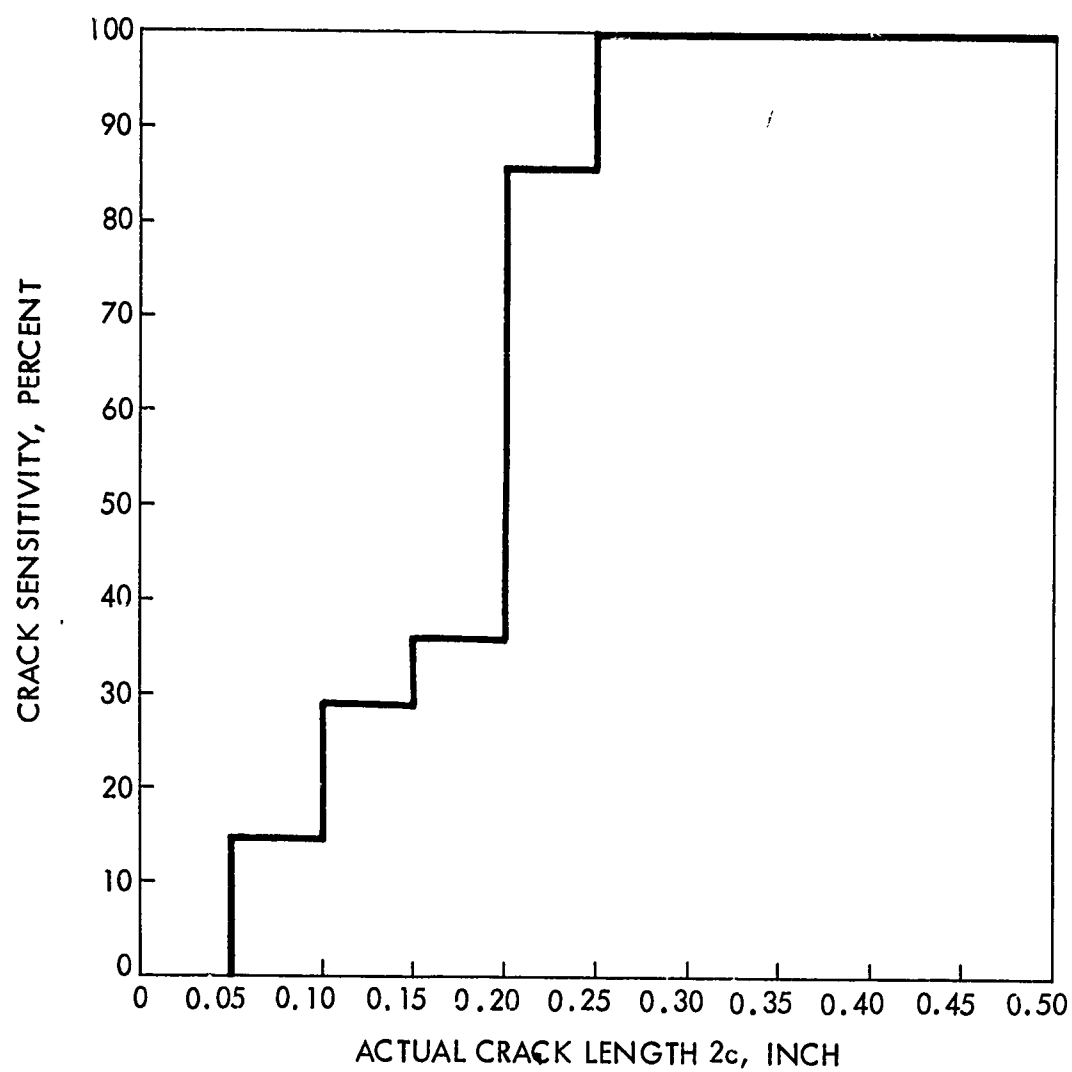
FIGURE 7i – SENSITIVITY OF DYE PENETRANT – ALUMINUM CYLINDERS
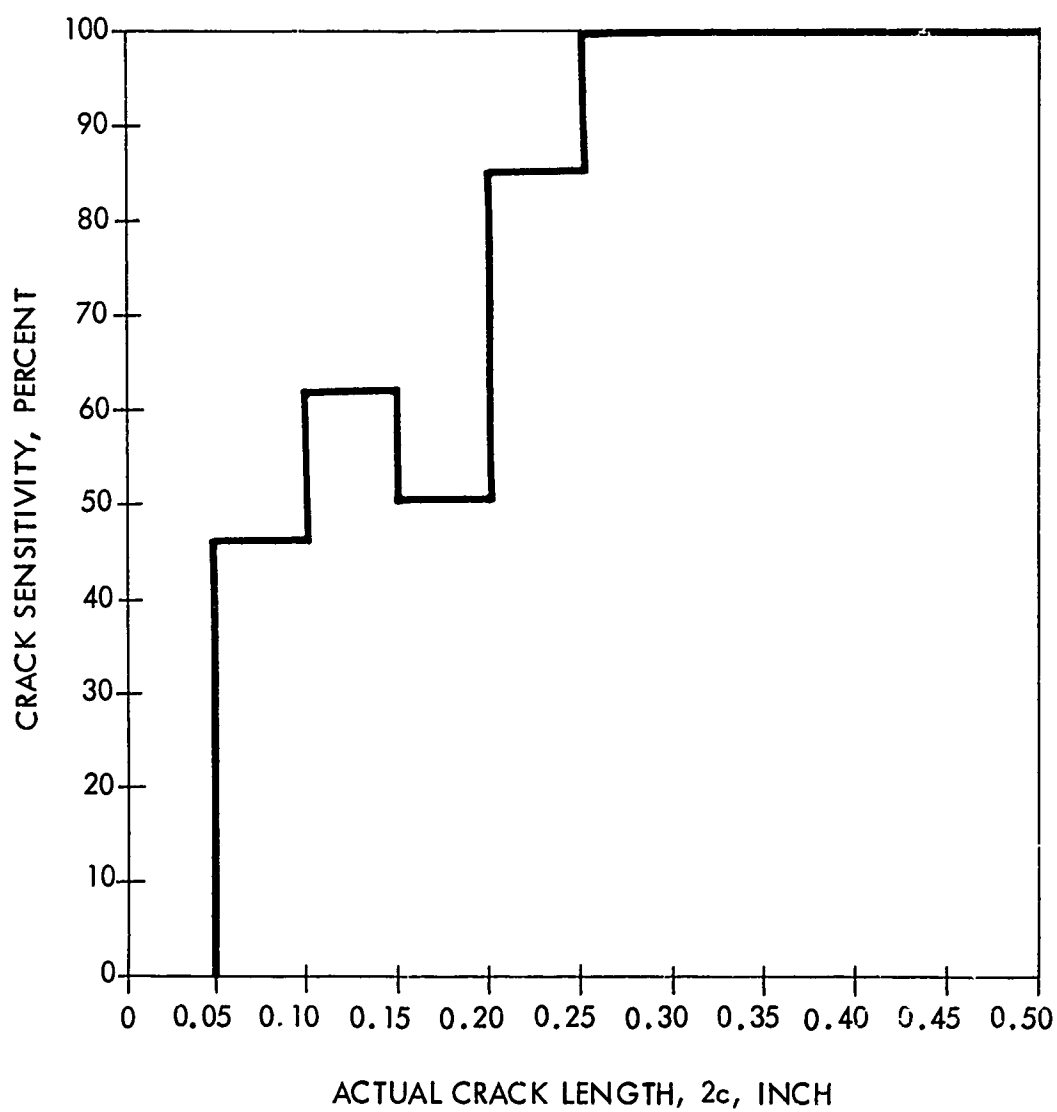
FIGURE 72 - SENSITIVITY OF ULTRASONICS - ALUMINUM CYLINDERS

103

Due to the extremely poor sensitivity of the X-ray method, it was decided not to measure the accuracy of the crack length or crack location obtained using X-rays.

It is interesting to note in Figures 73 and 74 that the accuracy of the crack length is higher using penetrant than using ultrasonics. The penetrant accuracy of crack length varied between 0.75 and 0.92, while only one crack size range (0.05 to 0.10 inch) was poor and gave an accuracy of 0.25. The ultrasonic measurements accuracy was relatively constant, varying between 0.65 and 0.75 for all crack ranges from 0.05 to 0.50 inches. No measurements could be obtained on specimens containing cracks smaller than 0.050 inch.

The accuracy of the crack location by penetrant is shown in Figures 75 and 76. In all cases, the accuracy of location ℓ is greater than 0.98, and the accuracy of θ is higher than 0.92. It appears that, once the crack is found by the penetrant, one can be extremely sure that the indication occurs there and not at some other point.

Figures 77 and 78 show the accuracy of the crack location ℓ and θ, obtained by ultrasonics. Again, all accuracies are greater than 0.95 for ℓ and greater than 0.92 for θ. It is interesting to note that the lowest accuracy of θ obtained was on cracks in the size range of 0.45 to 0.50 inch. This can be seen in both the penetrant and ultrasonic measurements.

Figures 79 and 80 and Table XII give the results of the reliability index for each of the NDT inspection methods used on the 7075-T6511 cylinders. The reliability index of X-rays was obtained only from the sensitivity and is included only for comparison.

The highest reliability index obtained was 0.88. This shows that the reliability that can be placed on NDT is poor at present. Several conclusions can be drawn from the data presented in Figure 81 and Table XII.

Figure 81 is a comparison plot of the reliability index for each of the three NDT methods used in the experimental program. It is evident that, in the small crack sizes from 0.001 to 0.20 inch, all NDT methods have a low reliability index. No values greater than 0.55 were obtained from any method in this crack size range, although the ultrasonics method was better than the penetrant and X-ray methods. This would indicate that the best potential method for detecting small cracks would be ultrasonics. In the intermediate crack size range from 0.20 to 0.45 inch, the penetrant method is superior to both the ultrasonic and X-ray methods. This is surprising, since both the ultrasonic and penetrant methods increase their reliability index in this range.

X-ray is an extremely reliable method for large defects, such as porosity in castings, inclusion and stringers, lack of fusion in weld zones, and other cases where the defect size may exceed 0.5 inch.

NDT Results, 4330V Modified Steel Cylinders

The experimental results obtained from the NDT inspection of the 4330V Modified steel cylinders are shown in Figures 82 to 98 and summarized in Table XIII.

Figures 82 to 85 show the sensitivity of the four NDT methods in detecting fatigue cracks. The sensitivity of the X-ray method in detecting the cracks is poor. The method is not able to detect more than 50% of the cracks even though the crack length is over 0.45 inch. No consistent pattern for X-ray sensitivity variation with crack length could be detected.

The sensitivity of the penetrant system is shown in Figure 83. The sensitivity is greater than that found for the X-ray method of the same cylinders. For crack sizes above 0.35 inch,

104
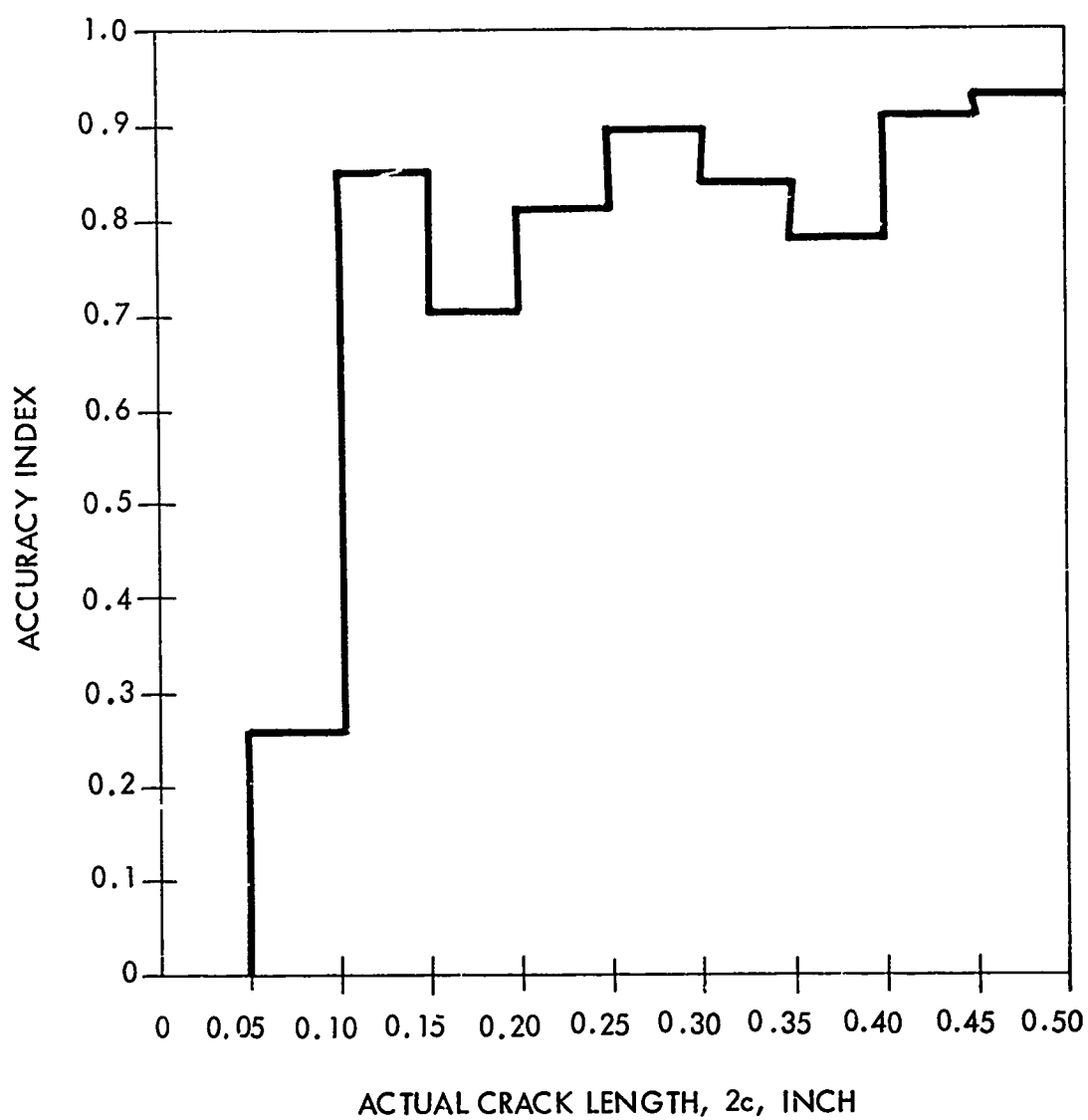
FIGURE 73 - ACCURACY OF CRACK LENGTH INDICATION, 2c, DYE PENETRANT -
ALUMINUM CYLINDERS

105
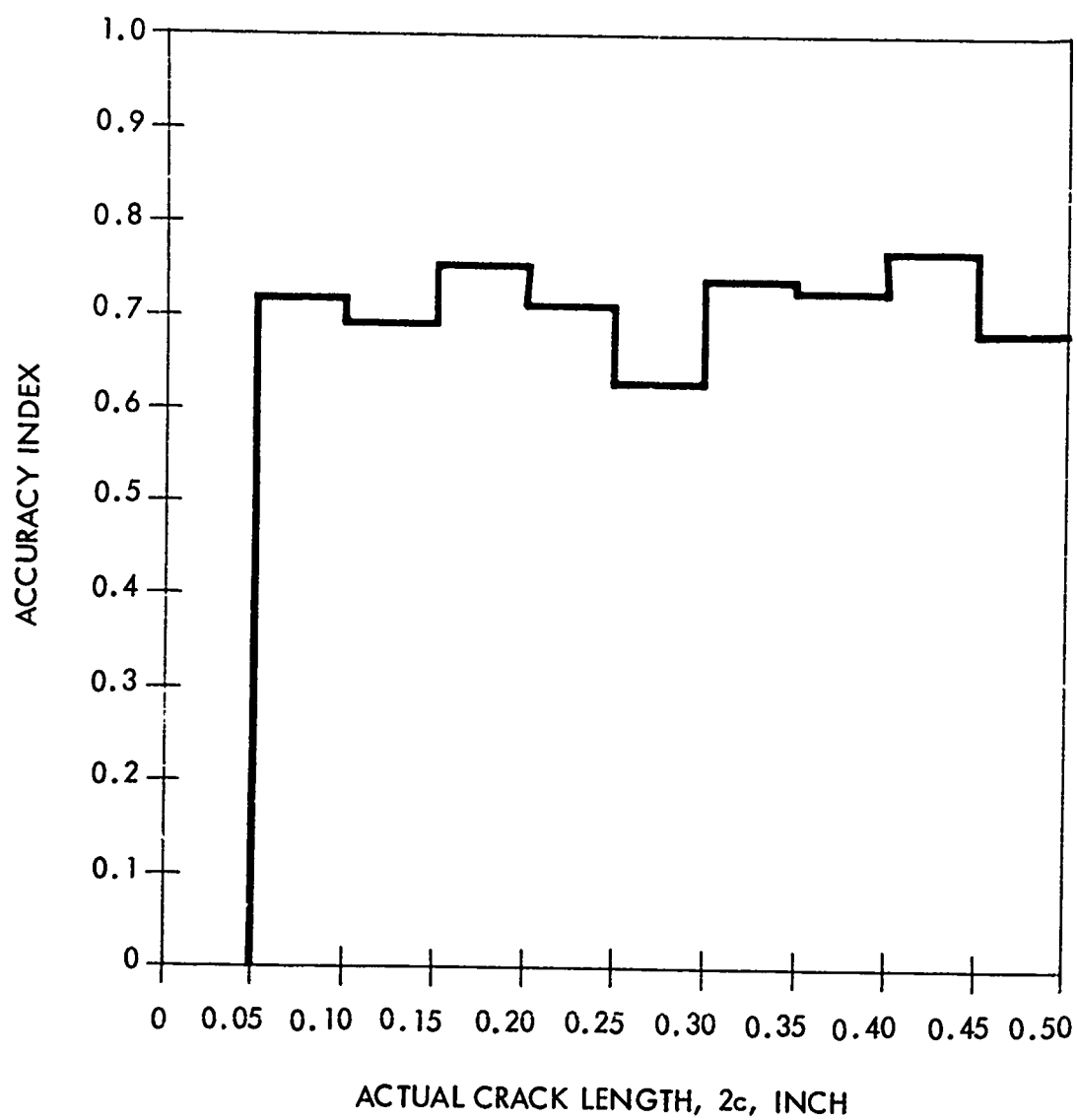
FIGURE 74 – ACCURACY OF CRACK LENGTH INDICATION, 2c, ULTRASONICS –
ALUMINUM CYLINDERS
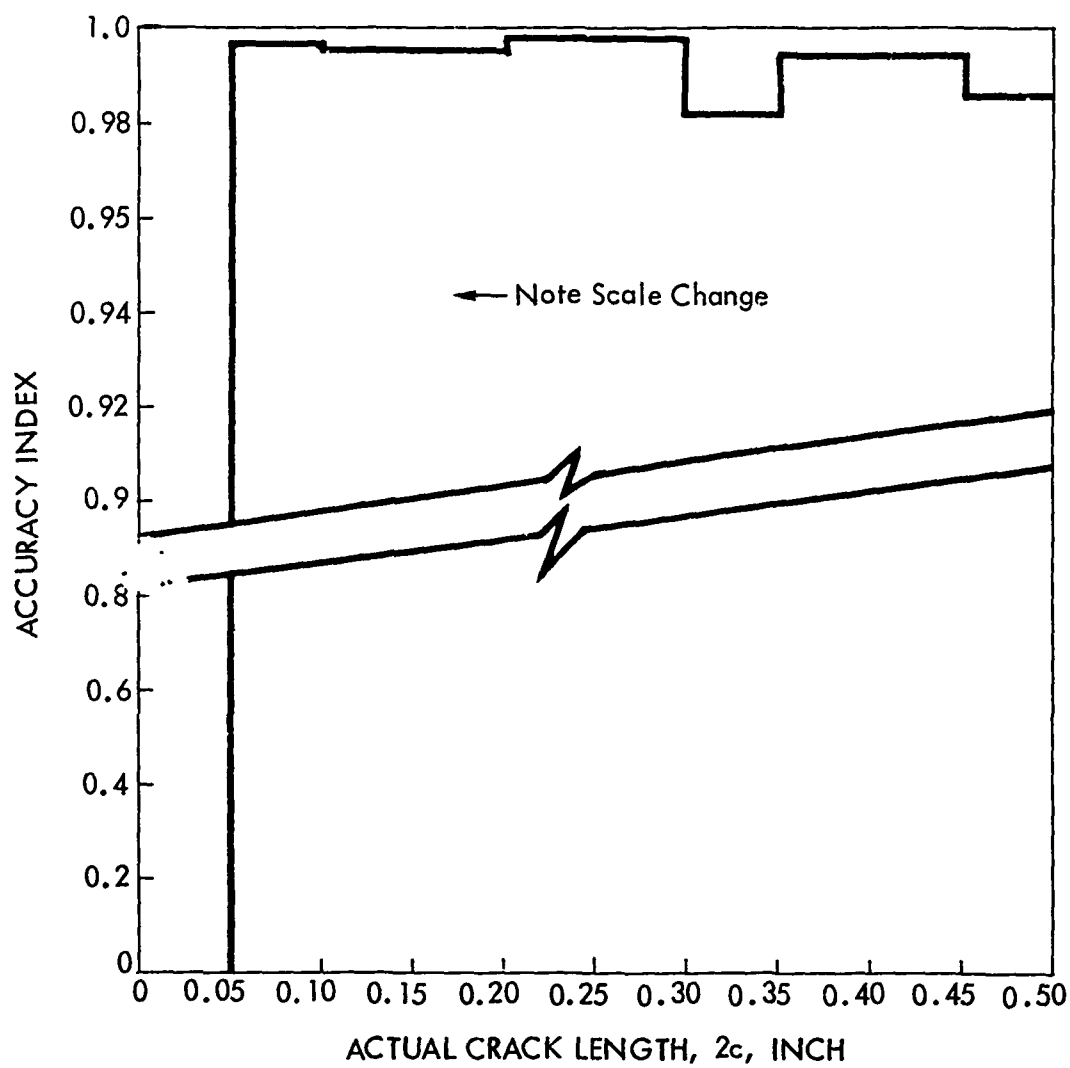
FIGURE 75 – ACCURACY OF CRACK LOCATION, ℓ , DYE PENETRANT – ALUMINUM CYLINDERS

107
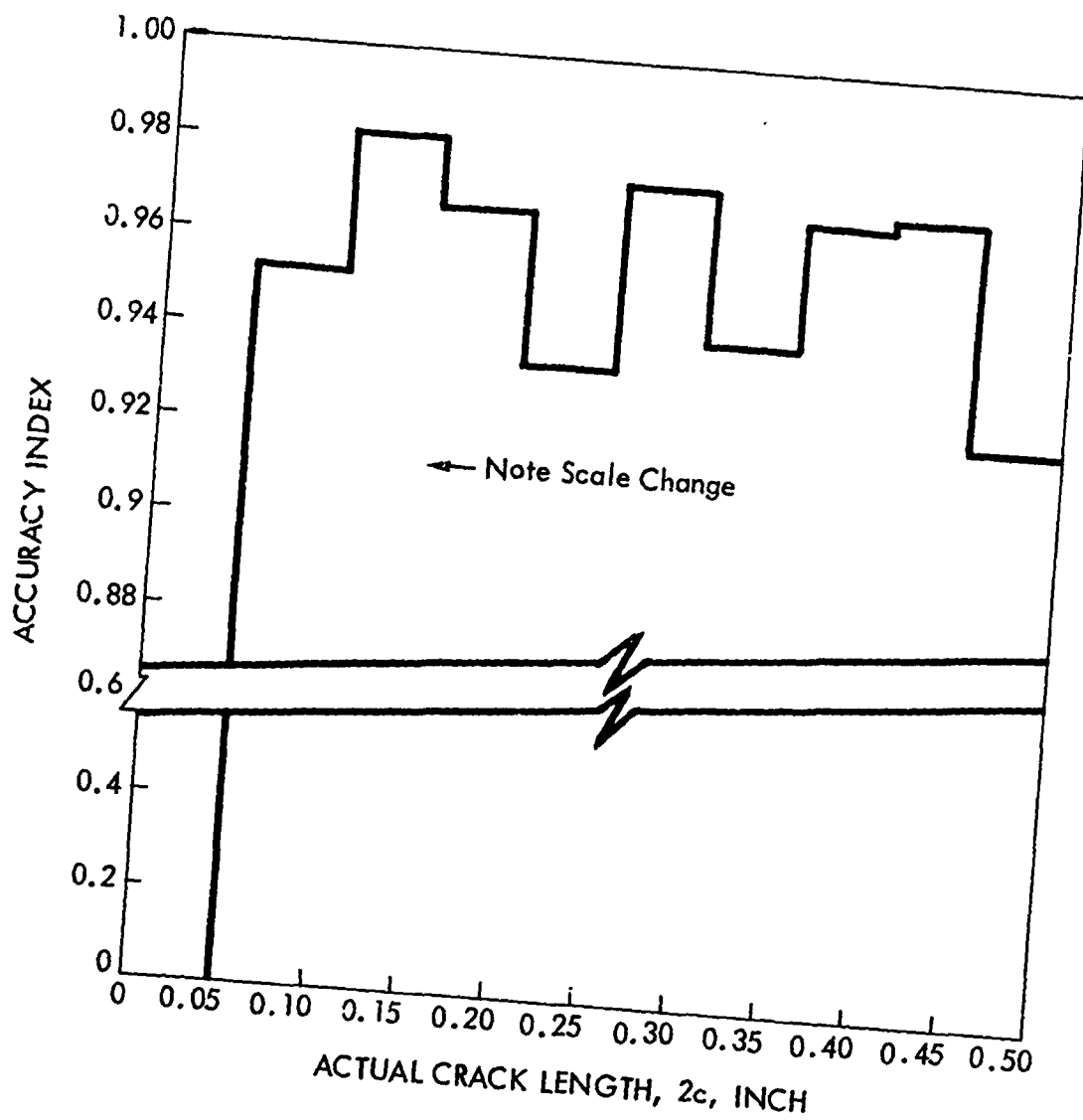
FIGURE 76 — ACCURACY OF CRACK LOCATION ANGLE, θ , DYE PENETRANT
ALUMINUM CYLINDERS
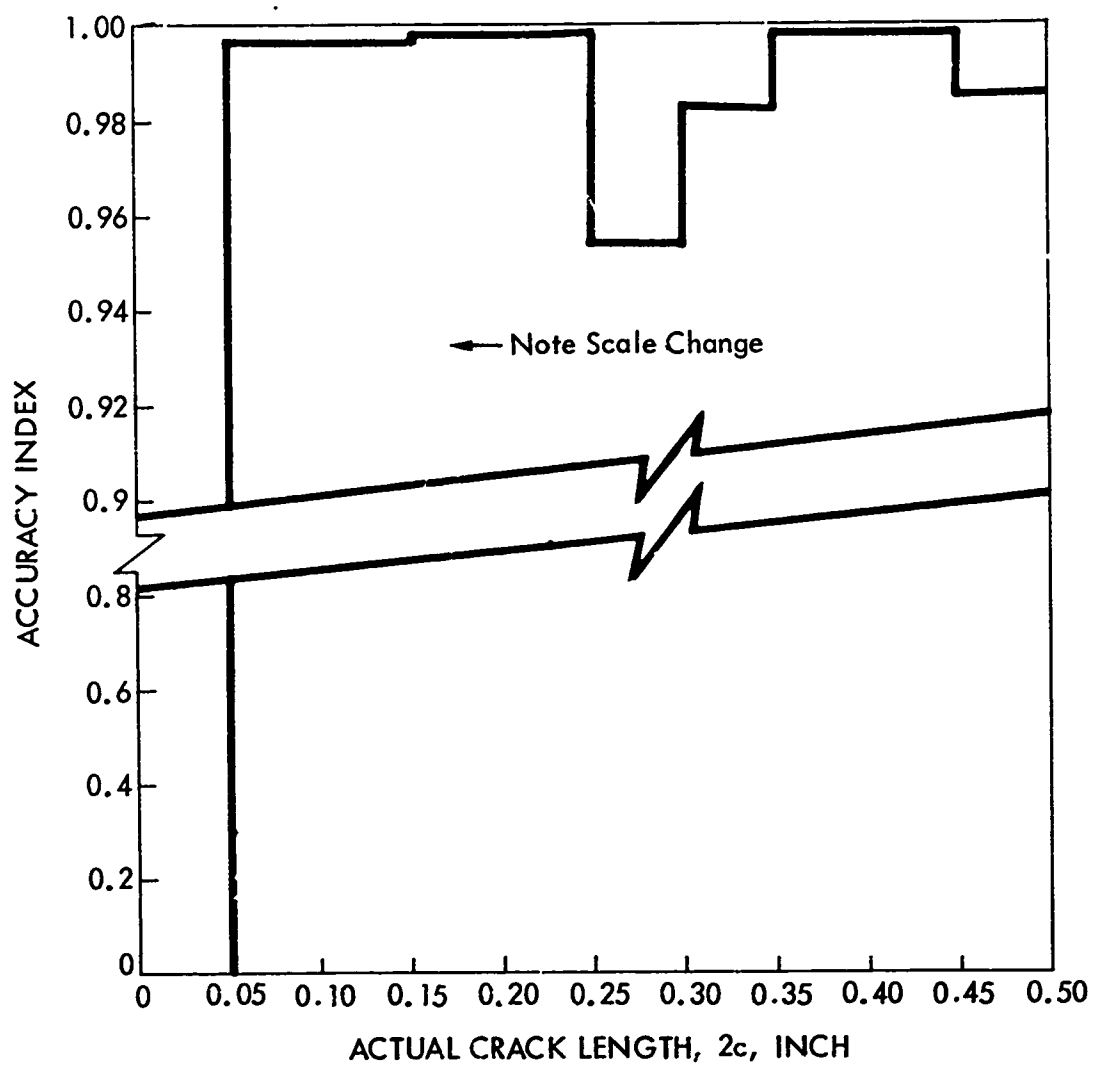
FIGURE 77 — ACCURACY OF CRACK LOCATION ℓ, ULTRASONICS –
ALUMINUM CYLINDERS
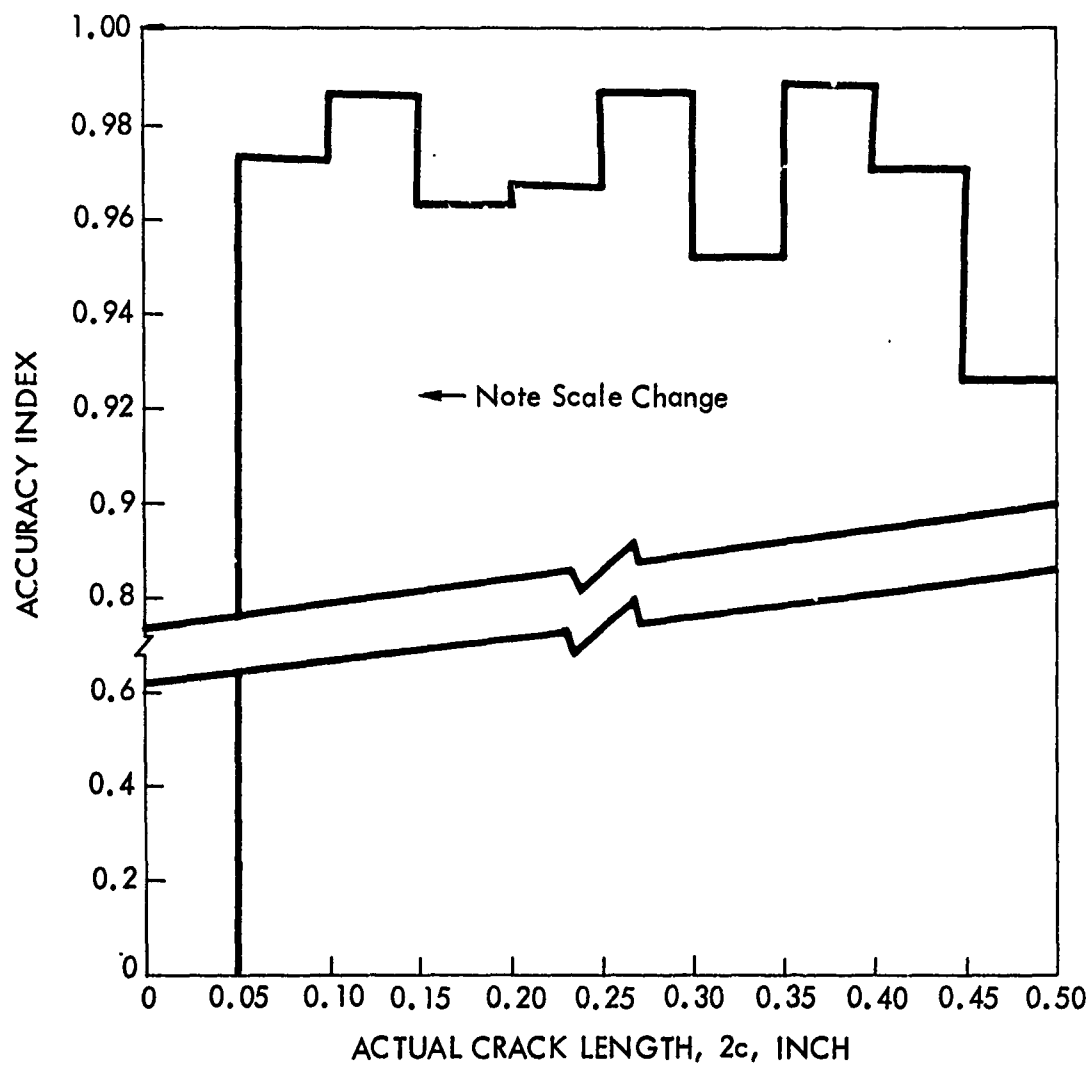
FIGURE 78 – ACCURACY OF CRACK LOCATION ANGLE, θ , ULTRASONICS
ALUMINUM CYLINDERS

110
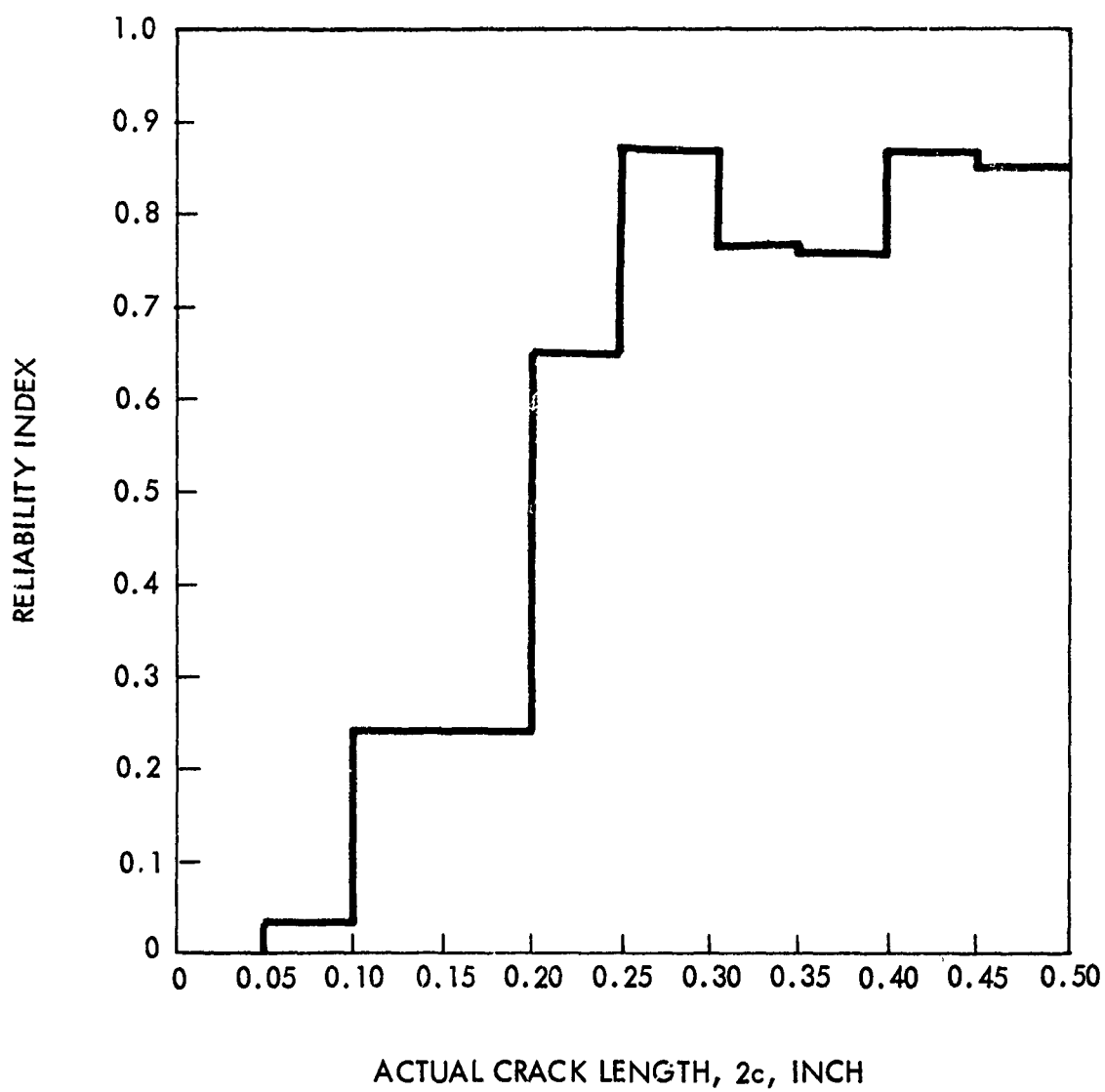
FIGURE 79   RELIABILITY INDEX DYE PENETRANT – ALUMINUM CYLINDERS

111
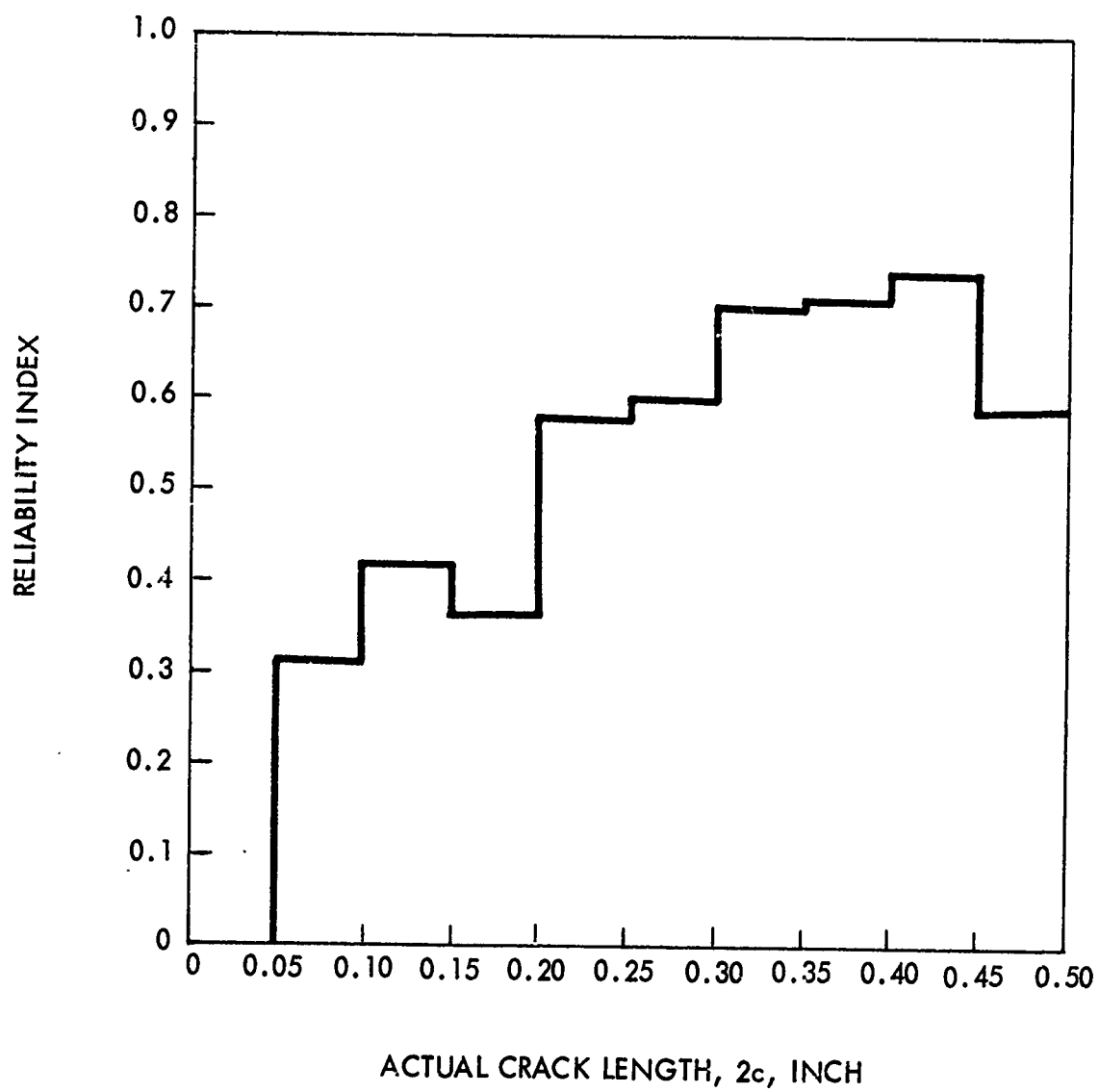
FIGURE 80   RELIABILITY INDEX, ULTRASONICS – ALUMINUM CYLINDERS

112
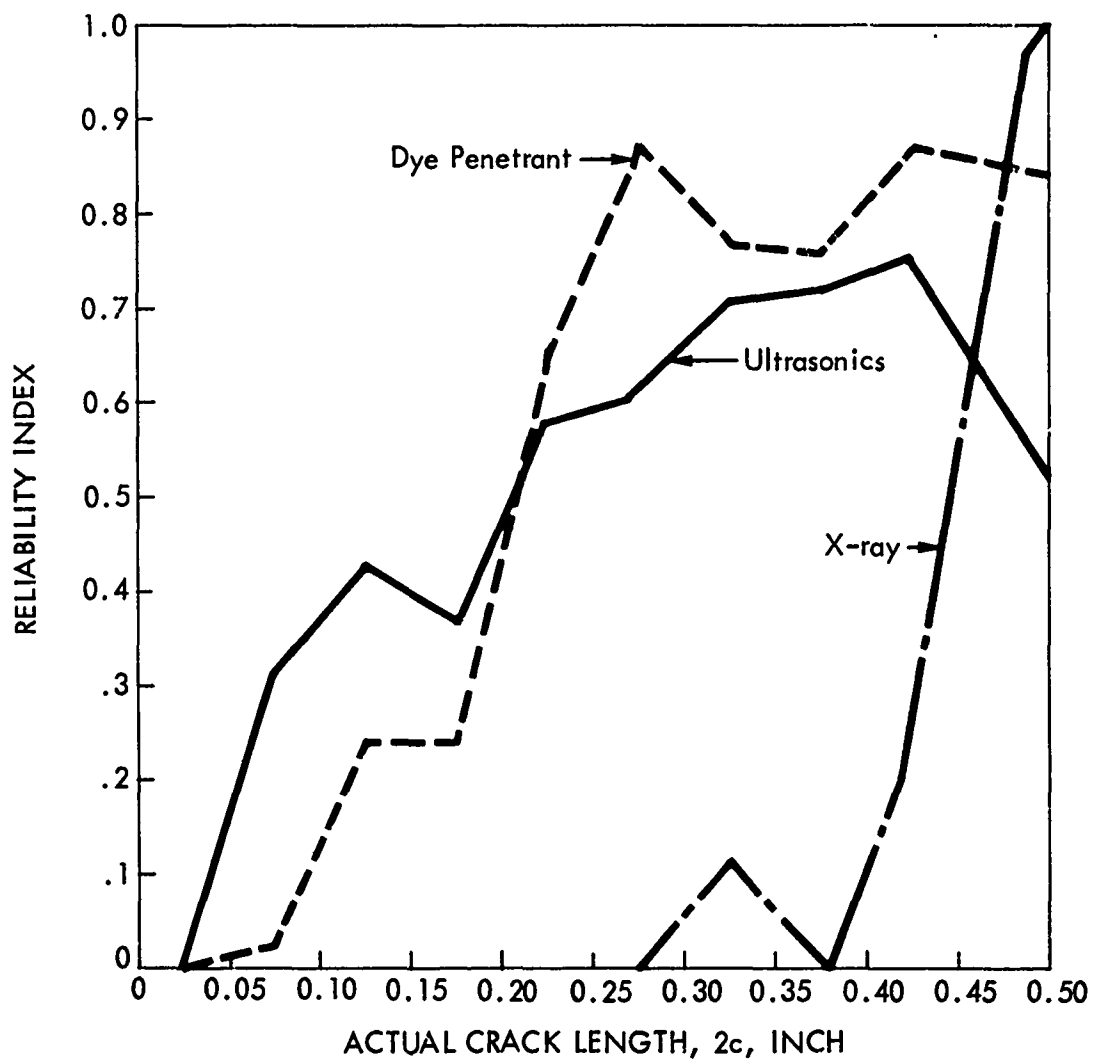
FIGURE 81 COMPARISON OF 3 NDT METHODS ON RELIABILITY OF FLAW
INDICATIONS IN ALUMINUM CYLINDERS

113

TABLE XIII

RELIABILITY INDICES FOR NDT INSPECTION OF STEEL CYLINDERS

Actual crack range (2c) (inch)	Accuracy									Sensitivity				Reliability index			
	Penetrant			Ultrasonics			Magnetic particle			Penetrant	Ultrasonics	Magnetic particle	X-ray	Penetrant	Ultrasonics	Magnetic particle	X-ray
	Crack length	Crack location ℓ	Crack location θ	Crack length	Crack location ℓ	Crack location θ	Crack length	Crack location ℓ	Crack location θ								
No crack	---	---	---	---	---	---	---	---	---	0.8889	0.7778	0.7778	---	---	---	---	---
0.001-0.050	0.0000	0.0000	0.0000	0.0000	0.0000	0.0000	0.0000	0.0000	0.0000	0.1111	0.2222	0.2222	0.390	---	---	---	---
0.051-0.100	0.3587	0.9972	0.9822	0.6632	0.9929	0.9882	0.4130	0.9979	0.9869	0.4000	0.4000	0.6000	0.0000	0.1405	0.2615	0.2426	0.0000
0.101-0.150	0.6381	0.9976	0.9894	0.6987	0.9972	0.9038	0.4527	0.9972	0.9459	0.5333	0.8000	0.9333	0.0000	0.2099	0.5038	0.3985	0.0000
0.151-0.200	0.2220	0.9760	0.9757	0.6493	0.9969	0.9841	0.8564	0.9966	0.9878	0.3000	0.9000	0.9333	0.0000	0.0647	0.5733	0.7868	0.0000
0.201-0.250	0.7731	0.9987	0.9563	0.6687	0.9962	0.9811	0.8097	0.9976	0.9837	0.6000	1.0000	0.9000	0.0000	0.4430	0.6836	0.7151	0.0000
0.251-0.300	0.7652	0.9986	0.9884	0.7478	0.9966	0.9885	0.7503	0.9984	0.9898	0.7978	1.0000	0.8889	0.2222	0.5874	0.7367	0.6591	0.2222
0.301-0.350	0.7571	0.9981	0.9621	0.6639	0.9984	0.9871	0.7838	0.9968	0.9704	0.6250	0.8750	1.0000	0.1250	0.4544	0.5725	0.7582	0.1250
0.351-0.400	0.8880	0.9850	0.9422	0.5793	0.9968	0.9448	0.7483	0.9979	0.9545	1.0000	1.0000	1.0000	0.0000	0.8241	0.5456	0.7128	0.0000
0.401-0.450	0.5491	0.9988	0.8970	0.6484	0.9784	0.9105	0.7917	0.9989	0.9513	1.0000	1.0000	1.0000	0.0000	0.4920	0.5776	0.7523	0.0000
0.451-0.500	0.8007	0.9970	0.8424	0.5458	0.9977	0.9307	0.8408	0.9984	0.9872	1.0000	1.0000	1.0000	0.5000	0.6725	0.5068	0.8287	0.5000
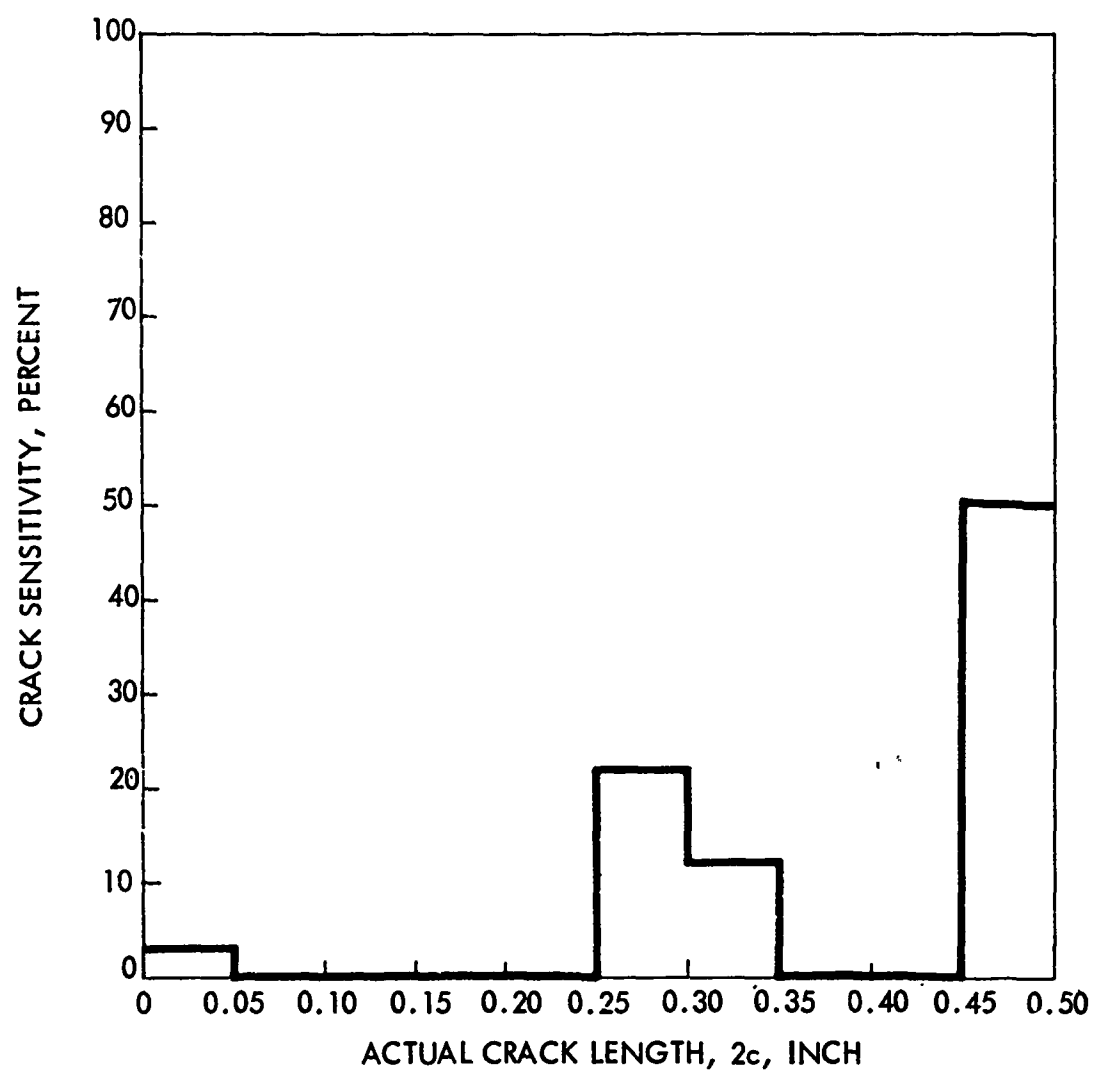
FIGURE 82   SENSITIVITY OF X-RAY METHOD – STEEL CYLINDERS
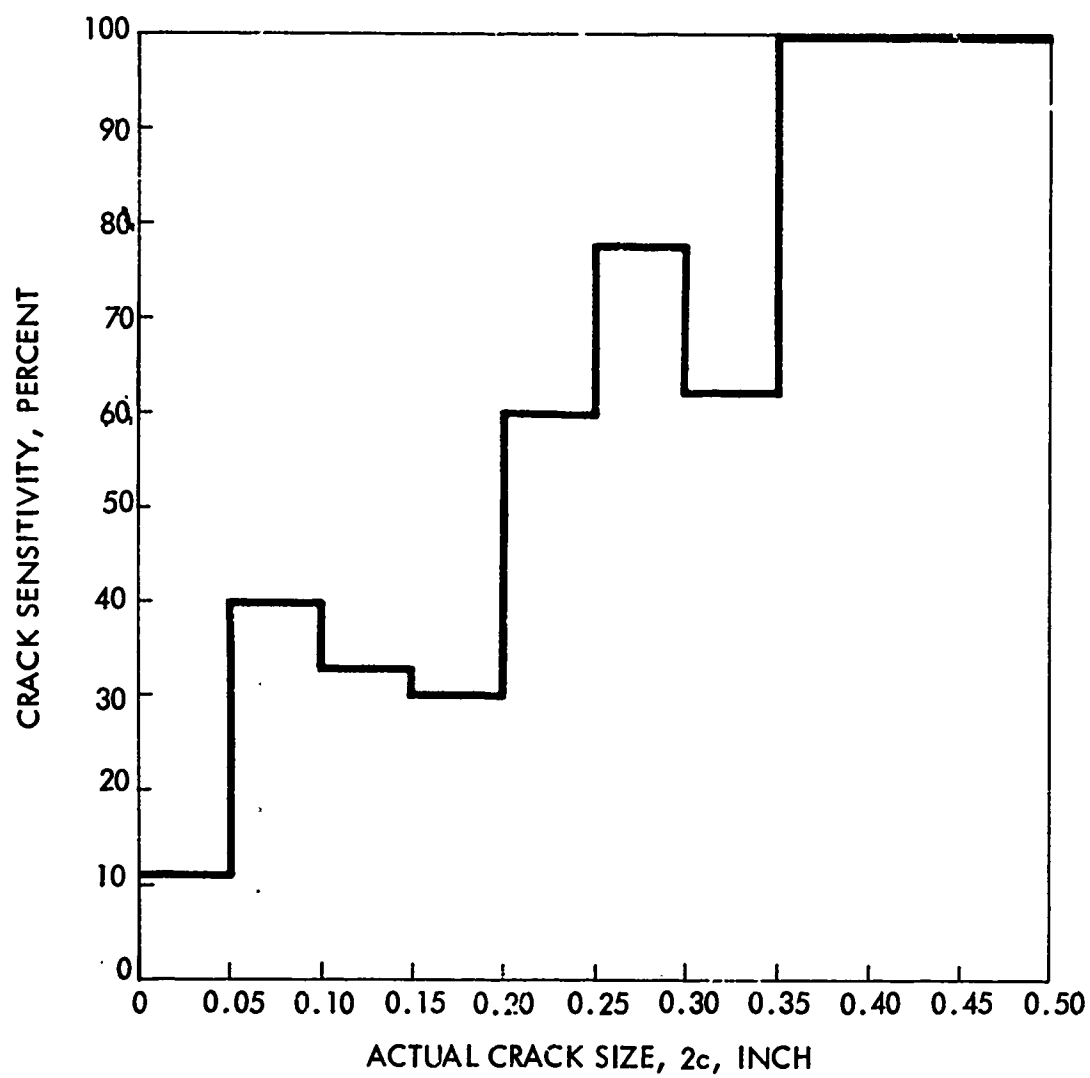
FIGURE 83   SENSITIVITY OF PENETRANT METHOD – STEEL CYLINDERS

116

100% of the cracks were detected. The sensitivity increases from 22% for cracks 0.05 inch long to a maximum of 78% as the crack size increases to 0.30 inch. There is a drop in sensitivity in the crack size range from 0.30 to 0.35 inch.

Figure 84 shows the sensitivity of the magnetic particle method. This method consistently exhibits a high sensitivity in all crack sizes above 0.05 inch. For cracks in the size range of 0.10 to 0.30 inch, about 90% of the cracks were detected. For cracks larger than 0.30 inch, 100% were detected. As was expected, the sensitivity dropped as the crack size decreased.

The ultrasonic sensitivity is shown in Figure 85. The sensitivity increases from 22% at small crack sizes to 100% for cracks larger than 0.20 inch. There is a drop in sensitivity in the crack range from 0.30 to 0.35 inch. This may be due to the particular combination of transducer size and operating frequency. However, the ultrasonic method appears to be sensitive in all of the crack sizes investigated.

Because of the poor sensitivity of the X-ray method, it was also decided not to measure the accuracy of the crack length and crack location of the steel specimens.

Figures 86 to 88 show the accuracy of the indicated crack length obtained using penetrant, magnetic-particle, and ultrasonic inspection methods. For crack lengths from 0.20 to 0.50 inch, both penetrant and magnetic particle methods are approximately equal in accuracy. However, magnetic-particle accuracies are less erratic than the penetrant accuracies. The penetrant accuracy drops to 0.55 for cracks in the 0.40 to 0.45 inch range. Penetrant inspection appears superior to magnetic-particle inspection in the 0.10 to 0.15 inch range. This result appears to be accidental, since the magnetic-particle method shows higher accuracies for other crack sizes. The ultrasonic crack length accuracies, Figure 88, appear to be the most consistent over the entire crack size range. No accurate indications were found for cracks less than 0.05 inch. For crack lengths greater than 0.05 inch, the accuracy of crack indication increases to 0.66.

The accuracy of crack location by penetrant is shown in Figures 89 and 90. In all cases the accuracy of location l is greater than 0.98; the accuracy of θ decreases as the crack length increases. Figure 90 shows that the decrease in accuracy is continuous as the crack length increases.

Figures 91 and 92 show the accuracy of crack location l and θ obtained using the magnetic-particle method. This method appears to have a high accuracy. The accuracies are greater than 0.995 for location l, and vary from 0.95 to 0.99 for θ. The accuracy of θ remains essentially the same throughout the whole crack size range and does not decrease for increasing crack sizes as much as do the penetrant accuracies.

The accuracy of the crack location by ultrasonics is shown in Figures 93 and 94. The accuracy of location l is high, over 0.99 for most crack sizes. The accuracy of θ is erratic, varying from 0.92 to 0.99 with a slight decrease in accuracy as the crack size increases.

Figures 95 to 98 and Table XIII summarize the results of the reliability indices for each of the NDT methods used to inspect the 4330V Modified steel cylinder. The highest reliability index obtained was 0.83. The results show that NDT techniques must be improved if they are to be used in conjunction with an FM analysis.

Figure 98 shows a comparison of the reliability index of all four NDT methods used on the 4330V Modified steel cylinders. No definite trends are evident, since the results overlap each other. However, several interesting conclusions can be drawn. It can be seen that

117
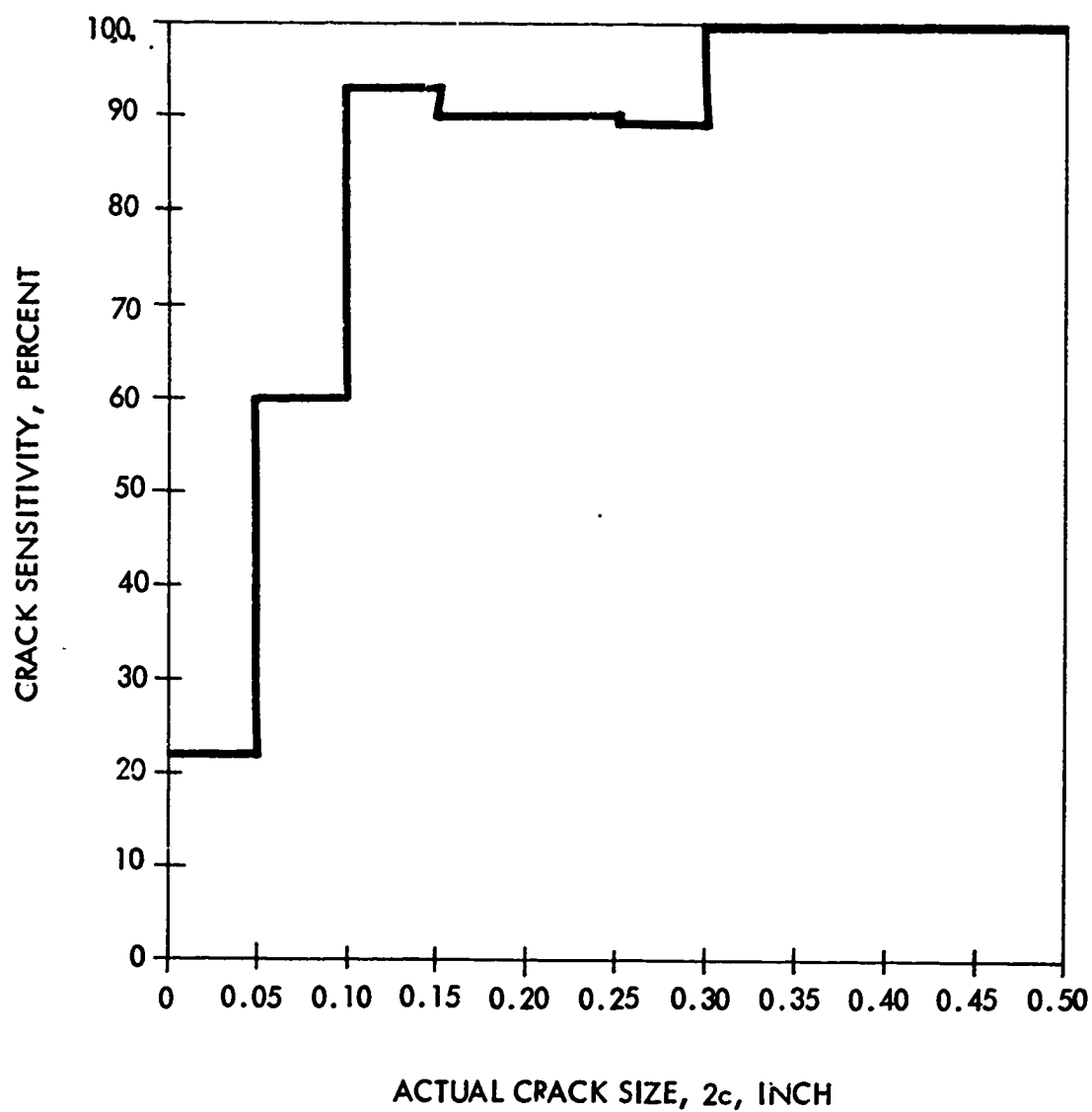
FIGURE 84   SENSITIVITY OF MAGNETIC PARTICLE METHOD – STEEL CYLINDERS
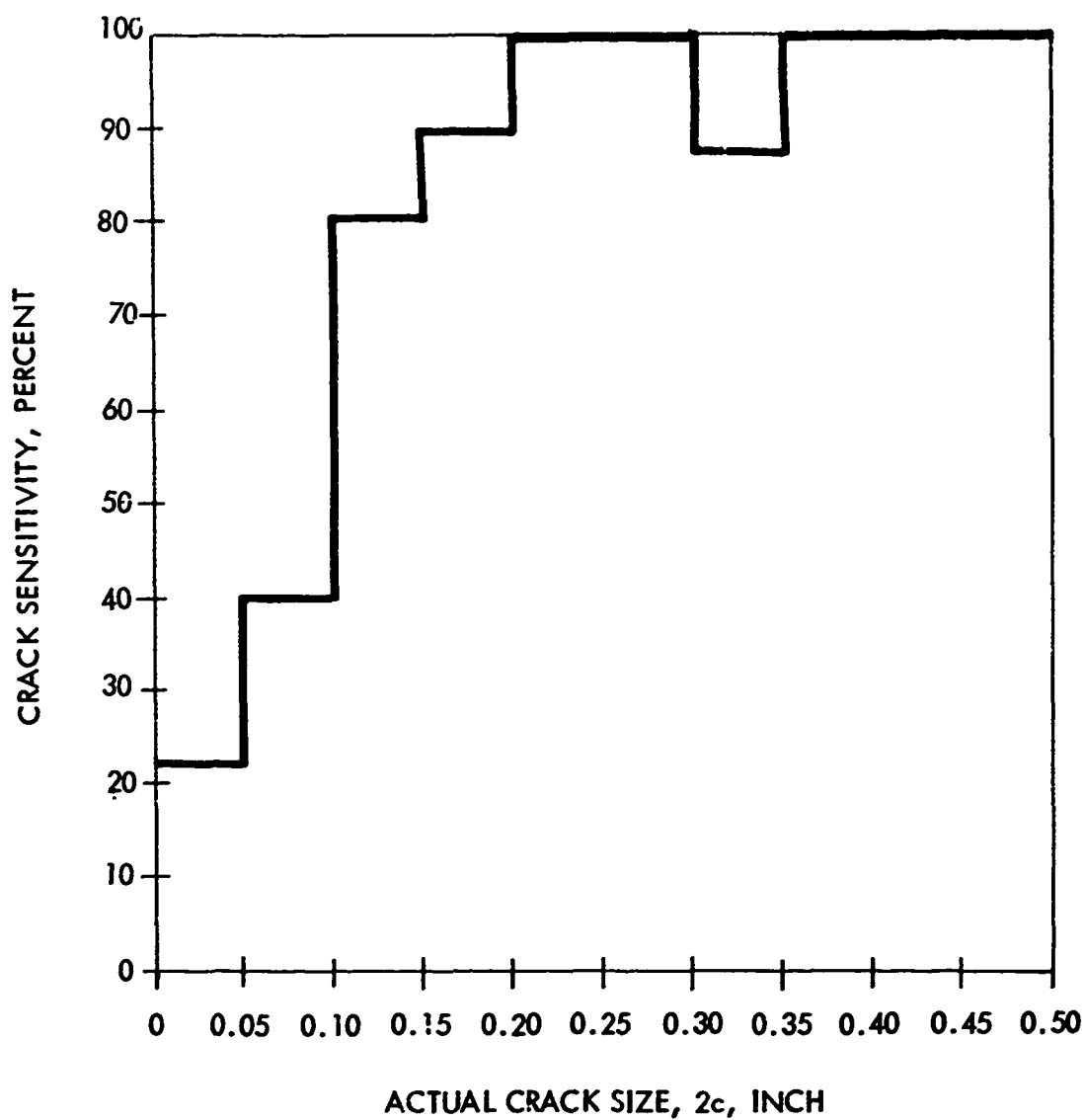
FIGURE 85   SENSITIVITY OF ULTRASONICS METHOD - STEEL CYLINDERS
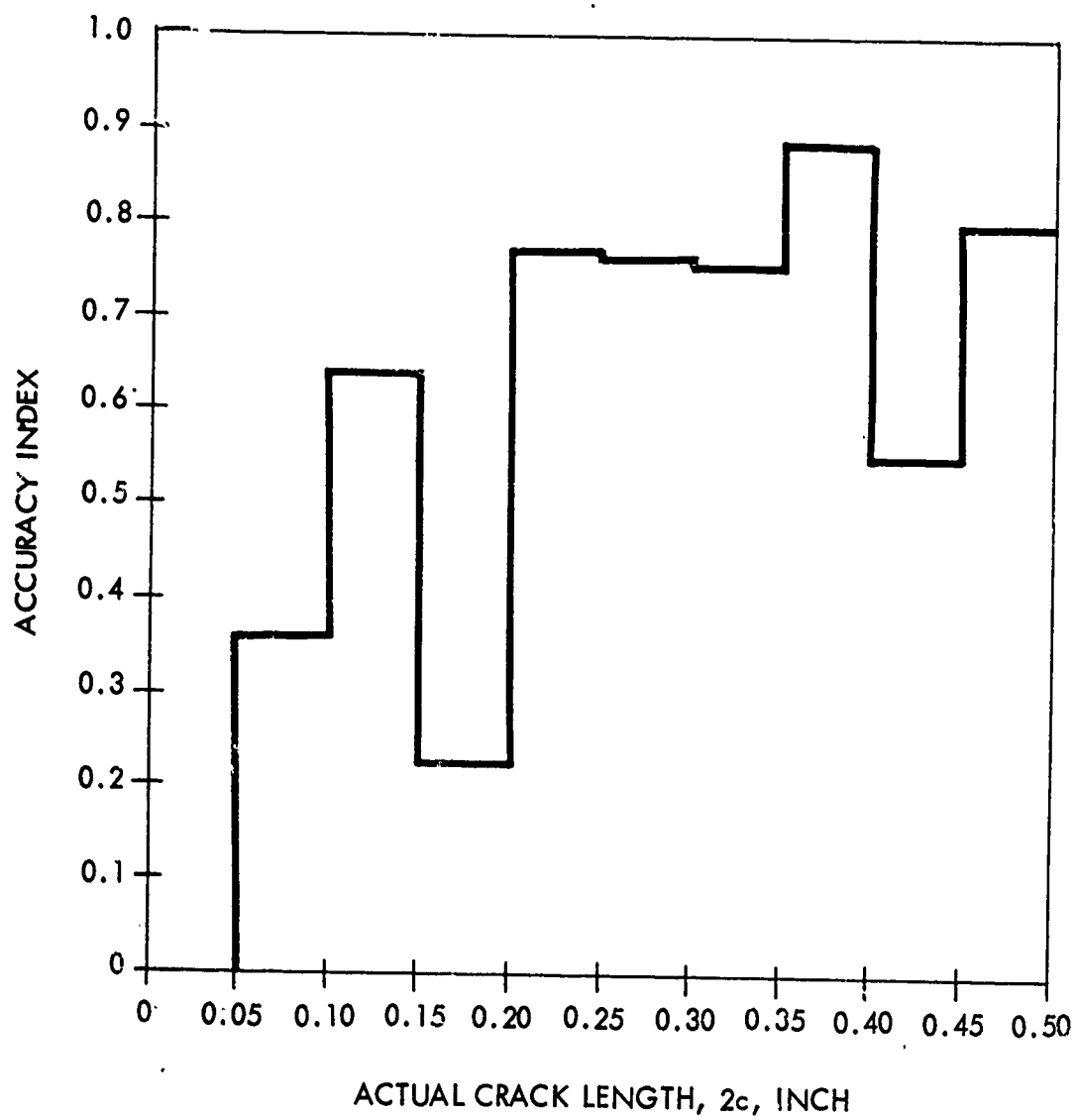
FIGURE 86   ACCURACY OF CRACK LENGTH, 2c, DYE PENETRANT –
STEEL CYLINDERS

120
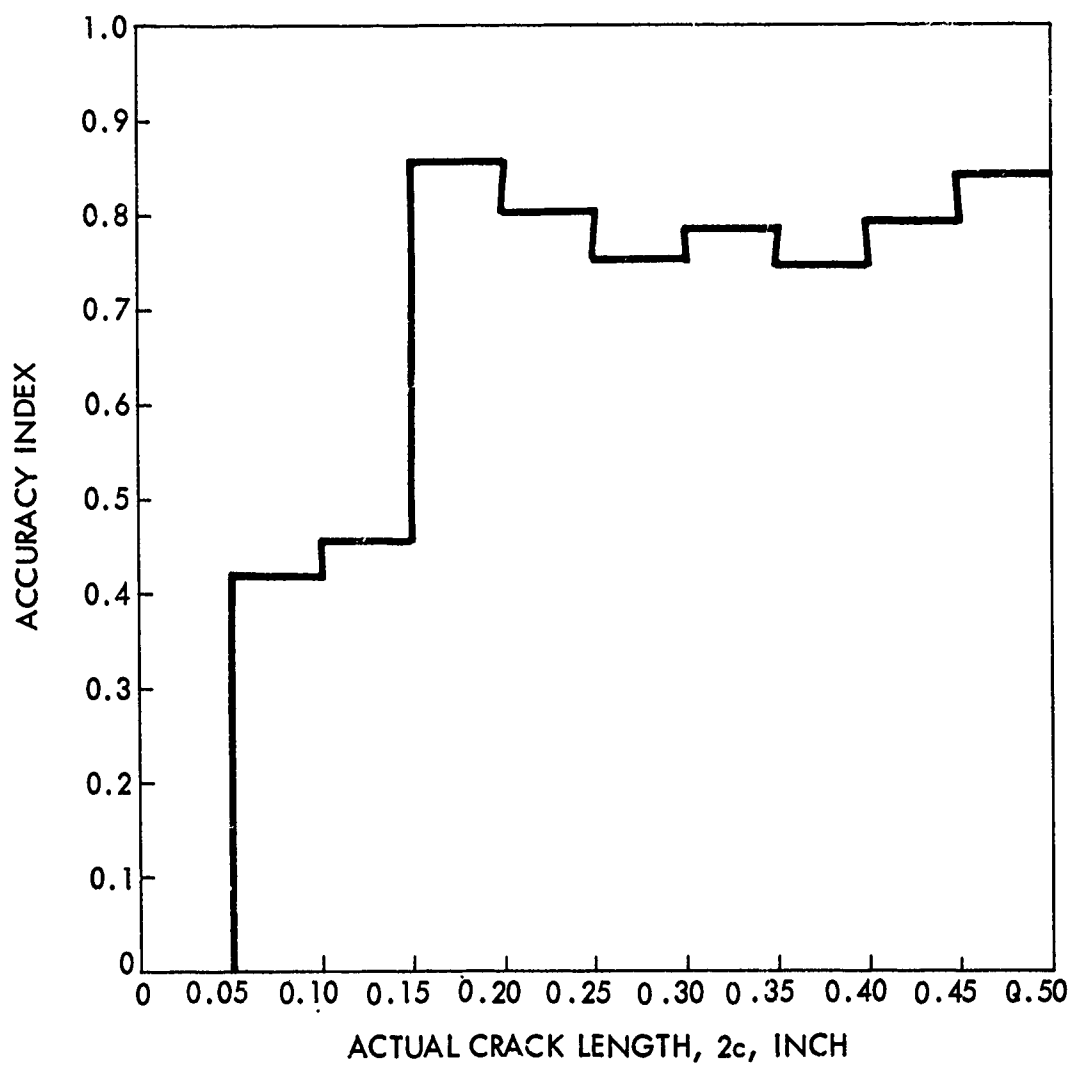
FIGURE 87 ACCURACY OF CRACK LENGTH, 2c, MAGNETIC PARTICLE –
STEEL CYLINDERS
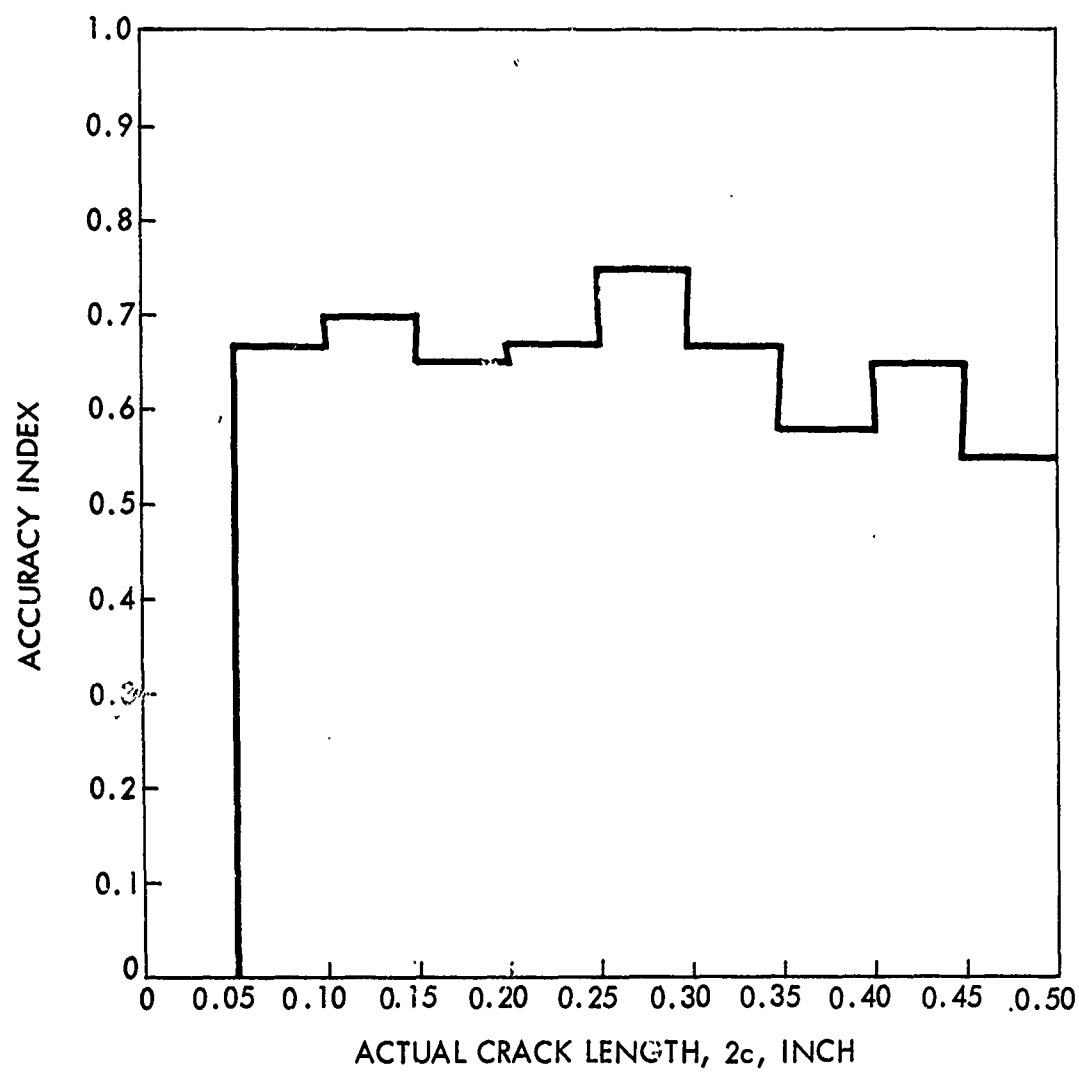
FIGURE 88 ACCURACY OF CRACK LENGTH, 2c, ULTRASONICS –
STEEL CYLINDERS
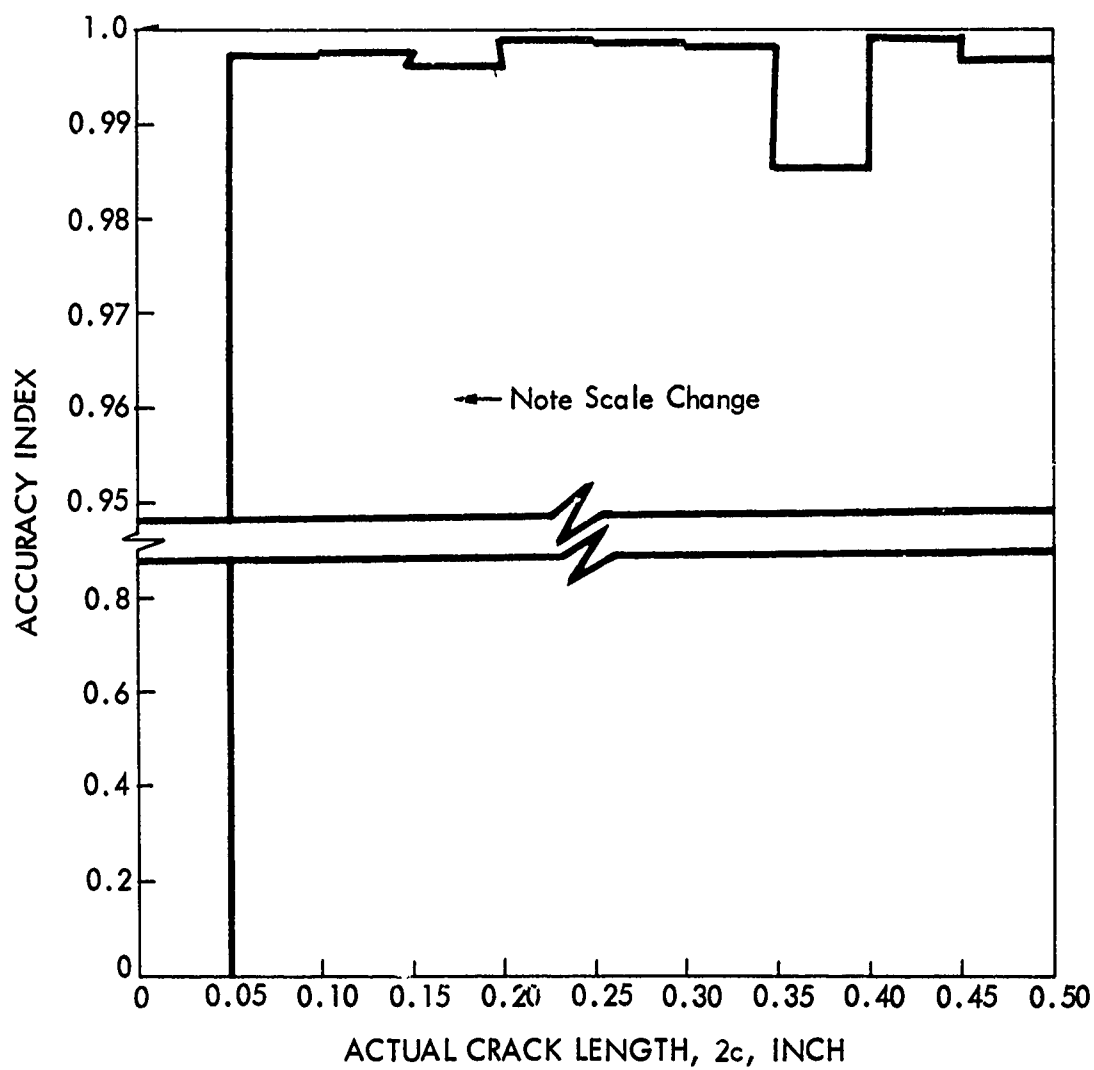
FIGURE 89   ACCURACY OF CRACK LOCATION, ℓ, DYE PENETRANT
STEEL CYLINDERS

123
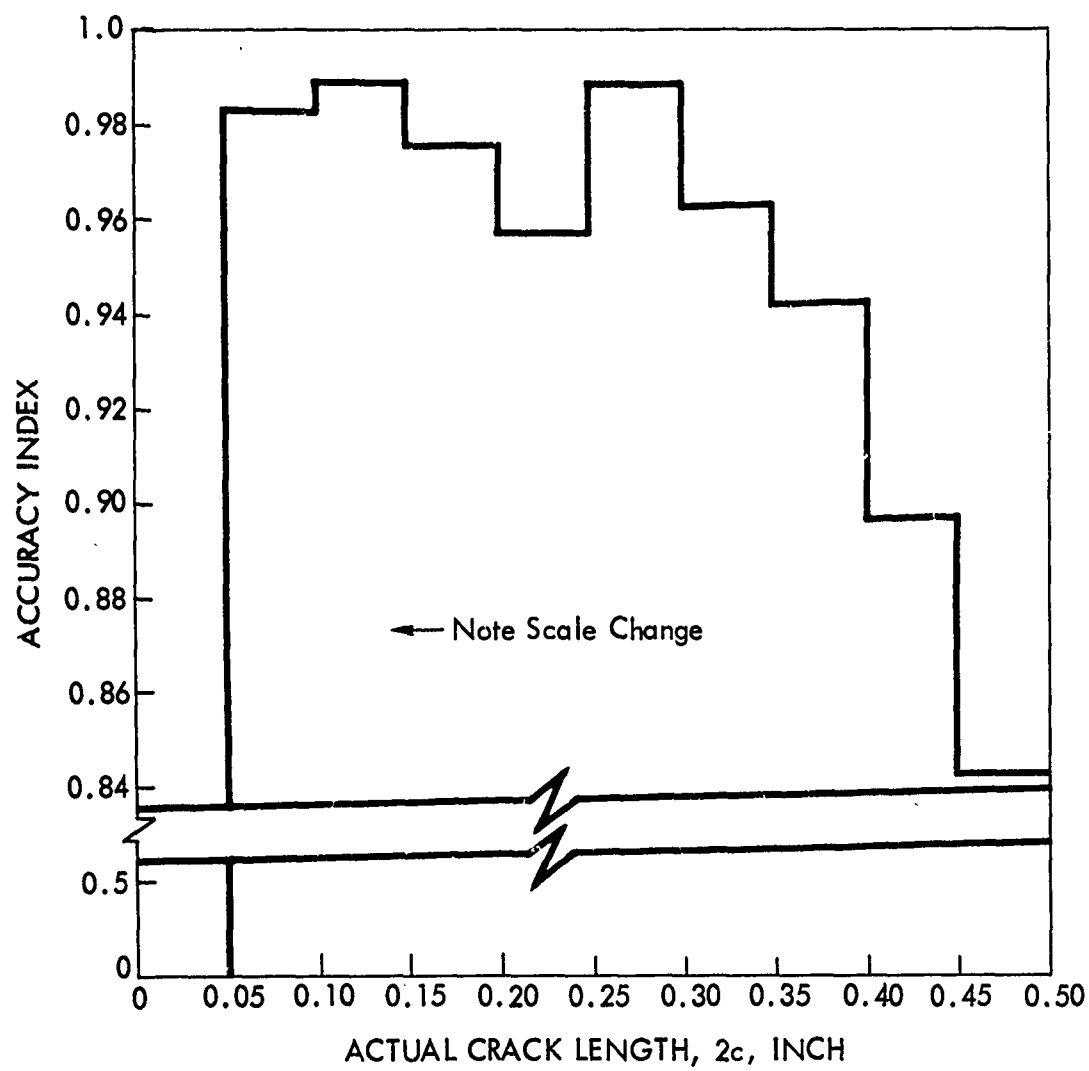
FIGURE 90   ACCURACY OF CRACK LOCATION ANGLE, θ,
            DYE PENETRANT - STEEL CYLINDERS
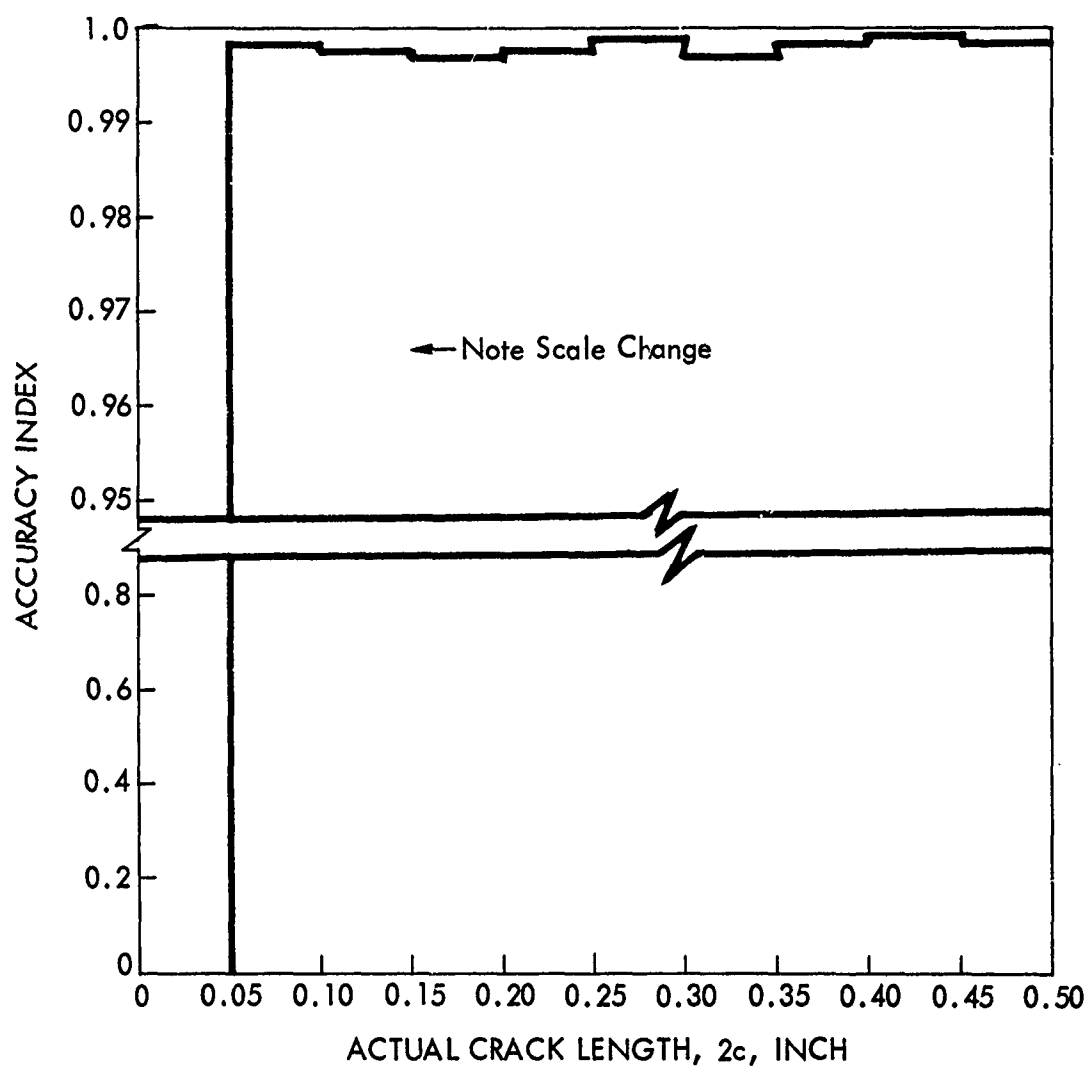
FIGURE 91 ACCURACY OF CRACK LOCATION, ℓ, MAGNETIC PARTICLE –
STEEL CYLINDERS
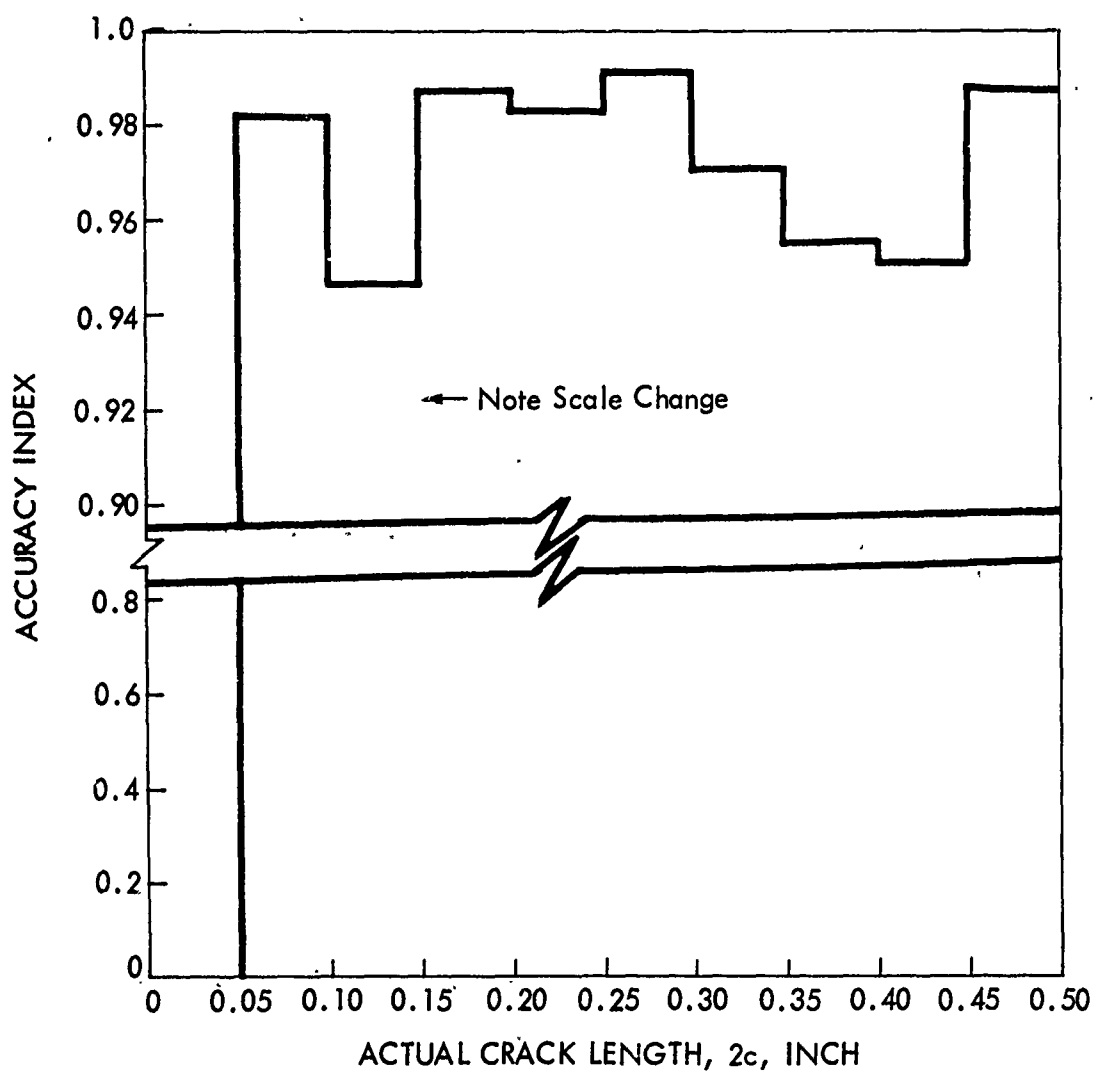
FIGURE 92   ACCURACY OF CRACK LOCATION ANGLE, θ,
MAGNETIC PARTICLE - STEEL CYLINDERS
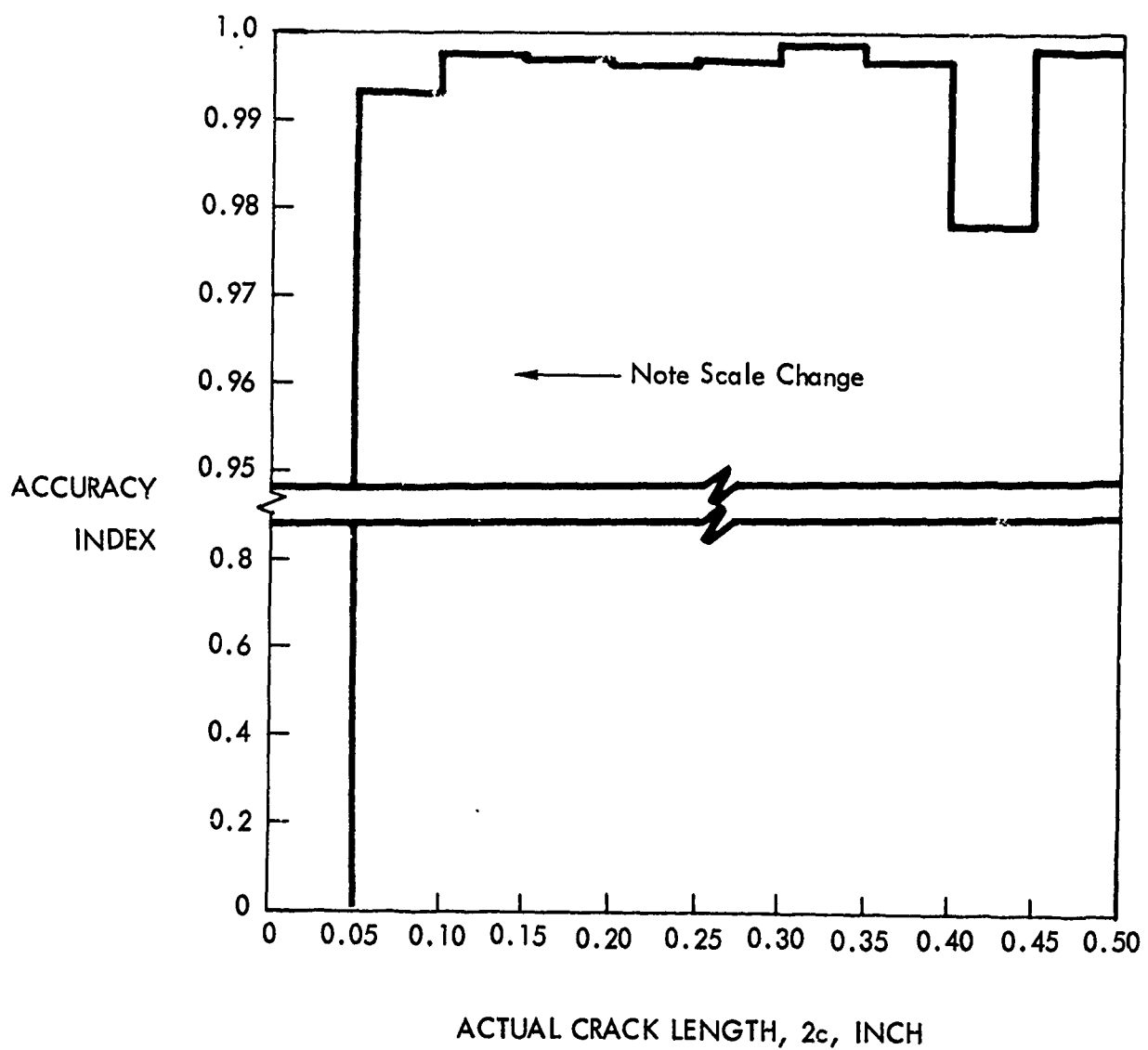
FIGURE 93   ACCURACY OF CRACK LOCATION, ℓ,
ULTRASONICS – STEEL CYLINDERS

ACCURACY INDEX

1.0
0.98
0.96
0.94
0.92
0.90
0.8
0.6
0.4
0.2
0

Note Scale Change

0   0.05   0.10   0.15   0.20   0.25   0.30   0.35   0.40   0.45   0.50

ACTUAL CRACK LENGTH, 2c, INCH
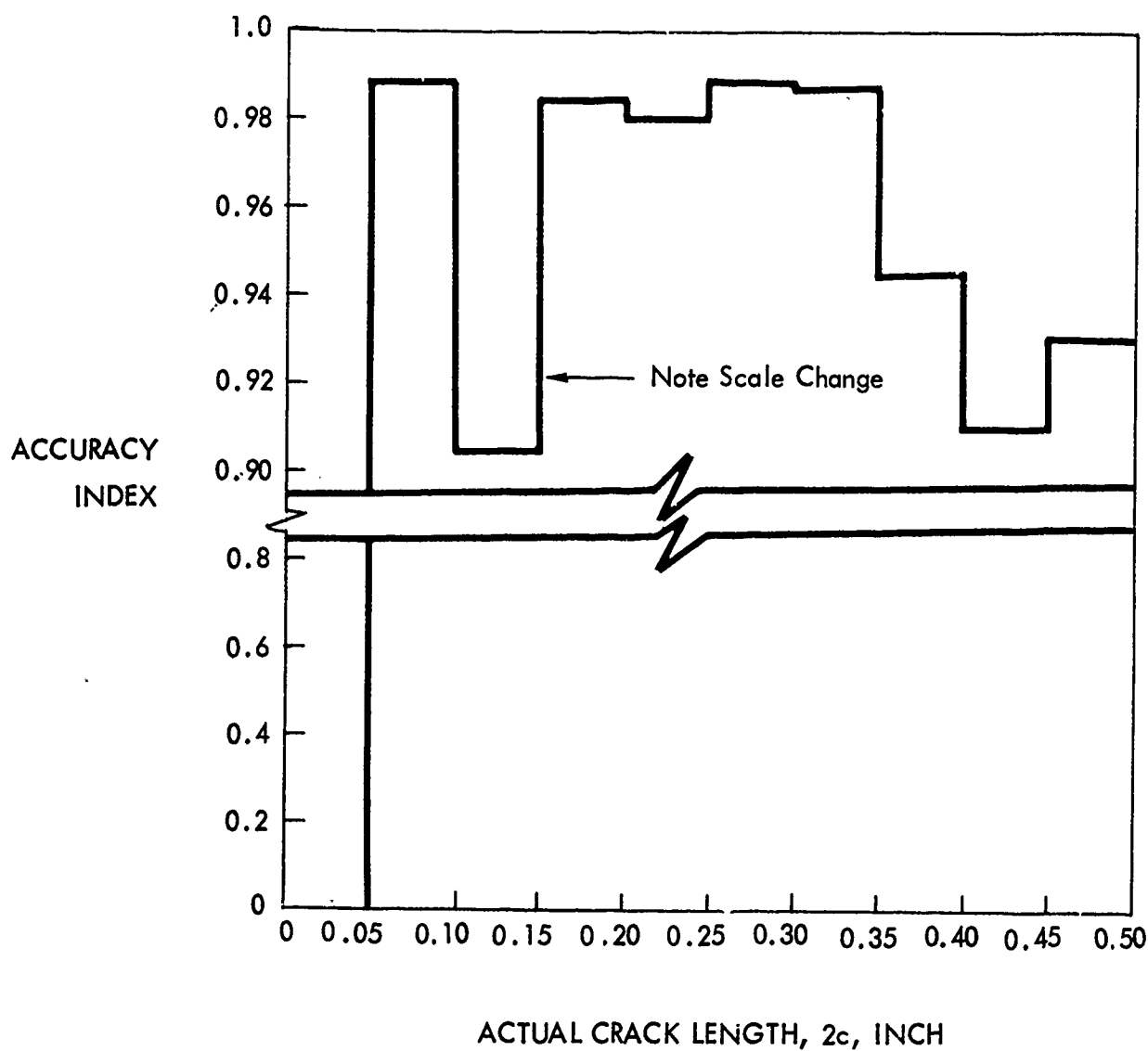
FIGURE 94   ACCURACY OF CRACK LOCATION ANGLE, θ,
ULTRASONICS - STEEL CYLINDERS
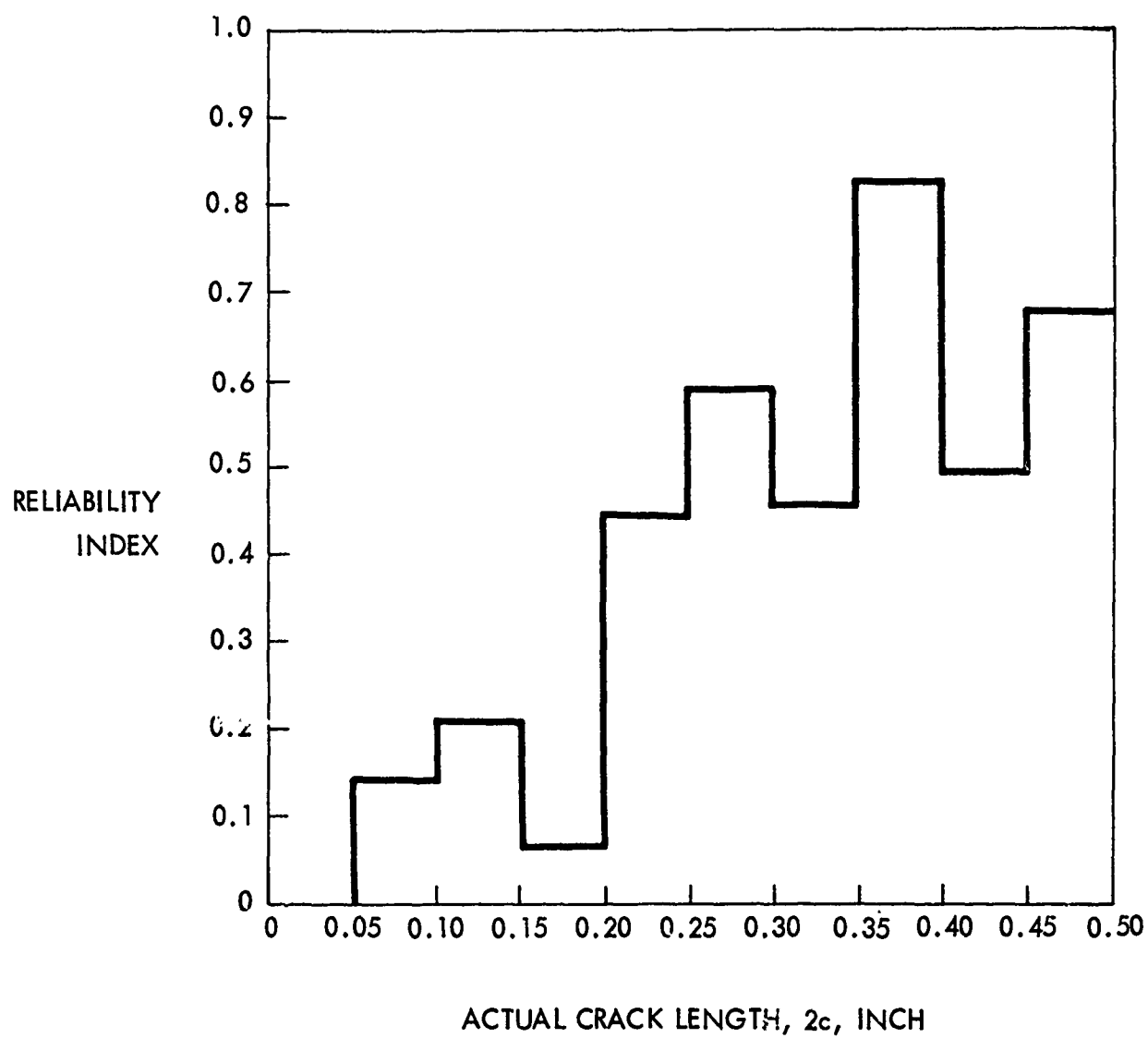
FIGURE 95   RELIABILITY INDEX, DYE PENETRANT – STEEL CYLINDERS

129
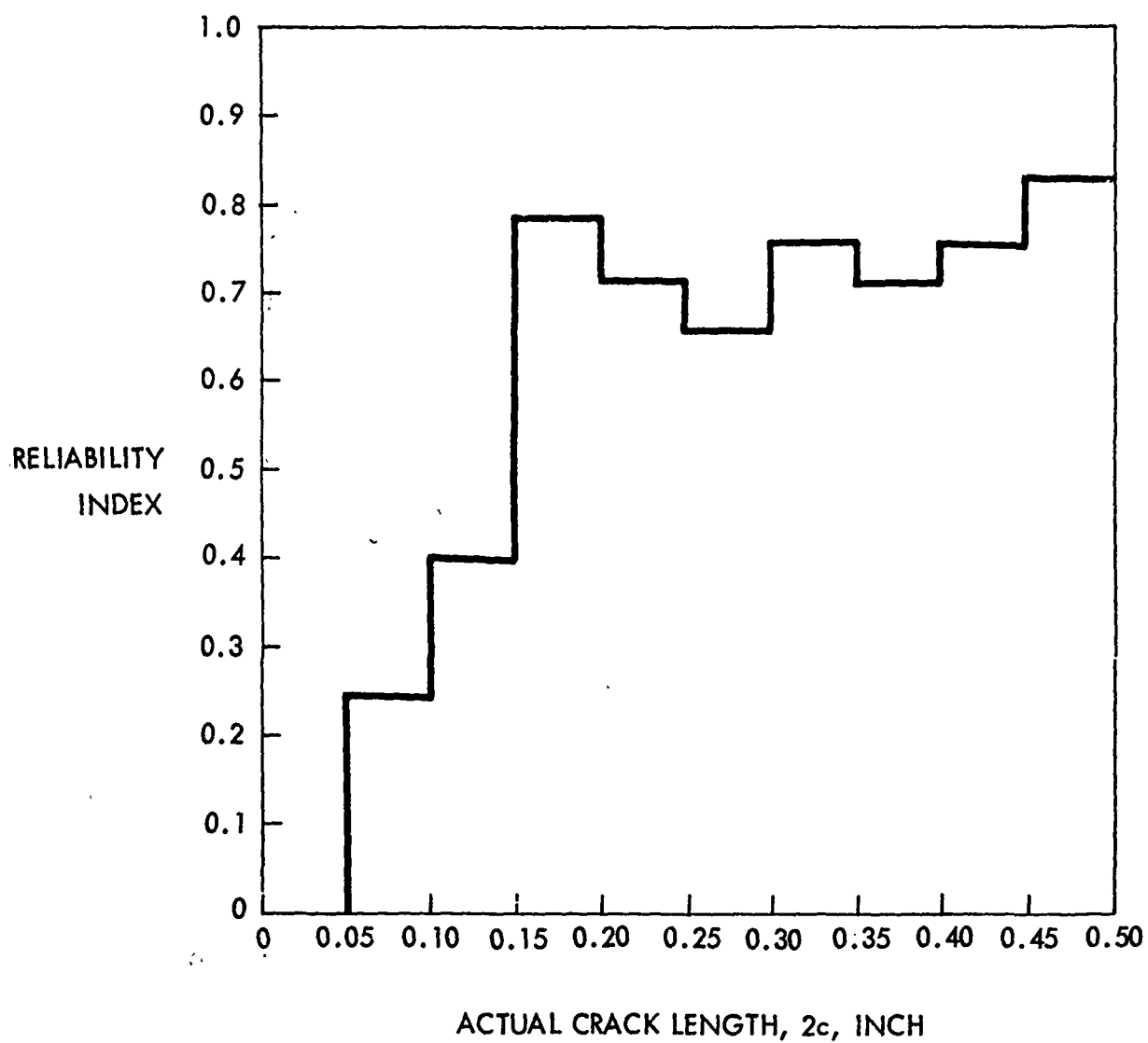
FIGURE 96   RELIABILITY INDEX, MAGNETIC PARTICLE – STEEL CYLINDERS

130
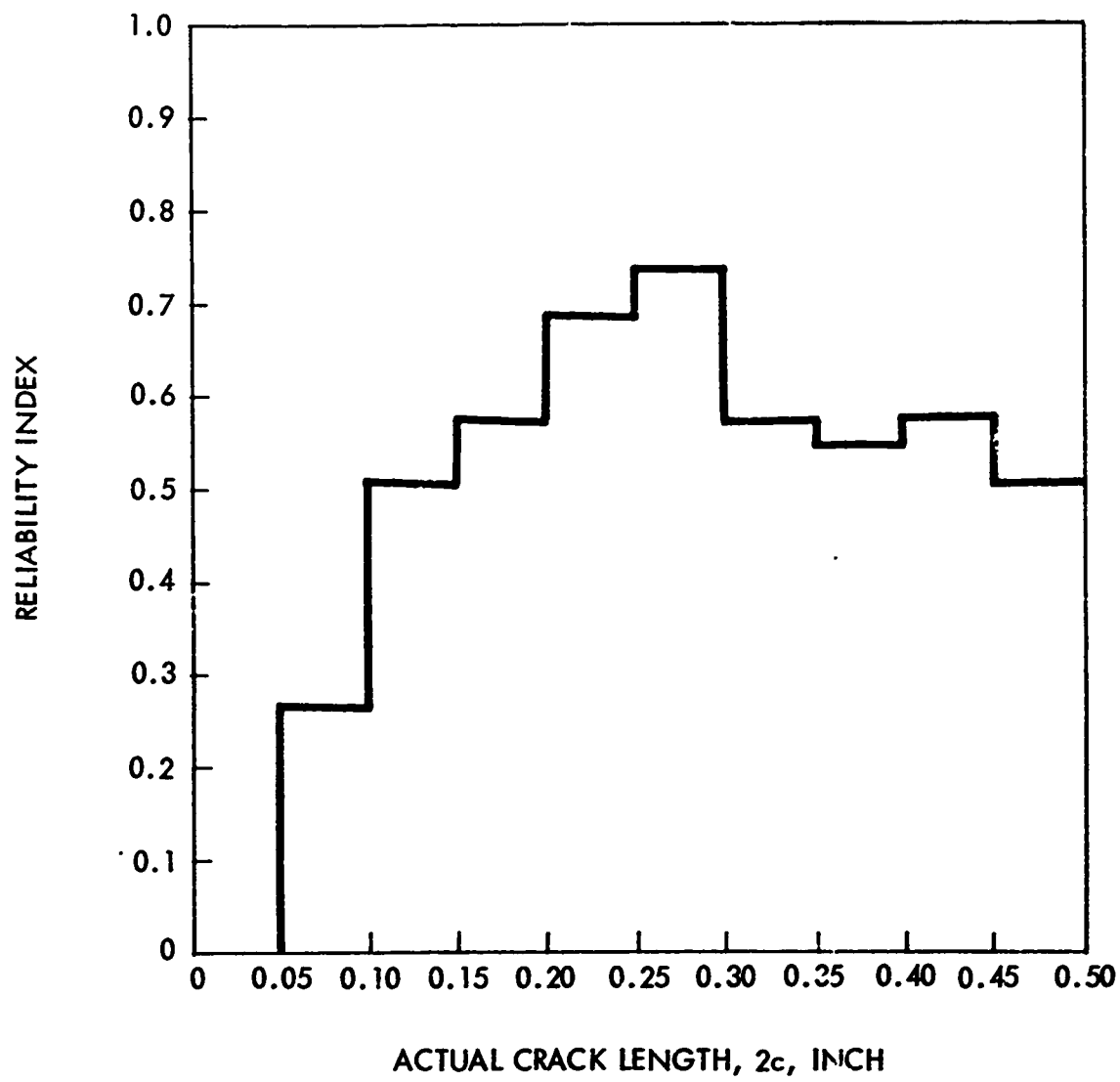
FIGURE 97 RELIABILITY INDEX, ULTRASONICS – STEEL CYLINDERS
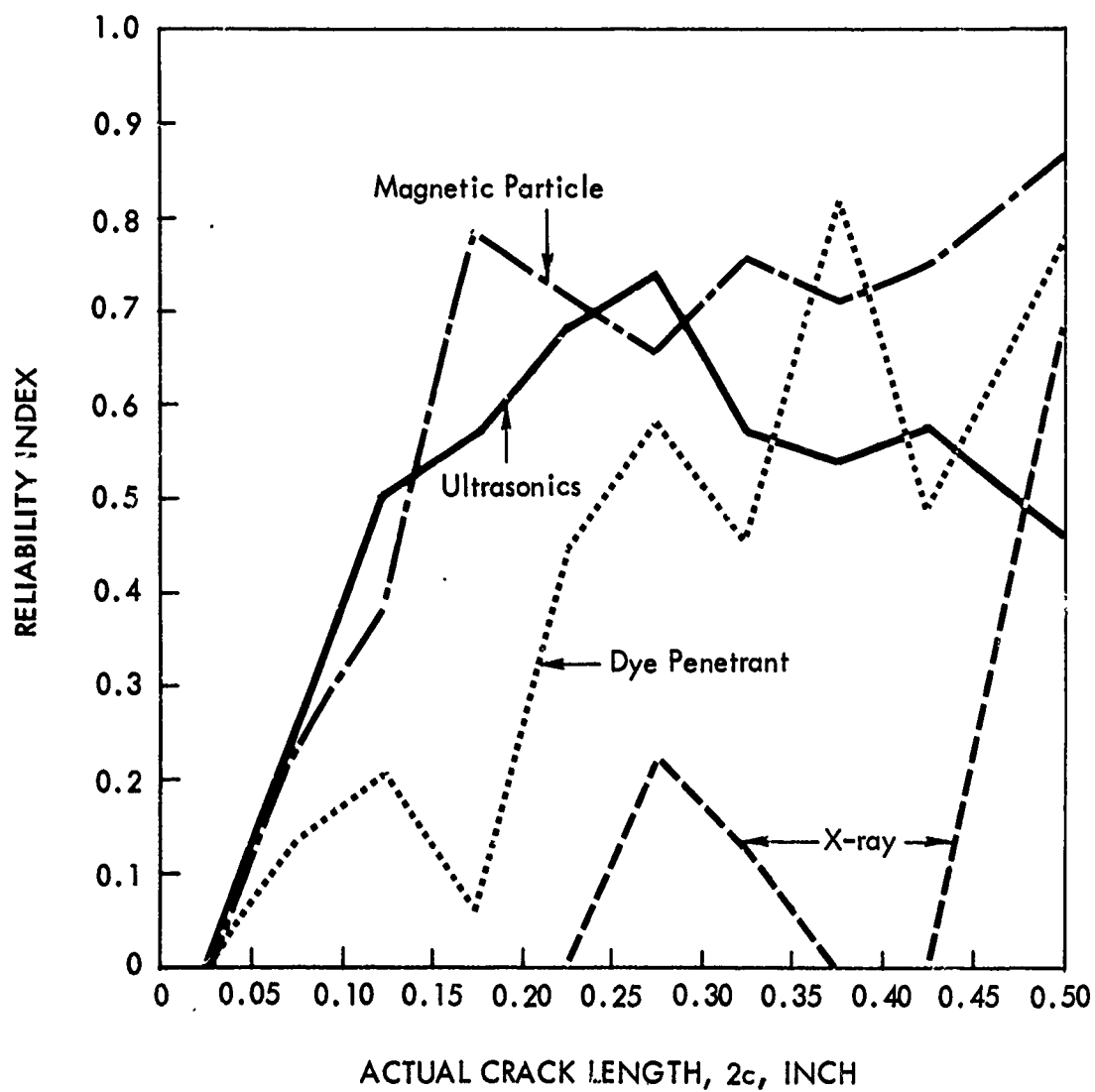
FIGURE 98 COMPARISON OF 4 NDT TECHNIQUES ON RELIABILITY
OF FLAW INDICATIONS IN STEEL CYLINDERS

all methods are inherently poor in the comparatively small crack sizes. As with the 7075-!
T6511 Aluminum, the ultrasonic method appears slightly more reliable in the crack size
range from 0.05 to 0.15 inch. However, the magnetic-particle method has a higher
reliability index for all other crack sizes.

The ultrasonic method shows a drop in reliability index as the crack size increases beyond
0.25 inch. This may be due to the choice of transducer size and operating frequency.

NDT Crack-Size Indications

The calculations given in Tables XIV and XV do not present a complete description of the
NDT method capabilities. The accuracy tabulations are based on the measurements from
those specimens containing cracks that were found to be in a particular crack-size range.
If a particular NDT method always overestimated the crack size, the accuracy tabulation
would be low, particularly if the estimate were off by more than 0.05 inch, for this would
then be out of the crack range.

Hence, it was decided to determine the range of actual crack lengths that would be indi-
cated by a particular crack length indication obtained from each NDT method. The actual
measured crack sizes would then give the error of the NDT method for that particular crack-
size range. Table XIV shows the mean, minimum and maximum crack lengths measured on
the fracture surfaces. A single parentheses (XXXX), indicates that the mean value of the
actual crack lengths is greater than the crack-length range as indicated by the NDT method.
This notation indicates when the NDT method underestimates the length of the crack. A
double parentheses ((XXXX)) indicates that the mean value of the actual crack length is
less than the crack-length range as indicated by the NDT method. Hence, this notation
shows when the NDT method overestimates the length of the crack.

Table XIV shows that the penetrant method underestimates the length of the crack in 5 out
of the 10 crack-length ranges for the 7075-T6511 Aluminum cylinders. The ultrasonic
method underestimates the size of the crack in 9 out of 10 crack-length ranges.

In the 4330V Modified steel cylinders, the penetrant method overestimates the crack length
in 4 out of 10 crack-length ranges and underestimates the length in 4 of the remaining. The
magnetic-particle method overestimates the crack length for large cracks and underestimates
the crack length for the small cracks. The ultrasonic appears to yield the same results; i.e.,
it overestimates the large cracks and underestimates the small cracks.

Production NDT, Experimental Results

It has been mentioned in the introduction that the aluminum and steel cylinders were in-
spected by production inspection whenever time permitted. There was no way of knowing
prior to the failure testing which cylinders contained the crack lengths of interest, and
hence no method or pre-selecting those cylinders that should be inspected by production
that would contain an adequate sampling of crack lengths. This difficulty was not encoun-
tered in laboratory inspection since 100% of the tubes were subjected to laboratory NDT.

Thus it is to be expected that the results of the production inspection are not complete.
This is true particularly where it is felt that an insufficient number of specimens containing
cracks were included in any one crack length range. The production inspection results are
given only in terms of sensitivity.

TABLE XIV

ACTUAL CRACK SIZES COMPARED TO THOSE INDICATED BY NDT

Crack size range as indicated by NDT (Inches)	Mean crack length actual (Inches)	Maximum crack length actual (Inches)	Minimum crack length actual (Inches)
7075-T6511 ALUMINUM CYLINDERS			
Penetrant			
0 -0.05	(0.1262)	0.2358	0.0524
0.05-0.10	(0.1517)	0.1900	0.1052
0.10-0.15	(0.1792)	0.2479	0.1792
0.15-0.20	0.1825	0.2665	0.0913
0.20-0.25	(0.3151)	0.3621	0.2422
0.25-0.30	0.2699	0.3297	0.7844
0.30-0.35	0.3357	0.3577	0.3142
0.35-0.40	0.3862	0.4284	0.3440
0.40-0.45	0.4153	0.4610	0.3475
0.45-0.50	(0.5356)	0.6042	0.4232
Ultrasonics			
0 -0.05	(0.1327)	0.2116	0.0524
0.05-0.10	(0.1470)	0.2620	0.0698
0.10-0.15	(0.2094)	0.2895	0.1309
0.15-0.20	(0.2810)	0.3440	0.1313
0.20-0.25	(0.2946)	0.4219	0.1324
0.25-0.30	(0.3611)	0.5768	0.2422
0.30-0.35	(0.4249)	0.4978	0.3142
0.35-0.40	0.3874	0.4307	0.3440
0.40-0.45	(0.4618)	0.5761	0.3475
0.45-0.50	(0.6042)	---	----
4330V MODIFIED STEEL CYLINDERS			
Penetrant			
0 -0.05	(0.1797)	---	----
0.05-0.10	---	---	----
0.10-0.15	(0.1726)	0.2618	0.1047
0.15-0.20	(0.2142)	0.2880	0.1306
0.20-0.25	(0.2762)	0.4460	0.1052
0.25-0.30	((0.2451))	0.3148	0.1324
0.30-0.35	((0.2674))	0.3937	0.1574
0.35-0.40	((0.3677))	---	----
0.40-0.45	((0.3938))	---	----
0.45-0.50	0.4780	0.5260	0.4200

(continued)

134

TABLE XIV (CONTINUED)

Crack size range as indicated by NDT (Inches)	Mean crack length actual (Inches)	Maximum crack length actual (Inches)	Minimum crack length actual (Inches)
4330V MODIFIED STEEL CYLINDERS (CONTINUED)			
Magnetic Particle			
0 -0.05	(0.1776)	0.2880	0.1000
0.05-0.10	(0.1500)	0.1500	0.1500
0.10-0.15	((0.1381))	0.1584	0.1200
0.15-0.20	0.1799	0.2880	0.1052
0.20-0.25	0.2126	0.3938	0.0700
0.25-0.30	0.2720	0.4460	0.1047
0.30-0.35	((0.2820))	0.4990	0.1300
0.35-0.40	0.3561	0.4722	0.2618
0.40-0.45	((0.3144))	---	---
0.45-0.50	((0.4995))	0.5260	0.4729
Ultrasonics			
0 -0.05	(0.1540)	0.3406	0.1000
0.05-0.10	(0.1396)	0.1836	0.0700
0.10-0.15	(0.2120)	0.4722	0.1309
0.15-0.20	(0.2279)	0.3938	0.1206
0.20-0.25	(0.2829)	0.4200	0.1309
0.25-0.30	(0.3625)	0.5260	0.2618
0.30-0.35	(0.4210)	0.4729	0.3440
0.35-0.40	(0.4990)	---	---
0.40-0.45	((0.3365))	---	---
0.45-0.50	((0.2880))	---	---

A double parentheses ((XXXX)) indicates that the mean value of the actual crack length is less than the crack-length range as indicated by the NDT method.

The production sensitivity results are shown in Table XV. The second column shows the ratio of the number of cracks found by production inspection divided by the total number of specimens containing cracks in that crack length range that were inspected by production. Those numbers in braces are based on a total of 3 specimens or less. For comparison the sensitivity of the laboratory NDT is shown in the adjacent column.

The results show that production inspection of 7075-T6511 Aluminum cylinders is as sensitive as laboratory inspection for the detection of crack lengths in the 0.20 to 0.50 inch range. Laboratory sensitivities are higher for small cracks. Production in penetrant inspection of 4330V Modified steel cylinders appears to be as sensitive as laboratory penetrant inspection for all crack lengths examined. The sensitivity of the production penetrant inspection of 4330V Modified steel in the small crack lengths (0.05 to 0.30 inch) appears to be as good or better than laboratory inspection. However, these results are inconclusive due to the small number of cylinders inspected by production.

Production magnetic-particle inspection of 4330V Modified steel cylinders appears equivalent to laboratory inspection for crack lengths over 0.25 inch. Both techniques can detect 100% of the cracks in this length range. For small cracks, laboratory sensitivity is slightly superior.

Many steel specimens were inspected by Eddy current techniques to determine if this method would be superior to ultrasonic inspection. These results are tabulated in Table XVI. Laboratory eddy-current inspection is as sensitive as laboratory ultrasonic inspection in detecting cracks 0.20 inch long or longer. Both techniques can detect 100% of the cracks in this range. For small cracks from 0.05 to 0.20 inch long, the ultrasonic method appears superior.

NDT Inspection-Conclusions

The results obtained from NDT inspection of the fatigue cracked cylinder can be summarized as follows:

o   The reliability of the NDT needs to be improved. No reliability index over 0.90 was obtained.

o   For 7075-T6511 Aluminum cylinders containing surface fatigue cracks, the order of preference for the NDT would be:

crack length less than 0.20 inch
1.   ultrasonics
2.   penetrant
3.   X-ray

crack length 0.20 to 0.50 inch

1.   penetrant
2.   ultrasonics
3.   X-ray

o   For 4330V Modified steel cylinders containing surface fatigue cracks, the order of preference for the NDT would be:

crack length less than 0.15 inch
1.   ultrasonics
2.   magnetic-particle
3.   penetrant
4.   X-ray

TABLE XV

COMPARISON BETWEEN
PRODUCTION AND LABORATORY NDT INSPECTION SENSITIVITIES

Actual crack size range 2c (Inches)	Production inspection	Laboratory inspection
Aluminum cylinders – penetrant inspection		
0 -0.05	NA	0.0667
0.05-0.10	0.0000	0.1538
0.10-0.15	0.0909	0.2917
0.15-0.20	0.0833	0.3636
0.20-0.25	1.0000	0.8571
0.25-0.30	{0.3333}	1.0000
0.30-0.35	{0.5000}	1.0000
0.35-0.40	NA*	1.0000
0.40-0.45	NA*	1.0000
0.45-0.50	{1.0000}	1.0000
Steel cylinders – penetrant inspection		
0 -0.05	NA*	0.1111
0.05-0.10	{0.5000}	0.4000
0.10-0.15	{1.0000}	0.3333
0.15-0.20	{0.6667}	0.3000
0.20-0.25	{1.0000}	0.6000
0.25-0.30	{1.0000}	0.7778
0.30-0.35	{1.0000}	0.6250
0.35-0.40	{1.0000}	1.0000
0.40-0.45	NA*	1.0000
0.45-0.50	{1.0000}	1.0000
Steel cylinders – magnetic particle inspection		
0 -0.05	0.2105	0.2222
0.05-0.10	{0.5000}	0.6000
0.10-0.15	0.6667	0.9333
0.15-0.20	0.7500	0.9000
0.20-0.25	0.6000	0.8889
0.25-0.30	1.0000	1.0000
0.30-0.35	1.0000	1.0000
0.35-0.40	1.0000	1.0000
0.40-0.45	NA*	1.0000
0.45-0.50	{1.0000}	1.0000

*Note: NA – No specimens containing crack of this size range were inspected by the particular technique.

Those numbers in {xxxx} are based on a total of 3 specimens or less.

137

TABLE XVI

COMPARISON OF EDDY CURRENT INSPECTION WITH ULTRASONIC INSPECTION OF STEEL CYLINDERS

Actual crack size range 2c (inches)	Eddy current laboratory	Ultrasonics laboratory
0 -0.05	0.0000	0.2222
0.05-0.10	0.2000	0.4000
0.10-0.15	0.1250	0.8000
0.15-0.20	0.2857	0.9000
0.20-0.25	{1.0000}	1.0000
0.25-0.30	{1.0000}	1.0000
0.30-0.35	{1.0000}	1.0000
0.35-0.40	{1.0000}	1.0000
0.40-0.45	NA*	1.0000
0.45-0.50	{1.0000}	1.0000

*Note: NA - No specimens containing crack of this size range were inspected by the particular technique.

Those numbers in braces {XXXX} are based on a total of 3 specimens or less.

crack length 0.15 to 0.50 inch

1. magnetic-particle
2. ultrasonics
3. penetrant
4. X-ray

o   All NDT methods obtained very high accuracies in location of the crack. (X-ray inspection was not included due to the low sensitivity of this technique). Low reliability indices are due to two factors; namely, (1) the inability of the method to measure the true crack length accurately for small cracks and, (2) the poor sensitivity of the methods in detecting cracks smaller than 0.20 inch.

o   The X-ray method used here was unable to detect small, tight surface fatigue cracks in aluminum and steel cylinders.

o   The sensitivity of the ultrasonics method to detect small cracks appears to be superior to all other methods examined.

o   Magnetic-particle inspection is superior to penetrant inspection for the 4330V Modified steel cylinders.

o   Production inspection methods are as sensitive to cracks of length from 0.20 to 0.50 inch as laboratory inspection methods. Laboratory methods appear to be more sensitive for small crack lengths.

o   Eddy-current inspection is less sensitive than ultrasonics for crack lengths smaller than 0.20 inch, but equal in sensitivity for cracks from 0.20 to 0.50 inch.

The X-ray method cannot be applied to detect small cracks in these specimens, as is evident by the poor results obtained by X-ray inspection. It is possible that, when combined with a penetrant technique to fill the crack with a radiation-absorbing material X-ray sensitivity may increase.

Penetrant techniques showed surprisingly high accuracies in detecting and locating small fatigue cracks.

Magnetic-particle methods were the most rewarding of all the methods investigated. For crack lengths over 0.25 inch, the results were better than those obtained by ultrasonics. It appears that magnetic-particle inspection has an excellent potential for detecting and locating fatigue cracks in these specimens.

The ultrasonic method appeared to show the greatest potential for detection of extremely small cracks. For crack lengths less than 0.20 inch, this method appeared to give the most consistent results. It is unfortunate that, for small crack lengths, no method was found to be very reliable.

It is felt that, once the NDT method has indicated that a crack exists, there is no doubt that the location of the crack is well known. This is true for all surface cracks investigated here. No results were obtained for subsurface cracks. It is recommended that further investigations be confined to increasing the sensitivity of the NDT methods to obtain better sensitivity for small cracks.

SECTION IV

FAILURE TEST PROGRAM

Test Cylinders

When the fatigue-cracking and NDT inspection were completed, the cylinders were tensile tested in accordance with Federal Test Method Standard #151a, Method 211.1. Using this Standard as a guide, steel plugs were made to fit inside the cylinders. The cylinders were held in special vee-type grips and tested to failure in one of two universal testing machines available in the Lockheed-Georgia Development Test Laboratory. The failure loads for the 4330V Modified steel specimens were calculated to be about 600,000 pounds, and 300,000 pounds for the 7075-T6511 Aluminum specimens. This required the use of slightly different test procedures, depending on the test machine used.

The 7075-T6511 Aluminum cylinders were tested to failure in a 400,000-pound capacity Baldwin Universal Testing Machine. Load values are accurate to ±0.5 percent at indicated load. An SR-4 type strainometer was mounted on the specimen in the center to measure elongation. The strainometer was calibrated to ASTM Class B-2 specifications. The specimen was loaded to failure at a constant rate of 0.006 in./in./min. A typical test configuration used in failure testing of the aluminum cylinders is shown in Figure 99. A detail photograph of the strainometer attachment is shown in Figure 100.

The 4330V Modified steel specimens in the 220-240 KSI heat-treated condition were tested to failure in a 1,200,000-pound capacity Baldwin Universal Testing Machine, Figure 101. The 600,000-pound load range was used. Load values are accurate to ±0.5 percent of indicated load. The initial tests were conducted using an SR-4 strainometer similar to the one used on the aluminum cylinders to measure elongation. A specimen failed at 450,000 pounds and damaged the strainometer. A Baldwin PD-1 Deflectometer, calibrated to ASTM Class C specifications, was used for the remainder of the tests. The sensitivity of the deflectometer is less than that of the strainometer due to the nature of measurement involved. The specimen is loaded at a constant loading rate of 1000 lb/sec. The test configuration used in failure-testing of the steel cylinders is shown in Figure 102. No difficulties were encountered in the test program on the cylinders.

Failure Test Results

Figure 103 is a plot of the failure load versus actual surface crack length 2c. Those specimens containing 1-inch-diameter bored holes are shown with open circles, and those specimens without holes are shown with solid circles. The data for specimens containing holes will be discussed in Section V. It can be seen that no loss in load occurs for the 7075-T6511 Aluminum cylinders until the surface crack length is over 0.20 inch. As the surface crack length increases, the failure loads continue to drop. Specimens that contain 1-inch-diameter holes show that, even with cracks less than 0.20 inch long, there is a reduction in failure load due to the crack. This reduction may be a considerable amount. For example, specimens containing surface cracks 0.10 to 0.15 inch long and a 1-inch-diameter hole failed at loads of 115 KIPS compared to 155 KIPS for specimens containing only the hole.

Figure 104 is a plot of the failure load versus actual surface crack length 2c for the steel cylinders. Those specimens containing 1-inch holes bored in the tube are shown with open circles; those specimens containing only surface cracks are shown as solid circles. The loss in strength associated with surface cracks only occurs at crack lengths over 0.15 inch. As
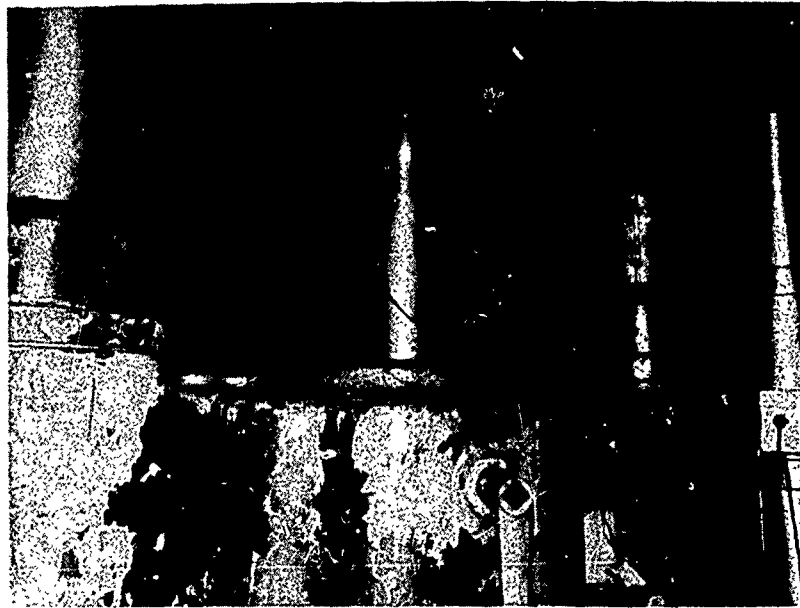
FIGURE 99   TEST CONFIGURATION FOR FRACTURE TESTING OF 7075-T6511
ALUMINUM CYLINDERS IN 400KIP MACHINE
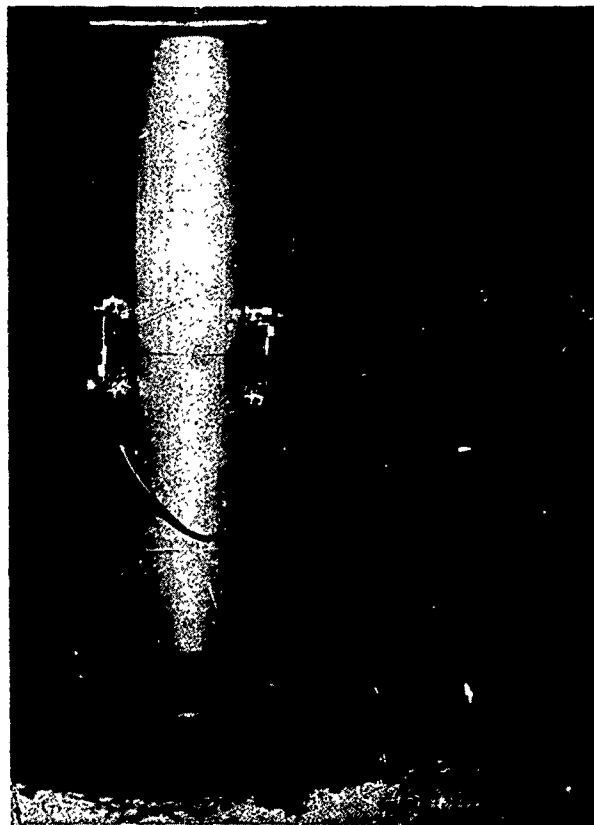
FIGURE 100   SR-4 STRAINOMETER MOUNTED ON
7075-T6511 ALUMINUM CYLINDERS
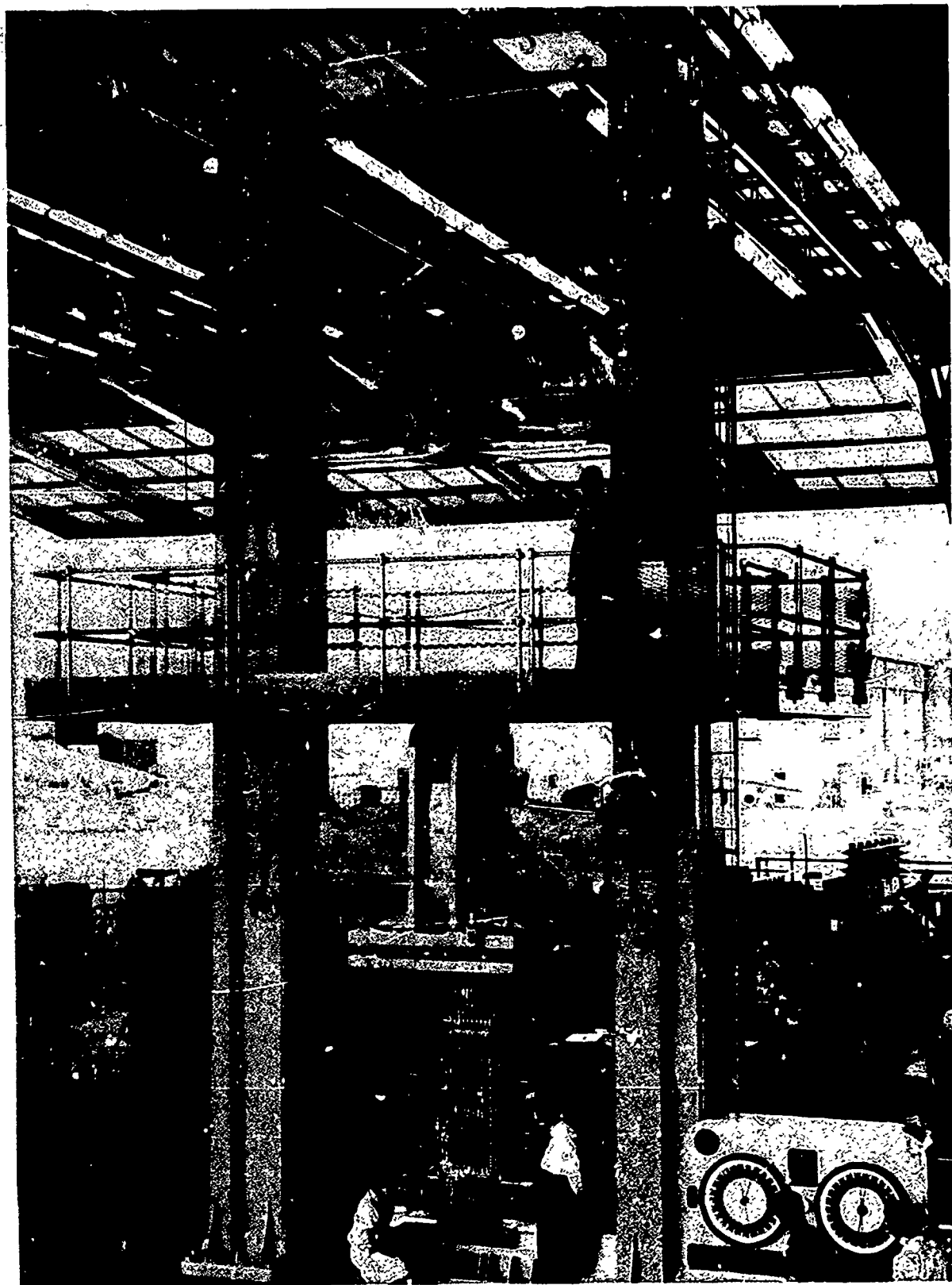
FIGURE 101 PHOTOGRAPH OF 1.2 MILLION POUND TEST MACHINE USES FOR
FRACTURE TESTING OF 4330V MODIFIED STEEL TUBES
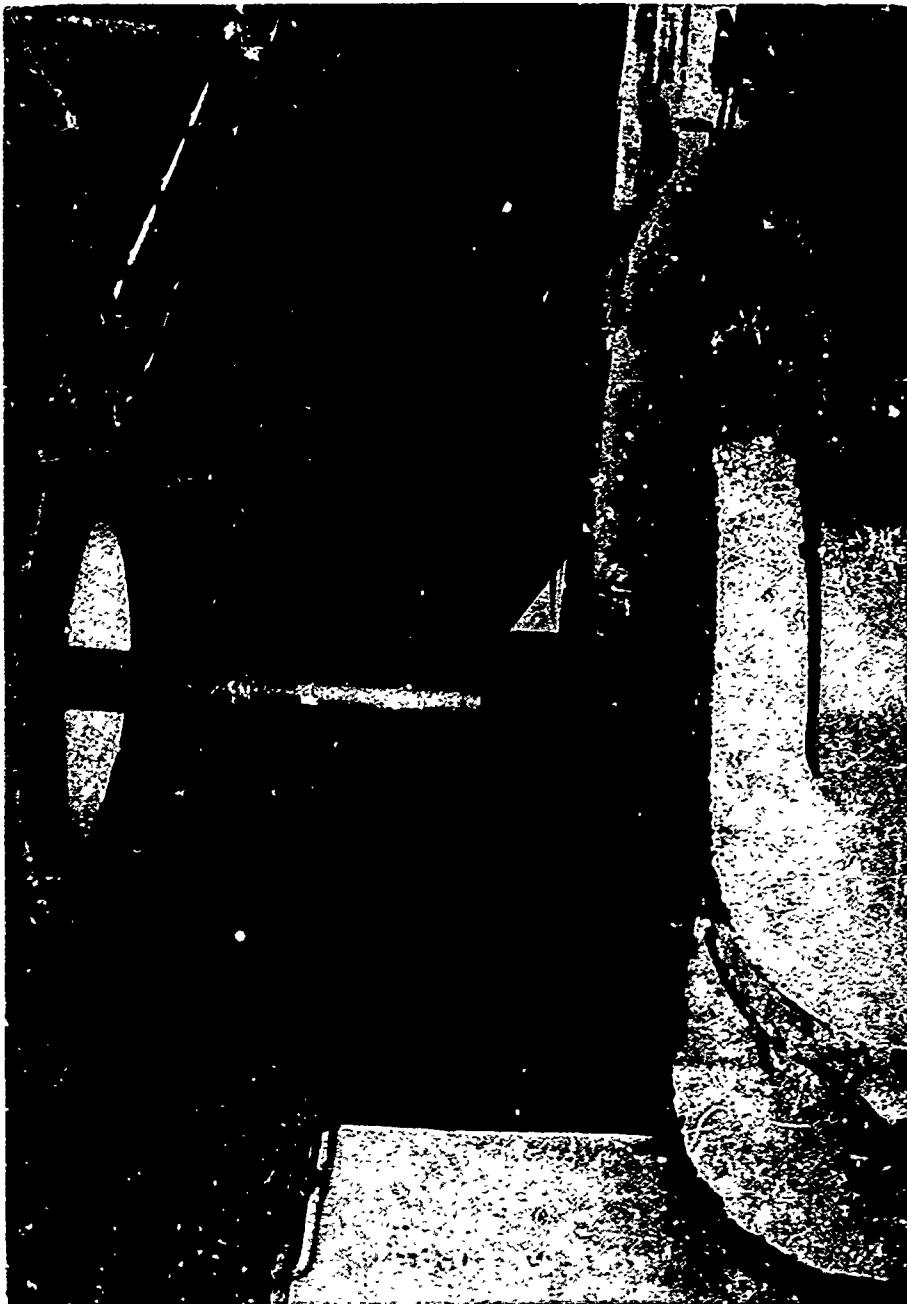
FIGURE 102 DETAIL PHOTOGRAPH SHOWING 4330V MODIFIED STEEL TUBE IN
UPPER GRIP OF 1.2 MILLION POUND TEST MACHINE
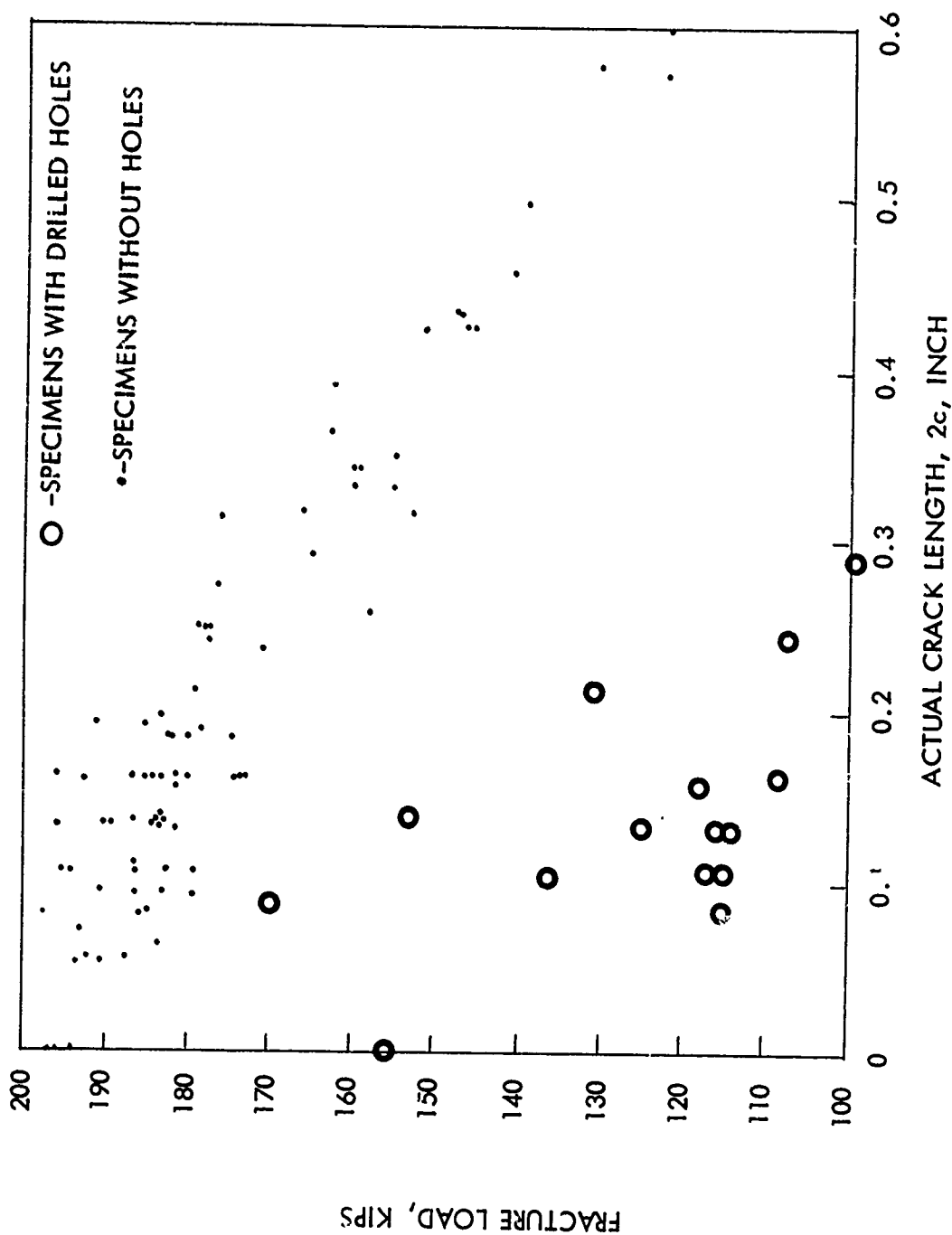
FIGURE 103   FAILURE LOAD VS. ACTUAL SURFACE CRACK SIZE FOR 7075–T6511 ALUMINUM CYLINDERS

144
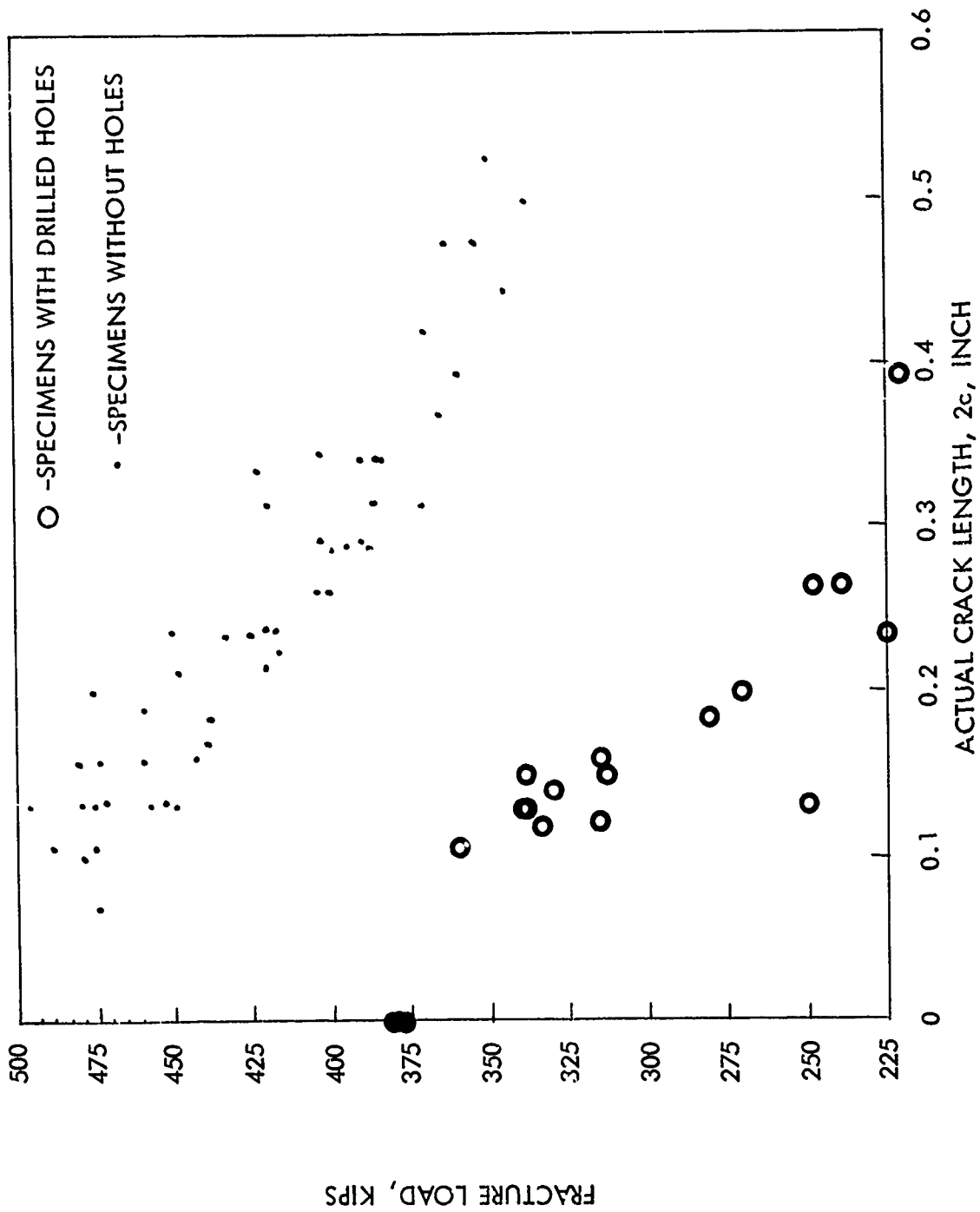
FIGURE 104   FAILURE LOAD VS ACTUAL SURFACE CRACK SIZE FOR 4330V MODIFIED STEEL CYLINDERS

145

was expected, failure load decreased as the crack length increased. It can be seen that the presence of the 1-inch-diameter hole reduces the failure load of the specimens containing small cracks. The effect of a small crack near the hole is on the same order of magnitude as was found for the aluminum specimens.

All of the cracks found in the cylinders were "thumbnail" cracks. For these specimens, the shape of the crack is usually given in terms of a flaw shape parameter Q. This is defined (3) as follows:

$$Q = \left[\phi^2 - 0.212 \left(\frac{\sigma_f}{\sigma_{yp}} \right)^2 \right] \tag{15}$$

where ϕ is the complete elliptic integral of the second kind

$$\phi = \int_0^{2\pi} \sqrt{1 - \frac{c^2 - a^2}{c^2} \sin^2\theta} \, d\theta \tag{16}$$

and σ_f is the gross stress at failure, σ_{yp} is the 0.2% offset yield stress. The function Q depends on the ratio of crack depth, a, to crack length, $2c$, and contains a correction for the plastic strains along the crack boundary.

Figure 105 shows the failure loads versus the flaw shape parameter a/Q for the 7075-T6511 Aluminum cylinders. The open circles are those cylinders containing the 1-inch bored hole. It can be seen that a loss in load-carrying ability of the cylinder is shown for all specimens containing both the hole and the crack, while no loss in load-carrying capacity is seen for the cylinders containing the crack alone until the a/Q value is over 0.06 inch. Figure 106 shows the failure load versus the flaw shape parameter a/Q for the 4330V Modified steel cylinders. It can be seen that, when the a/Q value is over 0.04, there is a loss in strength.

The Q value was calculated assuming that $\sigma_f / \sigma_{yp} = 1.0$ and should be corrected to account for the actual fracture stress as a function of the yield stress. This correction is made when the actual fracture stress is plotted as a function of the a/Q values, and will be shown in the next section.

Figure 107 shows the effect of crack depth, a, on the failure load of the 7075-T6511 Aluminum cylinders. It appears that surface flaws less than 0.10 inch deep did not affect the failure loads. With a 1-inch-diameter hole bored through the cylinder, flaws as shallow as 0.04 inch deep caused failure reduced loads.

Figure 108 shows the effect of crack depth, a, on the failure load of the 4330V Modified steel cylinders. It can be seen that these cylinders show a loss in failure loads when the crack depth is over 0.08 inch.

146

FIGURE 105   FAILURE LOAD VERSUS $\frac{a}{Q}$ FOR 7075-T6511 ALUMINUM CYLINDERS

147

FIGURE 106 FAILURE LOAD VERSUS a/Q FOR 4330V MODIFIED STEEL CYLINDERS

148
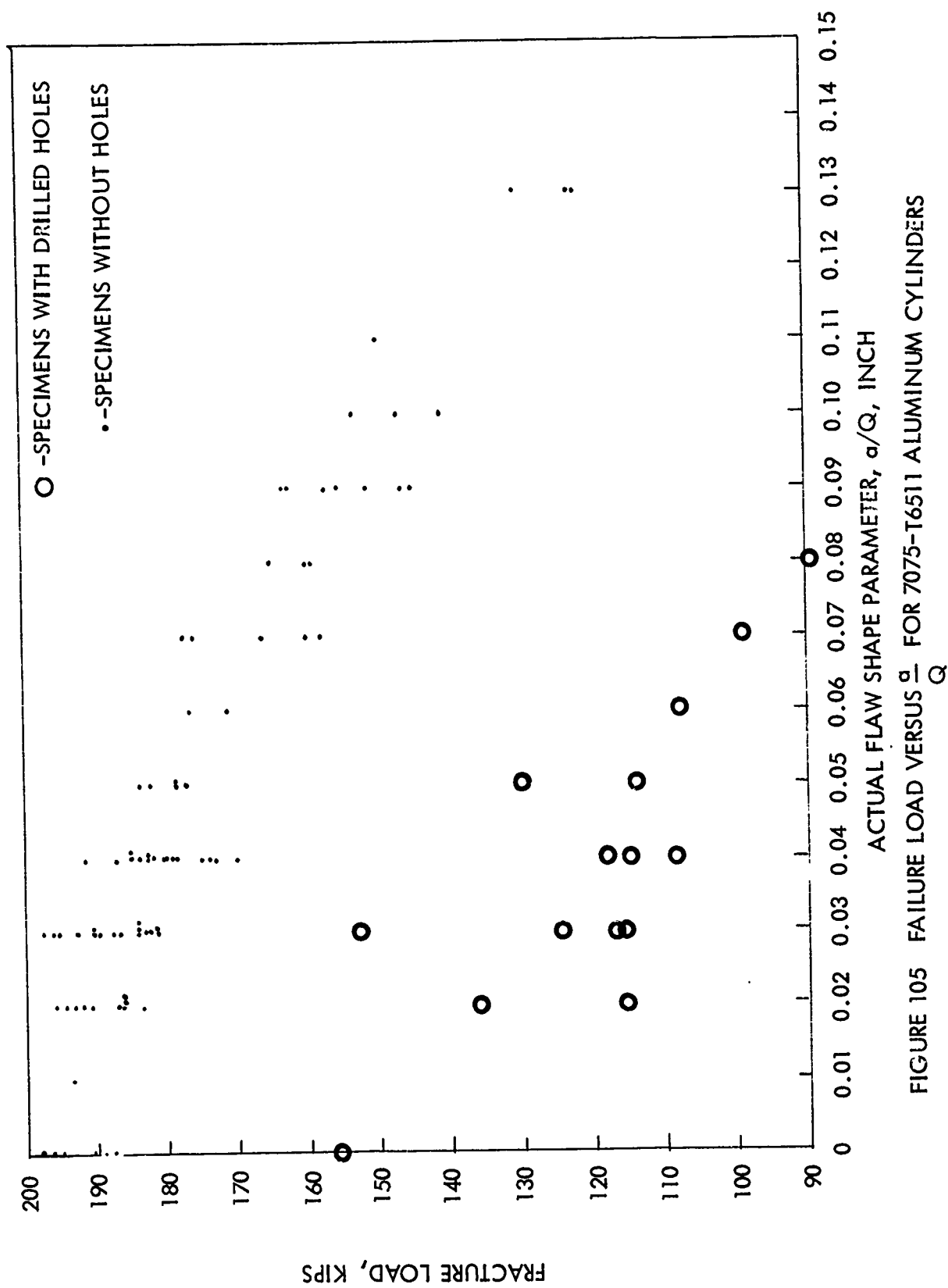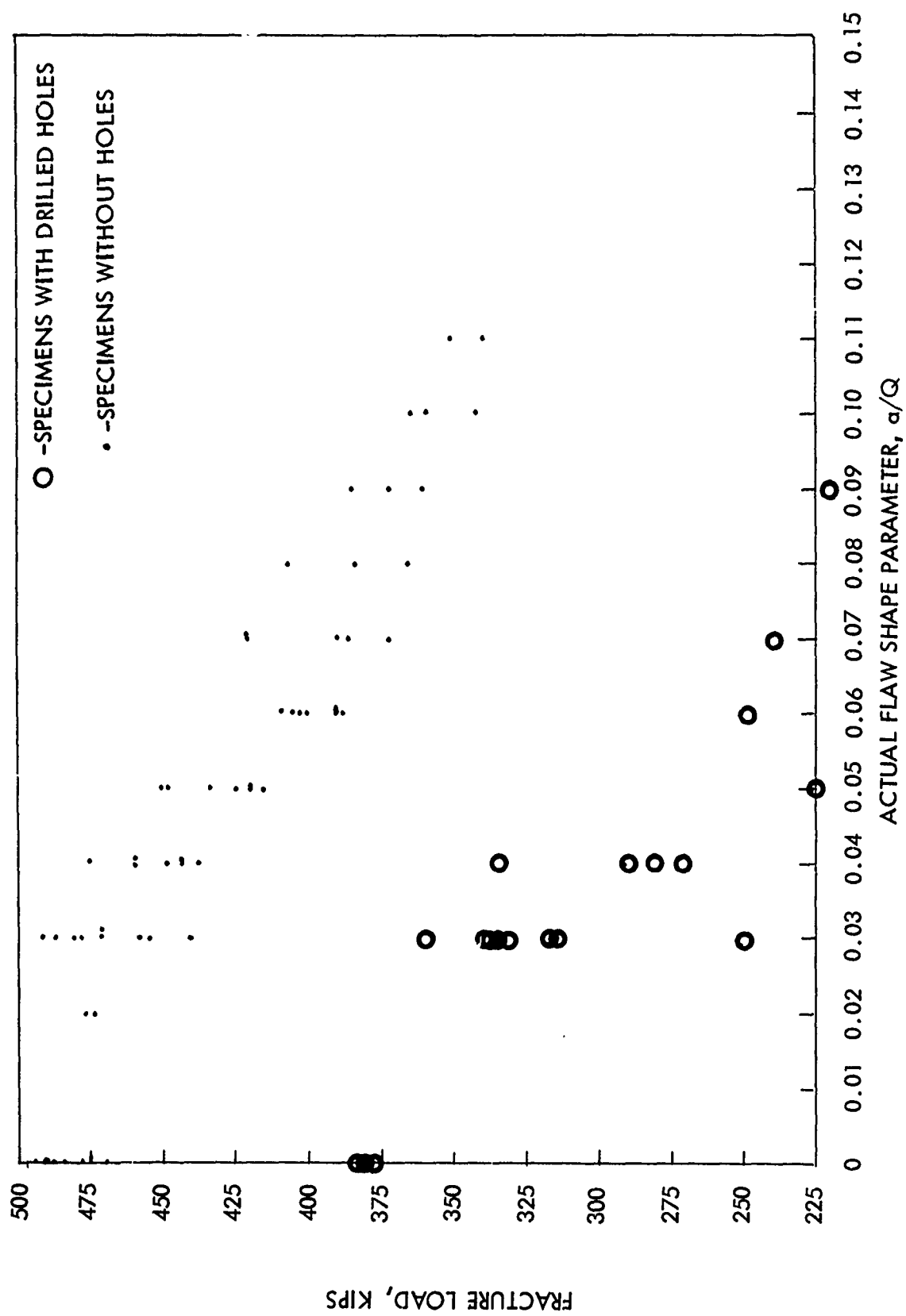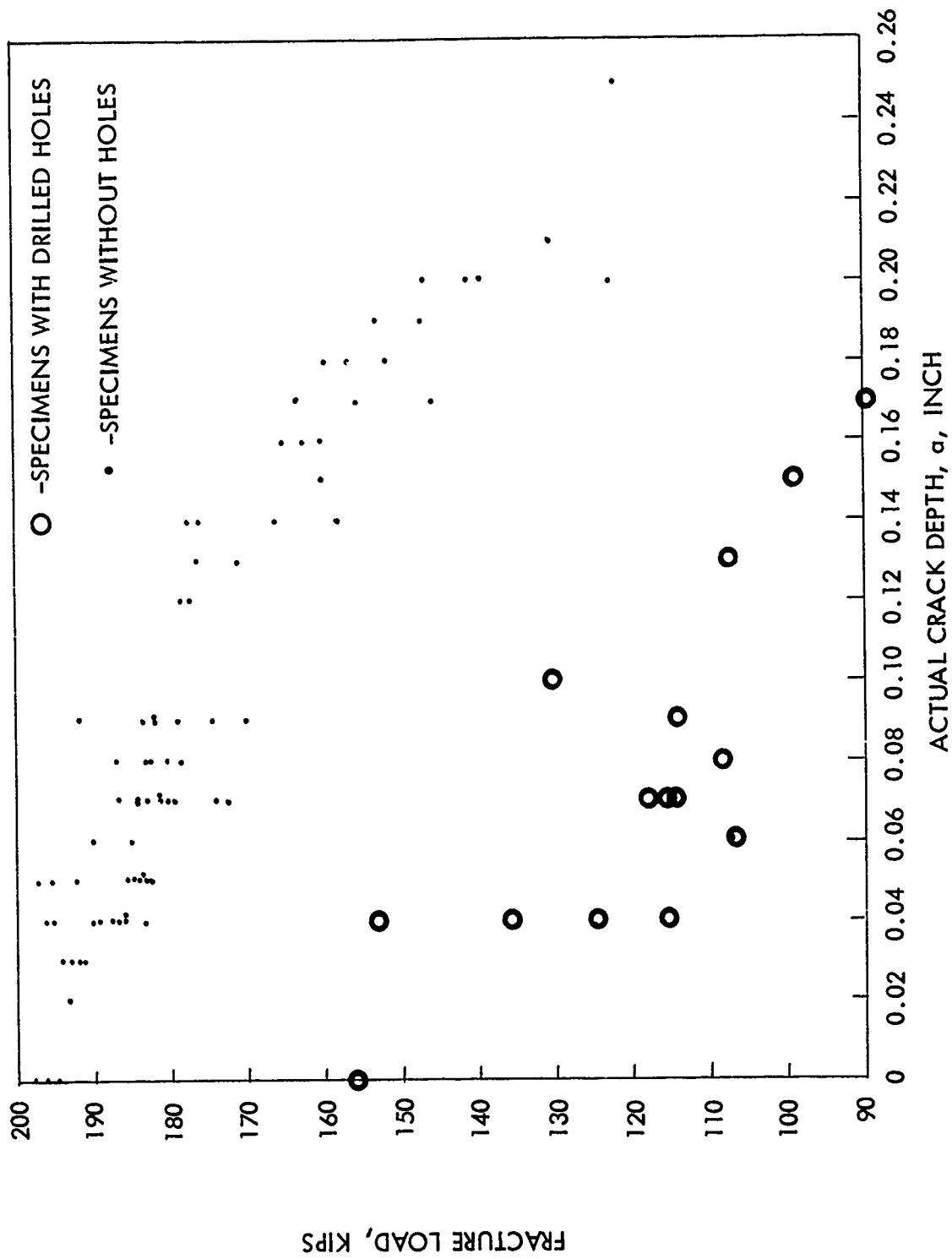
FIGURE 107   FAILURE LOAD VERSUS CRACK DEPTH, a, FOR 7075-T6511 ALUMINUM CYLINDERS

149
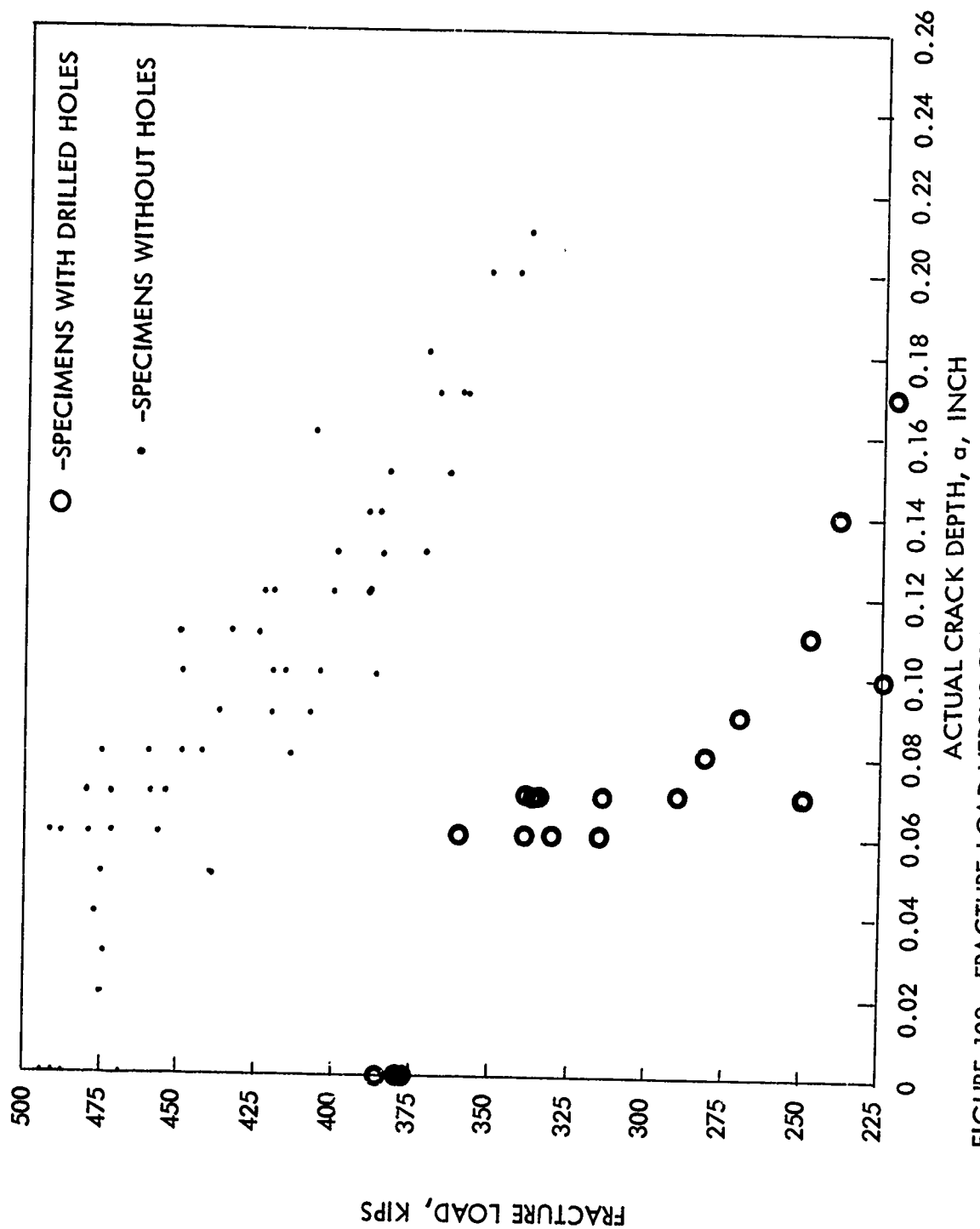
FIGURE 108   FRACTURE LOAD VERSUS CRACK DEPTH, a, FOR 4330V MODIFIED STEEL

Axis labels: ACTUAL CRACK DEPTH, a, INCH (horizontal); FRACTURE LOAD, KIPS (vertical)

Legend:
O – SPECIMENS WITH DRILLED HOLES
• – SPECIMENS WITHOUT HOLES

150

SECTION V

FRACTURE MECHANICS ANALYSIS

This section is divided into four parts. Part 1 presents the results of the literature survey of the available data conducted in an attempt to obtain a valid statistical analysis for K_{Ic} for the 7075-T6511 Aluminum and 4330V Modified steel. Part 2 presents the test program and test results obtained on round-center notched and precracked 4330V Modified steel specimens. Part 3 presents the analysis and results of the FM/NDT design in predicting the failure load and failure stress of the test cylinders. Part 4 presents the analysis and results of the FM/NDT design in predicting the failure load and failure stress of the test cylinders containing a 1-inch-diameter bored hole.

Part 1 - Analysis of Literature Data

Fracture-toughness testing has generated an enormous body of literature. For the purposes of this program, the literature survey was restricted to the following:

o 7075 Aluminum alloy in the T6, T65, T6511 heat-treat conditions

o 4330V Modified steel in the 220-240 KSI tensile ultimate heat-treat condition

o Tests conducted at near ambient temperatures in the absence of any detrimental environment

o Tests conducted according to ASTM fracture toughness procedures (2, 3)

o Analysis of data where the geometry and loads were tabulated and K_{Ic} could be calculated from individual specimens rather than an average K_{Ic} presented without individual test results.

Data from center-notched and fatigue-precracked specimens were initially selected for analysis. This type of specimen has been generally accepted in the literature as producing the most consistent results. The data available on round-center notched and fatigue-precracked specimens were also examined. Data obtained from single-edge tension and three- and four-point bending were also examined.

Approximately 1000 references were scanned. In addition, Defense Documentation Centers (39) and personal contacts with other aerospace fracture-testing personnel and material producers (40) were used to supplement the available data. It was discovered that no test data for K_{Ic} of 4330V Modified steel were available. There is considerable information available on 4335V Modified and 4340, but this was not used in the analysis. For this reason, it was decided to determine K_{Ic} by testing 25 longitudinal and 15 transverse fracture toughness specimens made from 4330V Modified steel heat-treated to 220-240 KSI. This subprogram is discussed in Part 2 of this section. The remainder of this Part deals with the results obtained from 7075 Aluminum alloys.

Approximately 800 data points obtained from 15 sources were analyzed. Table XVII shows the sets and the conditions of the material. Figure 109 shows the computer program that was designed to calculate the fracture toughness parameter K_{Ic}; typical inputs are shown. Table XVIII shows a typical output.

The computer program formulation for the center-notched and fatigue-precracked specimens is outlined below. The symbols used are as follows:

T	=	specimen thickness
W	=	specimen width
AP	=	1/2 crack length prior to pop-in
FGP	=	pop-in gross stress
FNP	=	pop-in net stress
AM	=	1/2 crack length at maximum load
FGM	=	gross stress at maximum load
FNM	=	net stress at maximum load
FTY	=	yield stress

152

TABLE XVII

7075 ALUMINUM SPECIMEN DATA

Set No.		Heat treatment	Fabrication process	Surface condition	Grain direction	Type of test	Data source	J	I	Type specimen
1	No buckling restraint	T6	Rolled	Bare	Long	Plane strain	Ref. 41	1	1	CN
2	No buckling restraint	T6	Rolled	Bare	Long	Plane stress	Ref. 41	2	1	CN
3	No buckling restraint	T6	Rolled	Bare	Long	Plane stress	Ref. 42	2	2	CN
4	No buckling restraint	T6	Rolled	Bare	Long	Plane strain	Ref. 40	3	3	CN
5	No buckling restraint	T6	Rolled	Bare	Long	Plane strain	Ref. 43	3	4	CN
6	No buckling restraint	T6	Rolled	Bare	Long	Plane stress	Ref. 44	4	5	CN
7	No buckling restraint	T6	Rolled	Bare	Trans	Plane strain	Ref. 41	5	6	CN
8	No buckling restraint	T6	Rolled	Bare	Trans	Plane stress	Ref. 42	6	7	CN
9	No buckling restraint	T6	Rolled	Bare	Trans	Plane strain	Ref. 42	7	8	CN
10	No buckling restraint	T6	Rolled	Bare	Trans	Plane strain	Ref. 41	7	9	CN
11	No buckling restraint	T6	Rolled	Clad	Long	Plane stress	Ref. 41	8	9	CN
12	No buckling restraint	T6	Rolled	Clad	Long	Plane stress	Ref. 41	9	9	CN
13	No buckling restraint	T6	Rolled	Clad	Long	Plane stress	Ref. 41	10	9	CN
14	No buckling restraint	T6	Rolled	Clad	Long	Plane strain	Ref. 41	11	10	CN
15	No buckling restraint	T6	Rolled	Clad	Long	Plane strain	Ref. 45	11	11	CN
16	No buckling restraint	T6	Rolled	Clad	Trans	Plane stress	Ref. 41	12	12	CN
17	No buckling restraint	T6	Rolled	Clad	Trans	Plane stress	Ref. 42	12	13	CN
18	No buckling restraint	T6	Extruded	Bare	Long	Plane stress	Ref. 45	13	14	CN
19	No buckling restraint	T6	Forged	Bare	Long	Plane strain	Ref. 41	14	15	CN
20	No buckling restraint	T651	Rolled	Bare	Long	Plane strain	Ref. 46	15	16	CN
21	No buckling restraint	T651	Rolled	Bare	Long	Plane strain	Ref. 40	15	17	CN
22	No buckling restraint	T651	Rolled	Bare	Trans	Plane strain	Ref. 46	16	18	CN
23	No buckling restraint	T651	Rolled	Bare	Trans	Plane strain	Ref. 42	16	19	CN
24	No buckling restraint	T651	Rolled	Bare	Trans	Plane strain	Ref. 47	16	20	CN
25	No buckling restraint	T7351	Rolled	Bare	Long	Plane strain	Ref. 46	17	21	CN
26	No buckling restraint	T7351	Rolled	Bare	Trans	Plane strain	Ref. 46	18	21	CN
27	With buckling restraint	T6	Rolled	Bare	Trans	Plane strain	Ref. 41	19	22	CN
28	With buckling restraint	T6	Rolled	Clad	Long	Plane strain	Ref. 41	20	22	CN

153

```
/ID
M.0073 ACTION IN PROGRESS.
M.0072 BEGIN ACTIVITY.
/INPUT
/JOB GO


/JOB GO
          IRD=5
          IWR=6
2         READ(IRD,1001)J,I,T,W,AP,FGP,FNP,AM,FGM,FNM,FTY
1001      FORMAT(2I3,F7.3,8F7.2)
          IF(J-JLAST)6,7,6
6         WRITE(IWR,8)
8         FORMAT(1H1)
          JLAST=J
          ILAST=0
          WRITE(IWR,1000)
1000      FORMAT(3X,65HJ  I    W     T     AP     VN     KN    KIC    AN     VS
     1    KS    KC )
7         IF(I-ILAST)3,4,3
3         WRITE(IWR,5)
5         FORMAT(//)
          ILAST=I
4         IF(FGP)10,20,10
10        THETAP=1.57529*AP/W
          VN=FNP/FTY-.8
          IF(VN)15,15,18
15        CHN=FGP/.91*(W*SIN(THETAP)/COS(THETAP))**.5
          THETAN=THETAP+.0755/W*(CHN/FTY)**2
          CHIC=FGP/.91*(W*SIN(THETAN)/COS(THETAN))**.5
          WRITE(IWR,2000)J,I,W,T,AP,VN,CHN,CHIC
2000      FORMAT(2I3,F5.2,F6.3,4F6.2)
          GO TO 2
18        WRITE(IWR,2000)J,I,W,T,AP,VN
          GO TO 2
20        THETAS=1.57529*AM/W
          VS=FNM/FTY-.8
          IF(VS)25,25,28
25        CHS=FGM*(W*SIN(THETAS)/COS(THETAS))**.5
          THETAC=THETAS+.25/W*(CHS/FTY)**2
          CHC=FGN*(W*SIN(THETAC)/COS(THETAC))**.5
          WRITE(IWR,2004)J,I,W,T,AM,VS,CHS,CHC
          T 2
28        WRITE(IWR,2000)J,I,W,T,AM,VS
2004      FORMAT(2I3,F6.2,F6.3 ,24X,4F6.2)
          GO TO 2
          END
/DATA
    2  1 0.079   29.94    00.00   00.00   00.00   16.26   13.10   28.67   75.10
    4  3 0.124   09.09    3.06    13.20   20.00   00.00   00.00   00.00   80.00
```

A.

FIGURE 109

COMPUTER PROGRAM USED TO CALCULATE K_{IC} AND $K_C(B)$.
TYPICAL INPUTS ARE ALSO SHOWN

A:1   VS

67   76.10
00   80.00

155

B.

BLANK PAGE

TABLE XVIII

TYPICAL COMPUTER DATA OUTPUT FOR 7075 ALUMINUM

J	I	W	T	AP	VN	KN	KIC	AM	VS	KS	KC
19	22	3.03	0.064	0.83	0.01						
19	22	24.00	0.065	8.64	-0.47	68.31	68.51				
19	22	24.00	0.064	8.54	-0.48	67.39	67.58				
19	22	24.00	0.062	8.66	-0.45	72.28	72.51				
19	22	24.00	0.062	8.36	-0.43	77.45	77.74				
19	22	24.00	0.064	8.62	-0.44	74.22	74.47				
19	22	24.00	0.062	8.68	-0.38	86.61	87.00				
19	22	24.00	0.064	8.90	-0.47	82.73	83.07				
19	22	24.00	0.064	8.70	-0.43	75.94	76.21				
19	22	24.00	0.064	9.20	-0.38	88.08	88.49				
19	22	24.00	0.064	8.50	-0.35	93.14	93.63				
19	22	24.00	0.062	7.10	-0.42	76.36	76.67				
19	22	22.00	0.062	3.52	-0.37	71.41	71.86				
19	22	20.00	0.062	3.60	-0.36	71.89	72.35				
19	22	16.00	0.062	3.40	-0.33	72.59	73.10				
19	22	12.00	0.062	3.00	-0.33	65.27	65.71				
19	22	10.00	0.062	3.26	-0.25	73.34	73.95				
19	22	8.00	0.062	3.44	-0.24	66.62	67.13				
19	22	7.00	0.062	3.12	-0.24	62.57	63.05				
19	22	24.00	0.064	7.00	-0.47	66.46	66.66				
19	22	24.00	0.064	7.10	-0.42	76.36	76.67				
19	22	21.00	0.064	6.25	-0.42	72.75	73.06				
19	22	18.00	0.064	5.50	-0.40	70.93	71.25				
19	22	15.00	0.064	4.00	-0.37	68.35	68.73				
19	22	12.00	0.064	3.50	-0.33	67.34	67.77				
19	22	10.00	0.064	2.50	-0.27	67.20	67.77				
19	22	6.00	0.064	1.70	-0.19	61.45	62.11				
19	22	4.50	0.064	1.23	-0.10	60.35	61.20				

ν = Poisson's ratio

KC = critical stress intensity factor associated with unstable plane-stress fracturing

KIC = critical stress-intensity factor associated with initiation of unstable plane-strain fracturing

J,I = numbers identifying each set of data, as shown in Table XVII

The results of each test were scanned to ascertain whether (1) the specimen had exhibited the crack pop-in that is characteristic of plane-strain fracturing and (2) VN = FNP/FTY − 0.8 ≤ 0. Calculations for K_{Ic} are considered invalid if these conditions are not met. Subsequently, values for the plane-strain fracture parameter were calculated both neglecting the plasticity correction term, and including the plasticity correction term. The following equations were used:

value, KN, neglecting plasticity term (17)

$$KN = FGP \left\{ \left[\frac{W}{(1-\nu^2)} \right] \tan \left(\frac{\pi \cdot AP}{W} \right) \right\}^{1/2}$$

value, KIC, including plasticity term (18)

$$KIC = FGP \left\{ \left[\frac{W}{(1-\nu^2)} \right] \tan \left[\left(\frac{\pi \cdot AP}{W} \right) + \left(\frac{0.0756}{W} \right) \left(\frac{KN}{FTY} \right)^2 \right] \right\}^{1/2}$$

Similarly, if the specimen exhibited no pop-in and VS = FNM/FTY − 0.8 ≤ 0 values for the plane-stress fracture toughness parameter were calculated neglecting the plasticity correction term and including the plasticity correction term. The following equations were used:

value, KS, neglecting plasticity term (19)

$$KS = FGM \left[W \cdot \tan \left(\frac{\pi \cdot AM}{W} \right) \right]^{1/2}$$

value, KC, including plasticity term (20)

$$KC = FGM \left\{ W \cdot \tan \left[\left(\frac{\pi \cdot AM}{W} \right) + \left(\frac{0.25}{W} \right) \left(\frac{KS}{FTY} \right)^2 \right] \right\}^{1/2}$$

158

The results of the K_{Ic} and $K_c(B)$ computations on the 7075 Aluminum data reveal the following:

o   A major portion of the references that were abstracted in a manner so as to report K_{Ic} data for 7075 did not contain any new data. The K_{Ic} values reported or used were obtained from previous references.

o   Many of the K_{Ic} values reported did not contain adequate supplementary information describing the specimen geometry to ascertain whether the test was valid for K_{Ic}.

o   The oldest references were found to contain invalid test geometries or used test procedures that were later discovered to introduce errors in the measurement of K_{Ic}. For example, all "ink staining" tests were not included based on the findings of Steigerwald, et al (47) regarding the detrimental effect of the ink and water base solutions on K_{Ic}.

o   The specimen geometry was such that, although K_{Ic} was reported, the width-to-thickness ratio was out of the range for a valid K_{Ic} test.

o   Many of the reported results are from tests conducted at low temperatures and could not be considered.

Those 7075-T6, T65, T6511 Aluminum specimens that were not eliminated were combined into three groups, with results as follows:

Group I - Material Producers: 80 Tests

  Average K_{Ic} - 30.15 KSI $(in)^{1/2}$

  Standard Deviation - 2.97

  Coefficient of variation - 0.099

Group II - Defense Information Center - 120 Tests

  Average K_{Ic} - 47.65 KSI $(in)^{1/2}$

  Standard Deviation - 15.86

  Coefficient of Variation - 8.33

Group III - Aerospace Industry and Others - 60 Tests

  Average K_{Ic} - 33.08 KSI $(in)^{1/2}$

  Standard Deviation - 2.32

  Coefficient of Variation - 0.07

Using these three sets of data, 90%, 95% and 99% confidence values can be established. The overbound 90% confidence value is given approximately by the mean value minus twice the standard deviation. As mentioned in the Introduction, this is called $K_{Ic}(B)$ and is the value that 90% of the material would be expected to exceed. The lower bound 95% confidence value is approximated by the mean K_{Ic} minus 2.5 standard deviations. The lower bound 99% confidence value, $K_{Ic}(A)$, is given by K_{Ic}(Mean) - 3.4 (Standard deviation). The results are as follows:

159

Group	I	II	III
Mean K_{Ic}	30.15 KSI $(in)^{1/2}$	47.65 KSI $(in)^{1/2}$	33.08 KSI $(in)^{1/2}$
lower bound 90% confidence Value K_{Ic}(B)	24.11 KSI $(in)^{1/2}$	NA	28.541 KSI $(in)^{1/2}$
lower bound 95% Confidence Value K_{Ic}	22.73 KSI $(in)^{1/2}$	NA	27.27 KSI $(in)^{1/2}$
lower bound 99% Confidence Value K_{Ic}(A)	20.05 KSI $(in)^{1/2}$	NA	25.18 KSI $(in)^{1/2}$

NA: Standard Deviation too high

160

Part 2 - Round Fracture Toughness Specimens

Because of the lack of available test data on K_{Ic} values for the 4330 V Modified steel, it was decided to test at least 25 specimens of 4330V Modified steel in the longitudinal grain direction and 15 specimens in the transverse grain direction. These specimens were designed using ASTM standards (2), and were round center-notched and fatigue-precracked specimens.

All specimens were made as shown in Figure 110. The specimens were machined to rough dimensions and finished-machined after heat-treatment. The specimens were then placed in an engine lathe and loaded to produce a fatigue crack in the base of the notch. Figures 111 and 112 show the experimental setup used to produce fatigue cracks. One end of the specimen was threaded into a collet mounted in a three-jaw chuck. The other end was threaded into a long collet that was loaded at the free end. The collet was supported near the specimen.

Several methods were tried to produce a constant bending moment at the base of the notch. Dead-weight loading was found to give the most constant results.

Specimens were fatigued for 10,000 cycles at 150 rpm, at which time they were inspected to determine if fatigue cracks developed in the base of the notch. If the fatigue crack was not sufficiently developed, the specimen was fatigued further. A special ultrasonic fatigue crack-measuring system was developed to detect and monitor the growth of the fatigue crack. This is described below.

An ultrasonic pulse-echo system, Sperry UM 721, was used to obtain a "C" scan of the plane of the circumferential notch. Flat, beam-pulsed, echo ultrasound was introduced into the specimen which was immersed in water. The surface of the specimen was sealed using a water-repellent tape and sealing wax. The X-Y scanning was coupled with the motion of the transducer. The passing of the signals obtained from the transducer through the uncracked material caused a dark recording on the "C" scan record. Typical fatigue cracks gave signals of saturated or near-saturated amplitude, causing white areas on the recording. Only moderate definition of the fatigue crack outline was obtained.

Typical "C" scan results on fatigued specimens are shown in Figures 113, 115, 117, and 118. The fracture surface of these specimens after failure is shown in Figures 114, 116, and 119. The actual fatigue area can be seen as a light surface reflection.

Figure 116 shows a typical fatigue cracked specimen. Figure 115 shows the "C" scan recording indicating that this specimen was cracked around the circumference. Figures 117 and 118 show two recordings taken from the same specimen #19 at two stages of fatigue. The first figure shows that the fatigue crack does not extend all around the specimen. The specimen was replaced in the lathe and fatiguing was continued. The second Figure (118) shows that the cracking was all around the base of the notch. Figure 119 shows the fracture surface of the specimen. This technique enables the test engineer to determine when his specimen has been fatigued for a sufficient time.

The results of the failure-testing of the specimens of 4330V Modified steel are given in Tables XIX and XX.

60±1°

0.001 ±0.0005 R

SECTION A

1.5 - 10 THREADS

0.03R TYP

1.50

A

1.050

1.50

1.250

2.50

5.00

ALL DIMENSIONS IN INCHES
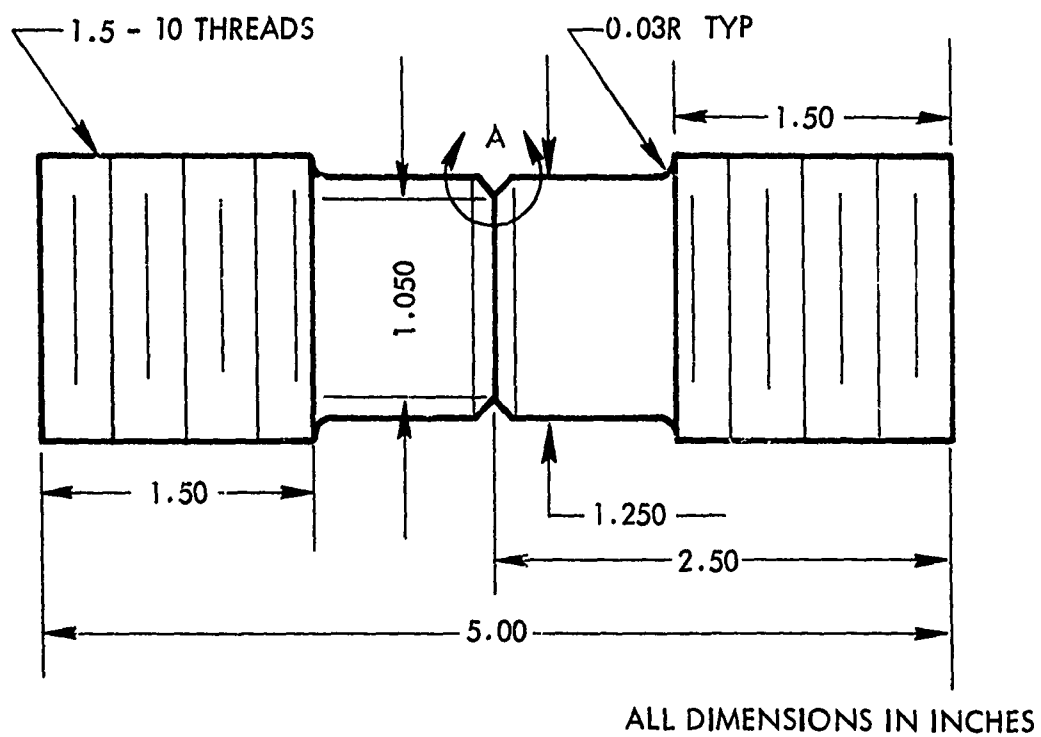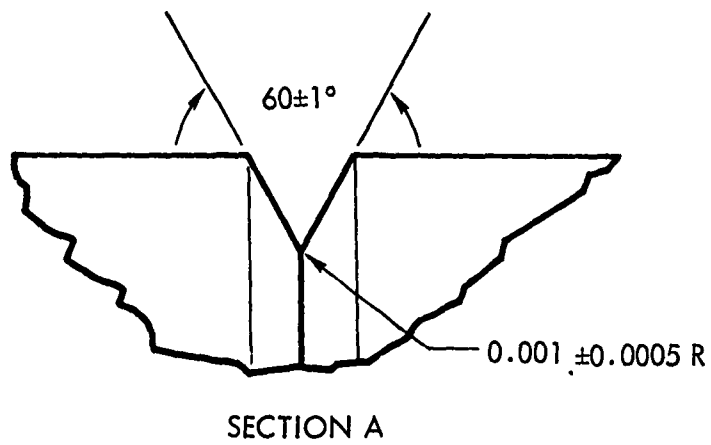
FIGURE 110   ROUND CENTER-NOTCHED FRACTURE TOUGHNESS SPECIMEN

162
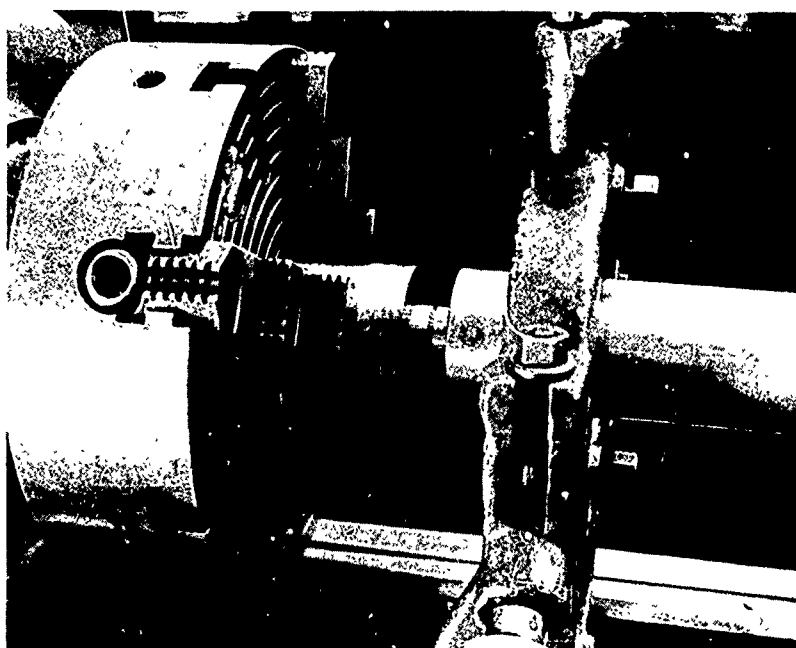
FIGURE 111 EXPERIMENTAL SET UP FOR FATIGUE CRACKING OF THE 4330V MODIFIED STEEL ROUND CENTER NOTCHED FRACTURE TOUGH-NESS SPECIMENS
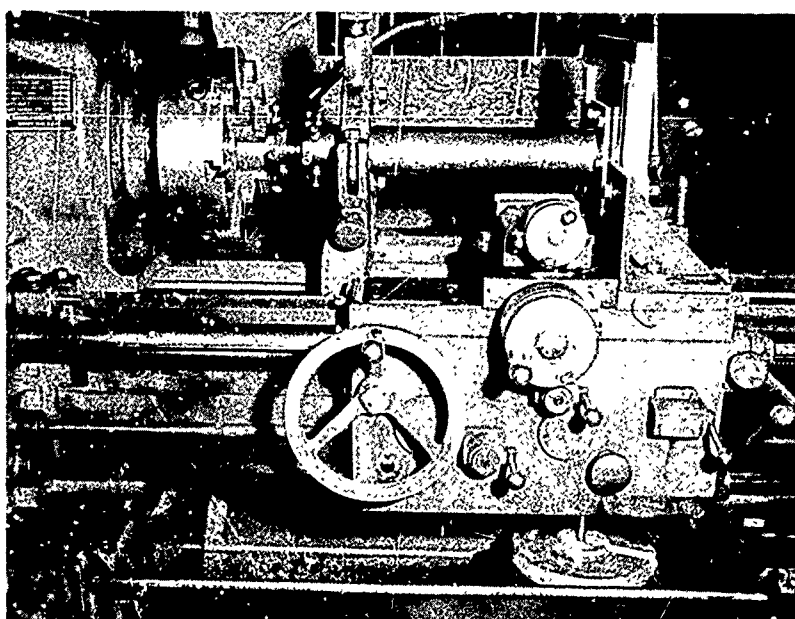
FIGURE 112 EXPERIMENTAL SET UP FOR FATIGUE CRACKING OF THE 4330V MODIFIED STEEL ROUND CENTER NOTCHED FRACTURE TOUGH-NESS SPECIMENS

163
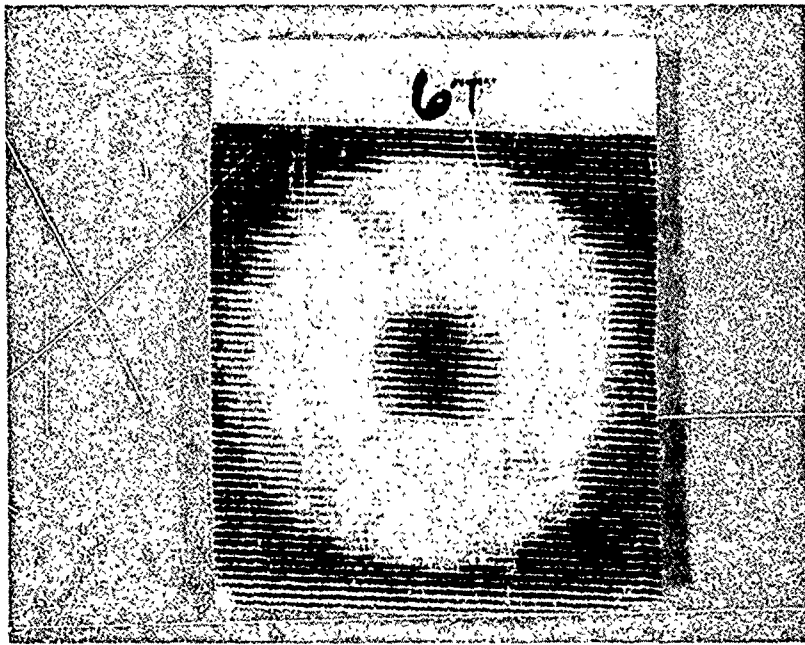
FIGURE 113   "C" SCAN OF SAMPLE 6T MADE DURING SAMPLE PRODUCTION
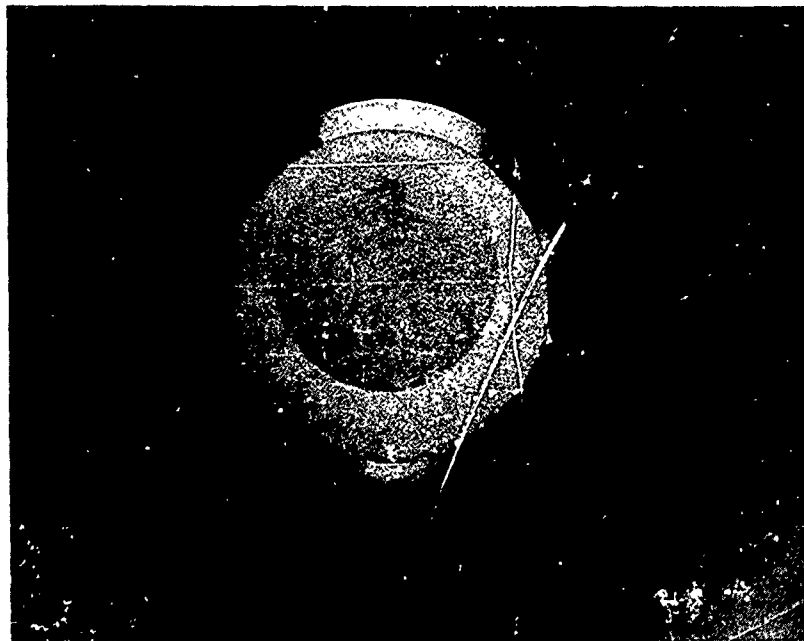
FIGURE 114   FRACTURE SURFACE OF SAMPLE 6T ROUND FRACTURE TOUGH-
NESS SPECIMEN
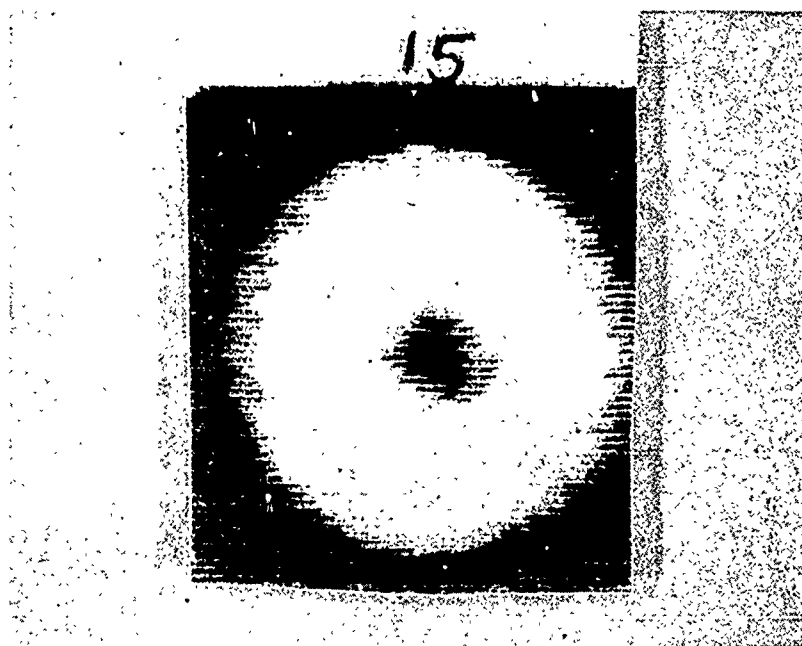
FIGURE 115   "C" SCAN OF SAMPLE 15 MADE DURING SAMPLE PRODUCTION

FIGURE 116   FRACTURE SURFACE OF SAMPLE 15, ROUND FRACTURE TOUGH-
NESS SPECIMEN

FIGURE 117   "C" SCAN OF INADEQUATELY FATIGUED SPECIMEN, SAMPLE 19
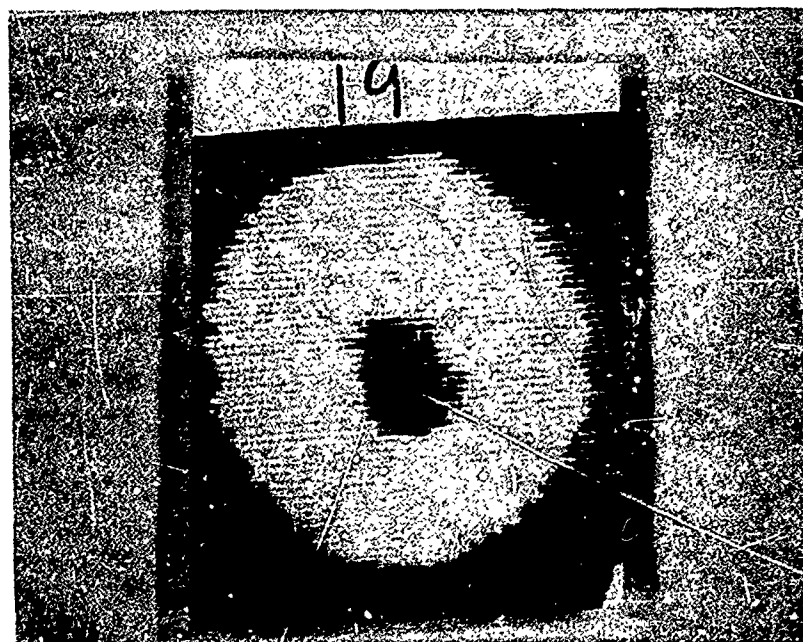
FIGURE 118   "C" SCAN OF FATIGUED SPECIMEN, SAMPLE 19
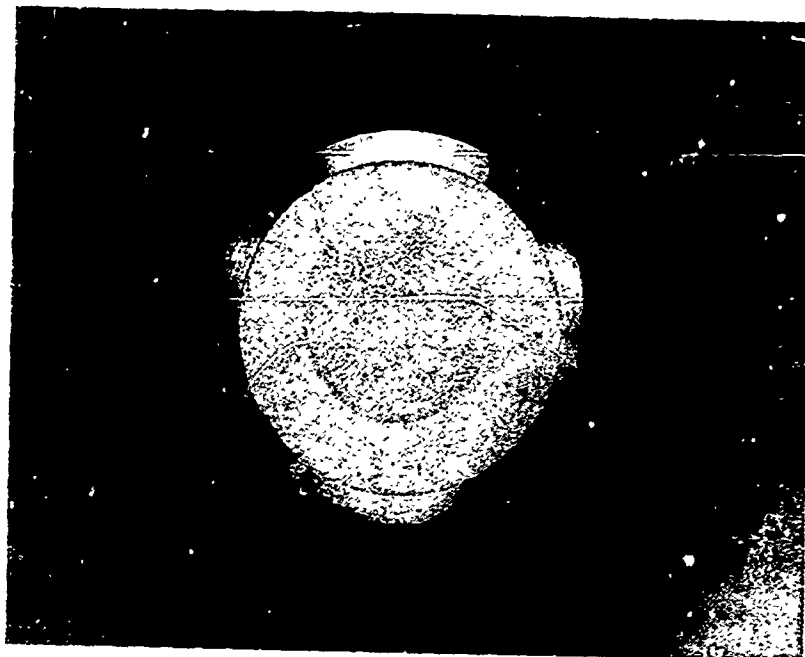
FIGURE 119   FRACTURE SURFACE OF SAMPLE 19 ROUND FRACTURE
TOUGHNESS SPECIMEN

TABLE XIX

RESULTS OF ROUND CENTER-NOTCHED AND FATIGUE-PRECRACKED K_{Ic} TESTS ON 4330V MODIFIED STEEL (220-240 KSI HEAT TREAT)-LONGITUDINAL

Specimen number	D''	d''	P, lbs	$\frac{D}{d}$	$1.72\frac{D}{d}$	Y	$D^{1/2}$	K_{Ic} KSI(in)$^{1/2}$
2	1.251	0.961	59,400	1.30	2.236	0.966	1.1185	51.3
3	1.253	0.797	38,800	1.57	2.700	1.430	1.1194	49.6
4	1.250	0.926	45,600	1.35	2.322	1.052	1.1181	42.9
5	1.253	0.887	41,890	1.41	2.425	1.155	1.1194	43.2
6	1.250	0.931	49,600	1.34	2.305	1.035	1.1181	45.9
7	1.250	0.797	36,000	1.57	2.700	1.430	1.1181	46.0
9	1.253	0.941	64,100	1.33	2.288	1.018	1.1194	53.3
10	1.251	0.858	45,000	1.46	2.511	1.241	1.1185	49.9
11	1.250	0.814	41,300	1.54	2.649	1.379	1.1181	50.9
12	1.253	0.808	40,700	1.55	2.666	1.396	1.1194	50.8
16	1.250	0.859	39,500	1.46	2.511	1.241	1.1181	43.8
18	1.254	0.832	41,100	1.51	2.597	1.327	1.1198	48.7
19	1.250	0.730	48,300	1.71	2.941	1.671	1.1181	72.2
20	1.250	0.787	34,600	1.59	2.735	1.465	1.1181	45.1
21	1.250	0.891	46,200	1.40	2.408	1.138	1.1181	47.0
22	1.251	0.912	49,200	1.37	2.356	1.086	1.1185	47.8
23	1.250	0.882	45,900	1.42	2.442	1.172	1.1181	48.1
24	1.250	0.767	28,700	1.63	2.804	1.534	1.1181	39.4
27	1.250	0.816	39,700	1.53	2.632	1.326	1.1181	48.4

Note: $Y = \left(1.72\frac{D}{d} - 1.27\right)$

Mean (M)   = 48.6

Std. Dev. (σ) = 6.7

$M - 2\sigma$ = 35.3

$M - 2.5\sigma$ = 31.9

$M - 3.4\sigma$ = 25.9

TABLE XX

RESULTS OF ROUND CENTER NOTCHED AND FATIGUE PRECRACKED K_{Ic} TESTS ON
4330V MODIFIED STEEL (220-240 KSI HEAT TREAT)-TRANSVERSE

Specimen number	D"	d"	P, lbs	$\frac{D}{d}$	$1.72\frac{D}{d}$	Y	$D^{1/2}$	K_{Ic} KSI(in)$^{1/2}$
1T	1.250	0.911	46,500	1.37	2.356	1.086	1.1181	45.2
2T	1.250	0.882	44,800	1.42	2.442	1.172	1.1181	47.0
3T	1.250	0.897	45,800	1.39	2.391	1.121	1.1181	45.9
4T	1.250	0.833	41,200	1.50	2.580	1.310	1.1181	48.3
6T	1.250	0.833	34,600	1.50	2.580	1.310	1.1181	40.5
7T	1.251	0.976	53,500	1.28	2.202	0.932	1.1185	44.6
8T	1.251	0.868	43,300	1.44	2.477	1.207	1.1185	46.7
9T	1.250	0.693	29,500	1.80	3.096	1.826	1.1181	48.2
12T	1.250	0.860	45,700	1.45	2.494	1.224	1.1181	50.0
13T	1.250	0.941	55,000	1.33	2.288	1.018	1.1181	50.1
14T	1.252	0.772	43,000	1.62	2.786	1.516	1.1189	58.3
15T	1.251	0.817	33,200	1.53	2.632	1.362	1.1185	40.2
16T	1.250	0.436	12,500	2.87	4.936	3.666	1.1181	41.0
18T	1.251	0.743	30,600	1.68	2.890	1.620	1.1185	44.3

Note: $Y = \left(1.72\frac{D}{d} - 1.27\right)$

Mean (M) $= 46.5$ KSI $\sqrt{in}$

Std. Dev. (σ) $= 4.70$

$M - 2\sigma = 37.1$

$M - 2.5\sigma = 34.7$

$M - 3.4\sigma = 30.5$

The analysis followed the procedure outlined in STP 410 (3). The K_{Ic} was calculated as follows:

$$K_{Ic} = \frac{P}{D^{1/2}} \quad (1.72 \frac{D}{d} - 1.27) \tag{21}$$

where D is the major diameter, d the fatigue notch diameter (corrected for plasticity), and P the applied load.

The mean value of K_{Ic} for the 4330V Modified steel heat treated to 220-240 KSI is 48.6 KSI $(in)^{1/2}$. In the longitudinal direction, the value of K_{Ic} that 90% of the material would be expected to exceed is $K_{Ic}(B) = 35.3$ KSI$(in)^{1/2}$ the value of $K_{Ic}(A) = 25.9$ KSI$(in)^{1/2}$. The $K_{Ic}(A)$ is the minimum that would be expected for the material.

The mean value of K_{Ic} for the transverse 4330V Modified steel specimens is 46.5 KSI$(in)^{1/2}$. As was expected, this is lower than the longitudinal value. However, due to the smaller scatter about the mean, the 90% confidence value is 37.1 KSI$(in)^{1/2}$.

The results seem to indicate that, although the average transverse K_{Ic} is lower than the longitudinal K_{Ic} value, there is less scatter in the results.

Part 3 - Fracture Mechanics Analysis

All of the tubes tested to failure were analyzed using a part through crack fracture toughness analysis. The analysis of Tiffany and Masters (2) was used for all cracks irrespective of the crack depth, a. It should be realized that, if the depth of the crack is more than halfway through the thickness, a magnification factor should be used to correct the K_{Ic} value. This correction for the nearness of the crack to the inside wall was made by superposition of additional K_{Ic} factors as described later.

Test Results

Figure 120 shows the failure stress of the 7075-T6511 Aluminum cylinders as a function of the actual crack length, 2c. The failure stress drops slightly with increasing crack length as was expected. The scatter in the data is due primarily to variations in crack depth, a, within a particular range of crack lengths, 2c; the lower values are specimens with a deeper crack depth. For crack lengths less than 0.2 inches there is no apparent loss in strength. Figure 121 shows the failure stress of the heat treated 4330V Modified steel cylinders as a function of the actual crack length, 2c. For this material, it appears that crack length of 0.1 inches or longer will reduce the failure stress. Again, the variations in failure stress for a constant value of 2c can be attributed to variations in crack depth, a. The drop in failure stress for these specimens with increasing 2c is greater than that observed for the aluminum cylinders.

Figure 122 shows the failure stress as a function of the actual crack depth, a, for the 7075-T6511 Aluminum cylinders. It can be seen that for a constant crack depth, a, there is some scatter due to the crack length, 2c. The failure stress for specimens containing cracks of depth from 0.00 to 0.10 is about 85 KSI, and drops to 55 KSI for cracks of depth 0.24 inches. Figure 123 shows the failure stress of the 4330V Modified steel cylinders as a function of crack depth, a. The variation in failure stress with crack depth is more pronounced for these specimens. For crack depths from 0.00 to 0.06 inches the failure stress remains essentially constant at 218 KSI. However, the stress drops to 155 KSI for cracks of depth 0.22 inches. As before, the scatter in the failure stress at a constant crack depth may be due to variations in the crack length.

Figure 124 shows the failure stress for the 7075-T6511 Aluminum cylinders as a function of the flaw shape parameter a/Q. This plot reduces the scatter in the failure stress considerably. This is to be expected, since the Q factor includes both a and 2c. The dependence on a/Q of the failure stress in the aluminum cylinders is of the same magnitude as the steel cylinders (Figure 125).

Stress Intensity Factors for 7075-T6511 Aluminum and 4330V Modified Steel

Figure 126 is a plot of the apparent critical stress intensity factor, K_{IX}, for the 7075-T6511 Aluminum cylinders versus the crack length, 2c. The equation used to determine the K_{IX} is as follows:

$$K_{IX} = 1.1 \sigma \sqrt{\pi \frac{a}{Q}} \tag{22}$$

The value of Q in these specimens is corrected for plasticity by using the ratio of failure stress to yield stress. The yield stress was measured directly on those specimens that exhibited yielding, and the failure stress was taken from each specimen. This was done to

171
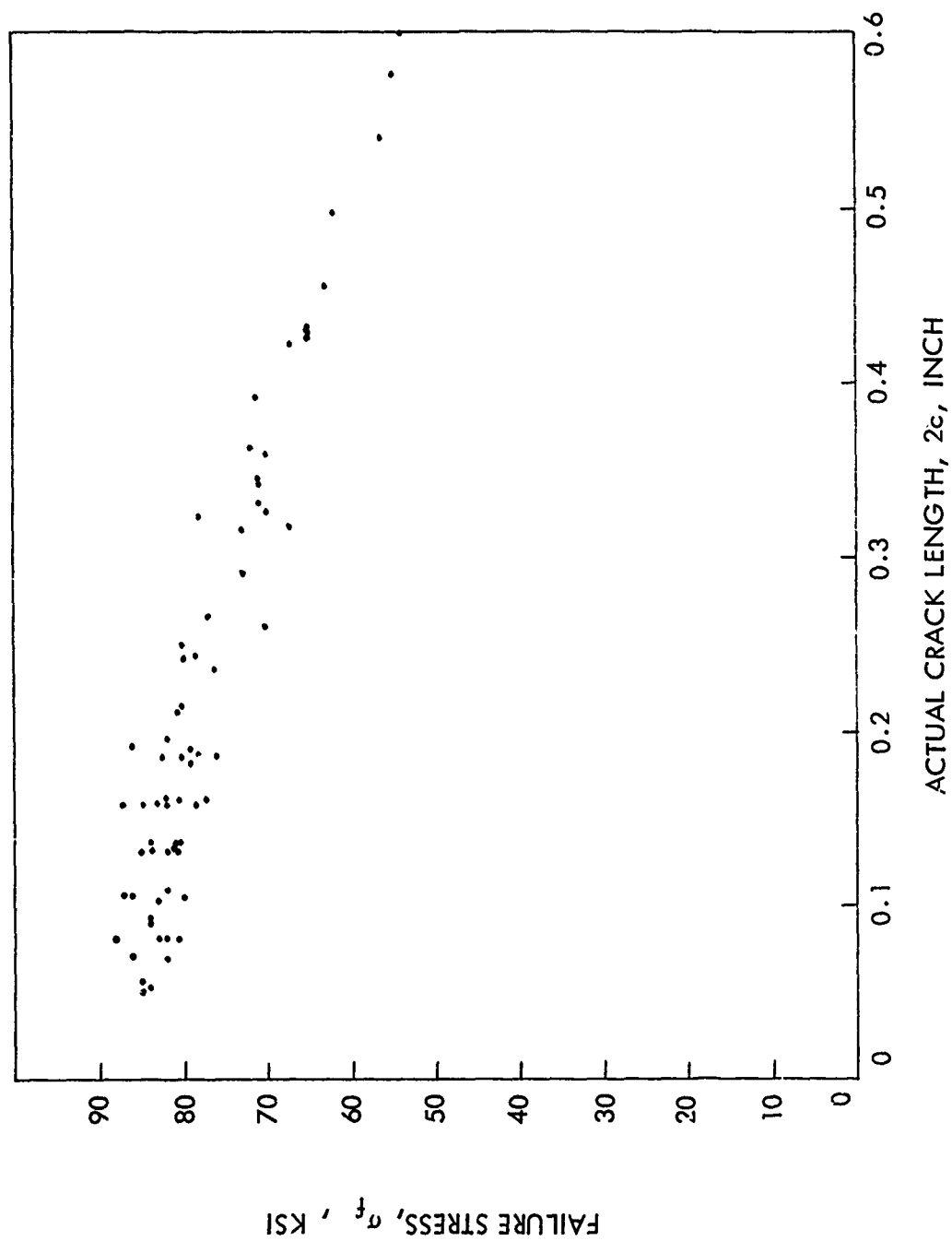
FIGURE 120 FAILURE STRESS VS ACTUAL CRACK LENGTH (2c) FOR 7075-T6511 ALUMINUM CYLINDERS
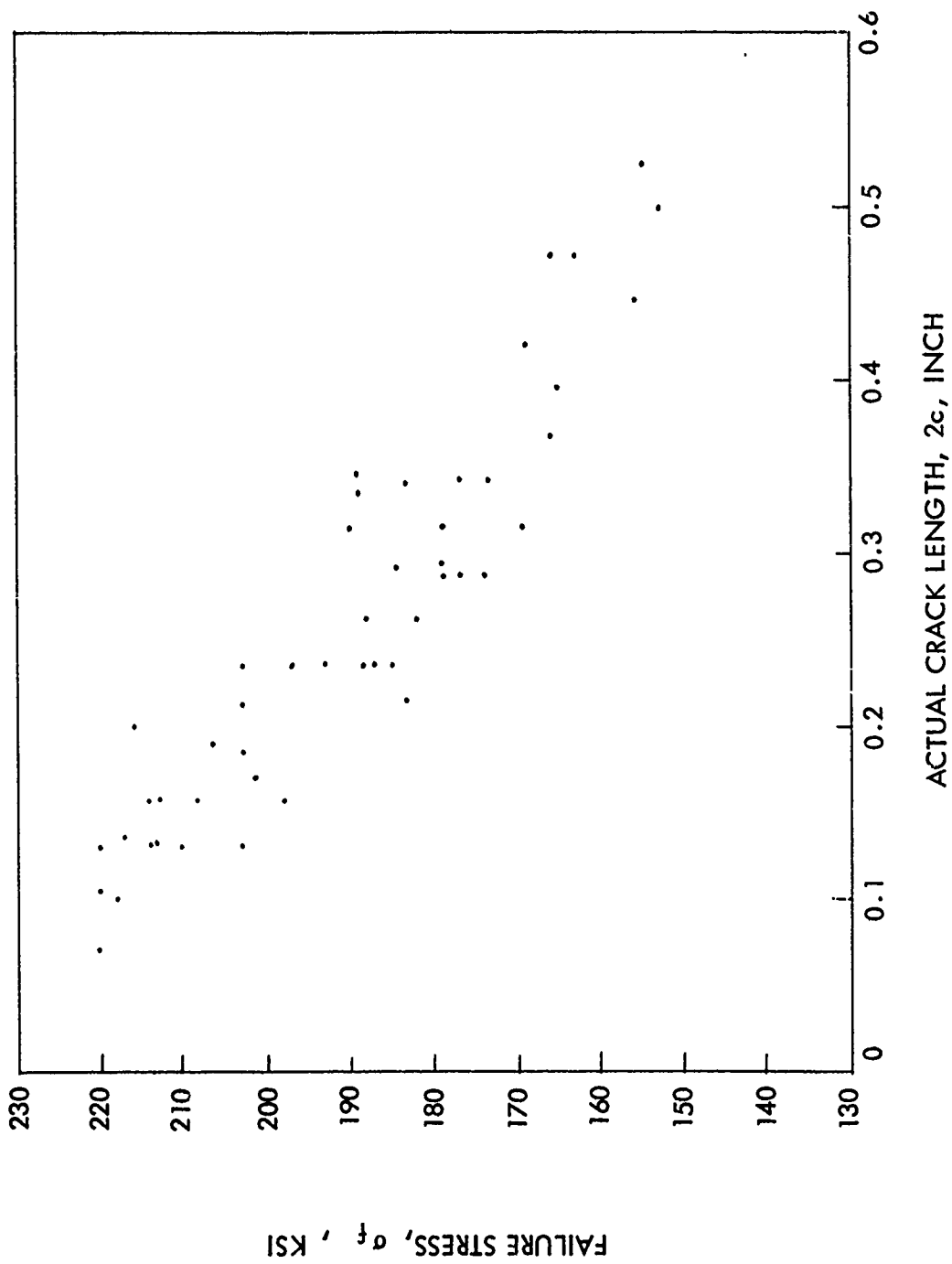
FIGURE 121   FAILURE STRESS VS ACTUAL CRACK LENGTH (2c) FOR 4330 V MODIFIED STEEL CYLINDERS
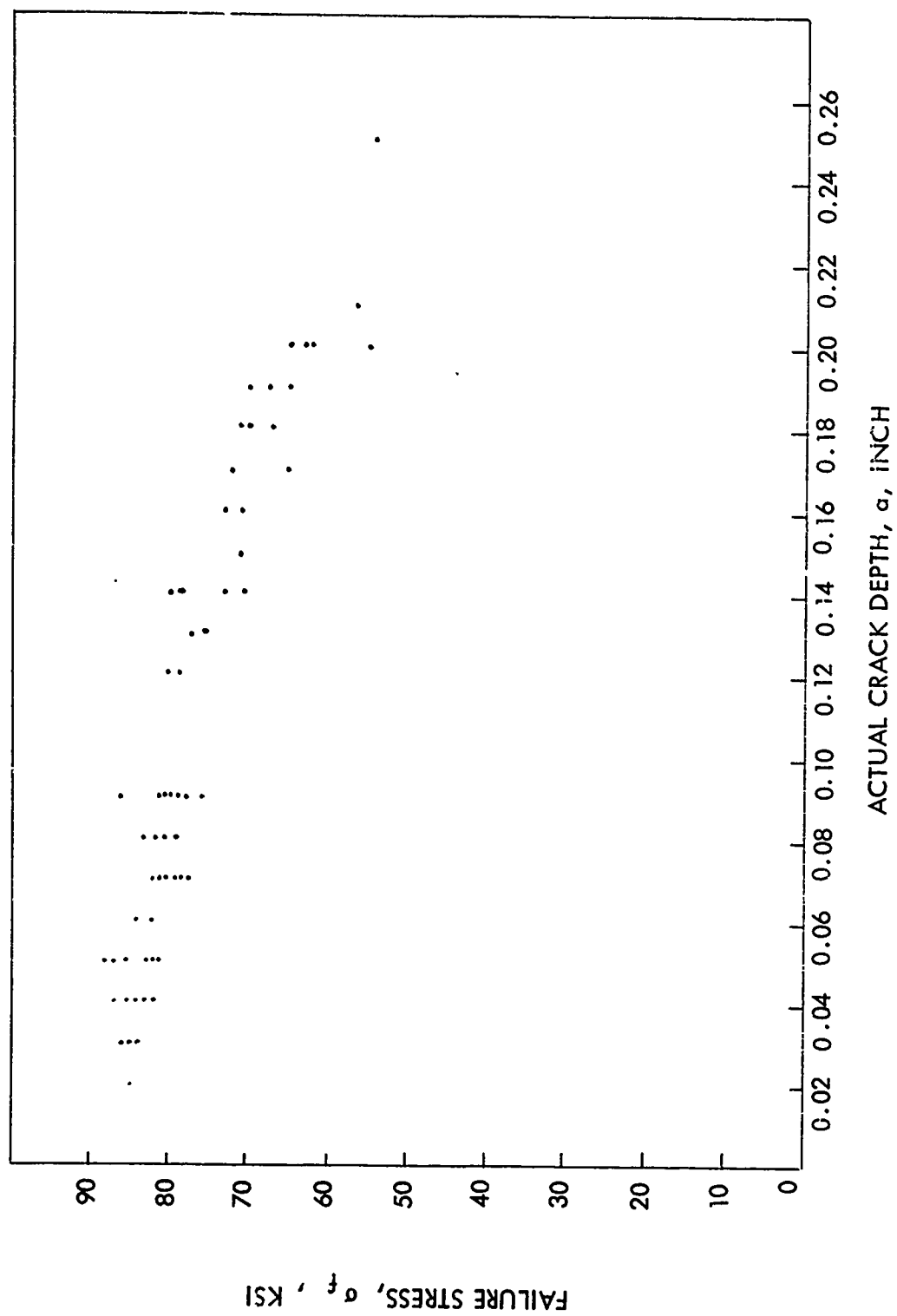
FIGURE 122   FAILURE STRESS VS ACTUAL CRACK DEPTH FOR 7075-T6511 ALUMINUM CYLINDERS

174
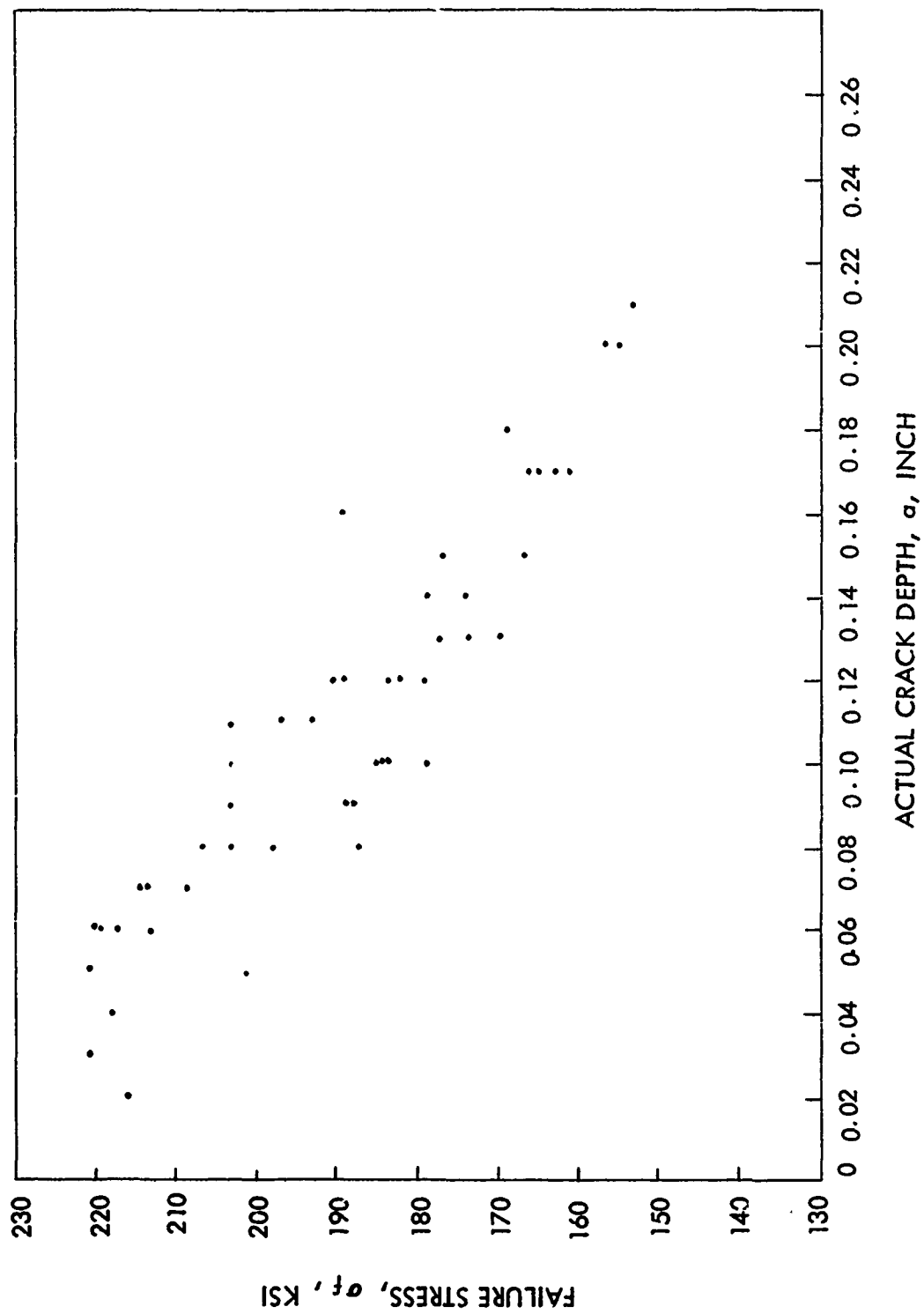
FIGURE 123 FAILURE STRESS VS ACTUAL CRACK DEPTH FOR 4330 V MODIFIED STEEL CYLINDERS

175

ACTUAL FLAW SHAPE PARAMETER, a/Q, INCH

FAILURE STRESS, σ_f, KSI
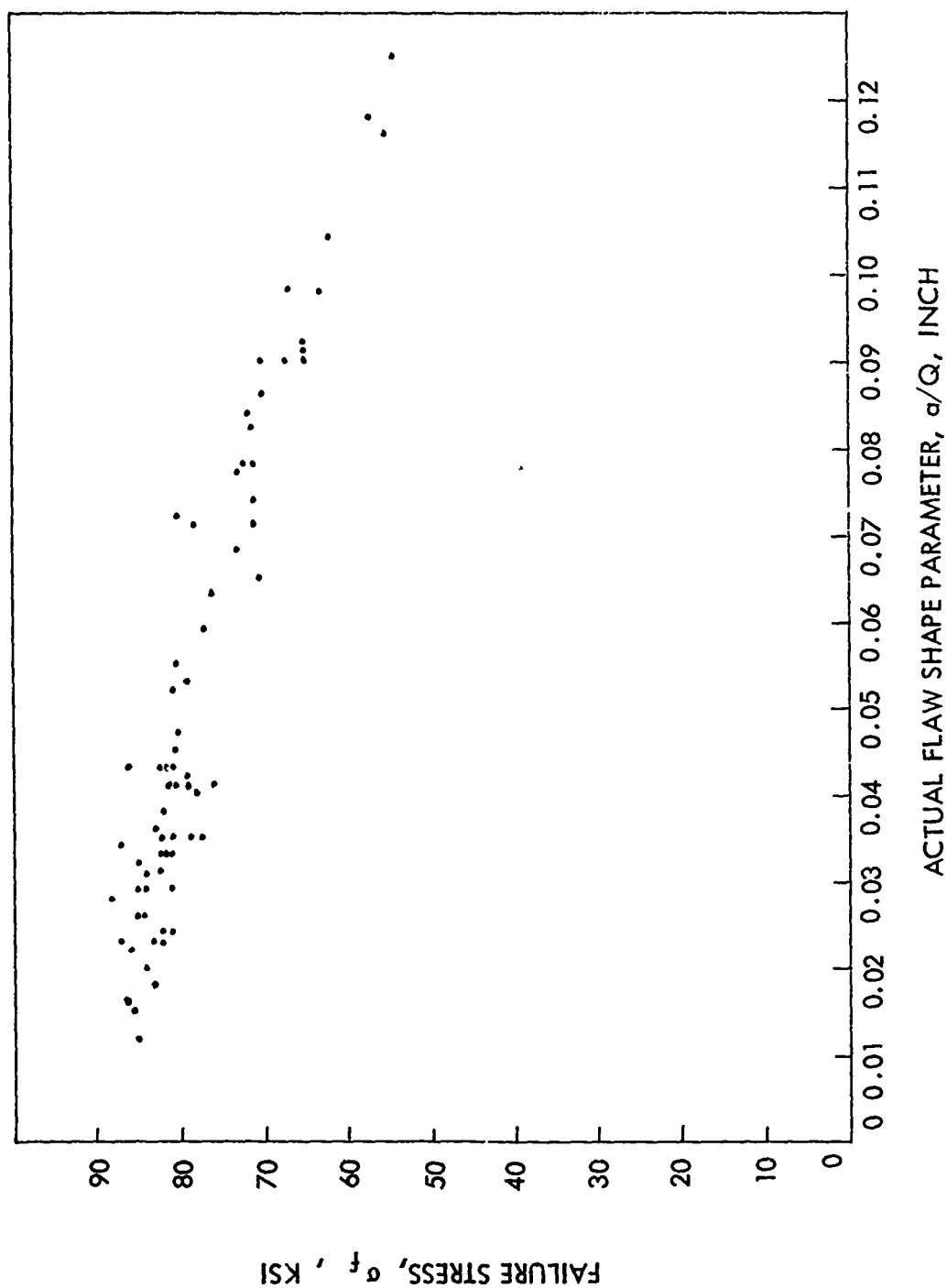
FIGURE 124   FAILURE STRESS VS $\frac{a}{Q}$ FOR 7075-T6511 ALUMINUM CYLINDERS

176

ACTUAL FLAW SHAPE PARAMETER a/Q, INCH

FAILURE STRESS, σ_f , KSI

FIGURE 125   FAILURE STRESS, σ_f VS ACTUAL FLAW SHAPE PARAMETER, a/Q FOR 4330 V MODIFIED STEEL CYLINDERS

177
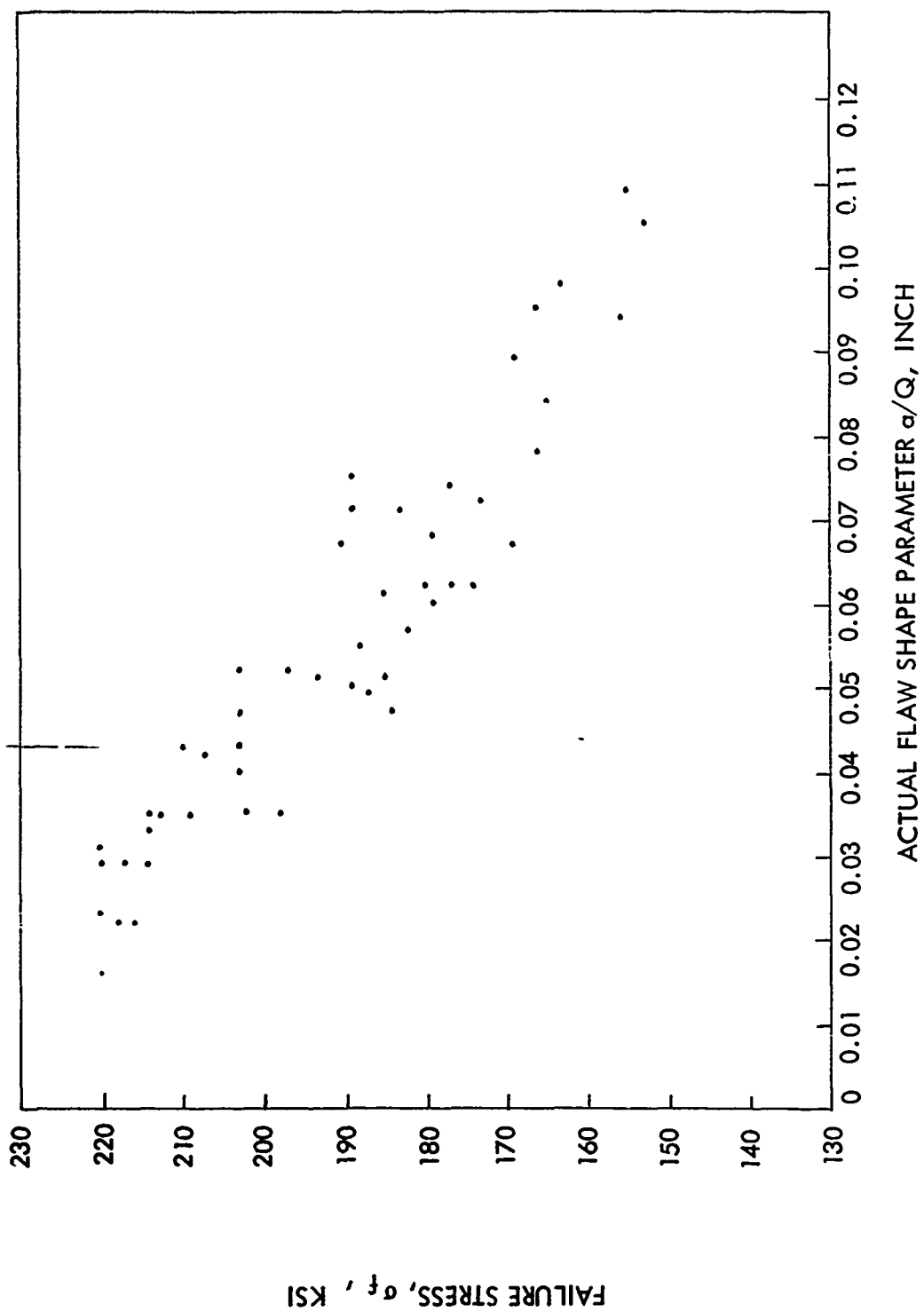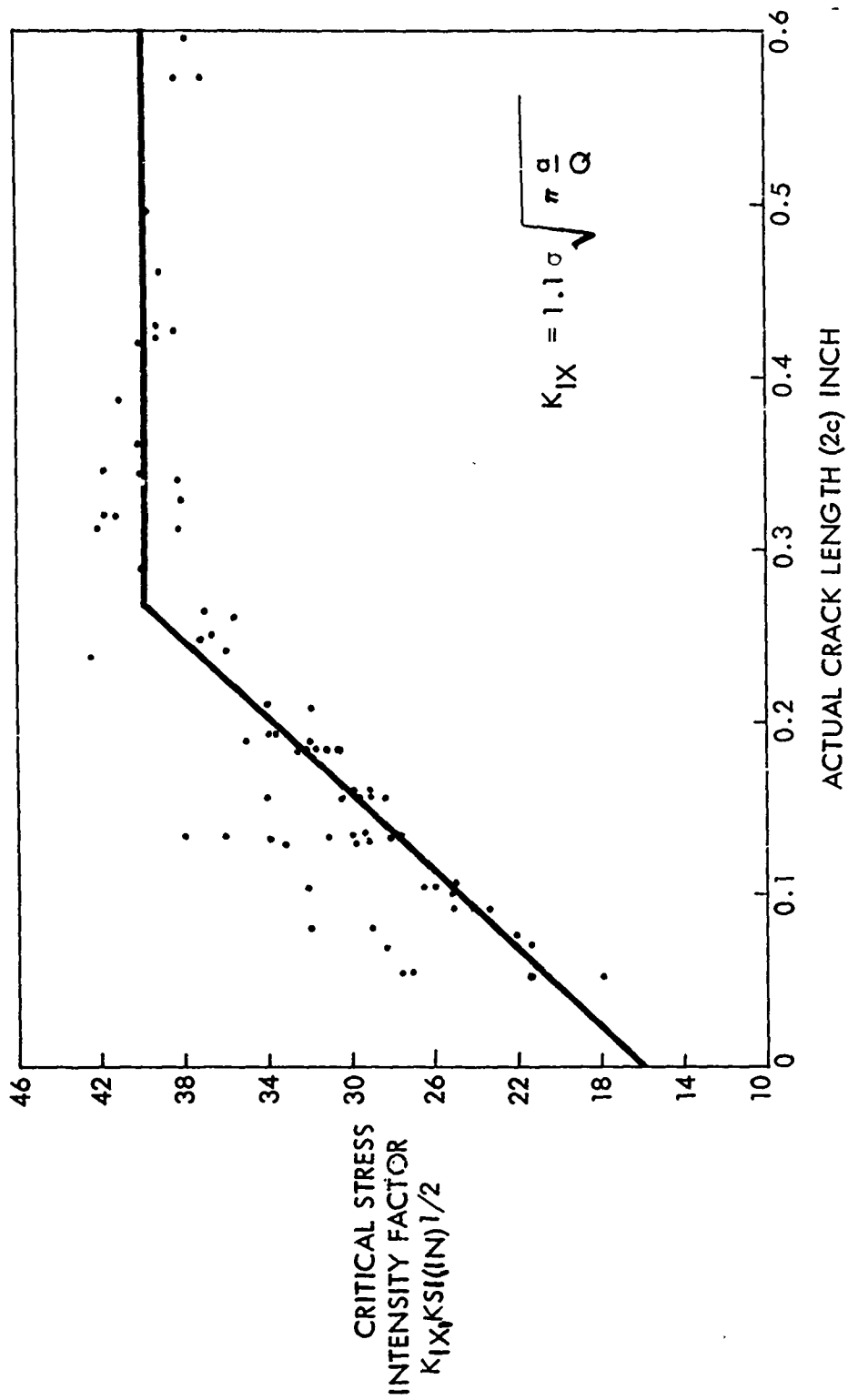
FIGURE 126   APPARENT CRITICAL STRESS INTENSITY FACTOR K_{IX} VS ACTUAL CRACK LENGTH
FOR 7075-T6511 ALUMINUM CYLINDERS

correct the Q value for the plasticity that occurred at the base of the crack, and is considered a standard procedure. The equation for Q is given in Section III, Equations 15 and 16. It should be realized that Equation 22 would not be expected to hold for crack geometries that are outside the specified ranges. In particular, if the crack depth, a, is over one half of the thickness, the K_{IX} that is obtained is too high. This is evident in Figure 126, where K_{IX} for the aluminum cylinders calculated using Equation 22 is plotted as a function of crack length, 2c, and in Figure 127, where K_{IX} is plotted as a function of crack depth, a. The K_{IX} for the Aluminum cylinders increases as the crack length, 2c, and crack depth, a, increase. For crack lengths over 0.30 inch and crack depths over 0.12 inch, K_{IX} remains essentially constant. When the K_{IX} is plotted as a function of the flaw shape parameter, a/Q (Figure 128), K_{IX} increases up to an a/Q value of about 0.6, and then remains constant. For the 7075-T6511 Aluminum cylinders the variation in K_{IX} KSI(in)$^{1/2}$ can be expressed in terms of the flaw geometry as follows:

$$K_{IX} = 17.0 + 140 \, c \qquad a, Q \text{ constant, } 2C < 0.275 \text{ inch} \qquad (23)$$

$$K_{IX} = 40 \qquad a, Q \text{ constant, } 2C > 0.275 \text{ inch}$$

$$K_{IX} = 17.0 + 180 \, a, \qquad 2c, \, Q \text{ constant } a < .125 \text{ inch} \qquad (24)$$

$$K_{IX} = 40 \qquad 2c, \, Q \text{ constant } a > .125 \text{ inch}$$

$$K_{IX} = 17.0 + 360 \frac{a}{Q}, \qquad \frac{a}{Q} < 0.625 \text{ inch} \qquad (25)$$

$$K_{IX} = 40 \qquad \frac{a}{Q} > 0.625 \text{ inch}$$

Figure 129 is a plot of the K_{IX} for the 4330V Modified steel cylinders versus actual crack length 2c. The K_{IX} was calculated using Equation 22 and the Q factor incorporated the plasticity correction as in the actual ratio of failure stress to yield stress. The K_{IX} increases linearly with crack length 2c. Figures 130 and 131 show the change in K_{IX} with crack depth, a, and flaw shape parameter, a/Q. In these cases, K_{IX} also increases linearly with the geometric variable.

For the 4330V Modified steel cylinders, the variation in K_{IX} KSI(in)$^{1/2}$ can be expressed in terms of the flaw geometry as follows:

$$K_{IX} = 64 + 145 \, c \qquad a, Q \text{ constant} \qquad (26)$$

$$K_{IX} = 64 + 220 \, a \qquad c, Q \text{ constant} \qquad (27)$$

$$K_{IX} = 64 + 400 \frac{a}{Q} \qquad (28)$$
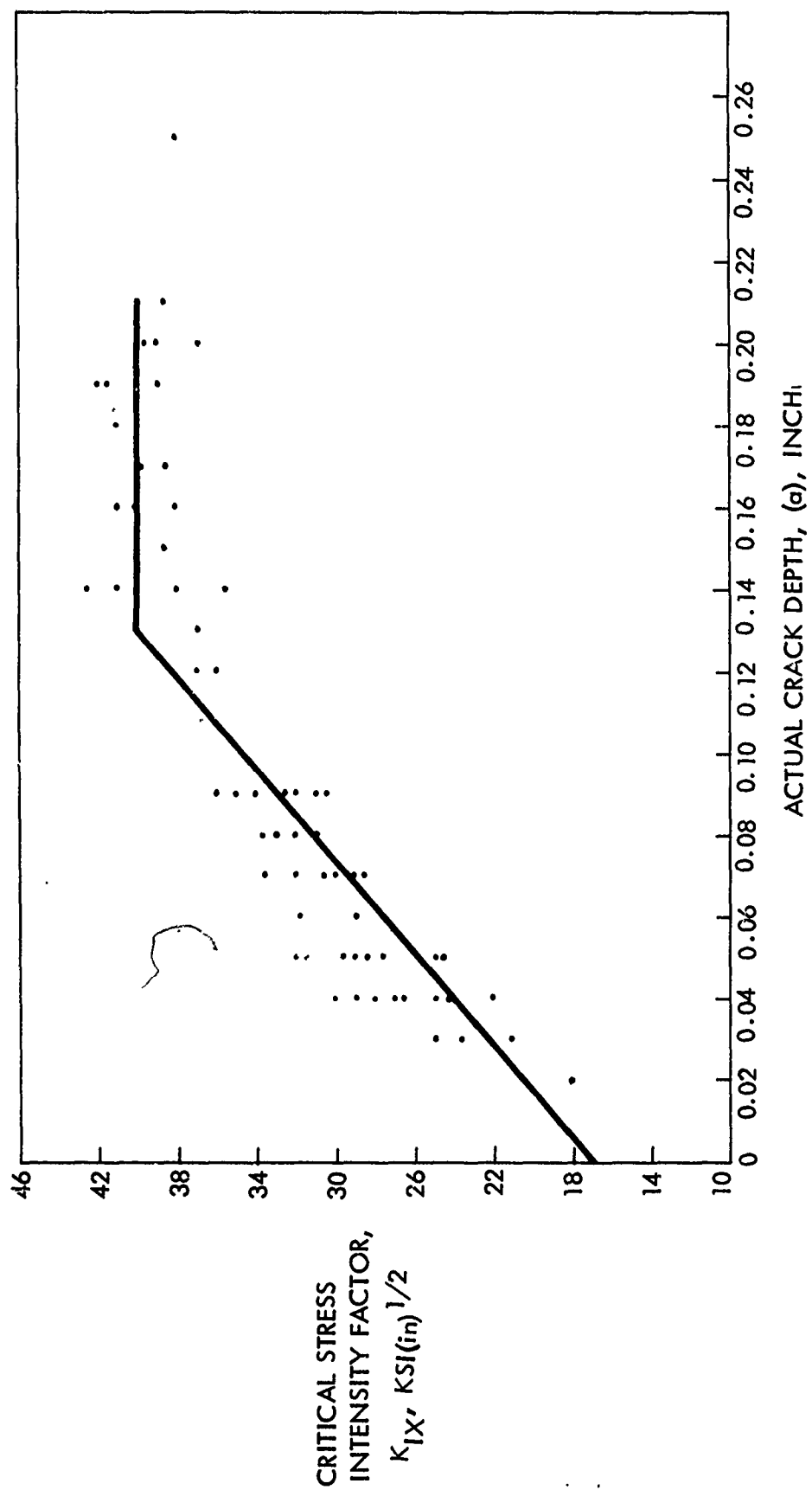
FIGURE 127 — APPARENT CRITICAL STRESS INTENSITY PARAMETER K_{IX} VS. ACTUAL CRACK DEPTH FOR 7075-T6511 ALUMINUM CYLINDERS
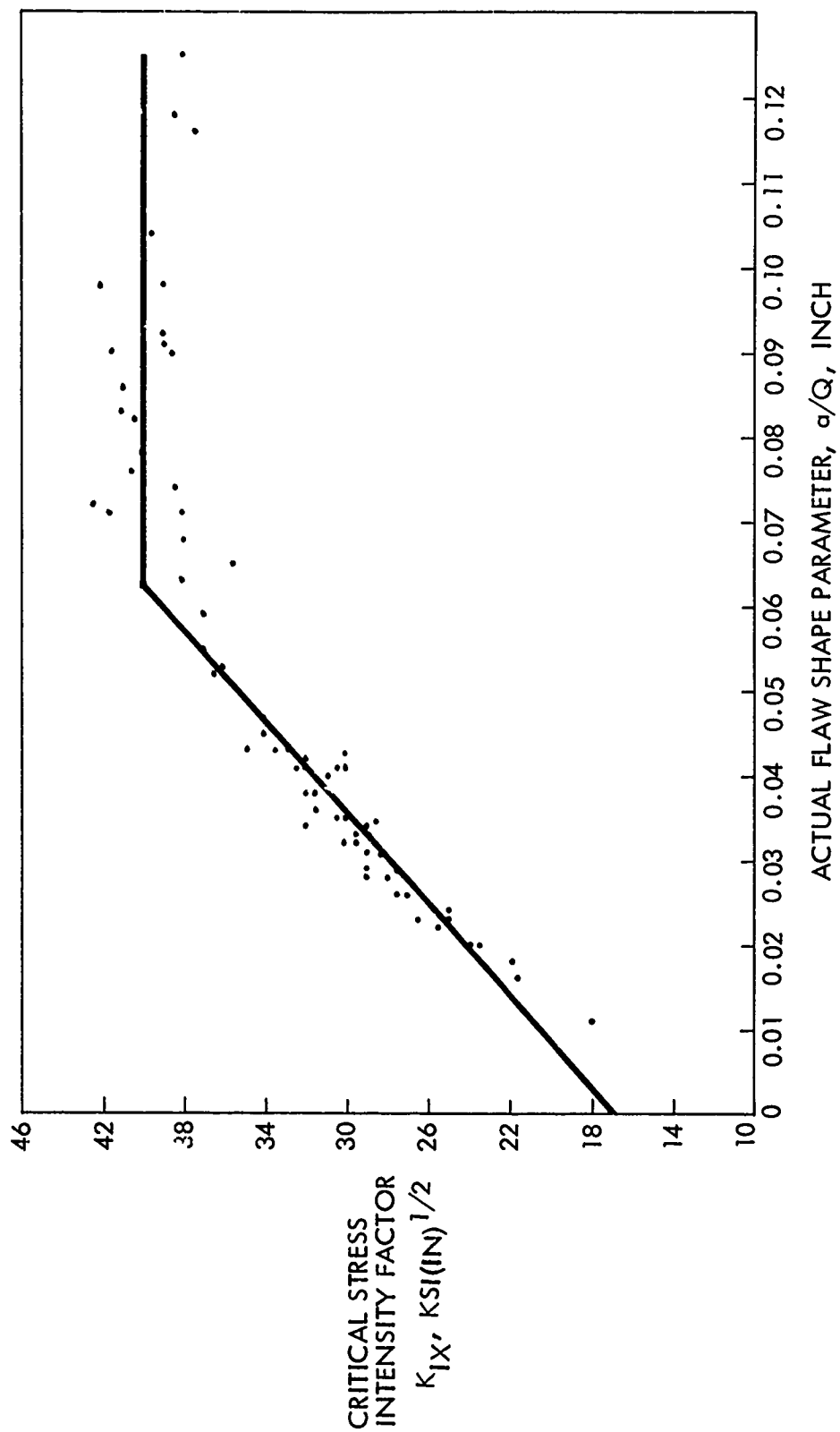
FIGURE 128 – APPARENT STRESS INTENSITY PARAMETER, K_{IX}, VS ACTUAL FLAW SHAPE PARAMETER, a/Q FOR 7075–T6511 ALUMINUM CYLINDERS

181
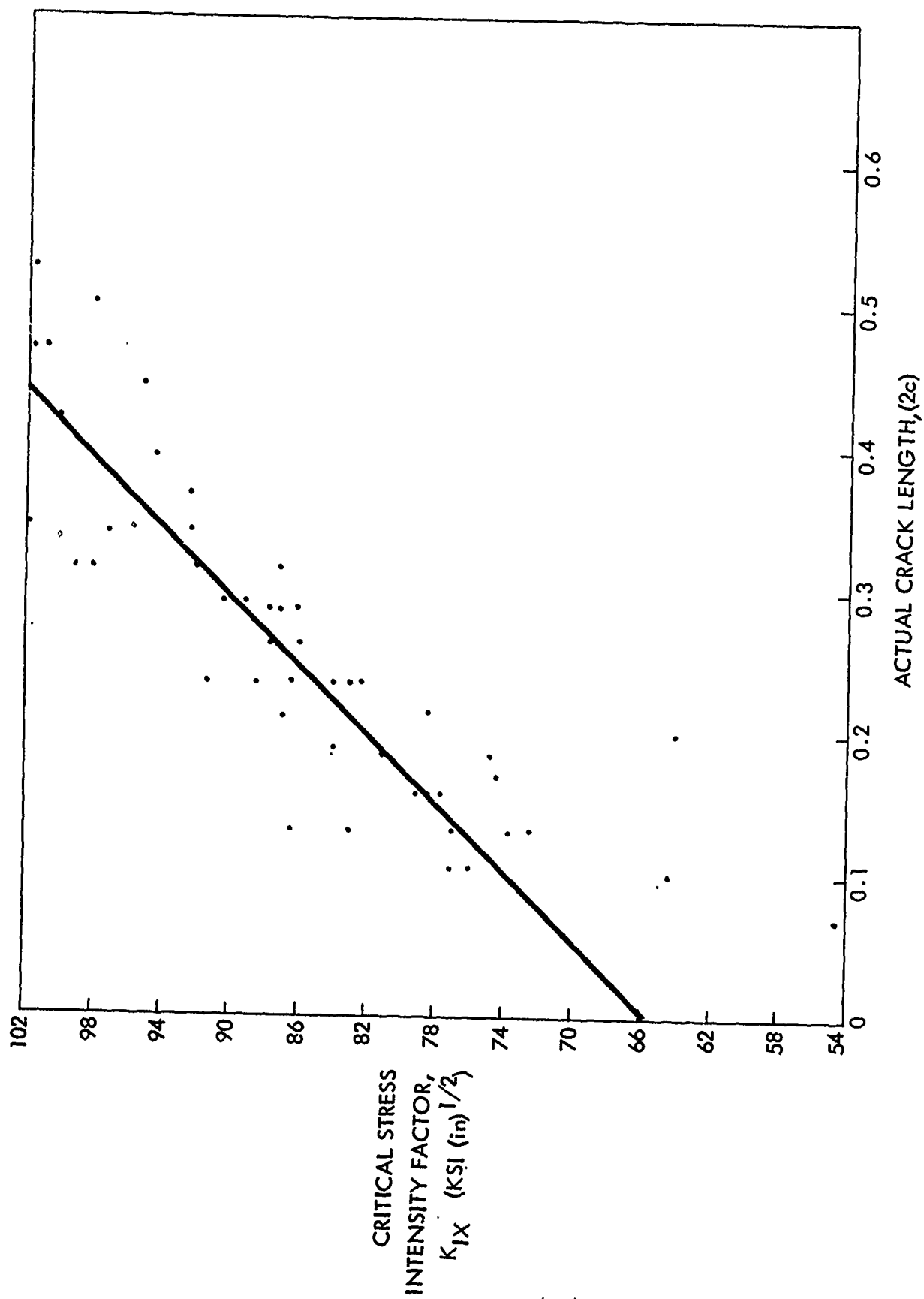
FIGURE 129 — STRESS INTENSITY PARAMETER K_{IX} VS. ACTUAL CRACK LENGTH, 2c, FOR 4330V MODIFIED STEEL CYLINDERS

182
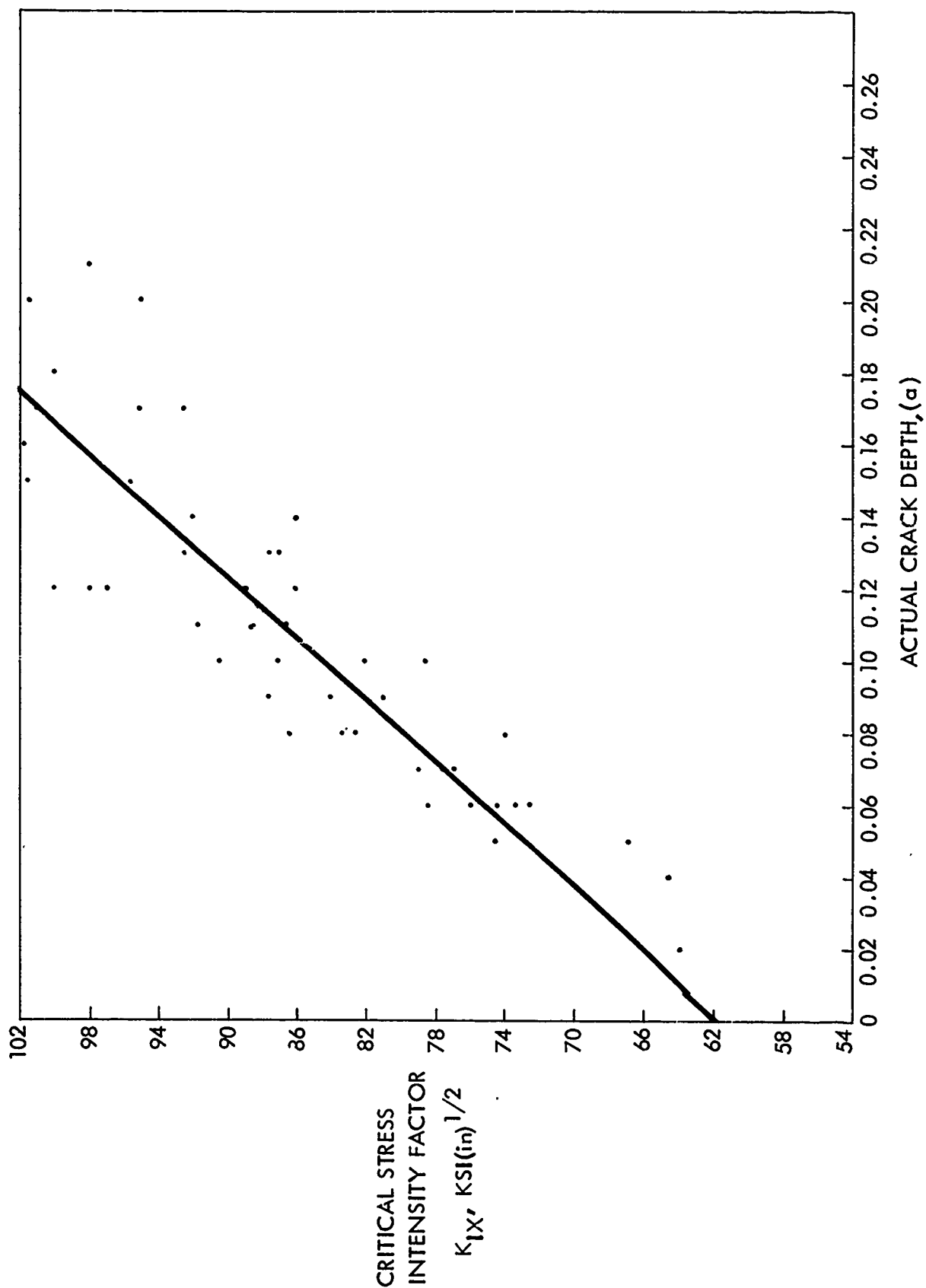
FIGURE 130 – STRESS INTENSITY PARAMETER, K_{IX} VS. ACTUAL CRACK DEPTH, a, FOR 4330V MODIFIED STEEL CYLINDERS
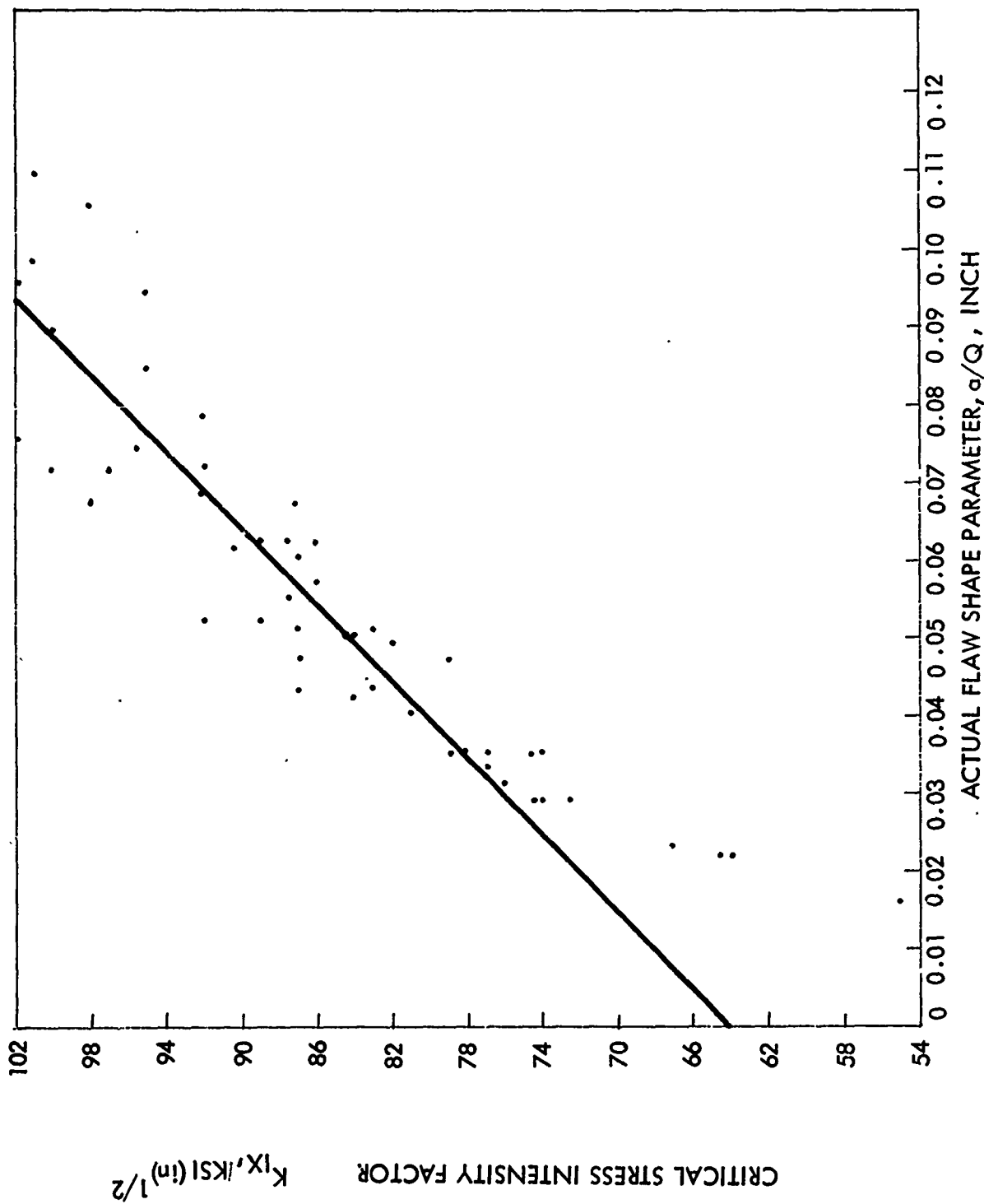
FIGURE 131   STRESS INTENSITY PARAMETER, K_{IX}, VS ACTUAL FLAW SHAPE PARAMETER, a/Q
FOR 4330V MODIFIED STEEL CYLINDERS

184

Plane Stress Corrections

The use of the terminology K_{IX} in Equations (23) to (28) is misleading since the original Tiffany analysis yielded K_{Ic} from Equation (22). The initial analysis of Tiffany assumes that the crack tip stress field is under plane strain conditions, and to insure this certain limitations were placed on the crack depth. A crack conforming to these limitations is shown in Figure 132a and 132c. In this experimental program the crack depth was allowed to vary, resulting in some cracks having the configuration shown in Figure 132b. As the depth of the crack increases, the constraint along the crack front changes.

Therefore, if Equation (22) is utilized the resulting stress intensity factor may not be K_{Ic}, the term restricted to plane-strain conditions, but some stress intensity factor, named K_{IX}. Note that K_{IX} is a function of the plane stress variations at the crack tip which results from a variation of depth; hence, K_{IX} is a function of crack depth and/or flaw shape. Therefore, $K_{IX} > K_{Ic}$ in the same manner as $K_c(B) > K_{Ic}$. This has been considered theoretically by Hall and Kobayashi (49), who consider the problem of two co-planar flaws. They then obtain a stress intensity magnification factor that accounts for this interaction. The use of the magnification factor adds complexity to the analysis as it is not a simple function. Observing the test data in Figures 126 and 129, it appears that a simple linear correction is possible.

If one examines a curve of $K_c(B)$ vs plate thickness for a through crack analysis, one observes that the $K_c(B)$ approaches K_{Ic} as the thickness increases. Hence, using Figure 133 as a schematic, one may write the following empirical relationship between the plane stress intensity factor, $K_c(B)$, and the plane strain stress intensity factor, K_{Ic}

$$K_c(B) = \left[f(B) \right] K_{Ic}$$

Assuming that the $K_c(B)$ vs B curve is a straight line in the decreasing portion of the curve $B > B^*$ and using the slope intercept form of the straight line one then has

$$K_c(B) = m' B + W$$

where m is the slope and W the intercept at $B = 0$. Using the fact that the intercept may be considered to be some multiple of K_{Ic}, i.e., $W = \beta' K_{Ic}$, and assuming that the slope m' is a constant, one may rewrite the equation as follows:

$$K_c(B) = m' B + \beta' K_{Ic}$$

since

$$K_{IX} \propto K_c(B)$$

or

$$K_c(B) = A K_{IX} \text{ where A is a constant}$$

$$K_{Ic} = \frac{A K_{IX} - m' B}{\beta'}$$
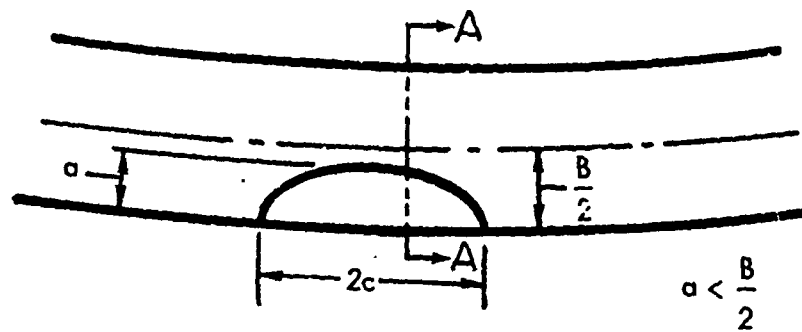
a) PLANE STRAIN GEOMETRY

b) PLANE STRESS-PLANE STRAIN GEOMETRY

c) CROSS SECTION VIEW OF CRACK
SECTION AA
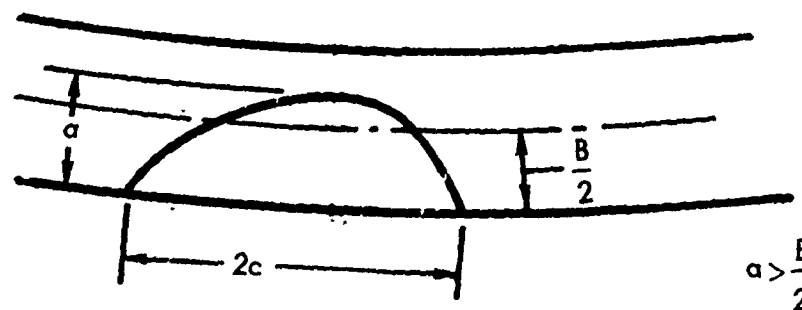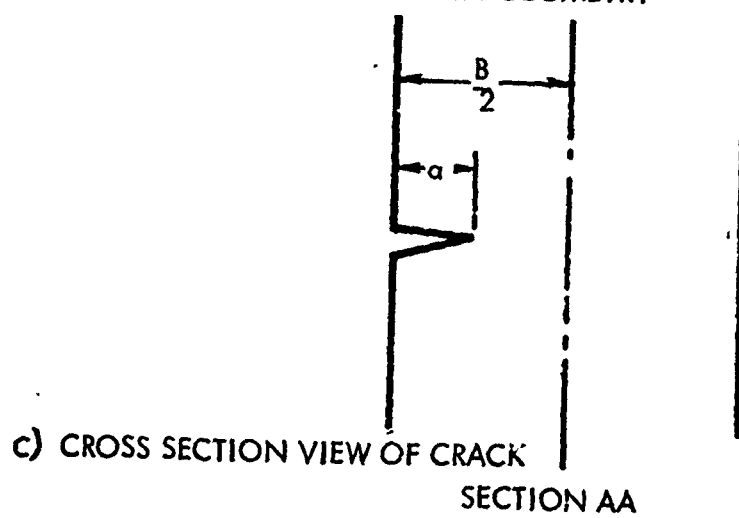
FIGURE 132   GEOMETRIC CONFIGURATIONS USED FOR SUPERPOSITION OF
K_{Ic} VALUES TO CORRECT FOR PLANE STRESS CONDITIONS
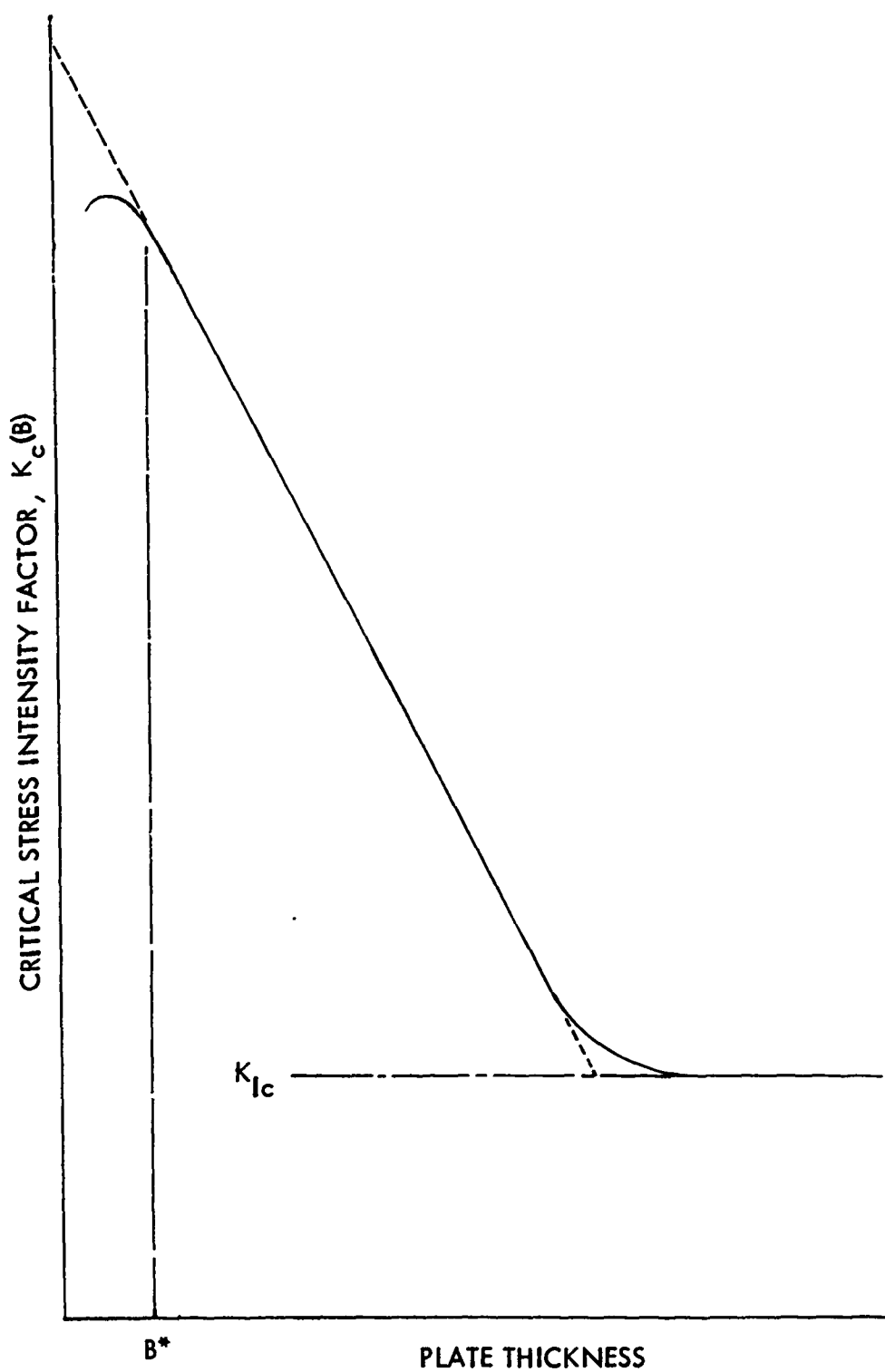
FIGURE 133 VARIATION OF $K_c(B)$ WITH PLATE THICKNESS,
B, FOR THROUGH-THE-THICKNESS CRACKS.

since A, m', and β' are constants dividing by A would not alter the results.

$$K_{Ic} = \frac{K_{IX} - m\,B}{\beta}$$

where $m = m'/A$ and $\beta = \beta'/A$. (29)

This analysis was conducted for a through crack to account for the plane stress-plane strain variations in the stress field that occur due to varying the plate thickness B. However, for the part-through crack analysis this plane stress-plane strain transition is a function of the crack depth, a. If $a = B$, the situation is a through-the-thickness crack and the conventional equations should apply. If $a < [1/2]B$, Equation (22) should yield K_{Ic}, or either gross yielding occurs and fracture mechanics is not applicable. As a approaches B, interaction between the crack front and the back surface occurs and one would expect some high value for stress intensity, approaching $K_c(B)$ for that particular wall thickness obtained from a through-crack test. Therefore, it appears that an equation of the form of Equation (29) with B replaced by B – a can be utilized. Thus,

$$K_{Ic} = \frac{K_{IX} - \xi(B - a)}{\eta}$$

(30)

where ξ and η are constants dependent on the material.

The data plotted in Figures 126 and 129 were analyzed by Equation (30) and the results are shown in Figure 134 for 4330V Modified Steel and Figure 135 for 7075-T6511 Aluminum. The following values were determined from the test data as being valid for these materials:

	ξ	η
4330V Modified Steel	224	2.46
7075-T6511 Aluminum	16.0	1.28

The critical stress intensity factor, K_{Ic}, for the steel now is a constant as it should be; however, the aluminum K_{Ic} is much less improved. If the criterion of failure stress less than yield stress is applied, all the aluminum data containing cracks shorter than 0.2 inches long are discarded as invalid and the results shown in Figure 136 remain. Now it appears that the aluminum data have been properly corrected to yield a valid K_{Ic}.

Fracture Mechanics Failure-Load Predictions

The failure-load predictions for the cylinders are made using the following equation:

$$P = \frac{K_{IX}}{1.1\sqrt{\pi}} \frac{A}{\sqrt{\frac{a}{Q}}}$$

(31)

where A is the area of the specimen.

188
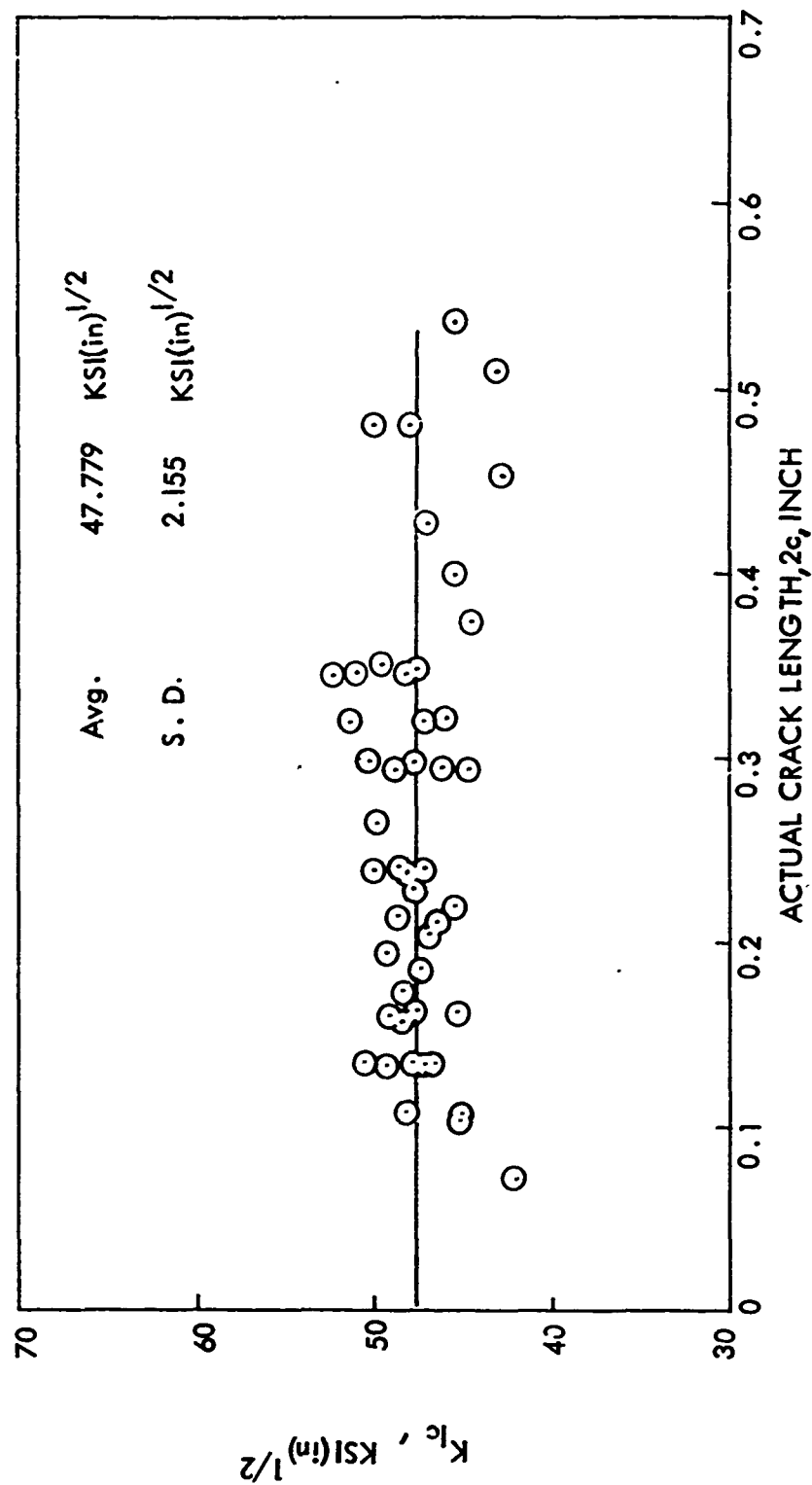
FIGURE 134 – CORRECTED K_{Ic} VERSUS 2c–4330V MODIFIED STEEL CYLINDERS

189
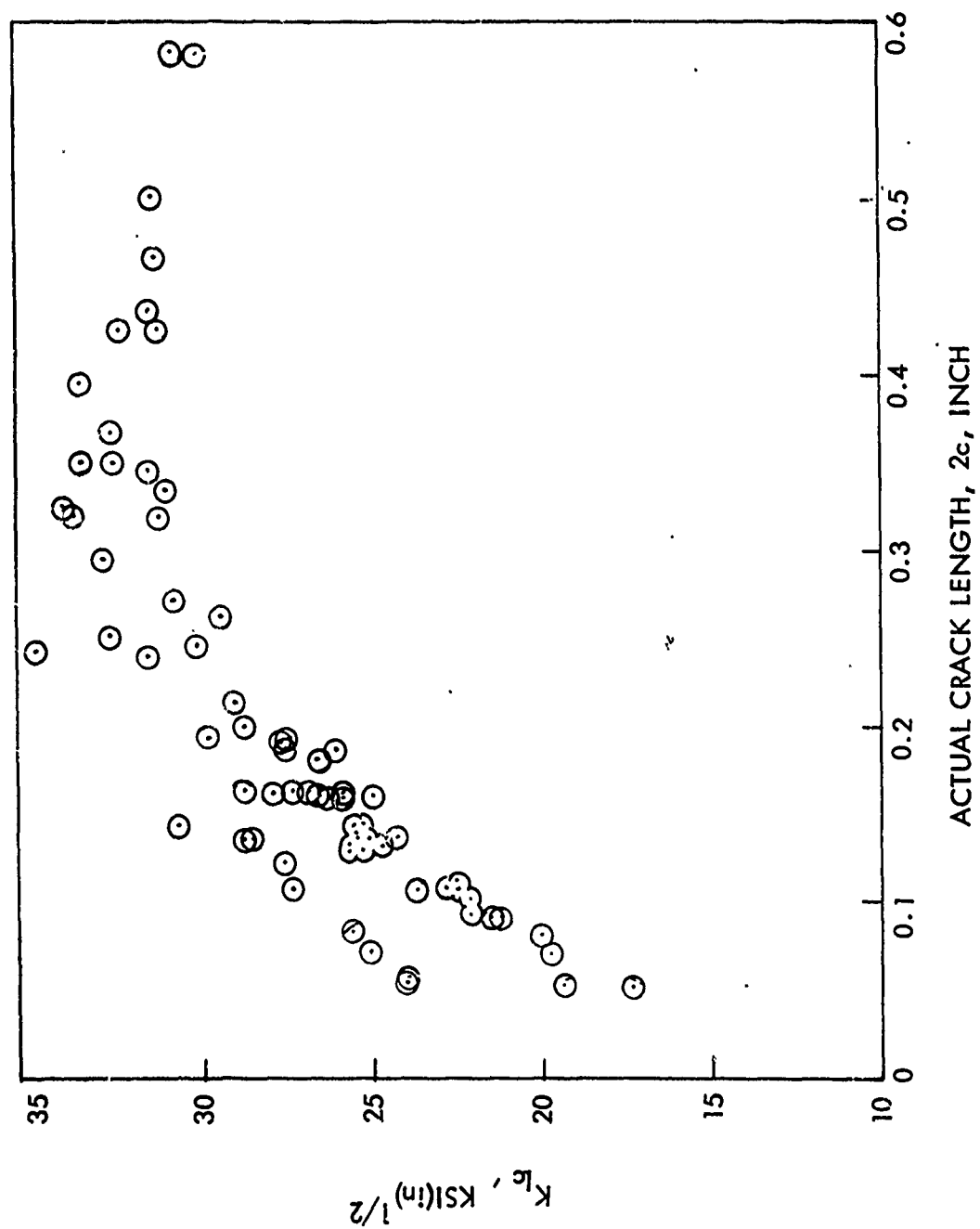
FIGURE 135   CORRECTED K_{Ic} VERSUS $2c$ FOR 7075-T6511 ALUMINUM CYLINDERS

190
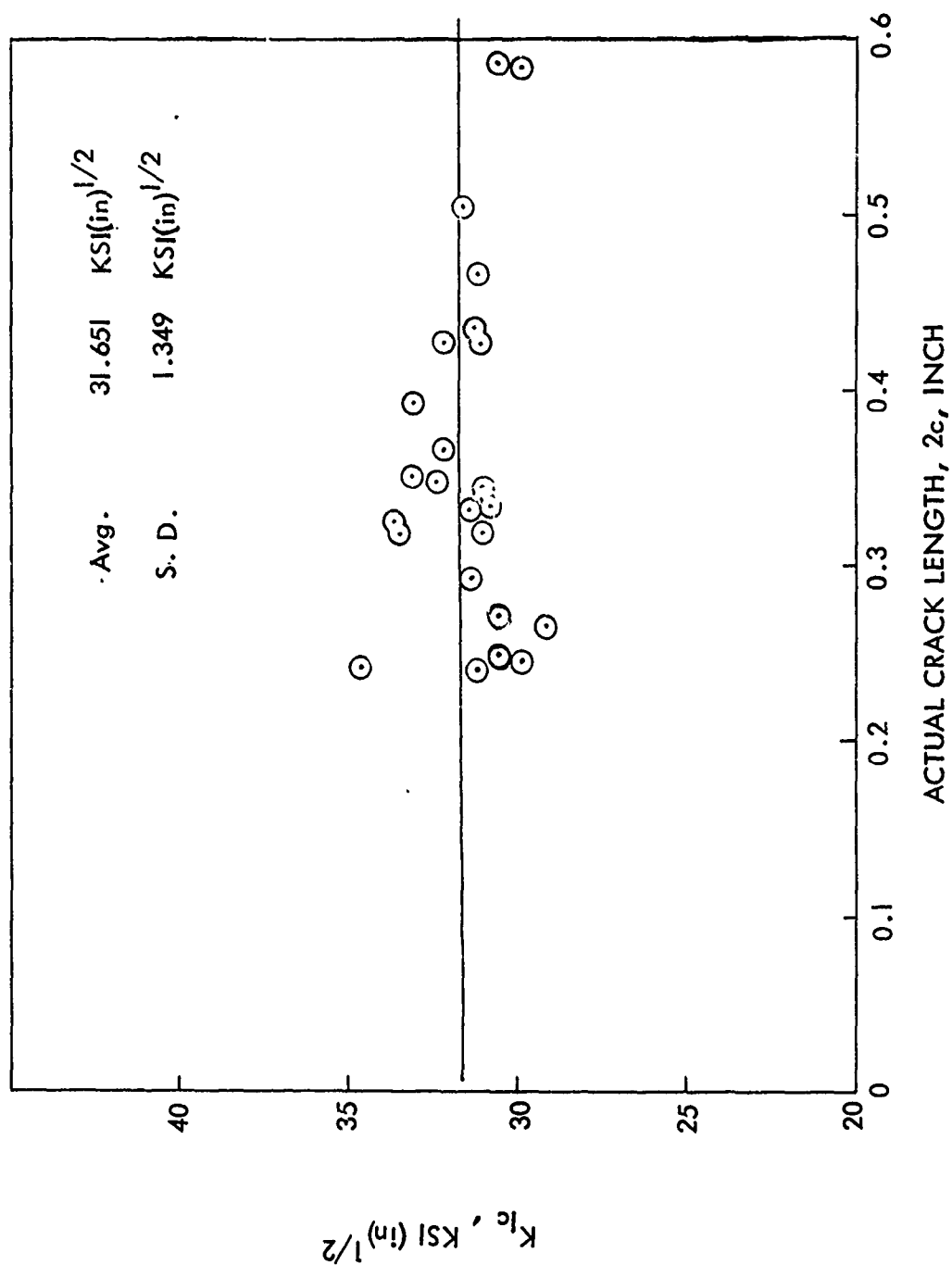
FIGURE 136 – CORRECTED K_{Ic} VERSUS $2c$ FOR 7075-T6511 ALUMINUM CYLINDERS

Avg.   31.651 $KSI(in)^{1/2}$

S. D.   1.349 $KSI(in)^{1/2}$

ACTUAL CRACK LENGTH, $2c$, INCH

K_{Ic} , $KSI (in)^{1/2}$

191

The value of K_{IX} used for the predictions is given in Equation (23) for 7075 T6511 Aluminum and Equation (26) for 4330V Modified steel. Figure 137 plots differences between the failure-load prediction and the actual failure load as a function of crack length, 2c. For each crack length range, the average deviation has been drawn as a horizontal line. A zero deviation obviously means that the fracture mechanics prediction agreed with the observed failure load. A positive deviation indicated that the fracture mechanics analysis overestimated the failure load, while negative deviations mean that the fracture mechanics analysis underestimated the failure loads.

For the 7075-T6511 Aluminum cylinders, the analysis usually underestimated the failure load. This was true in all ranges of crack sizes except for the cracks from 0.05 to 0.10 inch long. For these small cracks, the analysis overestimated the failure loads. This is to be expected, since for small cracks, gross yielding occurs prior to failure, and the fracture mechanics analysis would not apply.

Using the failure load of specimens not containing cracks as a basis, two error bands have been drawn. The outer two lines correspond to a ± 10 percent error based on a mean load of 195 KIPS, for aluminum, while the inner two lines correspond to a ±5 percent error. It can be seen that most predictions fall within ± 5 percent.

For comparison, the deviation from the failure-load predictions using a standard analysis are drawn on the same curve. This uses $P = \sigma_{tu} A$. The deviation is small for small cracks but increases as the crack length increases. Using standard analysis, the failure load is overestimated, since the decrease in load-carrying capacity due to the crack is not considered. If the crack exceeds 0.20 inch in length, the fracture mechanics analysis results in a better estimate of the failure load of the material than does the standard analysis.

The deviations between the true failure load and the failure load predicted using fracture mechanics is shown in Figure 138 for the 4330V Modified steel cylinders. Again two bands have been drawn, showing the ±10 percent and ±5 percent error based on an average failure load of 490 KIPS. In this case, the fracture mechanics overestimates the failure load in the majority of crack sizes. However, almost all of the average deviations fall within ±5 percent of the predicted failure loads. This is in excellent agreement, and it could be improved slightly by a more judicious choice of K_{IX}. As was expected, the largest deviation occurred with small cracks.

The deviations of the actual failure load from that predicted using a standard analysis on 4330V Modified steel are drawn for comparison in Figure 138. As before, the standard analysis is correct for small cracks up to 0.15 inch long. However, for cracks larger than 0.15 inch long, the deviations increase. The standard analysis again overestimates the failure load of specimens containing cracks. Here the error exceeds + 10 percent for cracks over 0.20 inch long. The fracture mechanics predictions are much more accurate for all cracks over 0.20 inch long.

Fracture Mechanics/NDT Failure-Load Predictions

Figures 139 through 141 show the deviation of the failure-load predictions from the actual failure load verses the actual crack length, 2c, made using fracture mechanics and the crack length as measured by each NDT method. Again, each point represents a single cylinder, and the average deviations are shown as straight lines for each crack range.

192
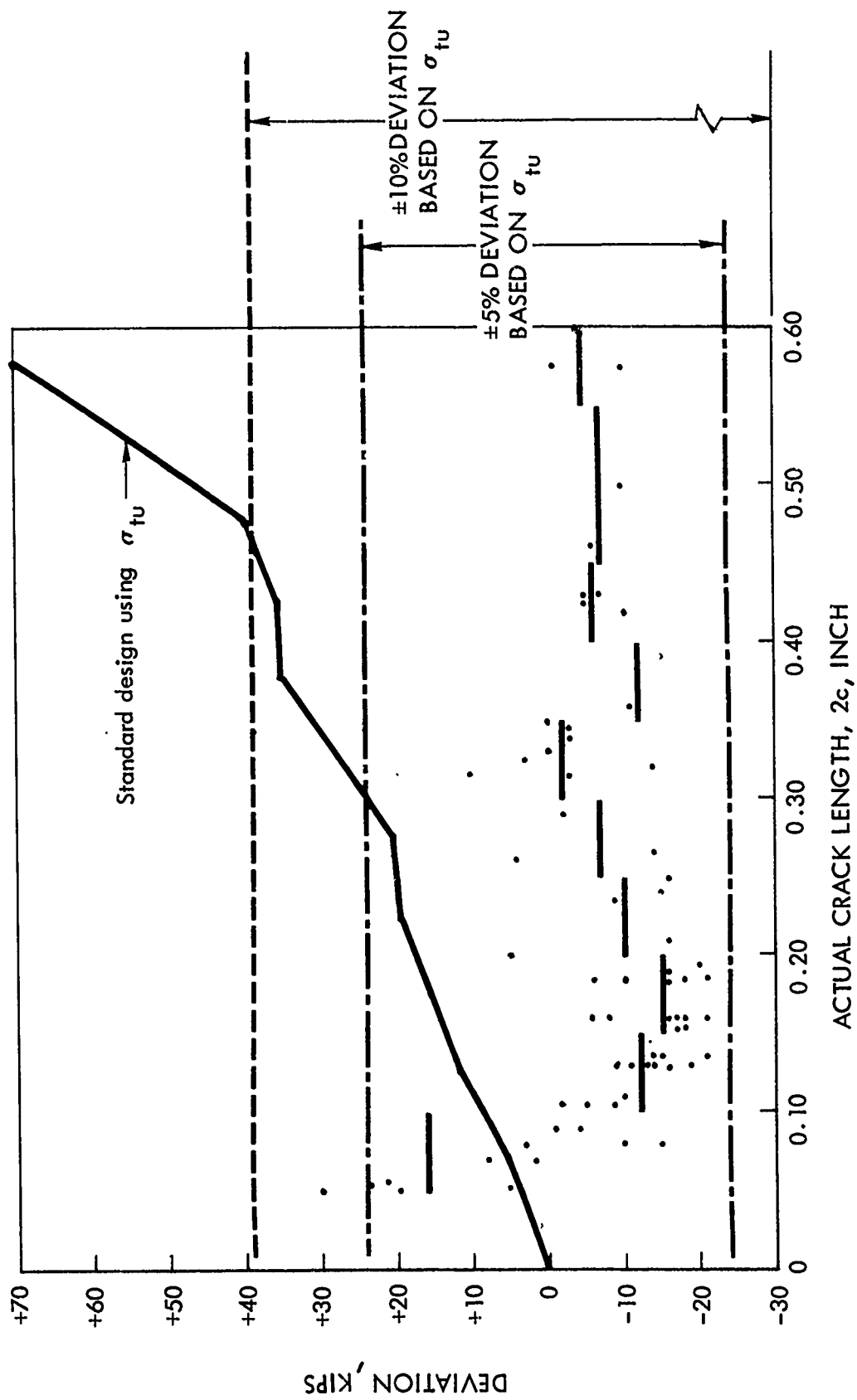
FIGURE 137   DEVIATION OF FAILURE LOAD PREDICTION USING FRACTURE MECHANICS FROM ACTUAL FAILURE LOAD 7075-T6511 ALUMINUM CYLINDERS

193
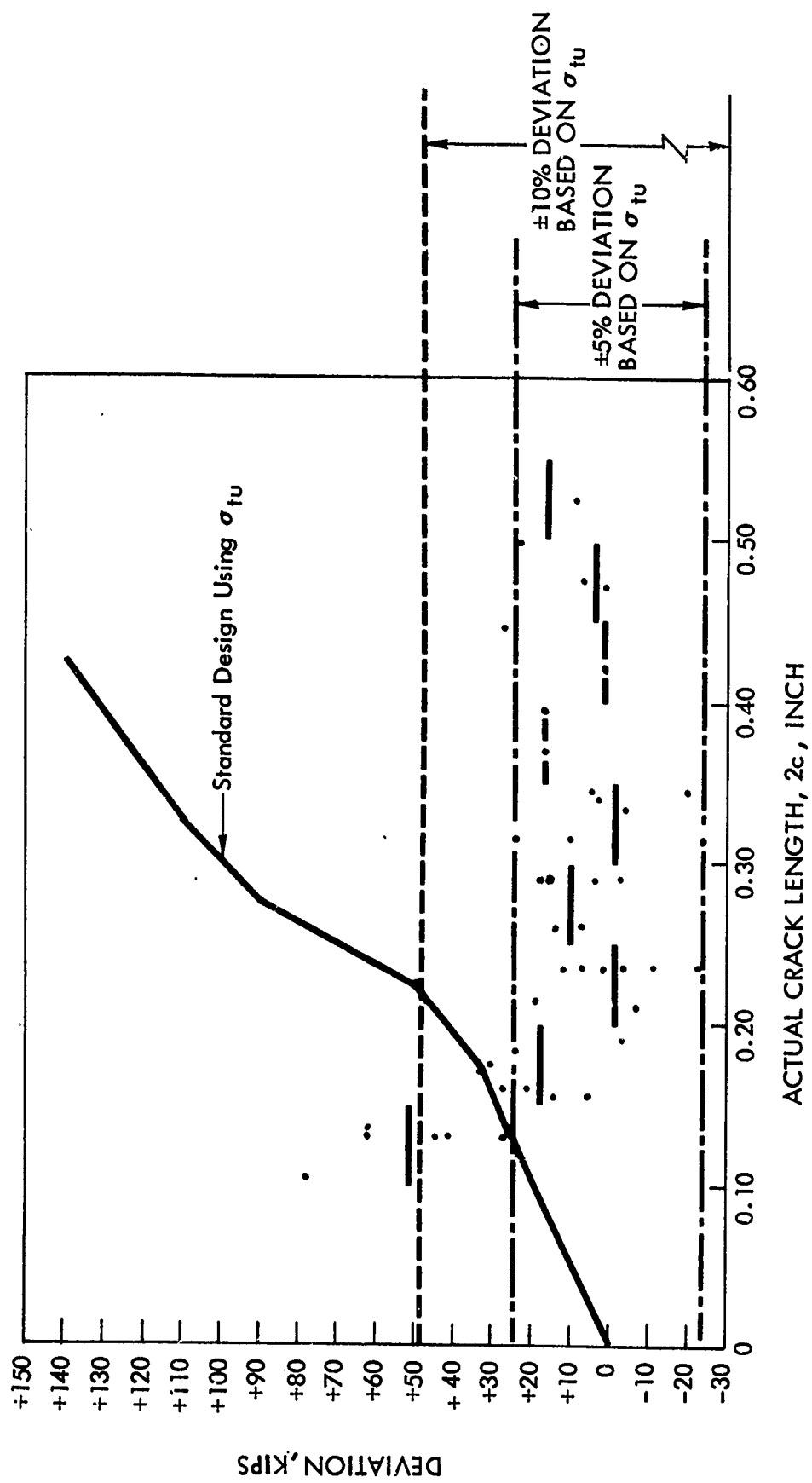
FIG. 138   DEVIATION OF FAILURE LOAD PREDICTION USING FRACTURE MECHANICS
FROM ACTUAL FAILURE LOAD   4330 V MODIFIED STEEL CYLINDERS

194

Figure 139 shows the failure-load prediction deviations using X-ray inspection to measure the cracks. In Section III it was mentioned that X-ray could not detect small cracks, so crack lengths less than 0.30 could not be included in this plot. Since the sensitivity of the X-ray method was poor, only a few failure-load predictions could be made. The results show that all of the FM/X-ray predictions correctly predict the actual failure load to within 5 percent of the actual failure load. X-ray always overestimates the actual failure load.

Figure 140 shows the FM/penetrant-inspection predictions as a function of actual crack length, 2c. All of the deviations between the actual failure loads and the predicted failure loads are within ± 5 percent. For crack sizes larger than 0.25 inch long, the penetrant-inspection predictions are very close to the actual failure loads.

Figure 141 shows the deviations of the failure-load predictions from the actual failure loads for the FM/ultrasonic inspection. Except for the small crack lengths (0.05 to 0.10 inch) and the large cracks (0.45 inch), all of the failure load predictions are within ± 5 percent. The FM/ultrasonic technique underestimates the failure loads of specimens containing cracks from 0.10 to 0.40 inch long.

Figures 142 through 145 show the deviations between the actual failure load and the failure load predictions made using the NDT methods for the 4330V Modified steel cylinders, as a function of actual crack length.

Figure 142 shows the results of the FM/X-ray inspection failure load predictions. At no time did the failure load prediction do better than ± 10 percent. No consistant pattern can be observed due to the small number of points. This is due primarily to the low sensitivity of X-rays to fatigue cracks in this material.

Figure 143 shows the results of the FM/penetrant predictions on the failure load of the 4330V Modified steel cylinders. Except for one case, all of the average deviations overestimated the actual failure loads. The deviations varied between + 3 percent and + 9 percent based on the actual tensile stress. One crack size, from 0.15 to 0.20 inch long was underestimated.

Figure 144 shows the results of the FM/magnetic-particle predictions on the failure load of the 4330V Modified steel cylinders. The average deviations always overestimate the actual failure load. There appears to be a continually increasing deviation, and for crack lengths below 0.25 inch, the predictions are within + 5 percent. Above 0.25 inch long, the predictions are greater than 5 percent, but the average deviation never exceeds 10 percent.

Figure 145 shows the deviation from the actual failure loads and the failure loads predicted using FM/ultrasonics. In this case the results are surprisingly poor. The average deviation is always over 10 percent. The method overestimates the failure load by more than 150 KIPS for small cracks. For cracks between 0.30 and 0.50 inch long, the method consistently overestimates the failure loads by more than 10 percent.

Figure 146 is a summary plot showing the average deviations between the actual failure loads and the failure load prediction made using fracture mechanics and each NDT method. The deviations from the actual failure load and the standard design using σ_{tu} is also shown for comparison. It can be seen that, for all of the methods used, the average deviation is within ± 5 percent of the actual failure load; this is surprisingly accurate. The most accurate predictions occur in the crack length range from 0.25 to 0.50 inch. The techniques are always in error for small crack lengths.

195
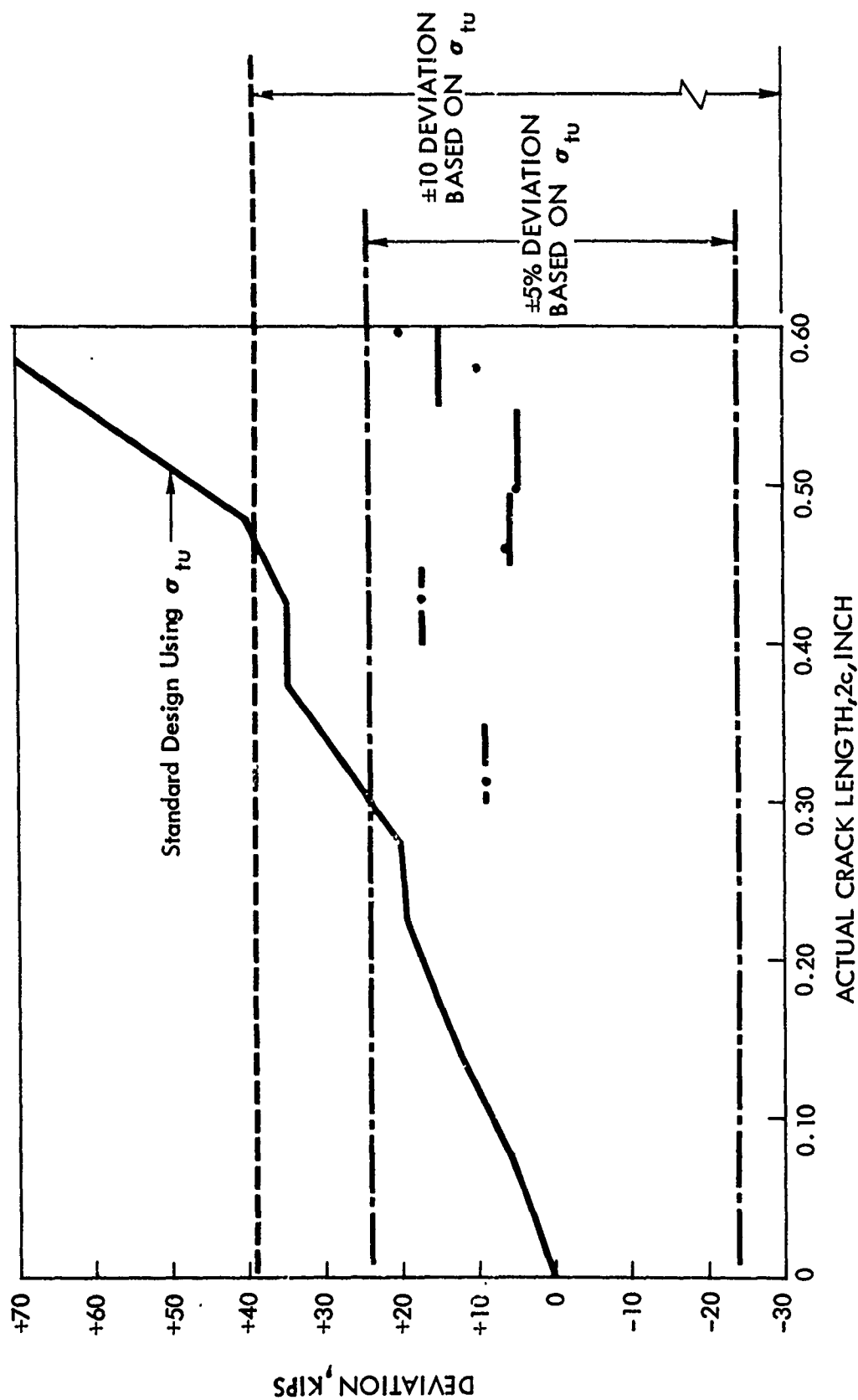
FIG 139   DEVIATION OF FAILURE LOAD PREDICTION USING FM/X-RAY INSPECTION
           FROM ACTUAL FAILURE LOAD 7075-T6511 ALUMINUM CYLINDERS

196
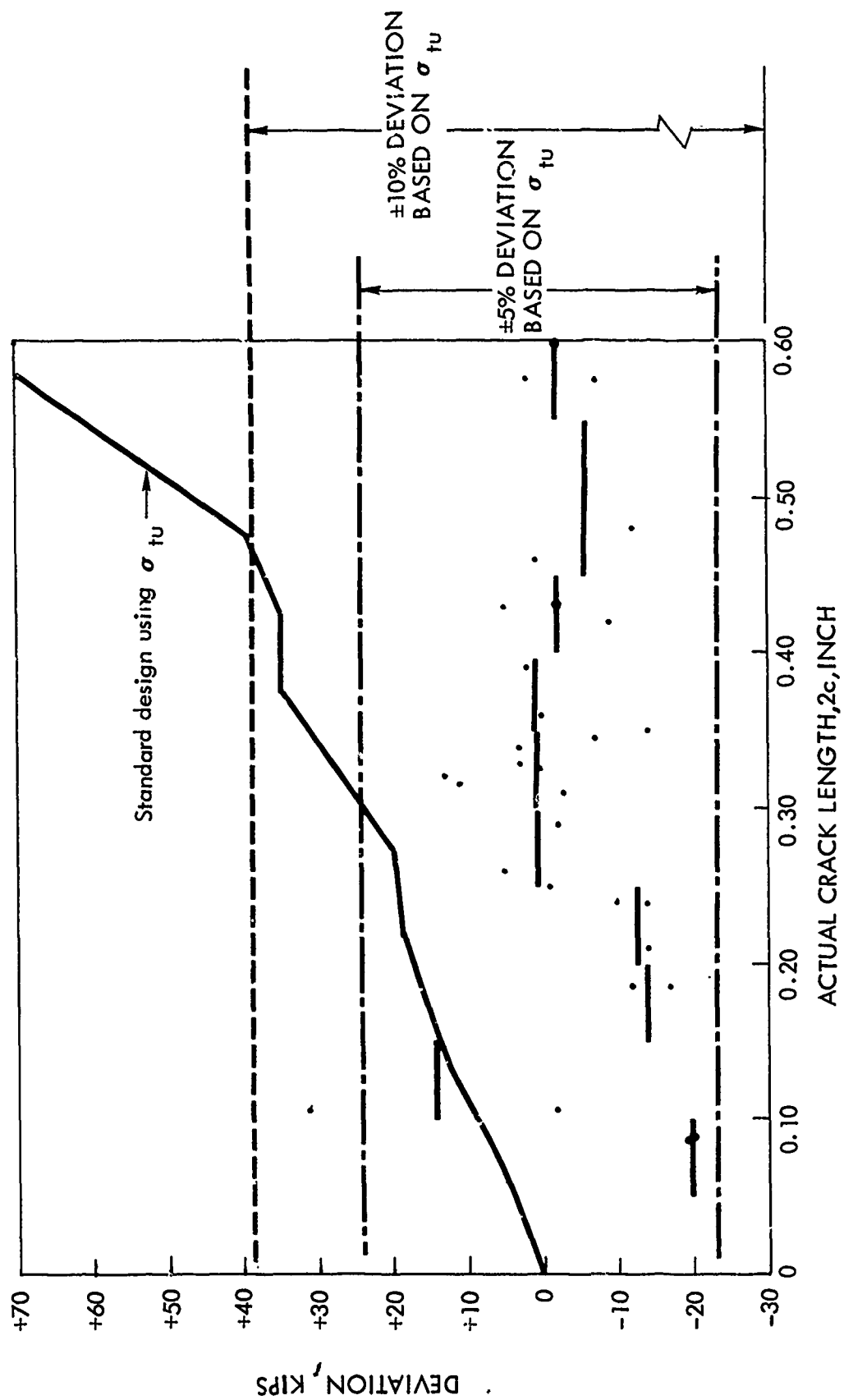
FIGURE 140   DEVIATIONS OF FAILURE LOAD PREDICTIONS USING FM-PENETRANT INSPECTION
FROM ACTUAL FAILURE LOADS–7075–T6511 ALUMINUM CYLINDERS

197
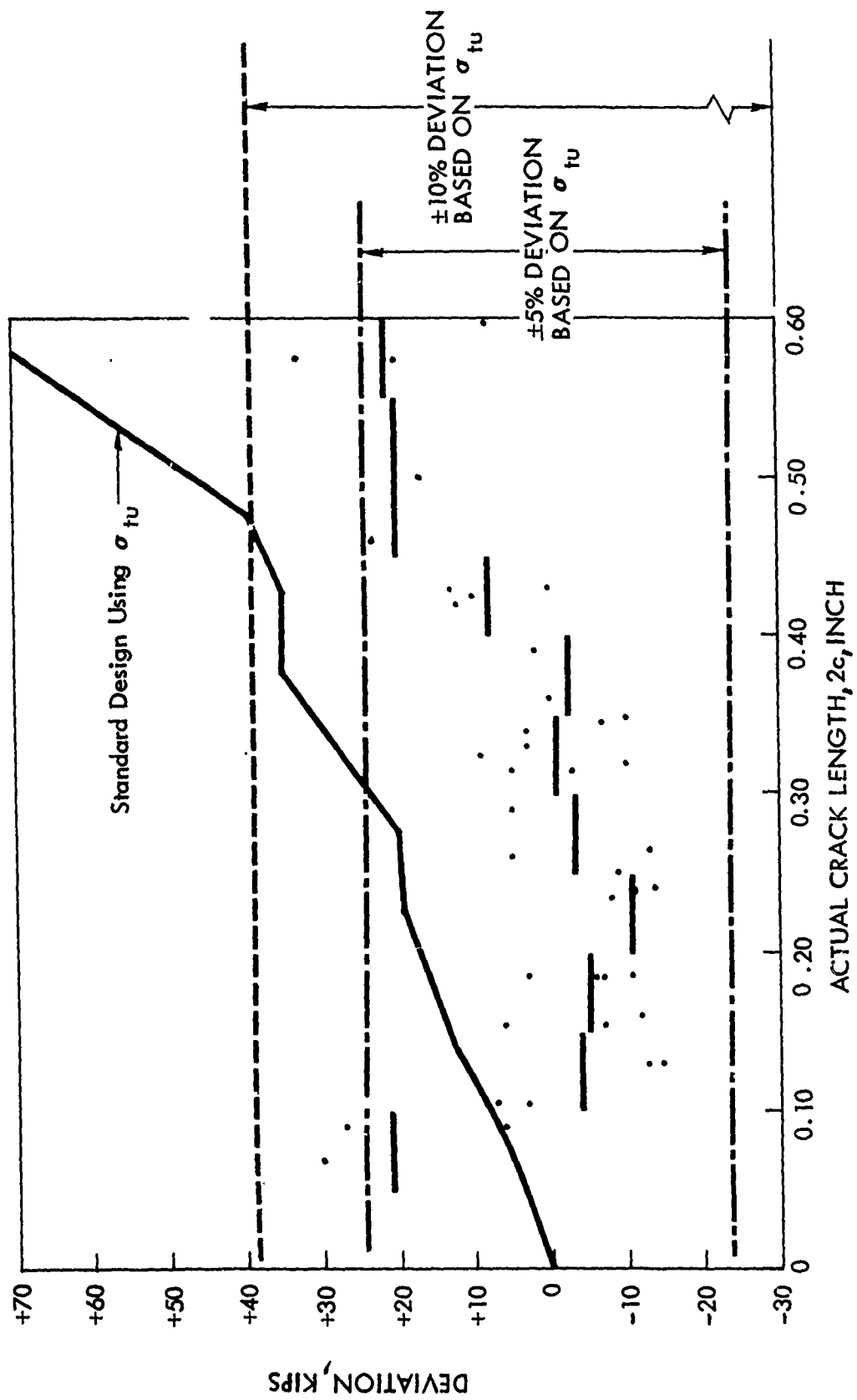
FIG 141   DEVIATIONS OF FAILURE LOAD PREDICTION USING FM- ULTRASONICS FROM ACTUAL FAILURE LOAD–7075–T6511 ALUMINUM CYLINDERS

198
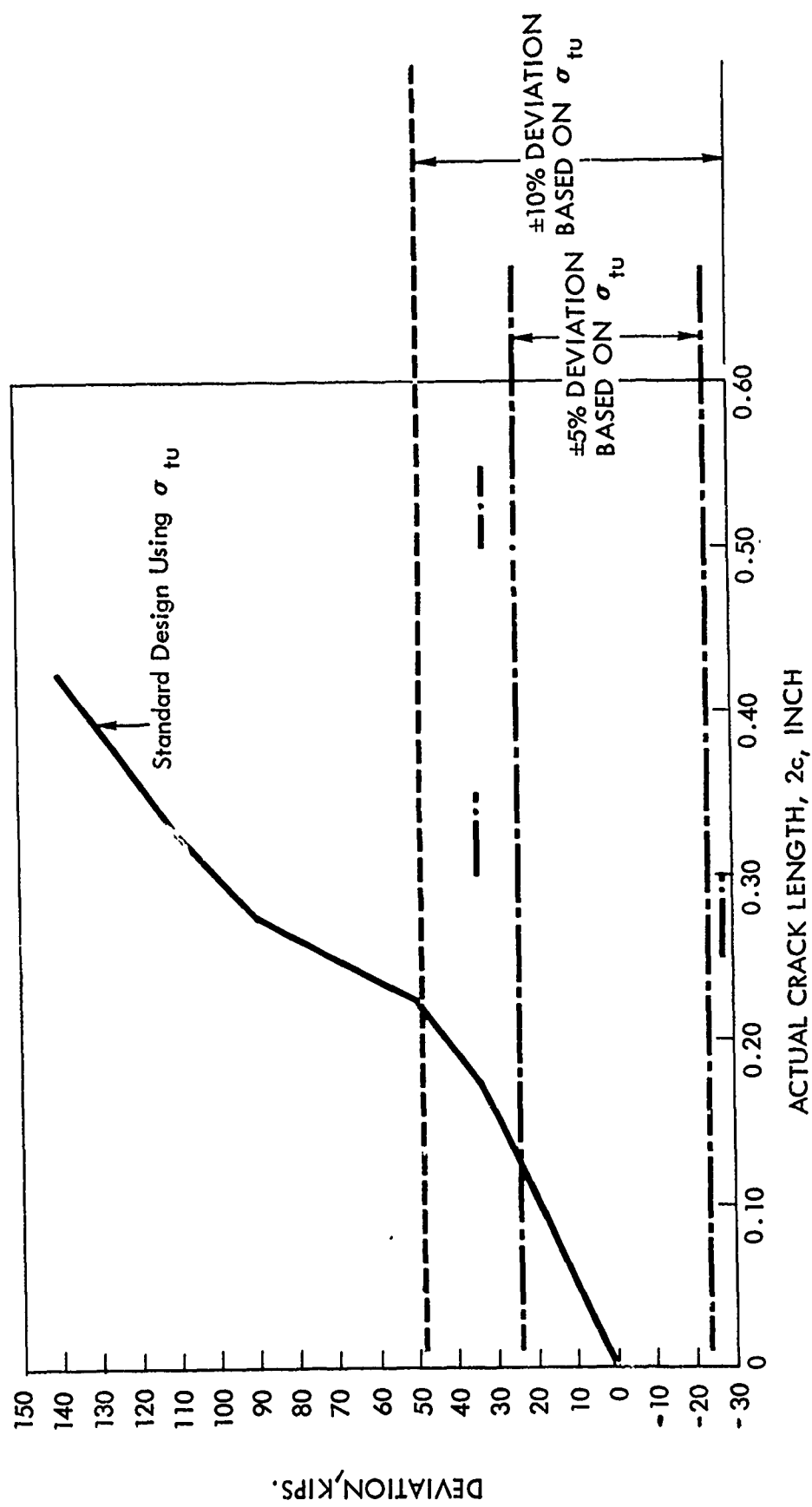
FIG 142 DEVIATION OF FAILURE LOAD PREDICTION USING FM-XRAY INSPECTION FROM ACTUAL FAILURE LOAD ~4330V MODIFIED STEEL CYLINDERS

199
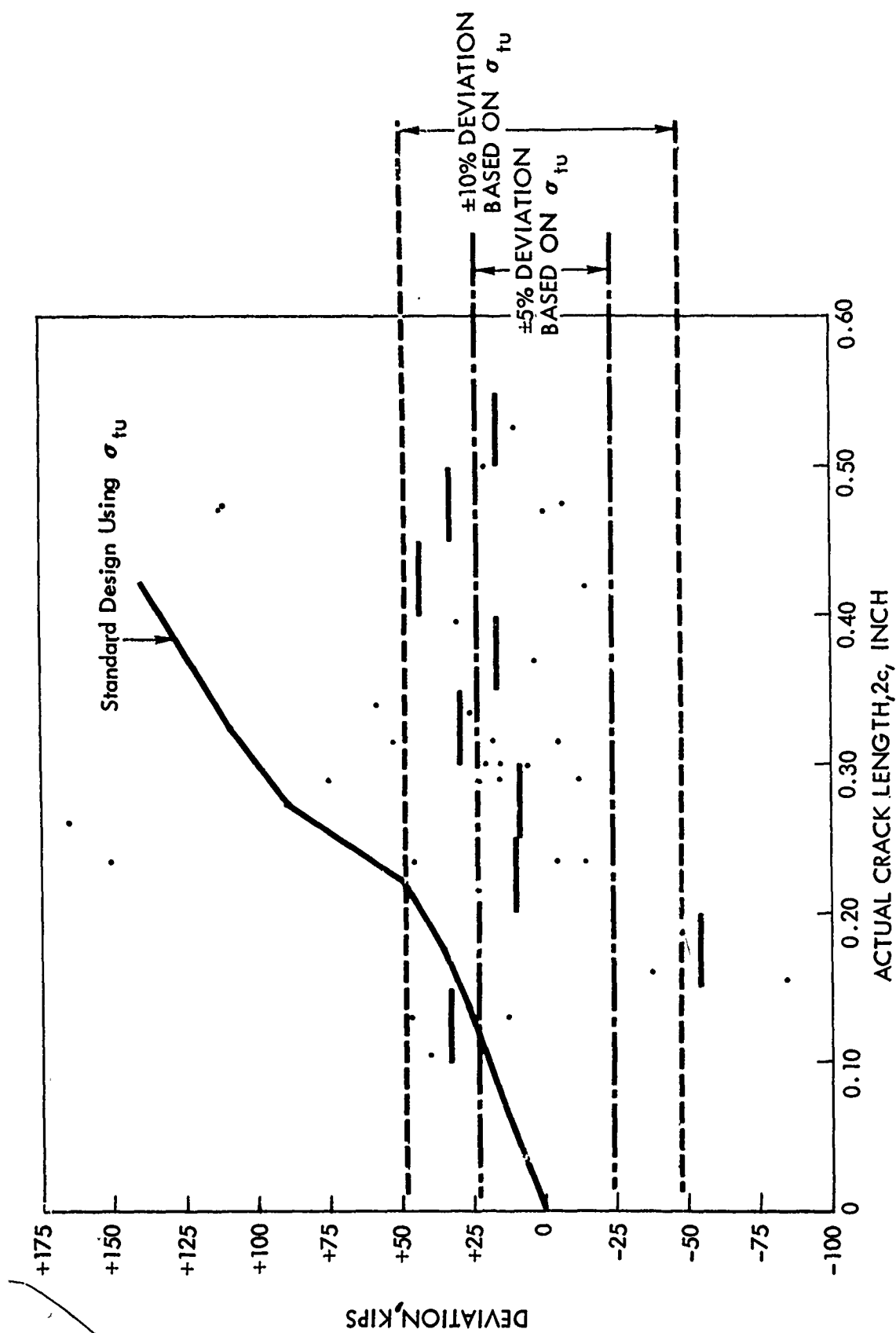
FIG 143 DEVIATION OF FAILURE LOAD PREDICTION USING FRACTURE MECHANICS – PENETRANT FROM ACTUAL FAILURE LOAD–4330V MODIFIED STEEL CYLINDERS.

200
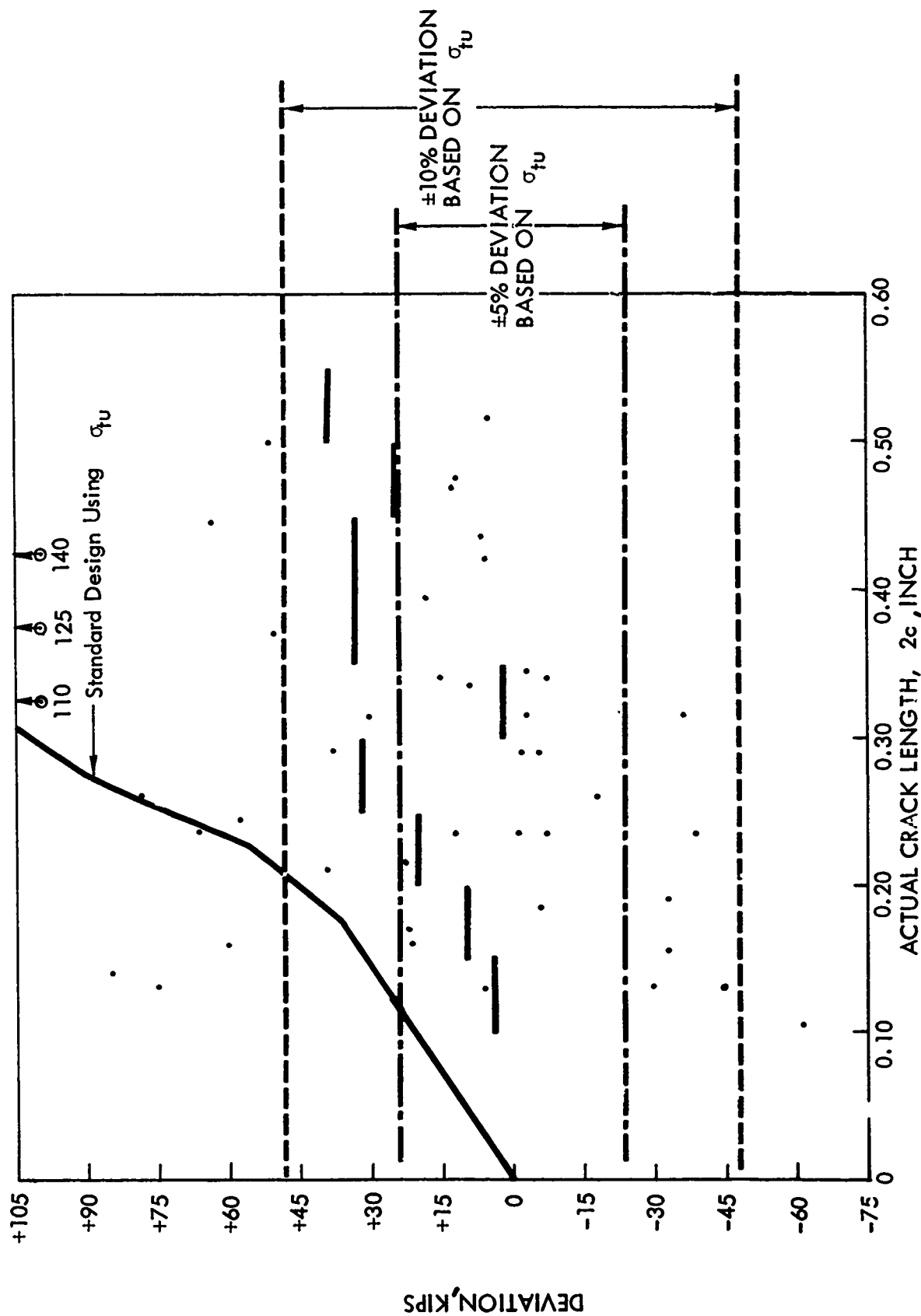
FIG 144   DEVIATIONS OF FAILURE LOAD PREDICTION USING FM–MAGNETIC PARTICLE
INSPECTION FROM ACTUAL FAILURE LOAD – 4330 V MODIFIED STEEL CYLINDERS

FIGURE 145
DEVIATION OF FAILURE
LOAD PREDICTION USING
FM-ULTRASONICS FROM
ACTUAL FAILURE LOAD –
4330 V MODIFIED STEEL
CYLINDERS

Standard Design Using σ_{tu}

±10% DEVIATION
BASED ON σ_{tu}

±5% DEVIATION
BASED ON σ_{tu}

ACTUAL CRACK LENGTH, 2c, iNCH

DEVIATION, KIPS

202
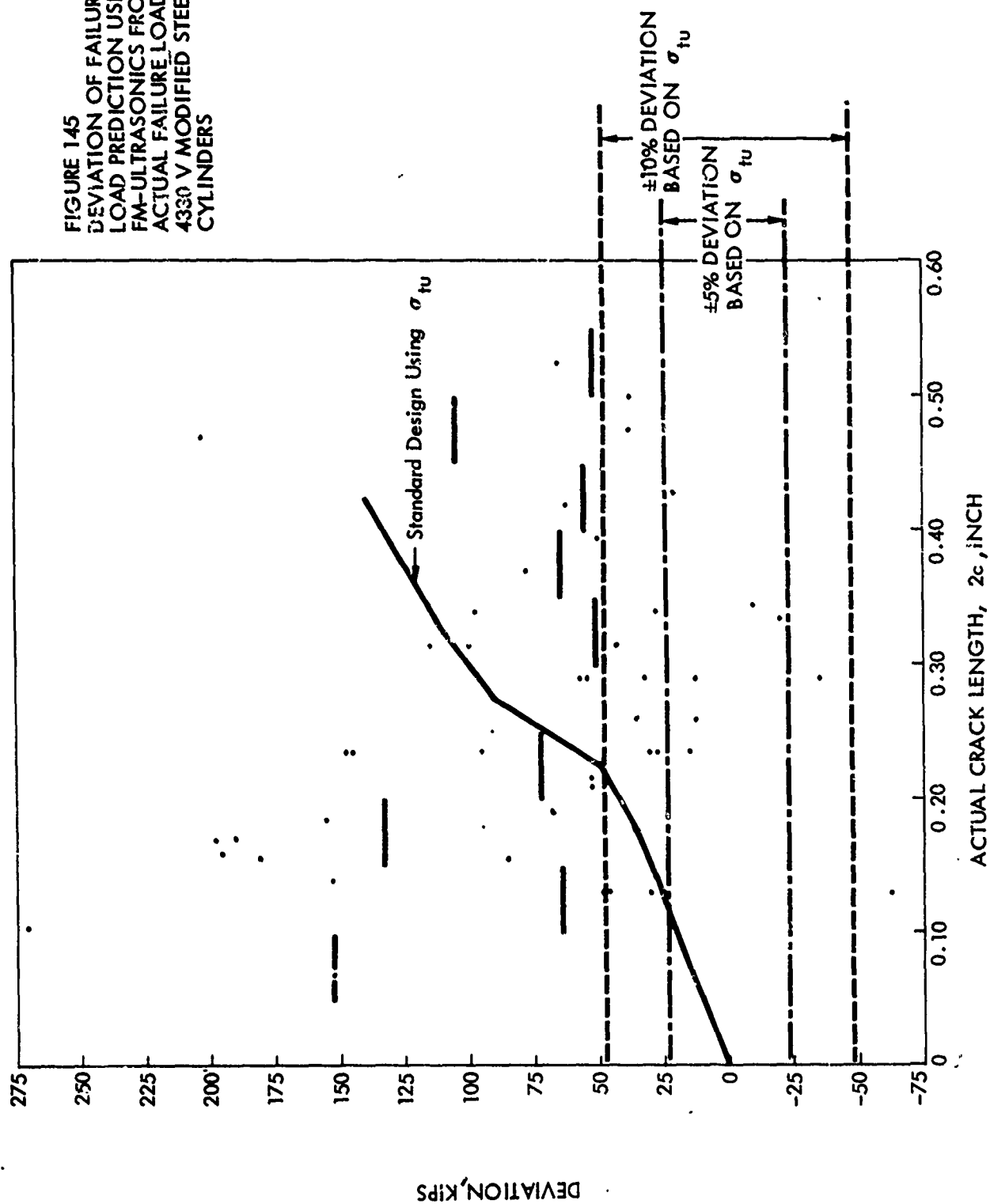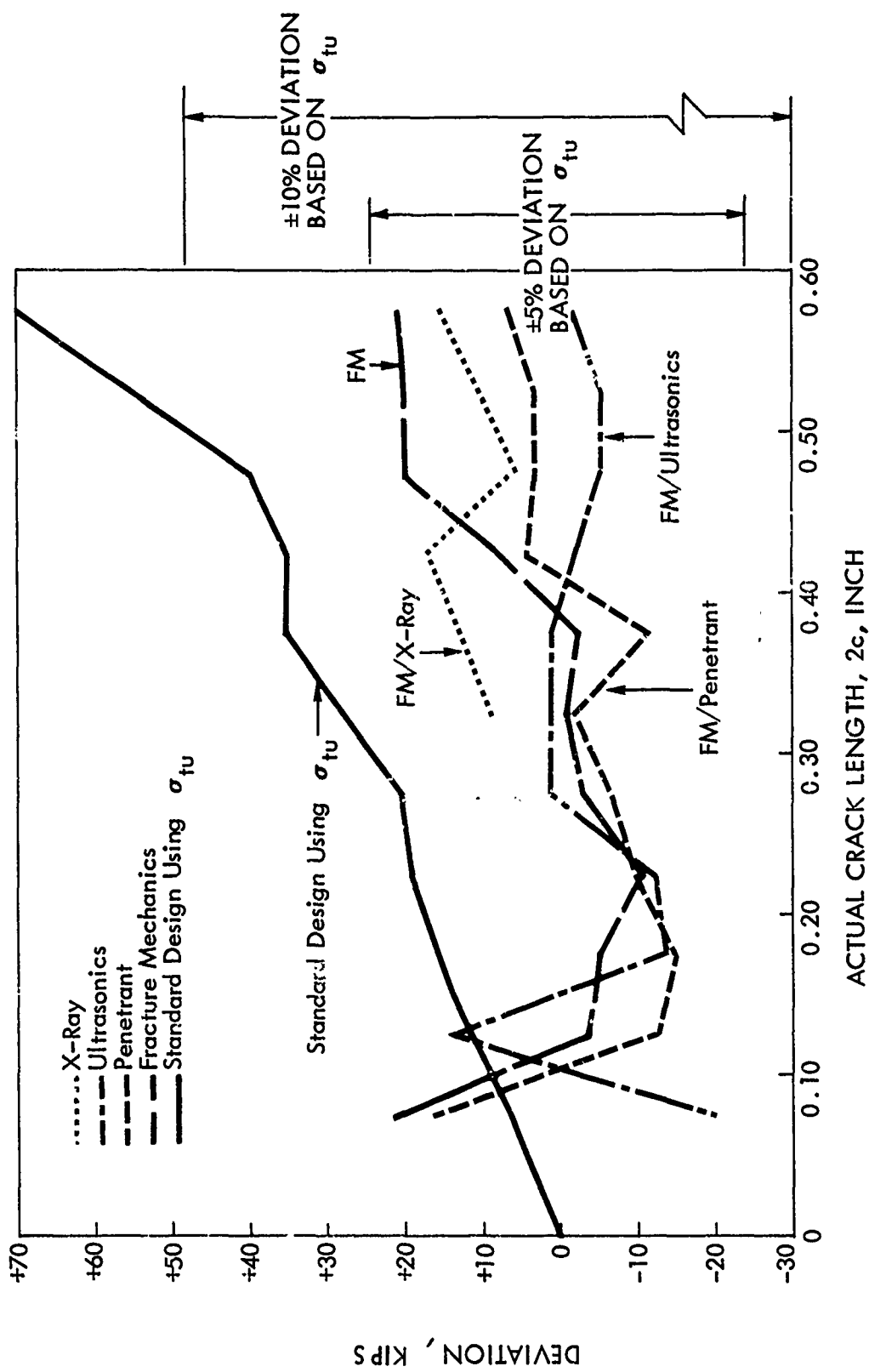
FIG 146 COMPARISON BETWEEN AVERAGE DEVIATION FROM ACTUAL FAILURE LOAD AND
FAILURE LOAD PREDICTION USING FRACTURE MECHANICS AND NONDESTRUCTIVE TESTING—
7075-T6511 ALUMINUM CYLINDERS

Several interesting facts are shown in Figure 146. Each of the FM/NDT procedures results in more accurate predictions of the failure load than FM using the actual crack lengths for cracks over 0.40 inch long. For example, using the crack length range from 0.45 to 0.50 inch, fracture mechanics theory and the actual crack length overestimates the failure load by an average of 20 KIPS. However, FM/X-ray, in that crack length range, is only off by 5 KIPS, while FM/penetrant is off by only 3 KIPS. The FM/ultrasonic predictions underestimate the loads by an average of 5 KIPS. In all cases of cylinders containing cracks the estimate of failure load is closer to the actual failure load than standard design assuming no cracks.

Figure 147 is a summary plot showing the average deviations between the actual failure loads and the failure-load predictions made using fracture mechanics and each NDT method. In this plot, all of the FM/NDT predictions are within 10 percent of the actual failure loads except for those made using ultrasonics. The FM/ultrasonics method is poor in comparison to penetrant, magnetic-particle and X-rays. It does not appear to be the fault of the FM analysis, since the predictions made using the actual crack length and fracture mechanics is within 5 percent of the actual failure loads. The FM/X-ray results are more accurate than those using FM/ultrasonics.

The results of the failure-load predictions are very encouraging and show the potential of a combined FM/NDT inspection procedure in predicting true failure loads. Two factors should be mentioned briefly at this point. First, the failure load predictions are very dependent on the choice of K_{Ic} or K_{Ix}. Since there can be large scatter in the actual value of K_{Ic}, the predictions could be very poor if the wrong value of K_{Ic} were used in the analysis. Second, it should be realized that in all of these predictions, the value of crack depth, a, was estimated from the NDT value of 2c. This is because there is no accurate method by which crack depth can be measured directly.

The ultrasonic technique offered the only potential method for measuring, a, directly, but the results were so inaccurate that they were not included in the analysis. In this example, the value of a was chosen based on the average value of $\frac{a}{2c}$ determined by measurements on the fracture surface. For example, for the 7075-T6511 the average $\frac{a}{2c}$ was 0.4832 and for 4330V Modified steel the average $\frac{a}{2c}$ was 0.4285. Most of the cracks showed a semicircular appearance on the fracture surface.

In the final analysis when part through cracks are used, the choice of crack depth, a, remains a difficult problem. However, it is expected that improved NDT procedures can be found that will result in more accurate estimates of crack depth. The accuracies of crack length, 2c, were sufficiently high to permit all failure-load predictions, with the exception of those discussed previously to be correct to within ± 10 percent.
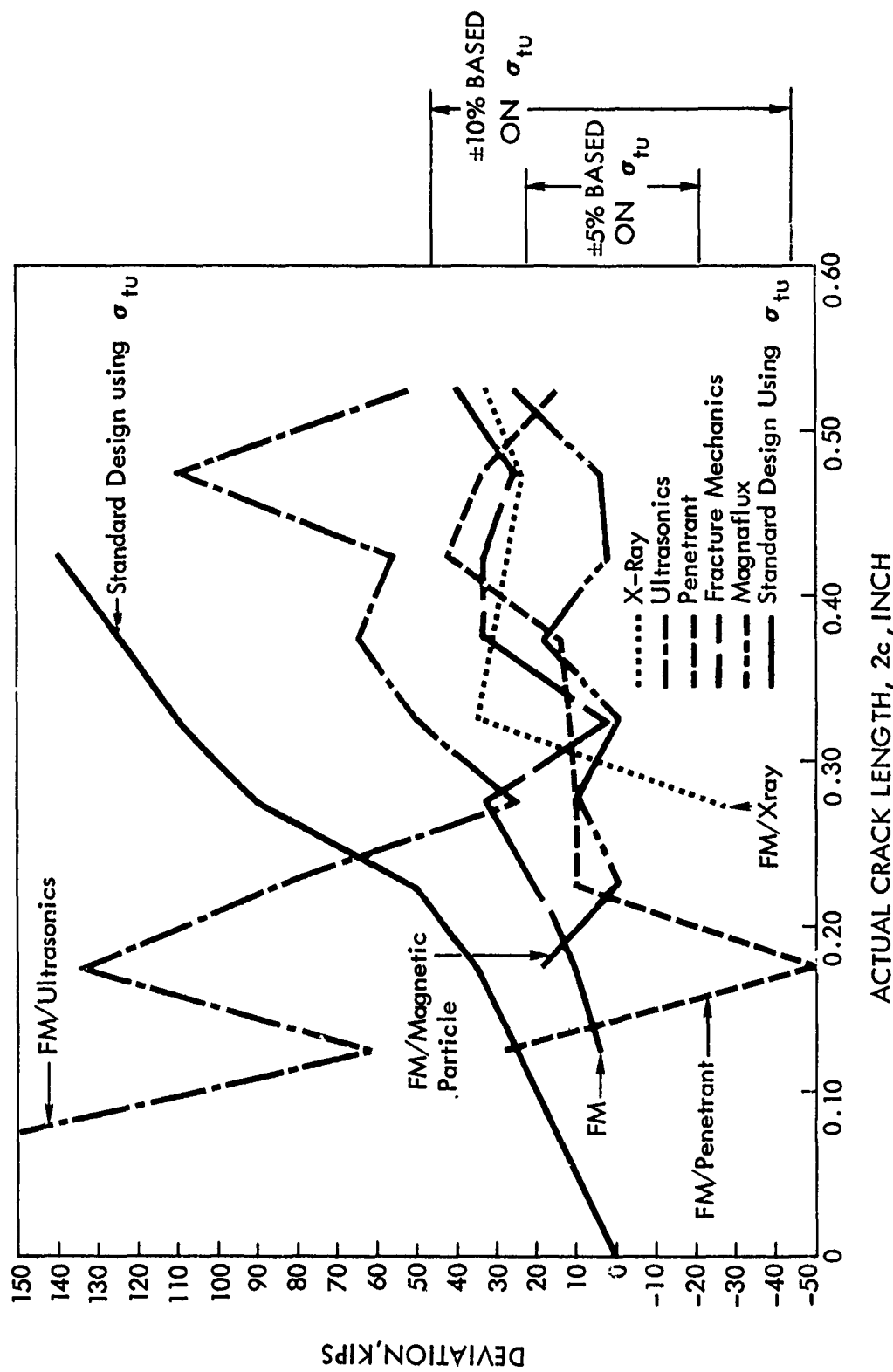
FIGURE 147   COMPARISON BETWEEN AVERAGE DEVIATION FROM ACTUAL FAILURE LOAD AND
FAILURE LOAD PREDICTION USING FRACTURE MECHANICS AND NONDESTRUCTIVE
TESTING – 4330 V MODIFIED STEEL CYLINDERS

Part 4 – Analysis of Cylinders Containing Circular Cutouts

Theoretical analyses of the stress distribution in the vicinity of a circular hole cut in a cylindrical shell have been made by Van Dyke (50) and Lurie (51). Experimental work on the stress distribution of such specimens was performed by Houghton (52) using a frozen stress technique. Later experimental work was extended to include elliptical cutouts and reinforced circular cutouts (53,54).

The tangential stress σ_ϕ at the edge of the circular hole in a cylindrical shell under uniaxial loading is given by

$$\frac{\sigma_\phi}{\sigma_1} = \left[1 + 2\cos 2\phi + \sqrt{3(1 - \nu^2)}\left(\frac{\pi m^2}{4RB}\right)\left(2 + 3\cos 2\phi\right)\right] \qquad (32)$$

This equation consists of the flat-plate solution plus a correction term for the curvature. Here σ_ϕ is the tangential stress, σ_1 the applied stress (P/ area), ϕ the angle of incline from the x axis, m the radius of the circular cutout, R the mean radius of the cylinder, and B the cylinder thickness. The stress distribution observed by Houghton follows the flat plate theory (55). Figure 148 shows the difference between the tangential stress σ_ϕ observed by Houghton and the theoretical values of σ_ϕ based on flat-plate theory as a function of incline ϕ.

The effect of cylinder radius R on the maximum stress concentration factor is shown in Figure 149. It was found that flat-plate theory is applicable to cylindrical shells containing circular holes whose geometries satisfy: $m^2/RB \leq 0.88$. A value for the cutout radius (m = 0.5") was determined by substituting the cylinder dimensions (R = 1.5" and B = 0.25") into this equation. According to the graph shown in Figure 149, the maximum stress concentration factor under uniaxial loading lies between 2.85 and 3.0.

Flat-plate theory was used to calculate the stress distribution around the hole for the test cylinders.

For an infinite flat plate under uniaxial tension containing a circular hole, the stress in the x direction, σ_x, and the stress in the y direction, σ_y, at distances r from the cutout are given by (56).

$$\sigma_y = \frac{\sigma_1}{2}\left[2 + \left[\frac{m}{r}\right]^2 + 3\left[\frac{m}{r}\right]^4\right] \qquad (33)$$

$$\sigma_x = \frac{\sigma_1}{2}\left[\left[\frac{m}{r}\right]^2 - 3\left[\frac{m}{r}\right]^4\right] \qquad (34)$$

The maximum σ_y stress is $3\sigma_1$ when m/r = 1.0; the minimum σ_x stress is $-\sigma_1$. The variation in stress as a function of the distance from the cutout is shown in Figure 150. Figure 150 also shows the variation in tangential stress plotted in polar coordinates. By suitable combination of Equations (32), (33), and (34) the stress parallel to the applied load at a distance r from the center of the cutout can be obtained.
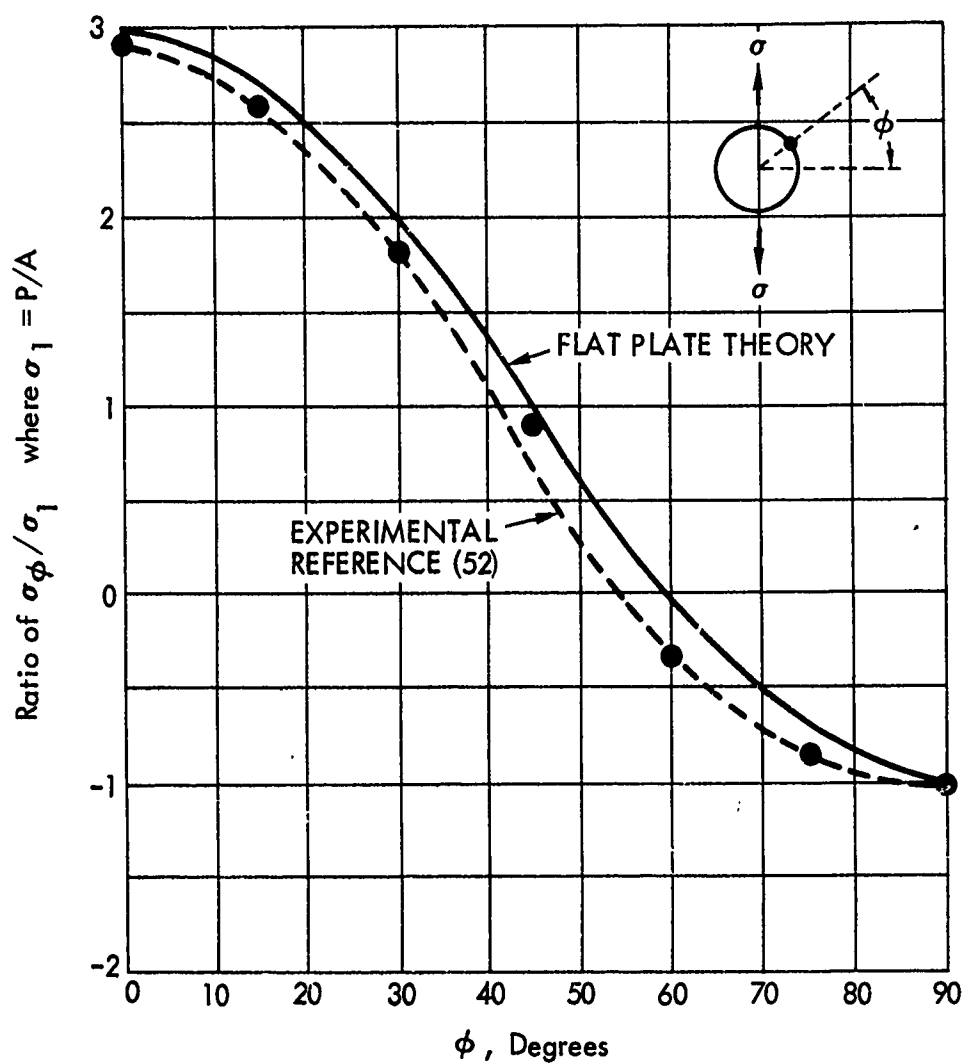
FIGURE 148 DIFFERENCE BETWEEN EXPERIMENTAL AND THEORETICAL VALUES
OF σ_ϕ AS A FUNCTION OF ϕ
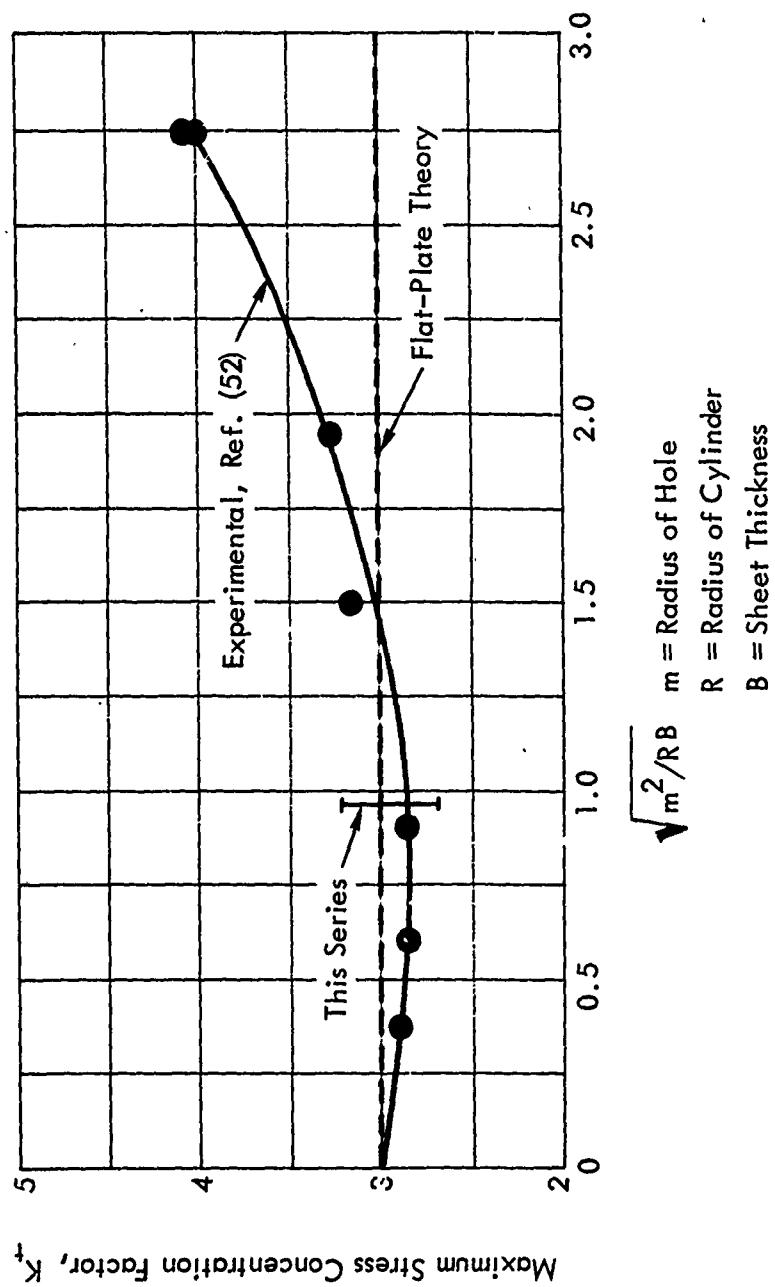
FIGURE 149 EFFECT OF CYLINDER RADIUS, CYLINDER THICKNESS, AND HOLE RADIUS ON THE MAXIMUM STRESS CONCENTRATION FACTOR

208
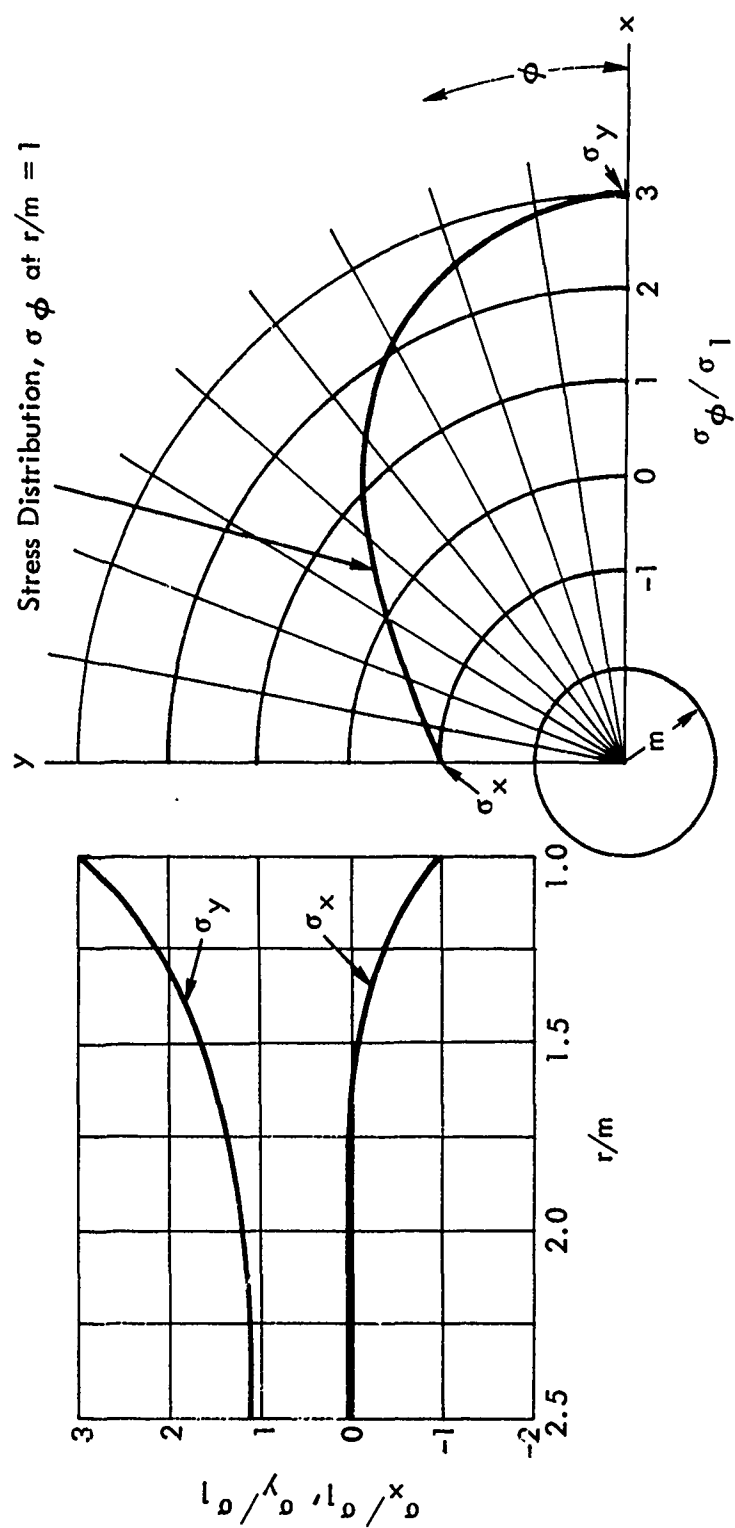
FIGURE 150 STRESS DISTRIBUTION AROUND CIRCULAR CUTOUT IN FLAT PLATE
UNDER UNIAXIAL TENSION

209

Failure Load Predictions of Cylinders Containing Cracks

For this limited series of tests, it was decided to hold the angle ϕ constant. The value of $\phi = 0°$ was chosen, since for this value of ϕ, equation (33) could be used directly in the calculations. Given $m = 0.50$ inch, the local stress at a distance, x, from the edge of the hole due to a uniform uniaxial stress σ_0 is given as

$$\sigma_{x_1} = \sigma_1 \left[\frac{2 + \left(\frac{0.50}{0.50 + x_1}\right)^2 + 3\left(\frac{0.50}{0.50 + x_1}\right)^4}{2} \right] \tag{35}$$

This stress, σ_{x_1}, is the local stress that is seen by the crack. This is shown schematically in Figure 151.[1] If the near edge of the crack was located at x_1, the material would fail when σ_x reached σ_f. Hence, using the part-through-crack analysis of Tiffany and Masters (2), the value of the fracture stress is given as

$$\sigma_{x_1} = \sigma_f = \frac{K_{Ic}}{1.1\sqrt{\pi} \sqrt{\frac{a}{Q}}} \tag{36}$$

Hence, replacing σ_f by σ_{x_1} in terms of the applied stress σ_0, the uniform axial stress required to cause failure is given by

$$\sigma_1 = \frac{2K_{Ic}}{1.1\sqrt{\pi} \sqrt{\frac{a}{Q}} \left\{ 2 + \left(\frac{0.50}{0.50 + x_1}\right)^2 + 3\left(\frac{0.50}{0.50 + x_1}\right)^4 \right\}} \tag{37}$$

By multiplying σ_1 by the area of the tube A, the failure load can be obtained:

$$P_x = \frac{A K_{Ic}}{1.1\sqrt{\pi} \sqrt{\frac{a}{Q}} K_{x_1}} \tag{38}$$

where P_x is used to designate the failure load prediction by this analysis

and

$$K_{x_1} = \left\{ \frac{2 + \left(\frac{0.50}{0.50 + x_1}\right)^2 + 3\left(\frac{0.50}{0.50 + x_1}\right)^4}{2} \right\} \tag{39}$$

and is the equivalent value of the stress concentration factor K_t at a distance x_1, from the hole.

The local stress concentration factor at the opposite end of the crack (not facing the hole) was also calculated. This is done simply by replacing x_1 by $x_2 = x_1 + 2c$ in Equations (35) to (39). The failure-load prediction, Equation (38), was also calculated assuming that the local stress experienced by the crack was the average of x_1 and x_2. This was called $K_{x(AVG)}$.

FIGURE 151 LOCAL STRESS AT TIP OF CRACK LOCATED AT DISTANCE, x_1, FROM HOLE IN SPECIMEN UNDER UNIAXIAL TENSION, σ_1
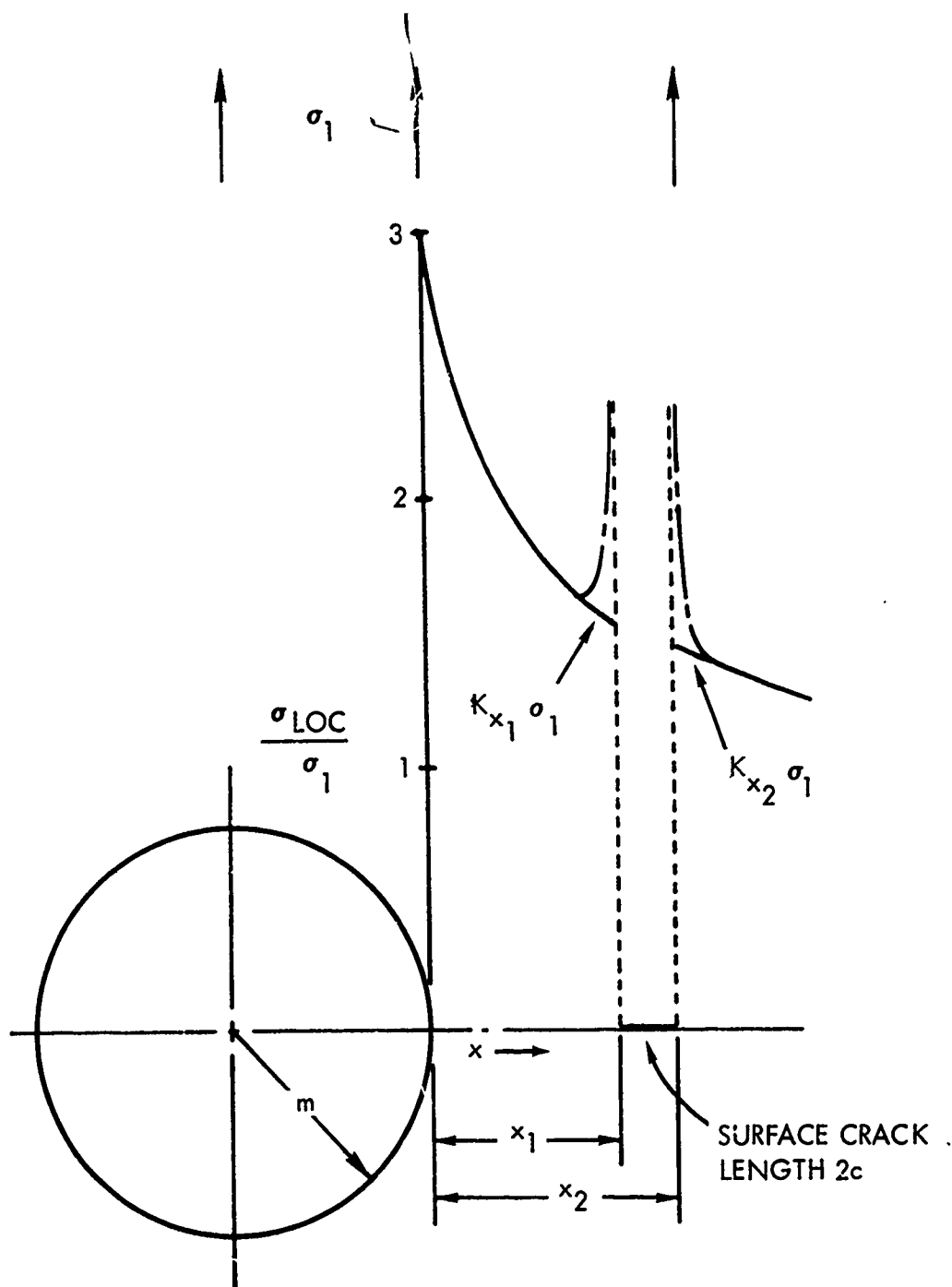
σ_{LOC} is the local stress in the y direction due to both the hole and the crack

A photograph of the failed surface of a 7075-T6511 Aluminum cylinder containing a 1-inch-diameter bored hole is shown in Figure 152. Figure 153 shows a side view of the same failed cylinder. It is evident that failure occurred in the section containing the cracks. Figure 154 shows a detail of the failure surface of a 4330V Modified steel cylinder containing a 1-inch-diameter bored hole. The primary failure passed through the section containing the cracks.

The values of x_1, x_2, $2c$, and a were measured directly on the failure surface. The location of the crack ℓ_1, ℓ_2, θ_1, and θ_2 were also measured. These measurements were used also in evaluation of the NDT and were incorporated in the results reported in Section III. However, for completeness, they are reported here in Tables XXI and XXII. These tables present the failure load predictions for the specimens containing both the hole and the crack. The K_{Ic} chosen was 48.6 KSI(in)$^{1/2}$ for the 4330V Modified steel in the 220-240 KSI heat-treat range and 31.8 KSI(in)$^{1/2}$ for the 7075-T6511 Aluminum.

For the 7075-T6511 Aluminum cylinders, the results are tabulated in the last three columns of Table XXI. The best results were obtained using the value of K_x where x_1 is the nearest point of the crack to the hole. The deviations are given in the last column. In all cases, the theoretical analysis overestimated the true failure load. This is perhaps due to the high value of K_{Ic} chosen.

The average overestimation is 13.9 KIPS too high. This is about a 9% error based on the failure load of the specimens containing the holes alone. The largest deviations, over-estimations of 50.5 KIPS, 44.0 KIPS, and 29.4 KIPS were found to occur for cracks with depths of 0.04 inch. This is not surprising, for these shallow cracks are not normally considered deep enough for the fracture mechanics to apply.

For the 4330V Modified steel cylinders, the results are tabulated in the last three columns of Table XXII. The best results were obtained using the value of K_{x_1} where x_1 is the nearest point of the crack to the hole. The deviations of the predicted loads from the actual loads are given in the last column. In most of the cases, the analysis overestimated the failure load. No particular pattern for the overestimation or underestimation was found; for example, with a crack depth of 0.07 inch, two specimens were overestimated and three underestimated.

The average deviation from the failure loads is +19.8 KIPS. The deviation was 5.2% based on the average failure load of the steel cylinder containing only the holes and was less than the average deviation found for the aluminum cylinders. Thus, it appears that the theory is more applicable to failure predictions for the steel cylinders than for the aluminum cylinders. This was to be expected, since the fracture mechanics theory is expected to be more accurate for the more brittle materials.

Several specimens failed in a manner shown in Figure 155. The failure appears to result from the crack's first growing into the hole and then propagating around the circumference of the cylinder. The right end of the crack is blunted by growing into the hole, and some plastic deformation is obtained on the periphery of the bored hole opposite the crack. The hole thus acts as a crack-stopper for one end of the crack.

This condition could also be approximated by a central hole with a single crack. This has been treated in detail by Paris and Sih (2). The failure-load prediction for this configuration, $\underline{P}$, is given by

FIGURE 152   FRACTURE SURFACE OF 4330V MODIFIED STEEL CYLINDER

FIGURE 153   FAILED SECTION OF 4330V MODIFIED STEEL CYLINDER
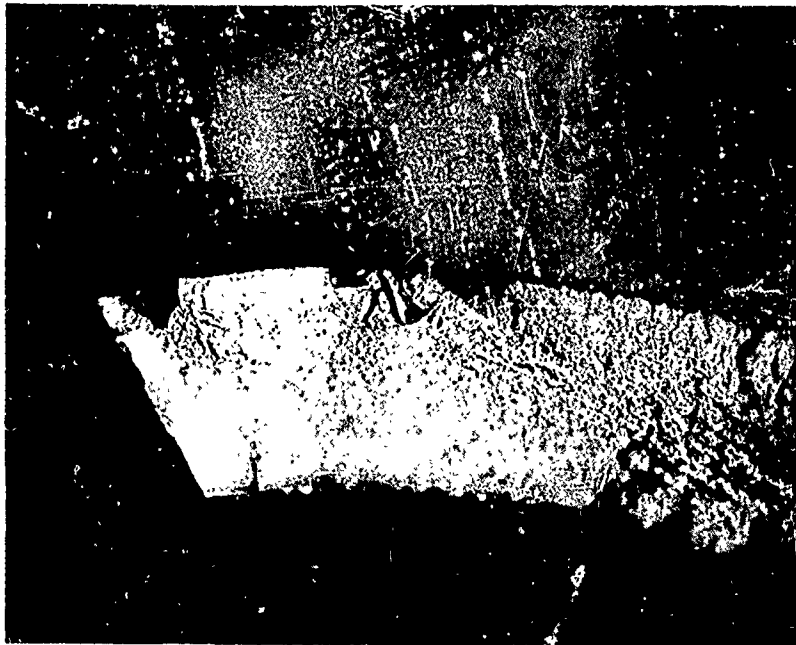
FIGURE 154   FRACTURE SURFACE 4330V MODIFIED STEEL

FIGURE 155 SECTION OF 4330V MODIFIED STEEL TUBE CYLINDER FAILED UNDER MONOTONIC TENSION TEST

TABLE XXI

FAILURE LOAD PREDICTIONS ON 7075-T6511 ALUMINUM CYLINDERS CONTAINING CRACKS AND HOLES

Specimen number	a, inch	$2c$, inch	x_1, inch	x_2, inch	Actual failure load, KIPS	K_{x_1}	K_{x_2}	$K_{x_{avg}}$	P_x min	P_x avg	$\underline{P}$** hole	dev.*
A47	0.07	0.105	0.14	0.25	115.0	1.864	1.518	1.691	116.4	128.3	53.7	− 1.4
A53	0.06	0.105	0.13	0.23	117.0	1.910	1.564	1.737	132.8	146.1	56.7	+ 15.8
A55	0.04	0.081	0.12	0.22	115.5	1.960	1.564	1.762	165.0	183.6	55.8	+ 50.5
A54	0.07	0.132	0.18	0.31	116.0	1.709	1.408	1.558	141.5	155.2	51.2	+ 24.5
A56	0.07	0.158	0.17	0.32	118.0	1.744	1.393	1.568	132.6	147.5	49.8	+ 14.0
A59	0.08	0.162	0.12	0.28	108.5	1.960	1.958	1.709	117.2	134.4	50.8	+ 8.7
A49	0.04	0.132	0.15	0.28	124.5	1.821	1.458	1.639	144.5	160.5	50.7	+ 20.0
A51		no crack			156.0							
A52	0.04	0.105	0.17	0.27	136.0	1.744	1.477	1.610	165.4	179.1	52.1	+ 29.4
A86	0.09	0.132	0.23	0.41	114.0	1.564	1.287	1.425	121.7	133.6	49.5	+ 8.7
A87	0.17	0.357	0.23	0.58	89.5	1.564	1.176	1.370	89.4	113.5	44.5	+ 9.9
A70	0.04	0.136	0.38	0.50	153.0	1.318	1.219	1.268	197.0	204.8	48.5	+ 44.0
A91	0.13	0.242	0.24	0.48	107.5	1.541	1.233	1.387	117.1	130.1	50.3	+ 9.6
A92	0.15	0.289	0.24	0.53	99.0	1.541	1.201	1.371	108.7	122.2	46.9	+ 9.7
A93	0.10	0.210	0.54	0.75	130.1	1.196	1.118	1.157	168.4	174.0	45.7	+ 37.9

Avg. dev.: +13.9

% dev.: 9%

*Deviation between actual failure load, and P_x min

** $\underline{P}$ (hole) using FM and equation (40)

217

TABLE XXII

FAILURE LOAD PREDICTIONS ON 4330V MODIFIED STEEL CYLINDERS CONTAINING CRACKS AND HOLES

Specimen number	a, inch	$2c$, inch	x_1, inch	x_2, inch	Actual failure load, KIPS	K_{x_1}	K_{x_2}	$K_{x\,avg.}$	P_x min	P_x avg	$\bar{P}$ hole **	dev. *
S34		crack not in fracture	0.06	0.13	377.0							
S75		no crack			386.0							
S76		no crack			377.0							
S63	0.07	0.13	0.19	0.32	337.0	1.676	1.393	1.534	317.6	347.0	112.6	− 19.4
S61	0.07	0.12	0.17	0.28	334.0	1.744	1.458	1.601	289.9	315.8	118.8	45.0
S62	0.06	0.12	0.15	0.28	316.0	1.821	1.458	1.640	201.5	223.8	120.1	114.5
S71	0.07	0.15	0.18	0.34	314.0	1.709	1.365	1.537	317.0	352.4	110.5	− 3.0
S72	0.06	0.105	0.19	0.28	360.0	1.676	1.450	1.567	336.4	359.9	121.8	− 23.6
S64	0.08	0.183	0.17	0.36	281.0	1.744	1.340	1.542	285.1	322.4	120.8	+ 4.1
S67	0.07	0.130	0.11	0.24	250.0	2.013	1.541	1.777	277.9	314.8	138.9	+ 27.9
S70	0.10	0.235	0.19	0.39	225.0	1.676	1.307	1.492	264.5	297.2	116.4	+ 39.5
S80	0.07	0.158	0.06	0.22	290.0	2.352	1.590	1.971	217.7	259.8	117.3	72.3
S59	0.06	0.15	0.23	0.38	339.0	1.564	1.318	1.441	343.5	372.9	115.5	+ 4.3
S66	0.07	0.13	0.23	0.36	339.0	1.564	1.340	1.452	345.7	372.3	120.3	+ 6.7
S49	0.06	0.14	0.21	0.34	331.0	1.617	1.365	1.491	339.8	368.5	108.3	+ 8.8
S65	0.11	0.263	0.21	0.47	248.0	1.617	1.239	1.428	250.6	283.7	110.0	+ 2.6
S60	0.09	0.20	0.24	0.44	271.0	1.541	1.261	1.401	306.9	337.6	108.6	+ 35.9
S74	0.14	0.263	0.21	0.49	239.0	1.617	1.225	1.421	240.0	273.1	111.6	+ 1.0
S86					387.0							
S88		no crack / crack not in fracture	0.29	0.37	384.0							
S73	0.17	0.393	0.28	0.68	221.0	1.459	1.138	1.298	233.8	262.7	109.1	12.0
S87		no crack			380.0							
S84		crack not in fracture	0.19	0.29	377.0							

Avg.dev.: +19.8 KIPS
Avg. no crack failure load: 381.1 KIPS
% dev.: 5.2%

*Deviation between actual failure load, and P_x min

** $\underline{P}$ (hole) using FM and equation (40)

218

$$\underline{P} = \frac{K_{Ic} A}{\sqrt{L\pi} f\left(\frac{L}{m}\right)} \tag{40}$$

and where L is the length of the initial crack plus the distance from the crack to the hole. $f(L/m)$ is tabulated as follows:

Stress-Intensity Factor Coefficients of (L/m) for
Cracks Emanating from a Circular Hole (2)

L/m	f(L/m) single crack uniaxial stress
0.00	3.39
0.10	2.73
0.20	2.30
0.30	2.04
0.40	1.86
0.50	1.73
0.60	1.64
0.80	1.47
1.00	1.37
1.50	1.18
2.0	1.06
3.0	0.94
5.0	0.81
10.0	0.75
∞	0.707

The results are given in Tables XXI and XXII under the column marked $\underline{P}$.

It is evident that these failure-load predictions are poor. The predicted failure loads are usually less than 50% of the actual failure loads.

Conclusions

The conclusions that can be drawn as a result of analysis of the fracture mechanics – nondestructive testing program are as follows:

o The present status of available literature concerning K_{Ic} values for 7075-T6511 Aluminum alloys is too scattered to be used as a design value in a FM/NDT design criterion.

o The available test information of K_{Ic} for most materials is, at best, marginal for use in the design of critical components and the scatter in reported values of K_{Ic} is too large, even at room temperature, so that the 90% confidence values of K_{Ic} based on the standard deviations would be so low as to render the design impractical.

o No information is available in the literature concerning K_{Ic} for 4330V Modified steel in the 220–240 KSI heat-treat range.

o The most consistent data for K_{Ic} appear to be available from the material producer, and next from the aerospace companies. The data from other sources showed an

extremely large scatter. This may be due to primary emphasis on devising new test techniques for K_{Ic}.

o The uncorrected plane-strain stress intensity factors obtained from tests conducted on the 7075-T6511 Aluminum cylinders show the K_{IX} to vary as follows:

$$K_{IX} = 17.0 + 140\ c \qquad\qquad \text{a, Q constant, } 2c < 0.275 \text{ inch}$$

$$K_{IX} = 40 \qquad\qquad \text{a, Q constant, } 2c > 0.275 \text{ inch}$$

$$K_{IX} = 17.0 + 180\ a \qquad\qquad 2c, Q \text{ constant, } a < 0.125 \text{ inch}$$

$$K_{IX} = 40 \qquad\qquad 2c, Q \text{ constant, } a > 0.125 \text{ inch}$$

$$K_{IX} = 17.0 + \frac{a}{Q} \qquad\qquad \frac{a}{Q} < 0.625 \text{ inch}$$

$$K_{IX} = 40 \qquad\qquad \frac{a}{Q} > 0.625 \text{ inch}$$

o The uncorrected plane-strain/stress intensity factors obtained from tests conducted on the 4330V Modified steel cylinders heat-treated to 220-240 KSI show the K_{IX} to vary as follows:

$$K_{IX} = 64 + 145\ c \qquad\qquad \text{a, Q constant}$$

$$K_{IX} = 64 + 220\ a \qquad\qquad \text{c, Q constant}$$

$$K_{IX} = 64 + 400\ \frac{a}{Q}$$

o A correction factor when applied to the K_{IX} to account for the plane stress-to-plane strain variation at the tip of cracks whose depths are greater than 1/2 the thickness reduces the K_{IX} obtained for deep cracks to K_{Ic}.

o The fracture mechanics failure load predictions using the actual crack length, 2c, and actual crack depth, a, are all within ±10% for both the aluminum and steel cylinders. This is in excellent agreement with the actual failure loads for these specimens.

o The fracture mechanics-nondestructive testing failure-load predictions are very dependent on the choice of K_{Ic} or K_{IX}. For the values of K_{IX} chosen, all FM/NDT predictions agreed with the failure-load to within ±10%. The one exception was FM/ultrasonics for the 4330V Modified steel cylinders.

o Except for the small crack lengths, the FM/NDT failure-load predictions for the aluminum cylinders were better than those predictions using standard design procedures.

o The failure-load predictions using FM/NDT for the 4330V Modified steel were all found to be more accurate than standard design predictions, with the exception of FM/ultrasonics.

220

o The failure-load predictions for test cylinders containing both a 1-inch-diameter hole and a small crack near the hole are in excellent agreement with the actual failure load. The average error for the 7075-T6511 Aluminum specimens was 9% and was 5.2% for the 4330V Modified steel.

SECTION VI

APPLICATIONS

The applicability of the FM/NDT design philosophy to actual aerospace components depends on two major factors; (1) The type of material used must be such that fracture theory would be applicable, and (2) the NDT procedure to be used must be specified in the design.

The material that is used should be of sufficient brittleness that there is a possibility of failure at stresses less than the yield stress. Some typical materials that might be used in a FM/NDT analysis are: (57)

Steels

    HP 9-4-25
    D6AC
    H-11
    4340, 4335V Modified
    4330V Modified
    300M
    18 percent Ni Maraging

Titanium Alloys

    6Al-4V
    6Al-6V-6Sn
    8Al-1Mo-1V
    6Al 6V-2Sn
    13Cr-11Mo-3Al

Aluminum Alloys

    2014-T6
    2020-T6
    2024-T6 T8 T651
    2219-T87
    7075-T6 T651, T6511
    7079-T6 T651

There are many others, but this partial list shows the potential alloy systems that may be used in the analysis. The fracture toughness of these alloys is such that the possibility of a brittle fracture at low stresses should not be ignored.

It is mandatory that the NDT procedure to be used in the design be specified in the design procedure. Since an assumption is made in the FM/NDT method regarding the pre-existance of flaws, the size of the flaw used in the design procedure should be detectable. The confidence in the design is based on the reliability of the NDT procedure to detect the size flaw.

If the sensitivity of the NDT method were 100 percent, there would be a high degree of reliability in the NDT procedure. On the other hand, if the sensitivity of the NDT were only 50 percent at that flaw size range, only 50 percent of the cracks would be found by the NDT. Thus, one of the cracks that was overlooked could be the cause of the failure.

The reliability of the combined FM/NDT failure-load prediction is the product of the reliability index of the NDT method and the confidence limit of the value of K_{Ic}. For example, if a flaw size of 0.30 inch were used, Figure 98 shows that the penetrant reliability index would be 0.53, the magnetic-particle index 0.72, and the ultrasonic index 0.66. Thus, using a 90 percent lower bound confidence value of K_{Ic} equal to 35.3 KSI(in)$^{1/2}$ for 4330V Modified steel, the relative confidence, R_f, that could be placed on the failure load predictions is as follows:

Penetrant: R_f	=	(0.9)(0.53)	=	0.48
Magnetic-Particle: R_f	=	(0.9)(0.72)	=	0.65
Ultrasonics: R_f	=	(0.9)(0.66)	=	0.59

The following paragraphs describe the general procedures that could be used in applying FM/NDT as a design method.

Case A: Tensile Loading

Failure stresses have been calculated for arbitrary conditions and flaw dimensions in a 20-inch wide flat plate to illustrate the results that may be expected. The basic equation used to evaluate each condition for susceptibility to fracture includes specimen width and local plasticity effects. The relationship used to calculate the fracture stress is as follows (2):

$$\sigma_f = \sqrt{\frac{K_{Ic}^2(1-\nu^2)}{W \tan\left\{\frac{\pi}{W}\left[c + \frac{K_{Ic}^2(1-\nu^2)}{6\pi\sigma_{ty}^2}\right]\right\}}} \tag{41}$$

where:

σ_f = Predicted gross stress at failure

K_{Ic} = Critical stress intensity factor for the plane-strain condition

ν = Poisson's ratio (use .3)

W = Specimen width

$2c$ = Flaw length

σ_{ty} = Yield stress of the material

Example 1 - Smooth Specimen, Flaw Detected

Specimen Data:

Material	7075-T6511 Extruded Plate
Thickness	0.250 inch
Width	20 inches
Yield Stress	80 KSI (Typical)
K_{Ic}	31.75 KSI(in)$^{1/2}$

223

Results:

NDT Technique	Flaw Size	Predicted Failure Stress
X-Ray	0.125 Inch	45.5 KSI
Penetrant	0.100 Inch	48.1 KSI
Ultrasonics	0.250 Inch	38.0 KSI

Example II - Smooth Specimen, No Flaw Detected

Specimen Data:

Material	7075-T6511 Extruded Plate
Thickness	0.250 Inch
Width	20 Inches
Yield Stress	80 KSI (Typical)
K_{Ic}	31.75 KSI$(in)^{1/2}$

Results:

NDT Technique	Minimum Flaw Size Detectable	Predicted Failure Stress*
X-Ray	0.40 Inch	32.5 KSI
Penetrant	0.20 Inch	40.7 KSI
Ultrasonics	0.15 Inch	43.9 KSI

*For preliminary design, the estimated gross stress at failure may be considered equal to the ultimate strength of the material for these conditions.

Example III - Specimen Containing 1-Inch-Diameter Bored Hole and Crack

The flaw is assumed to be located close to the edge of the hole and oriented in the plane of the specimen containing the minimum cross-sectional area with respect to the direction of loading. This location is the most critical in terms of the stress field surrounding the flaw. A solution for the stress analysis around a hole in a plate subjected to an axial load is given in Section V, Part 4.

Specimen Data:

Material	7075-T6511 Extruded Plate	Hole:	
Thickness	0.500 Inch		
Width	20 Inches	Centrally located	
Yield Stress	80 KSI (Typical)	Radius (m) 0.5 Inch	
K_{Ic}	31.75 KSI$(in)^{1/2}$		
Q	2.26		

224

Results:

NDT Technique	Flaw Size, 2c	Flaw Location	Predicted Failure Stress
Ultrasonics	0.242 Inch	0.17 Inch From Hole	40.7 KSI
Penetrant	0.158 Inch	0.24 Inch From Hole	59.3 KSI
X-Ray	0.400 inch*	0.23 (estimated)	25.0 KSI

*No flaw detected. Minimum flaw size detectable with X-ray is used.

Case B: Fatigue Loading

An elementary approach is used to illustrate the general form in which fracture mechanics-NDT concepts can be utilized in fatigue analysis. In this type of analysis, the objective is to obtain an estimate of the crack growth during fatigue-cycling. The initial crack size is taken to be compatible with the maximum size of a crack that would not be detected during the initial inspection. If this crack did exist, it could grow during the fatigue loading. Thus, the analysis assumes that the crack was not detected and calculates the final size of the crack after the fatigue loading. If this final size is such that it will not grow catastrophically upon reloading, the design is considered safe.

The introduction of alternating stresses introduces several complications into the analysis. First, it is assumed that the crack grows only during the tension portion of the loading. Second, it is assumed that the fatigue crack grows with a growth rate, da/dN, proportional to the applied stress intensity, K_I. A curve such as shown in Figure 156 is used. This plots the rate of crack growth, da/dN, in microinches per cycle against the applied stress intensity. In figure 156, for example, if the maximum applied stress, $\sigma_{applied}$, and crack geometry were such that:

Example IV: Simple Fatigue Loading

$\sigma_{applied}$ = 22.5 KSI (maximum alternating stress)

a = 0.15 inch

Q = 2.20

N = 10,000 cycles

The K_I would be given by

$$K_i = 1.1\sqrt{\pi}(22.5)\sqrt{\frac{.15}{2.20}} = 11.5 \text{ KSI (in)}^{1/2}$$

For this applied stress intensity, the crack growth rate would be about .20 microinches per cycle. Thus, with 10000 cycles of fatigue applied, the crack would grow .20 micro-inch/cycle(10000 cycles) = 0.0020 inch. For this example, a part through crack was used. If the crack were completely through the thickness, a different equation would be used for computation of the K_I.

This analysis may be extended to calculate the final crack size after a series of fatigue loads was applied. In this example, the crack would grow (or not grow if K_I were too low) to an intermediate size a_i. This new a_i would then be used with the second stress to

225

$$K_I = \sigma_{max.} \ (1-R)^{1/2} \ (1.2 \ \pi \ a/Q)^{1/2}$$

FATIGUE CRACK GROWTH, μ INCH/CYCLE [da/dN]

K_I, KSI(in)$^{1/2}$
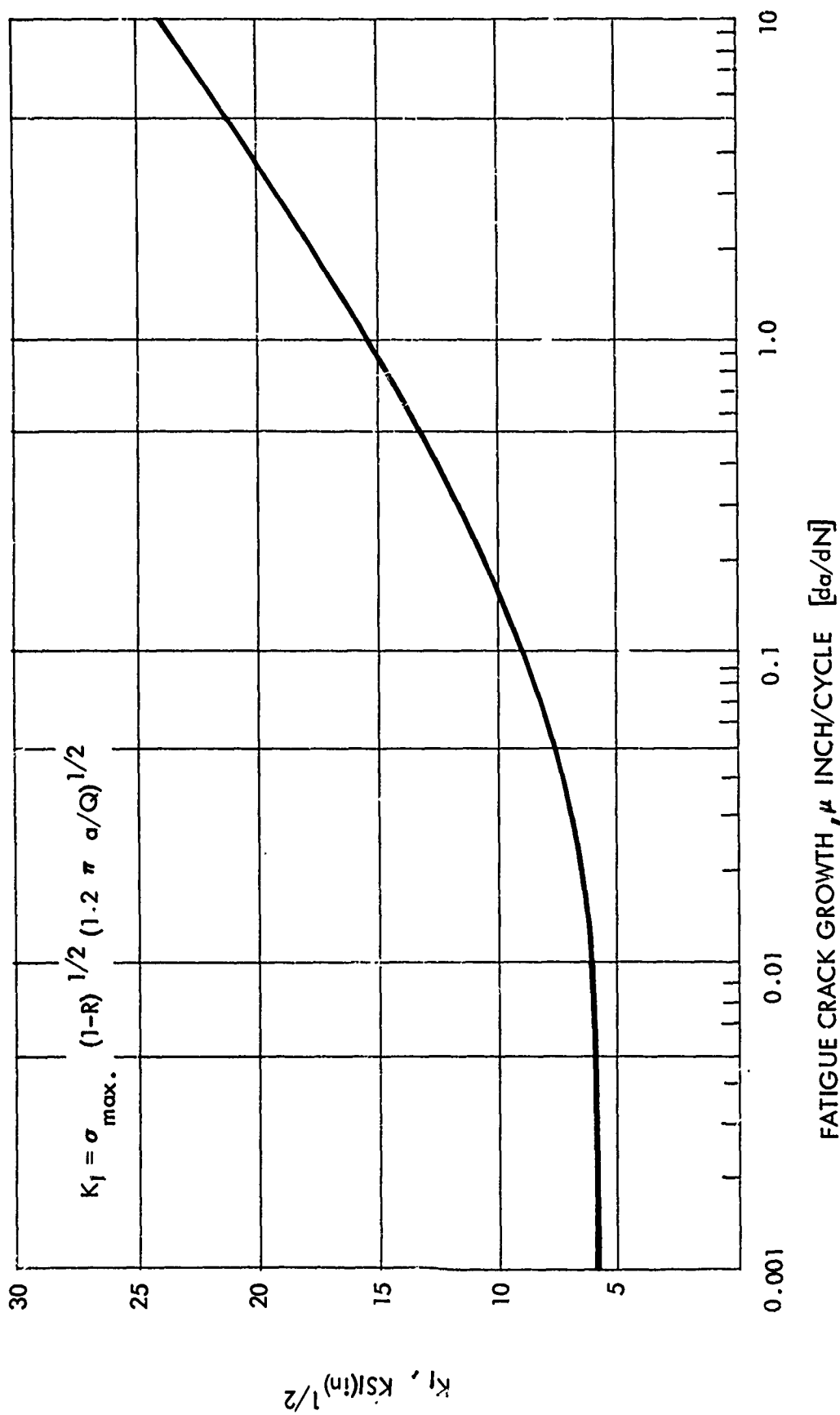
FIGURE 156 SCHEMATIC SHOWING FATIGUE CRACK GROWTH RATE AS A FUNCTION OF APPLIED STRESS INTENSITY FACTOR

226

calculate a new K_I; the crack growth rate for this new K_I is calculated and the new crack growth obtained by multiplying the da/dN by the number of cycles. Thus

Example V: Fatigue Loading (Complex Spectrum)

Maximum, Applied Stress	N
27,000 psi	6,000,000
45,000 psi	100,000
18,000 psi	10,000,000
30,000 psi	33,000

Initial flaw size $a = 0.030$ inch

$Q = 2.26$

$a_f =$ final crack size

A table is set up as follows:

Crack depth, inch	σ_{max}, KSI	K_I KSI$(in)^{1/2}$	da/dN, μ inch/cycle	N cycles	Crack depth, inch
0.030	27,000	6.06	.002	6×10^6	0.042
0.042	45,000	11.98	.330	1×10^5	0.075
0.075	18,000	6.39	.01	1×10^7	0.175
0.175	30,000	16.26	1.35	2×10^4	$0.220 = a_f$

Each calculation is made assuming that the value of Q remains the same. The final crack depth is 0.220 inch. If the material were now subjected to tensile loading, it would fail at

$$\sigma_f = \frac{K_{Ic}}{\sqrt{1.2 \, a_f / Q}} \text{ , KSI}$$

If this stress is higher than the maximum applied tensile load, the part is considered safe.

It should be realized that, in this and subsequent analyses, the value of Q is assumed to be constant. This implies that the crack depth growth is proportional to the crack length growth. If it were not, the variation in Q would have to be considered in calculating the K_I.

In fatigue loading, the type of cyclic stressing is often expressed in terms of "R." This is defined as the ratio of the minimum stress to maximum stress or:

$$R = \frac{\sigma_{mean} - \sigma_{alt}}{\sigma_{mean} + \sigma_{alt}}$$

An R of zero is loading from zero stress to some maximum stress; an R of -1 is tensile-compressive stressing. As mentioned previously, it is assumed that the maximum stress, and hence the maximum value of K_I, determines the fatigue-crack growth. However, it is possible that the K_I should incorporate the value of R. Hence, it is suggested that, for

fatigue with varying R values, the K_I be assumed as:

$$K_{IR} = \sigma_{max}(1-R)^{1/2}(1.2 \pi a/Q)^{1/2} , \quad (1-R) \geq 0$$

This is for a part-through crack. For other crack geometries, the K_I would be multiplied by the $\sigma_{max}(1-R)^{1/2}$ term. Hence, if the fatigue loading included different values of R, the analysis would be as follows:

Example VI: Fatigue Loading, Varying R Value

σ_{mean}	R	N
72,250	0.82	500,000
43,750	0.75	3,000,000
42,220	0.82	600,000
54,290	0.75	50,000

$a_i = 0.30$

$Q = 2.26$

In a manner similar to Example V, a table is set up. Now the calculation of K_I includes R, and hence is tabulated as K_{IR}.

Crack Depth inch	σ_{Max}	K_{IR}	da/dN	N	Crack Depth, a inch
0.030	80,000	7.64	0.045	5×10^5	0.053
0.053	45,000	6.70	0.020	3×10^6	0.113
0.113	50,000	9.28	0.110	6×10^5	0.178
0.178	60,000	16.40	1.10	5×10^4	$0.233 = a_f$

The final crack depth is 0.233 inch. As before, the remaining residual tensile stress is given by:

$$\sigma_f = \frac{K_{Ic}}{\sqrt{1.2\pi a_f/Q}}$$

In many aircraft situations, there is no way of knowing how many cycles of stress may be applied at any one time. It is known that the part will be subjected to several stages of fatigue, but the number of cycles at each particular stress level are unknown. The total number of cycles at each stress level is known. This would require a random application of the fatigue stresses for a random number of cycles at each stage. This is called "random fatigue spectrum loading." This problem may also be solved as follows:

Example VII: Random Fatigue Spectrum Loading

Stage	σ mean	R	N(total) cycles
1	27,500 psi	0.968	4,000,000
2	27,800 psi	0.943	1,800,000
3	28,100 psi	0.927	680,000
4	28,300	0.903	300,000

initial crack depth   a = 0.030 inch

Q value = 2.26

Using a table of random numbers a series of numbers were chosen and used in sets of three. The first number refers to the stage of loading, the second pair to the percent of the total N that is used during the fatigue. For example, if the following numbers were used:

$$135 \quad 442 \quad 415 \quad 363 \quad 793 \quad 227 \quad 152,$$

the first number states that a mean stress of 27,500 psi and an R of 0.968 were used for 35% of 4,000,000 cycles. This would then be the first entry for crack depth. The K_{IR} is calculated and the growth of the crack computed and added to the initial crack depth. The fourth numbered set would be used, i.e. 28,300 psi, R = 0.903 for 42% of 300,000 cycles. This procedure would be continued. A number that indicates a stage not in the sequence would be discarded. (Here 793 is discarded). When the stage is repeated, i.e. 152, the stress for stage 1 would be used, but 52% of the remaining number of cycles would be used in computing the fatigue cycles at this level. Hence, the second time stage 1 was reached, the calculation of crack growth would be based on 52% of (4,000,000- 42% of 4,000,000) cycles or 52% of 2,320,000 cycles. This is repeated for about 20 steps. At this time, the remaining fatigue lives are used one after the other. Since the first 20 steps used a random number of cycles, the last step would also use a random number of remaining cycles.

To do this calculation by hand would obviously be tedious, especially with a large number of fatigue stages. For this example, a computer program was set up. For a run of 20 stages, the final crack depth was about 0.20 inch. This was repeated 20 times with 20 different sets of random numbers. The values of final crack depth are given below.

0.150	0.210	0.201
0.231	0.214	0.197
0.188	0.215	0.193
0.189	0.213	0.185
0.212	0.205	0.188
0.192	0.196	0.219
0.177	0.202	

Avg: 0.1996

Standard deviation 0.1762

Upper bound 95% confidence limit - 0.206 inch

Using the average plus the 3.4 standard deviation gave the value of final crack size that would be equivalent to the 95% upper bound confidence limit. This is the crack size that 95% of the material would not be expected to exceed. This implies that if the process were

229

repeated for 100 random loading sequences, 95 of the numbers for final crack depth would be **below** this number.

The static strength remaining after this random loading would then be given by

$$\sigma_f = \frac{K_{Ic}}{\sqrt{1.2\,\pi\,a_f/Q}} \tag{47}$$

If the K_{Ic} is given with a 95% confidence factor, the confidence in this calculation would be .95 x .95 or 90%. This would be equivalent to a "B" confidence value for σ_{ty}.

Case C: Sustained Loading in Environment

It is well known that high-strength materials may fail in a brittle manner when subjected to sustained loading in the presence of external environments. To use the fracture mechanics-nondestructive testing design methodology for this type of an application, a curve such as that shown in Figure 157 must be determined experimentally. In this case, the flaw growth per unit of time is plotted against the applied stress intensity K_{ii} in a particular environment. The K_{ii} is determined by calculation using the initial flaw sizes and sustained applied stress. Thus, for a part through crack with the following geometry and stress:

Example VIII – Sustained Loading in Salt Water Environment

$$\sigma_{applied} = 22.5 \text{ KSI}$$
$$a = 0.15 \text{ inch}$$
$$Q = 2.20 \text{ inch}$$

The K_{ii} is 10 KSI $(in)^{1/2}$, and the flaw growth rate is 70 microinches/minute. Using a value of K_{Ic} of 30 KSI $(in)^{1/2}$, and the part through crack analysis, the part would fail when the crack grows to a depth of

$$a = \frac{K_{Ic}^2 \, Q}{1.2 \; \sigma^2 \pi} \tag{48}$$

$$a = 1.04 \text{ inches.}$$

At a rate of 70 microinches per minute, this would take about 1270 minutes or a little over 20 hours.

If the K_{ii} were less than 5 KSI $(in)^{1/2}$, the material would last indefinitely. This is commonly referred to as the K_{ISCC} value.

230

CRACK GROWTH RATE, da/dt, μ inches/minute
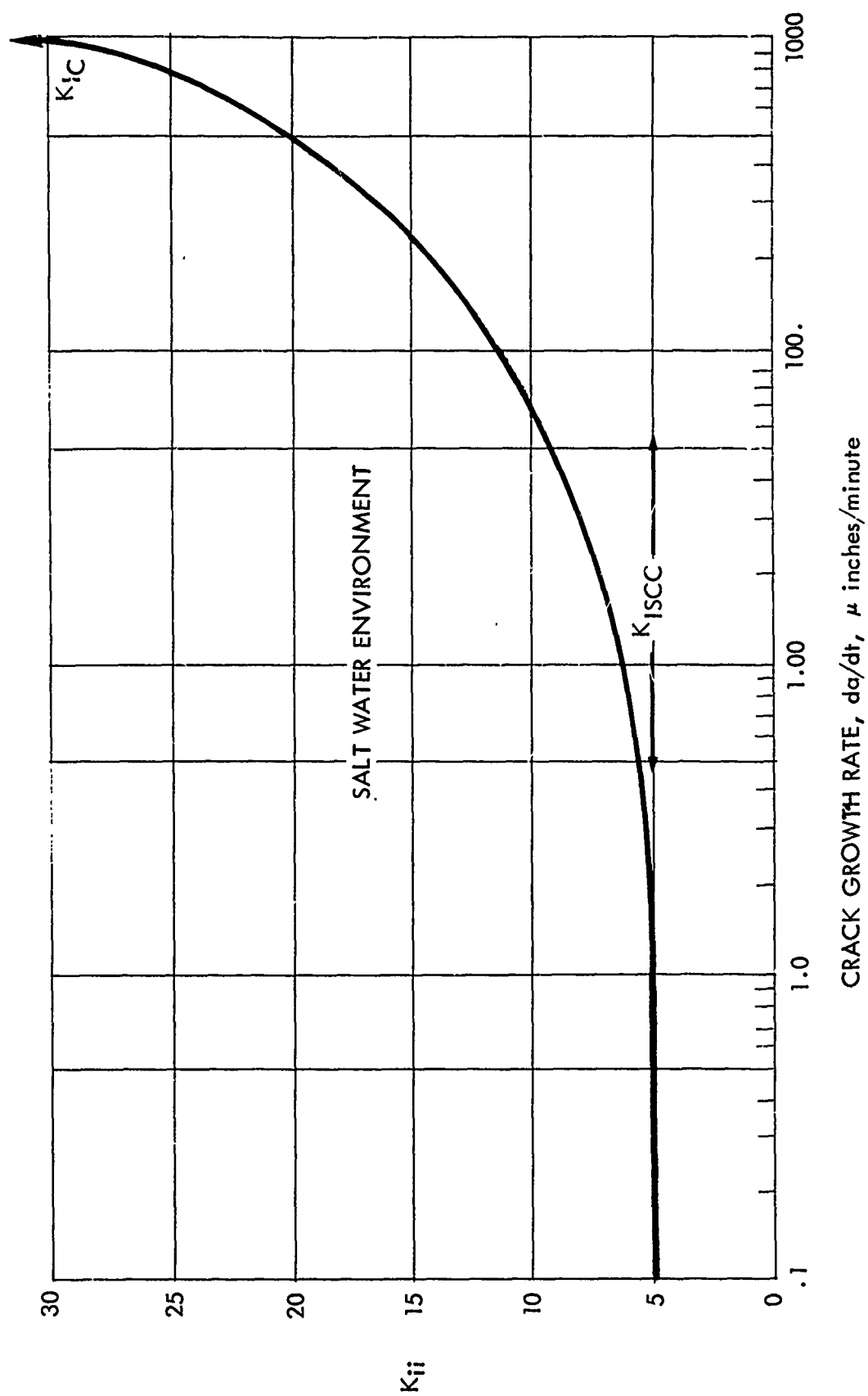
FIGURE 157   SCHEMATIC SHOWING THE CRACK GROWTH RATE AS A FUNCTION OF APPLIED STRESS INTENSITY FACTOR K_{ii} FOR SALT WATER ENVIRONMENT.

Aircraft Components

Test data from the following C-5A components were used in the full-scale test section of this program.

Center Wing Shear Panel (105A)	7075-T6511 Aluminum
Center Wing Shear Panel (107A)	7075-T6511 Aluminum
Center Wing Failsafe Panel	7075-T6511 Aluminum
Latch Assembly (Small)	4330V Modified Steel
Latch Assembly (Medium)	4330V Modified Steel
Latch Assembly (Large)	4330V Modified Steel

The center wing shear panels (105A and 107A) were the first components to be inspected and tested. Typical cross-section dimensions are listed below:

	Panel 105A	Panel 107A
Pitch	5.500"	5.500"
Flange Width	2.520"	2.520"
Skin Thickness	0.276"	0.224"
Riser Thickness	0.214"	0.156"
Flange Thickness	0.266"	0.199"
Riser Height*	3.938"	4.017"
Panel Width	30.00"	30.00"

*Riser Height is measured from upper skin surface to lower flange surface.

Penetrant inspection was carried out using Zyglo penetrant. Ultrasonic inspection was performed using a Reflectoscope model UM 715 with a 5 mHz contact transducer. The instrument was calibrated to detect a 1/64-inch flat-bottom hole at full-scale deflection. Neither method revealed a defect. X-ray inspection was performed by production inspectors. No flaw was detected.

The test setup that was used for testing the C-5A wing panels is shown in Figure 158. The panels were tested in a 1200-KIP Baldwin Universal Testing Machine.

The -105A and -107A shear panels were correlated using the load-strain data and the following Ramberg-Osgood properties obtained from furnished coupon data: For reference These values are as follows:

	-105A Panel	-107A Panel
$\sigma_{0.7}$	65,185 psi	68,179 psi
n	15.0	15.0

The unit strains in the test panels at failure were estimated from the load strain data to be .02 for the -105A panel and .03 for the -107A panel. Using these unit strains to determine the equivalent shear stress associated with them, the loads in the panels at failure were determined to be 13,168 lbs/in for the -105A panel and 10,804 lbs/in for the -107A panel. The predicted allowable loads were determined to be 10,633 lbs/in for the -105A panel and 9,026 lbs/in for the -107A panel.

The test loads are 2,535 lbs/in higher for the -105A panel and 1,778 lbs/in higher for the -107A panel than the predicted allowable loads. These differences were due to the large strains in the test panels. The predicted mode of failure is general yielding, which limits the stress to $\sigma_{0.1t}$ (the stress at which the tangent modulus is 1/10 the elastic modulus).

FIGURE 158 TEST CONFIGURATION FOR C-5A 7075-T6511 ALUMINUM WING
PANEL.   LOWER GRIP NOT IN PLACE

FIGURE 160 OUTER SURFACE OF FAILED C-5A
7075-T6511 ALUMINUM WING PANEL
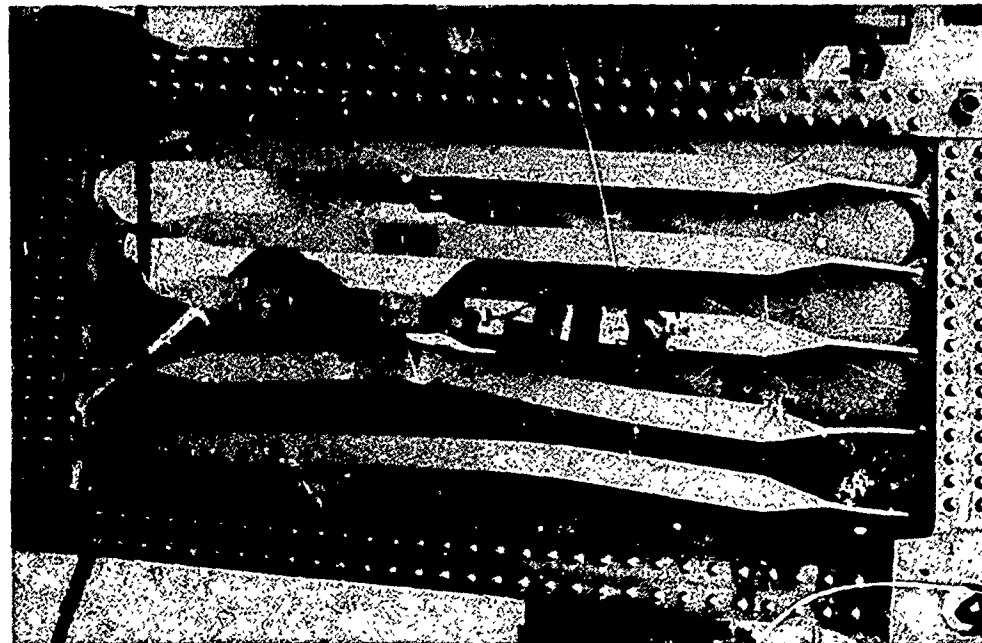
FIGURE 159 INNER SURFACE OF FAILED C-5A
7075-T6511 ALUMINUM WING PANEL

The ultimate loads carried by the test assemblies were 17,889 lbs/in for the -105A panel and 14,207 lbs/in for the -107A panel. These loads are 4,721 lbs/in higher for the -105A panel and 3,374 lbs/in higher for the -107A panel. Separate calculations indicated that the additional load was carried by the test frames.

The capacity of the test machine was reached prior to the catastrophic failure of panel -105A. The strain data indicated that the skin of the panel yielded at shear loads of approximately 9.0 KIP per inch.

Figures 159 and 160 show the inner surfaces of the failed -107A center wing panel. The panel failed due to tension failure of the skin and the risers and shear buckling of the skin. The risers underwent lateral buckling of the flanges. The bases of the risers failed in tension.

The shear panel is approximated by a center-cracked plate. The following maximum undetectable surface crack in each of the NDT methods is used:

Penetrant	2c	0.10 inch
X-ray	2c	0.30 inch
Ultrasonics	2c	0.05 inch

The value for K_{lc} used is 30 KSI (in)$^{1/2}$.

The failure load is calculated assuming that the failure starts in the thin section. However, some load, P', is taken up by the risers. The relative magnitudes of the total applied load, P, is assumed to be distributed proportional to the area of the skin and the risers.

Hence, for panel 105A each riser has an area of 1.456 in^2. The skin has an area of 8.28 in^2. There are five risers, hence, the total riser area is 7.37 in^2.

$$P_{riser} + P_{skin} = P_{total}$$

$$\frac{P_{riser}}{A_{riser}} = \frac{P_{skin}}{A_{skin}}$$

$$P_{skin} + P_{skin} \frac{A_{riser}}{A_{skin}} = P_{total}$$

$$P_{skin} \left(1 + \frac{A_{riser}}{A_{skin}} \right) = P_{total} \tag{49}$$

The predicted load in the skin at failure is given by

$$P_{skin}^2 = \frac{K_{lc}^2 W^2 B^2}{\pi c} \tag{50}$$

Hence,

$$P_{skin}^2 = \frac{(30)^2 (30)^2 (0.276)^2}{\pi (0.05)} \text{ KIPS}^2 \text{ (for penetrant)}$$

$$P_{skin} = 622,000 \text{ pounds (for penetrant)}$$

$$P^2_{skin} = \frac{(30)^2 \ (30)^2 \ (.276)^2}{\pi \ 0.15} \quad \text{(for X-ray)}$$

$$P_{skin} = 360,000 \text{ lbs. (for X-ray)}$$

$$P^2_{skin} = \frac{(30)^2 \ (30)^2 \ (.276)^2}{\pi \ 0.025} \quad \text{(for ultrasonics)}$$

$$P_{skin} = 880,000 \text{ lbs. (for ultrasonics)}$$

Using Equation 49, the predicted failure loads are then

$$P_{total} \text{ (penetrant)} = 622,000 \left[1 + \frac{7.37}{8.28} \right] = 1,170,000 \text{ pounds}$$

$$P_{total}(\text{X-ray}) = 680,000 \text{ pounds}$$

$$P_{total} \text{ (ultrasonics)} = 1,660,000 \text{ pounds}$$

These should be compared to the actual failure loads.

Predicted Load, lbs.		Actual Load, lbs.
Penetrant	1,170,000	1,053,000
X-ray	680,000	1,053,000
Ultrasonics	1,660,000	1,053,000

The percent errors are:

Penetrant	10%
X-ray	35%
Ultrasonics	59%

The most accurate prediction was made using the penetrant system which was 10 percent too high.

Figure 161 shows the medium-sized 4330V Modified steel cargo latch hook prior to testing. The hook-latch assembly (large) made from 4330V Modified steel was inspected using three methods. The magnetic-particle inspection was carried out using the coil shown in Figure 162. The part was inspected with the long axis normal to the coil axis, it was demagnetized and it was then inspected with the short axis normal to the coil axis. The ultrasonic methods were calibrated to detect an internal flaw equivalent to a 1/64-inch flat bottom hole. A 5 mHz transducer was used in conjunction with the Reflectoscope model UM 715 shown in Figure 163. X-ray inspection was performed by production inspection. None of the inspections revealed any abnormalities or flaws.

Hook-latch assemblies (medium and small) were inspected using magnetic-particle, ultrasonic, and penetrant (Zyglo) methods. The inspection procedures were the same as for the large hook. The inspections revealed no defects in either of the parts.

It was calculated that the medium-size hook would fail at section B-B and that the small and large hooks would fail at section A-A (Figure 151). The calculated ultimate loads are given below:

236
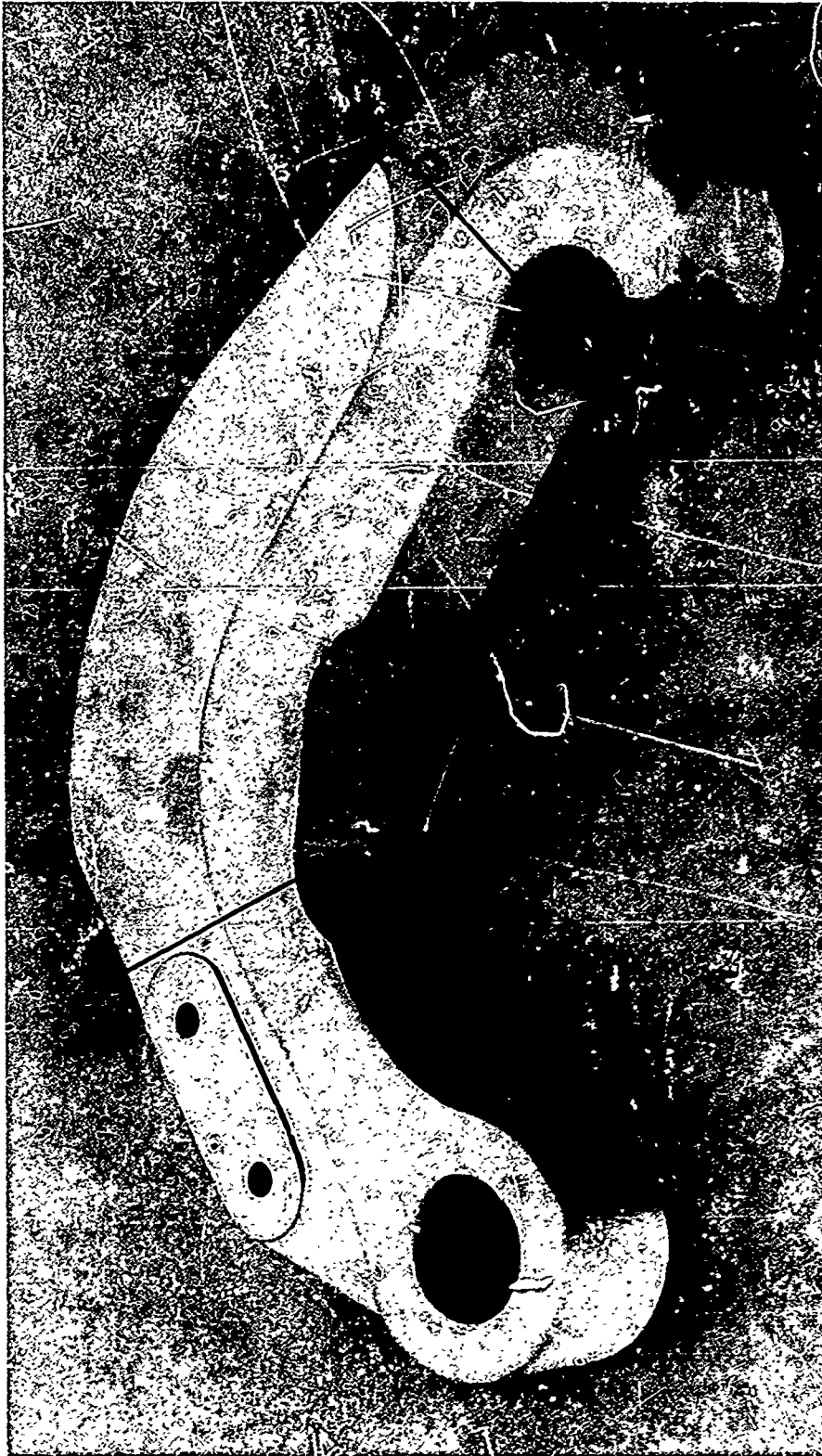
FIGURE 161 TYPICAL 4330V MODIFIED STEEL CARGO LATCH HOOK PRIOR
TO TESTING. SECTIONS A-A AND B-B ARE LOCATIONS OF
CRITICAL SECTIONS

FIGURE 162 MAGNETIC PARTICLE INSPECTION EQUIPMENT USED TO INSPECT
4330V MODIFIED CARGO LATCH HOOKS

FIGURE 163 PORTABLE PULSE REFLECTION ULTRASONIC INSPECTION UNIT
USED TO INSPECT 4330V MODIFIED CARGO LATCH HOOKS

Small Hook	31,400 pounds
Medium Hook	56,700 pounds
Large Hook	69,100 pounds

All three hooks were tested to failure. The results were as follows:

Small Hook	Failed at A-A	33,100 pounds
Medium Hook	Failed at B-B	57,100 pounds
Large Hook	Failed at B-B	79,800 pounds

Figure 164 shows the small 4330V Modified hook after failure. This hook failed in the A-A section, exhibiting necking of the areas surrounding the fracture. There was considerable distortion in the hook when examined. Figure 165 shows the appearance of the fracture surfaces of the small hook. The fracture surface is about 50 percent flat in the thick and the thin section. There is considerable doubt as to where the crack initiated, but two possible sites appear likely. The first is at a point about 1/16 inch from the surface, while the second appears to be a small inclusion located approximately in the center of the thick section. It is possible that both areas produced some crack growth prior to final failure.

Figure 166 is a photograph of the medium hook after failure. The failure initiated in the tensile section of the hook at a point about 1/16 inch from the surface. Figure 167 shows the fracture surface. The failure is essentially 70 percent flat fracture in the thick section and 90 percent flat fracture in the thin section. The crack started in one corner and propagated rapidly across the thick section. There was enough plastic deformation in the thin section to distort the lower connecting hole as shown in Figure 167.

Figure 168 shows the large 4330V Modified hook after failure. The fracture occured across the B-B section, with some distortion of the lower connecting hole. The fracture was about 90 percent flat for the thin section and about 80 percent flat for the thick section. Figure 169 shows the fracture surfaces of the large hook. Failure appears to have been caused by a crack that initiated at a point 1/16 inch from the inner surface and progressed rapidly in all directions.

Figures 170 and 171 show electron fractographs taken from replicas of the fracture surface of the medium-size hook. The replicas were taken from areas in the neighborhood of the crack initiation site. The fracture surface exhibited mostly dimple rupture with some evidence of cleavage.

A simple analysis will be used for each of the hooks. It is assumed that a small surface crack exists at the critical sections AA and BB. If the size of the crack is assumed as follows:

$$2c = 0.200 \text{ inch long}$$
$$a = 0.020 \text{ inch deep}$$
$$Q = 0.88 \qquad (\sigma_f = \sigma_{ty}),$$

This crack would not have been detected by the X-ray inspection or with any high degree of accuracy by any of the other inspection techniques. A crack length greater than 0.20 inch may have been used but would have been detected. Hence, the failure load is given by:

$$P = \frac{A \, K_{Ic}}{\sqrt{1.2 \, \pi \frac{a}{Q}}} \qquad (51)$$
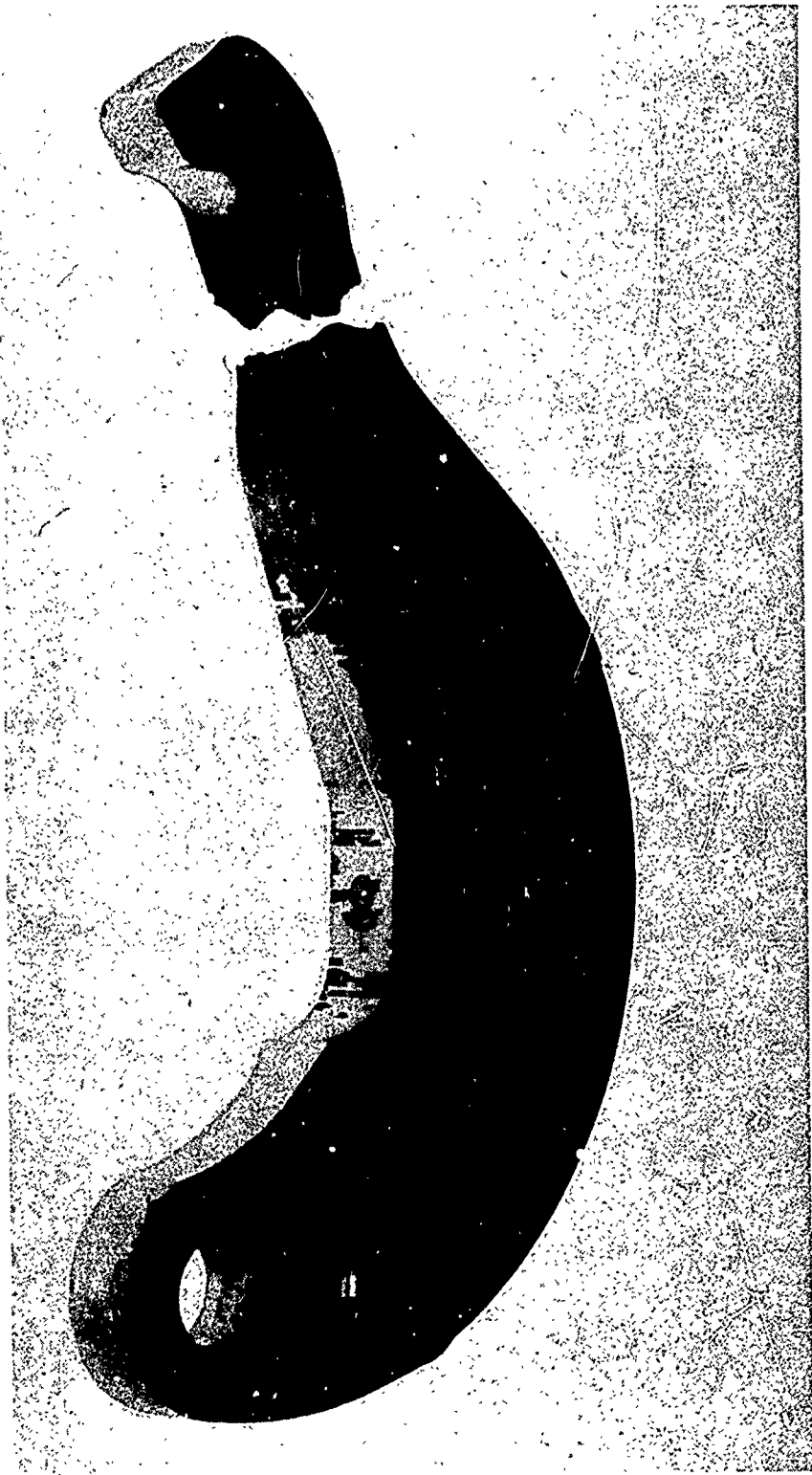
FIGURE 164 4330V MODIFIED STEEL CARGO LATCH HOOK AFTER TEST (SMALL SIZE)
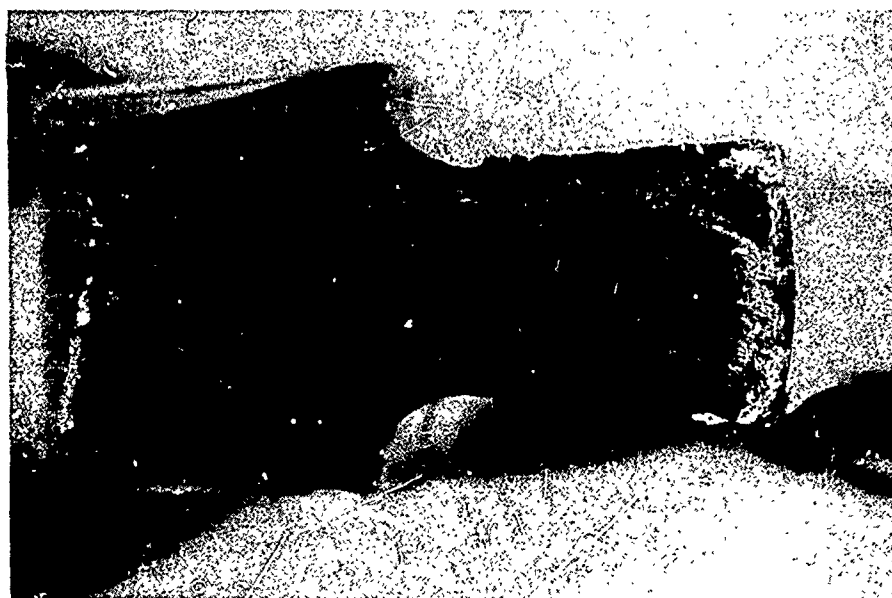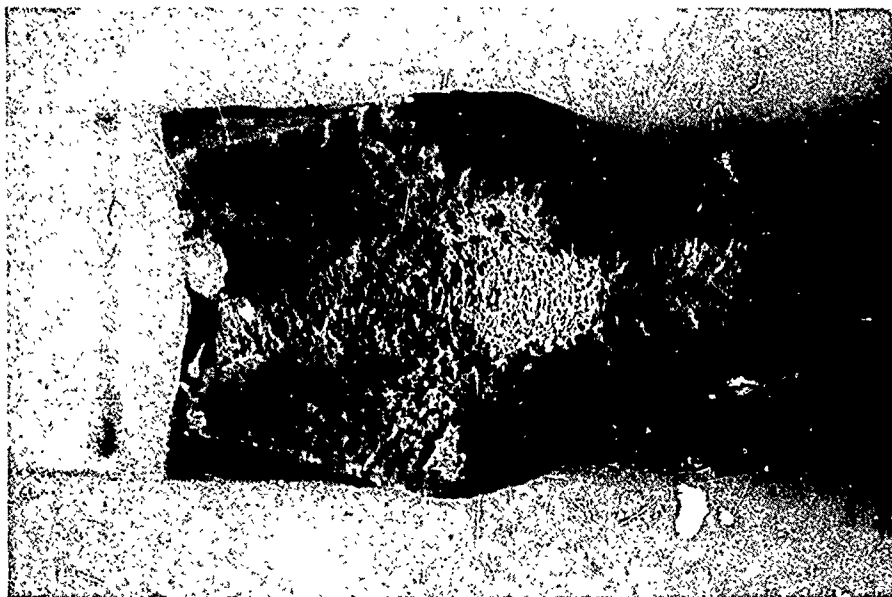
FIGURE 165 FRACTURE SURFACES OF FAILED 4330V MODIFIED STEEL CARGO LATCH HOOK (SMALL SIZE)

242

FIGURE 166 4330V MODIFIED STEEL CARGO LATCH HOOK AFTER TEST (MEDIUM SIZE)
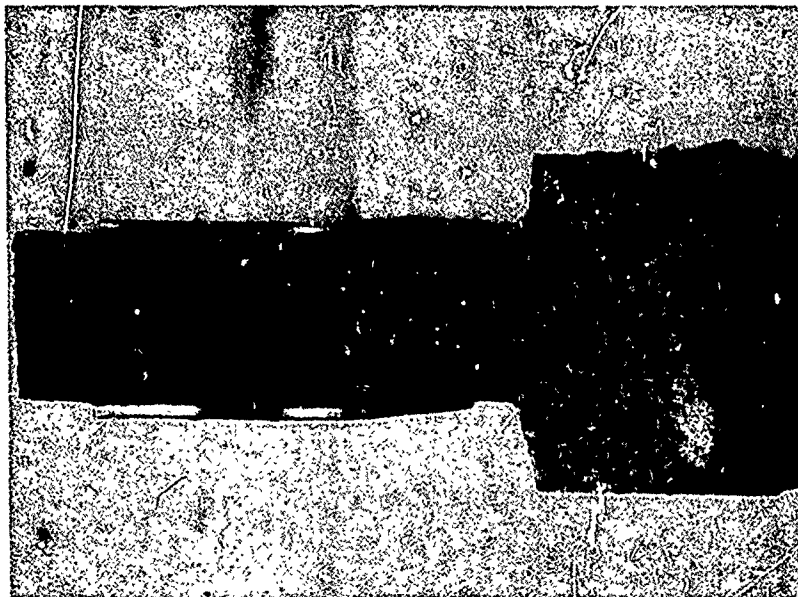
FIGURE 167 FRACTURE SURFACES OF FAILED 4330V MODIFIED STEEL CARGO LATCH HOOK (MEDIUM SIZE)
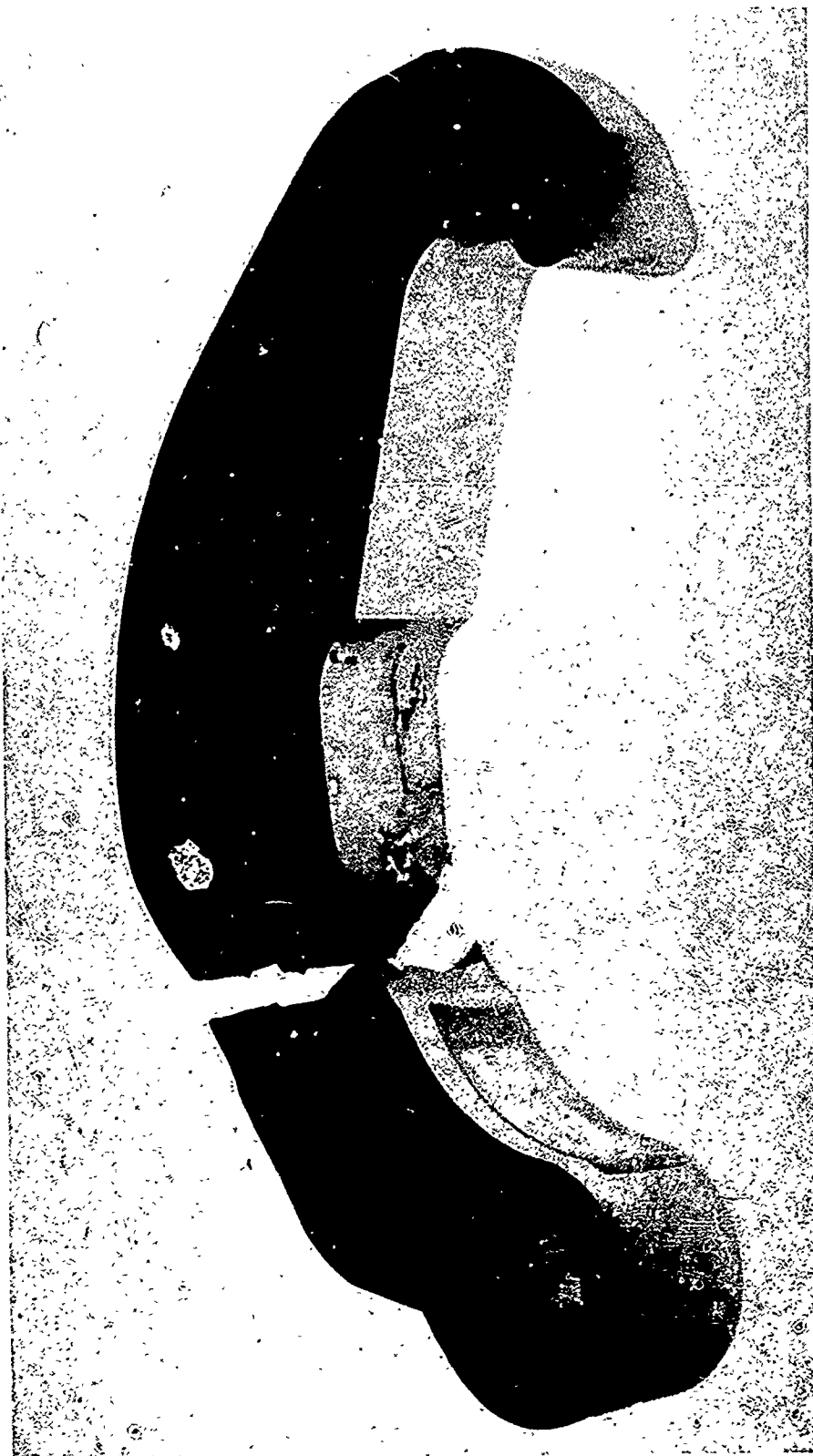
FIGURE 168   4330V MODIFIED STEEL CARGO LATCH HOOK AFTER TEST (LARGE SIZE)
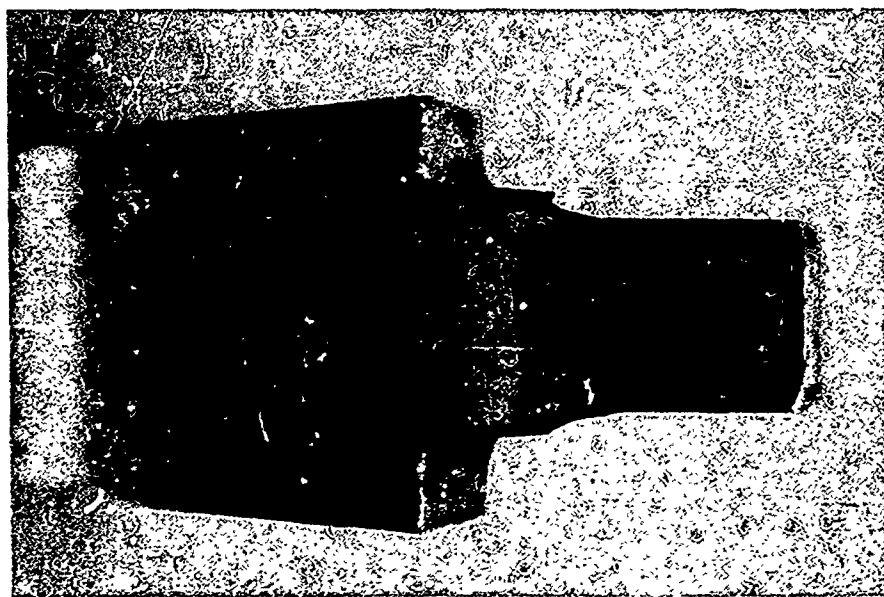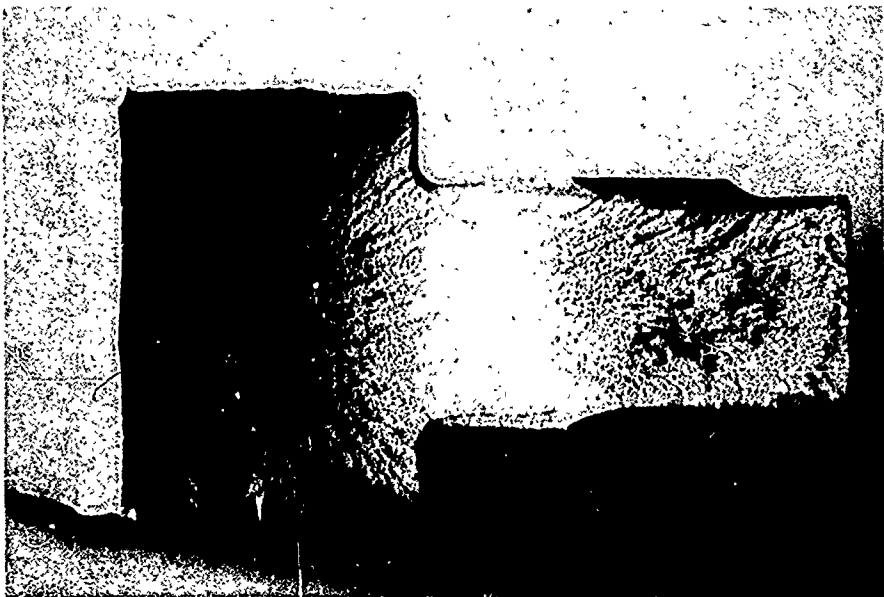
FIGURE 169 FRACTURE SURFACES OF FAILED 4330V MODIFIED STEEL CARGO
LATCH HOOK (LARGE SIZE)

246
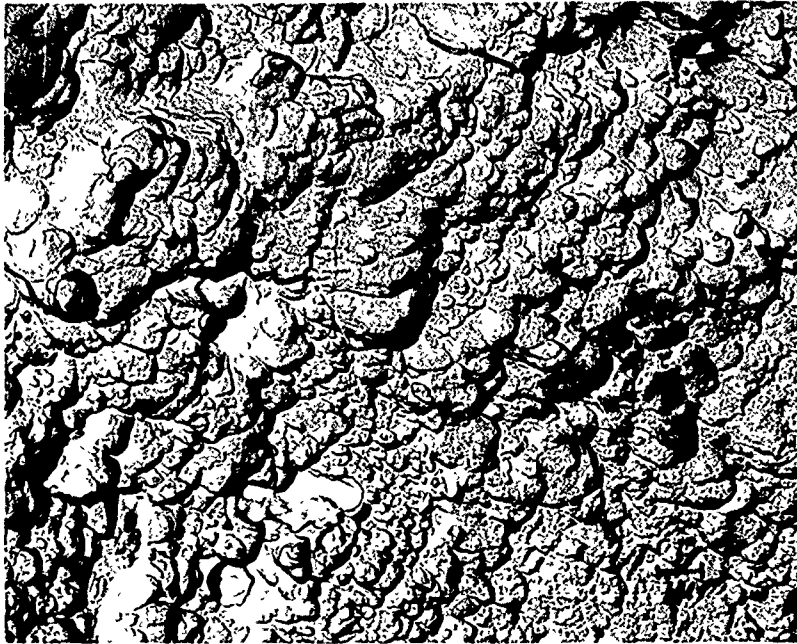
FIGURE 170 ELECTRON FRACTOGRAPH SHOWING DIMPLE RUPTURE 4330V
MODIFIED STEEL CARGO LATCH HOOK (MEDIUM SIZE) 6000X

FIGURE 171 ELECTRON FRACTOGRAPH SHOWING CLEAVAGE 4330V MODIFIED
STEEL CARGO LATCH HOOK (MEDIUM SIZE) 6000X

where A is the relative area of each hook determined by assuming

$$A = \frac{P_{actual}}{220,000 \text{ PSI}} \quad \text{or} \quad \frac{\text{load}}{\sigma_{tu}} \tag{52}$$

Hence, for each hook we find:

Small hook	$A = 0.150 \text{ in}^2$
Medium hook	$A = 0.259 \text{ in}^2$
Large hook	$A = 0.363 \text{ in}^2$

We further assume a value of $K_{Ic} = 49 \text{ KSI (in)}^{1/2}$. Hence, the predicted failure loads are as follows:

Small hook:

$$P = \frac{(49) \quad (.150)}{\sqrt{1.2 \, \pi \, \frac{0.02}{0.88}}} = 26,000 \text{ pounds}$$

Medium hook:

$$P = 43,400 \text{ pounds}$$

Large hook:

$$P = 60,700 \text{ pounds}$$

Comparing these predicted failure loads with the actual failure loads, the percent errors are as follows:

Small hook:	21%
Medium hook:	7%
Large hook:	24%

Each of these is less than the actual failure load. If a value of $K_{Ic} = 61 \text{ KSI (in)}^{1/2}$ were used, the failure loads would be:

Small hook:	31,200 pounds
Medium hook:	54,000 pounds
Large hook:	75,500 pounds

Thus, it may be assumed that each hook was made of material whose K_{Ic} value did not agree with the estimated lower bound for the K_{Ic}.

Since all of the hooks failed with some prior yielding, it appears that the FM approach will not apply to this case.

The Center Wing Failsafe Panel was a tension panel made from integrally stiffened 7075-T6511 Aluminum. The panel contained a center crack, 2c = 22.5 inches. The panel thickness

was 0.226 inch and the width was 67 inches. Testing was accomplished using the 1,200,000-pound-capacity Baldwin universal testing machine. Load was applied at a slow, even rate until failure occurred at 776,000 pounds. Pop-in occurred at 651,000 pounds.

A fracture mechanics estimate of the failure load is determined by considering a center-notched and fatigue-precracked specimen. For the analysis, it is assumed that no load is taken by the risers, since the panel is loaded directly across the skin.

Hence, we use

$$P = \frac{K_{Ic} \, W \, B}{\sqrt{\pi \, c}} \tag{53}$$

where

W = 67 inches
B = 0.226 inch
c = 11.25 inch

We assume $K_{Ic} = 30 \, KSI \, (in)^{1/2}$. Therefore, P = 700,000 pounds.

Comparing the actual failure load to the predicted load, we see that an error of only eleven percent was made. This is considered excellent agreement.

SECTION VII

SUMMARY

Discussion

The use of the concepts of linear elastic fracture mechanics-nondestructive testing in the development of an aerospace design criterion has been shown to be of merit. However, it is not yet possible to replace the present methodology of design by a Fracture Mechanics/Non-Destructive Testing design methodology. There are several reasons for this: (1) most of the materials now used in aircraft design are of sufficient ductility to render the fracture mechanics analysis invalid or inaccurate; (2) there is only limited use of thick sections in aircraft structures, and hence, the plane strain stress intensity factor has only limited usefulness; (3) the limitations of the present NDT techniques in accurately determining flaw geometry lower the overall reliability of the design analysis; and (4) the analyses relating the flaw geometry, applied stress, and stress intensity factor, K_{Ic}, are limited to relatively simple specimen configurations.

This does not mean to imply that an FM/NDT design criterion cannot find widespread applicability in aerospace design. On the contrary, the results presented in this report very encouragingly show that an FM/NDT design criterion can, in many instances, predict the failure load of a simple structure more accurately than does the present methodology. The concepts of FM/NDT could be used in a wide range of present applications such as fatigue, environmental failure, random fatigue loading and establishing the time between inspections, and the analysis of flaws found during inspection.

It is within the scope of this report to mention only briefly the methods by which these problems may be attacked by fracture mechanics. These problems do not lend themselves to simple solutions even with the present design methods, and they must be approached on an individual basis.

Many areas of development are required prior to the fruitful use of an FM/NDT design criterion for aerospace structures. Due to the requirements of DOD, plane-strain fracture analysis has been accelerated and proven successful in the missile technology fields. In the design of aircraft, handbook values of tensile ultimate stress and tensile yield stress would still be required in a fracture mechanics design.

It is to the next generation of aircraft and aerospace vehicles that this design procedure is projected. It is toward materials that are extremely light in weight and high in strength, with little ductility, that fracture mechanics and nondestructive testing can prove more accurate in predicting the true failure loads. The present trends in design are to use materials to the limit of their capabilities. Fracture mechanics can determine when these capabilities have been reached.

A primary factor advocating the need for FM/NDT design is the rising costs of materials. When a part was simple to make, and the material relatively inexpensive, a small flaw would result in the scrapping of the part. However, with rising material costs and the use of more exotic materials and materials that are difficult to fabricate, it becomes a difficult decision to throw out a complex part because it contains a small flaw. If it can be shown that the flaw will not grow sufficiently to cause failure, there is no reason to discard the part. This would save a great deal of money in repair and maintenance and operating costs.

This places the material producers in a difficult position. The material they produce must be of sufficiently high quality to pass increasingly more difficult acceptance standards. That the material producer has risen to the challenge is evidenced in the results of the literature survey conducted on the K_{Ic} values for 7075 Aluminum. The values that they have published are accurate estimates of the capabilities of their materials and do not show very large deviations. Perhaps the material producers are anticipating the eventual incorporation of fracture mechanics into specifications and are establishing a firm background in this area.

It is unfortunate that the scatter in K_{Ic} values is larger than the scatter in σ_{tu} and σ_{ty}. This makes it difficult to design using a statistical value of K_{Ic} that 99% of the material would be expected to exceed. This difficulty can possibly be overcome by standardizing on one type of K_{Ic} specimen and developing a large backlog of test data. Which particular specimen design or how to conduct the tests are matters open for discussion.

The inherent inaccuracies in NDT are not as formidable as they appear to be. In many cases, the NDT reliability index is only slightly below the values that would be needed to use them for reliable design. However, NDT needs to be improved, particularly in detecting and measuring small flaws. This present program has been limited to surface fatigue cracks. Other defect types should also be investigated. The accuracies of present NDT methods are extremely high in locating the flaw, but sensitivity and the accuracy of flaw-size measurement can be improved significantly. The most promising of the NDT methods appears to be ultrasonics, but penetrant and magnetic-particle methods as well as other electronic techniques should not be overlooked. These NDT techniques should move rapidly into the production lines, since little difference was found between the present laboratory NDT and production NDT sensitivities.

The theoretical difficulties in developing solutions for the K_{Ic} of complex shapes can be overcome by combining fracture mechanics with the theory of stress concentration factors.

It has been demonstrated here that combining the K_{Ic} and the stress distribution in the vicinity of a circular cutout yields a valid solution for predicting the failure load of a cylinder containing both a hole and a crack. This solution is more accurate than either fracture mechanics or stress concentration theory alone. It provides a strong bridge between the present stress analysis and the fracture mechanics analysis.

The test data obtained during the program would lend itself to many analyses in addition to those shown herein. Therefore, summaries of the 7075-T6511 Aluminum and 4330V Modified Steel test data are given in Tables XXIII and XXIV, respectively.

Conclusions

o The reliability of the NDT needs to be improved. No reliability index over 0.90 was obtained.

o For 7075-T6511 Aluminum cylinders containing surface fatigue cracks, the order of preference for the NDT would be:

251

crack length less than 0.20 inch –

1. ultrasonics
2. penetrant
3. X-ray

crack length 0.20 to 0.50 inch –

1. penetrant
2. ultrasonics
3. X-ray

o For 4330V Modified steel cylinders containing surface fatigue cracks, the order of preference for the NDT would be:

crack length less than 0.15 inch

1. ultrasonics
2. magnetic-particle
3. penetrant
4. X-ray

crack length 0.15 to 0.50 inch

1. magnetic-particle
2. ultrasonics
3. penetrant
4. X-ray

o All NDT methods obtained very high accuracies in location of the crack. (X-ray inspection was not included due to the low sensitivity of this technique.) Low relia- bility indices are due to two factors; namely, (1) the inability of the method to measure the true crack length accurately for small cracks and, (2) the poor sensitivity of the methods in detecting cracks smaller than 0.20 inch.

o The X-ray method used here was unable to detect small, tight surface fatigue cracks in aluminum and steel cylinders.

o The sensitivity of the ultrasonics method to detect small cracks appears to be superior to all other methods examined.

o Magnetic-particle inspection is superior to penetrant inspection for the 4330V Modified steel cylinders.

o Production inspection methods are as sensitive to cracks of length from 0.20 to 0.50 inch as laboratory inspection methods. Laboratory methods appear to be more sensitive for small crack lengths.

o Eddy-current inspection is less sensitive than ultrasonics for crack lengths smaller than 0.20 inch, but equal in sensitivity for cracks from 0.20 to 0.50 inch.

o The available test information of K_{Ic} for most materials is, at best, marginal for use in the design of critical components and the scatter in reported values of K_{Ic} is too large, even at room temperature, so that the 90% confidence values of K_{Ic} based on the standard deviations would be so low as to render the design impractical.

o The uncorrected plane-strain stress intensity factors obtained from tests conducted on the 7075-T6511 Aluminum cylinders show the K_{IX} to vary as follows:

$$K_{IX} = 17.0 + 140 \, c \qquad a, \, Q \text{ constant, } 2c < 0.275 \text{ inch}$$

$$K_{IX} = 40 \qquad a, \, Q \text{ constant, } 2c > 0.275 \text{ inch}$$

$$K_{IX} = 17.0 + 180 \, a \qquad 2c, \, Q \text{ constant, } a < 0.125 \text{ inch}$$

$$K_{IX} = 40 \qquad 2c, \, Q \text{ constant, } a > 0.125 \text{ inch}$$

$$K_{IX} = 17.0 + \frac{a}{Q} \qquad \frac{a}{Q} < 0.625 \text{ inch}$$

$$K_{IX} = 40 \qquad \frac{a}{Q} > 0.625 \text{ inch}$$

o The uncorrected plane-strain/stress intensity factors obtained from tests conducted on the 4330V Modified steel cylinders heat-treated to 220-240 KSI show the K_{IX} to vary as follows:

$$K_{IX} = 64 + 145 \, c \qquad a, \, Q \text{ constant}$$

$$K_{IX} = 64 + 220 \, a \qquad c, \, Q \text{ constant}$$

$$K_{IX} = 64 + 400 \, \frac{a}{Q}$$

o The fracture mechanics failure load predictions using the actual crack length, 2c, and actual crack depth, a, are all within ± 10% for both the aluminum and steel cylinders. This is in excellent agreement with the actual failure loads for these specimens.

o The fracture mechanics-nondestructive testing failure-load predictions are very dependent on the choice of K_{Ic} or K_{IX}. For the values of K_{IX} chosen, almost all FM/NDT predictions agreed with the failure load to within ±10%. The one exception was FM/ultrasonics for the 4330V Modified steel cylinders.

o Except for the small crack lengths, the FM/NDT failure-load predictions for the aluminum cylinders were better than those predictions using standard design procedures.

o The failure-load predictions using FM/NDT for the 4330V Modified steel were all found to be more accurate than standard design predictions, with the exception of FM/ultrasonics.

o In some instances the FM/NDT predictions are better than the failure load predictions made using fracture mechanics and actual crack sizes. This appears to occur due to the overestimation of the crack length, 2c, by some of the NDT methods.

o A correction factor, when applied to the K_{IX} to account for plane stress to plane strain variations at the tip of the crack whose depth is greater than 1/2 the thickness, reduced the K_{IX} obtained from deep cracks to K_{Ic}.

253

o The failure-load predictions for test cylinders containing both a 1-inch-diameter hole and a small crack near the hole are in excellent agreement with the actual failure load. The average error for the 7075-T6511 Aluminum specimens was 9% and was 5.2% for the 4330V Modified steel.

o A fracture mechanics/NDT analysis on the C-5A shear panels, made assuming maximum undetectable flaw sizes, yielded predicted loads that were in error by 10%, assuming penetrant maximum flaw size, 35% assuming X-ray maximum flaw size, and 59% assuming ultrasonic maximum flaw size. However, a fracture mechanics analysis appears not applicable because of the yielding encountered.

o Analysis of the small, medium, and large hooks by fracture mechanics yielded predicted loads that were 21%, 7%, and 24% in error, respectively. Again a maximum undetectable flaw size was chosen, but apparently due to prior yielding the fracture mechanics analysis would not be applicable.

o The center wing failsafe panel failed 11% above the predicted failure load made with a fracture mechanics analysis. Here a crack was present, fracture mechanics does apply, and the agreement is considered good.

Recommendations

In conclusion, the following recommendations are offered:

o A research effort should be directed toward determining the sensitivity, accuracy, and reliability of all present NDT methods to detect, locate, and measure all types of flaws in common aerospace materials. This should be conducted as a joint program with the Department of Defense, universities, and aerospace industry organizations.

o A standardized plane-strain specimen should be used in a "round robin" program to determine both a 99% confidence limit for K_{Ic} and a mean value of K_{Ic} for common aerospace materials.

o A program should be initiated to develop some standard method for determining plane stress, $K_c(B)$, at the particular thicknesses used by aerospace companies.

o The present FM/NDT design analysis should be extended to fluctuating loads and environmental loading design applications.

TABLE XXIII
SUMMARY OF TEST DATA FOR 7075-T6511 AL

SPEC	NUMBER OF CYCLES IN FATIGUE	ACTUAL CRACK GEOMETRY FROM FRACTURE SURFACE						SPECIMENS WITH HOLES, DISTANCE FROM HOLE		PENETRANT					MAGNETIC PARTICLE							ULTRASONICS			
		LENGTH 2c	DEPTH a	l_1	l_2	θ_1	θ_2	x_1	x_2	LENGTH 2c	l_1	l_2	θ_1	θ_2	LENGTH 2c	DEPTH a	l_1	l_2	θ_1	θ_2		LENGTH 2c	DEPTH a	l_1	l_2
A1	25,000	-	-	-	-	-	-	-	-	0	18.	0	5°	0								0	0	18 04	-
A2	46,000	.0810	.06	16.19	16.18	173°	176°	-	-	0	-	-	-	-								0	0	16.11	-
A3	22,190	.1884	.08	-	-	30°	37°	-	-	0	0	0	0	0								0	0	0	0
A4	30,000	7.3815	.26	16.83	16.97	160°	238°	-	-	6.545	16.7	15.6	208°	360°								2.985	-	16.69	16.69
A5	10,000	-	-	-	-	-	-	-	-	0	14.2	0	57°	0								0	0	0	0
A6	40,217	.1052	.05	-	-	172°	176°	-	-	0	0	0	0	0								.0785	.009	16.5	-
A7	23,700	.3889	.16	15.78	15.91	10°	24°	-	-	.3142	15.8	15.9	8°	20°								1832	11	15.85	15.9
A8	21,500	.0916	.05	-	-	74°	70.5°	-	-	0	0	0	0	0								.0785	-	15.13	-
A9	20,000	.0524	.03	-	-	101.5°	103.5°	-	-	0	0	0	0	0								-	.005	16.98	-
A10	5,000	N.C.	-	-	-	-	-	-	-	0	0	0	0	0								0	0	0	0
A11	15,000	N.C.	-	-	-	-	-	-	-	0	0	0	0	0								0	0	0	c
A12	22,500	.1309	.08	14.83	14.83	77°	82°	-	-	0	0	0	0	0								.1309	005	14.33	-
A13	22,200	-	-	-	-	-	-	-	-	-	-	-	-	-								-	-	-	-
A14	22,500	.0524	.02	13.18	13.18	265°	267°	-	-	0	0	0	0	0								0	0	0	0
A15	23,000	.2895	.16	-	-	217°	228°	-	-	2880	15.1	15.1	215	226								1309	.11	15.12	15.14
A16	23,000	-	-	-	-	-	-	-	-	0	0	0	0	0								0	0	0	0
A17	33,381	-	-	-	-	-	-	-	-	-	-	-	-	-								-	-	-	-
A18	20,000	.1052	.07	15.22	15.23	201°	205°	-	-	.1047	15.1	15.1	196°	200°								0	0	0	0
A19	10,800	-	-	-	-	-	-	-	-	-	-	-	-	-								-	-	-	-
A20	14,910	.1313	.05	18.69	18.70	76°	81°	-	-	0	0	0	0	0								0	0	0	0
A21	10,000	.0810	.05	15.85	15.83	104°	107°	-	-	0	0	0	0	0								0	0	0	0
A22	22,008	.2399	.14	16.96	16.91	108°	117°	-	-	.2710	16.98	17.05	104°	114°								.1621	07	17.03	17.04
A23	38,500	.2620	.14	19.74	19.75	200°	210°	-	-	.2618	16.10	16.00	198°	208°								.2880	.09	16.12	-
A24	18,500	.1857	.09	15.24	15.21	25°	32°	-	-	.1571	15.3	15.3	23°	29°								.2094	.05	15.28	-
A25	25,500	.5761	.20	17.32	17.31	241°	263°	-	-	.5498	16.3	16.3	245°	266°								3142	.15	16.56	-
A26	21,500	.0698	.05	16.80	16.80	288°	292°	-	-	0	0	0	0	0								.0524	.005	16.81	-
A27	61,200	N.C.	0	0	0	0	0	-	-	0	0	0	0	0								0	0	0	0
A28	27,900	.3440	.18	16.48	16.43	47°	60°	-	-	.3665	16.4	16.5	43°	57°								3665	.145	16.45	-
A29	30,900	.2358	.13	18.17	18.16	46°	55°	-	-	0	0	0	0	0								.2618	.017	18.23	-
A30	38,000	-	-	-	-	-	-	-	-	-	-	-	-	-								-	-	-	-
A31	30,000	.0785	.04	19.28	19.28	359°	2°	-	-	G	0	0	0	0								0	0	0	0
A32	24,350	.1584	.09	14.14	14.16	228°	234°	-	-	0	0	0	0	0								.1309	.10	14.17	-
A33	16,800	.0533	.04	15.87	15.88	262°	264°	-	-	0	0	0	0	0								0	0	0	0
A34	30,000	.1052	.04	14.70	14.69	257°	261°	-	-	0	0	0	0	0								.0785	.07	14.81	-
A35	27,800	.0533	.04	16.58	16.59	256°	258°	-	-	0	0	0	0	0								0	0	0	0
A36	19,000	.1313	.07	15.31	15.31	261°	266°	-	-	0	0	0	0	0								.1571	.10	15.33	15.37
A37	29,800	N.C.	0	0	0	0	0	-	-	0	0	0	0	0								0	0	0	0
A38	5,400	.1313	.07	16.08	16.07	275°	280°	-	-	0	0	0	0	0								0	0	0	0
A39	5,200	.1584	.07	15.92	15.94	203°	197°	-	-	0	0	0	0	0								0	0	0	0
A40	0	-	-	-	-	-	-	-	-	0	0	0	0	0								0	0	0	0
A41	7,050	.1857	.05	15.97	15.94	270°	277°	-	-	0	0	0	0	0								0	0	0	0
A42	6,750	.1900	.09	15.92	15.87	275°	282°	-	-	0	0	0	0	0								P.M.	.005	15.90	278
A43	5,980	1304	.07	15.92	15.72	266°	271°	-	-	0	15.9	0	266°	0								P.M.	.008	15.95	267
A44	4,700	.1343	.05	16.03	16.00	286°	291°	-	-	0	0	0	0	0								P.M.	.005	16.03	287
A45	4,400	.1324	.07	16.06	16.04	264.5°	269.5°	-	-	0	0	0	0	0								P.M.	.005	16.05	265
A46	1,800	.0913	.03	15.89	15.90	268°	271°	-	-	0	0	0	0	0								P.M.	.005	15 95	268
A47	4,560	.1052	.07	15.91	15.92	265°	769°	.14	.25	0	15.9	0	266°	0								P.M.	.005	15.93	264
A48	5,050	.1324	.08	16.01	16.03	288°	273°	-	-	0	0	0	0	0								P.M.	.005	16.03	290
A49	3,150	.1324	.04	15.95	15.97	293°	298°	.15	.28	0	0	0	0	0								P.M.	.005	15.96	292
A50	4,260	.1089	.05	16.02	15.99	258°	262°	-	-	0	0	0	0	0								P.M.	.006	16.03	259
A51	5,170	N.C.	0	0	0	0	0	0	0	-	-	-	-	-								P.M.	-	16.00	252
A52	6,480	.1052	.04	15.94	15.93	272°	276°	.17	.27	0	0	0	0	0								P.M.	.005	15.93	271
A53	2,850	.1054	.06	15.90	15.92	266°	270°	.13	.23	0	0	0	0	0								P.M.	-	15.91	268
A54	4,080	.1324	.07	15.93	15.91	271°	276°	.18	.31	0	0	0	0	0								P.M.	-	15.96	270
A55	3,880	.0810	.04	15.98	16.00	249°	252°	.12	.22	0	0	0	0	0								P.M.	-	16.03	253

NOTES: - = NO INFORMATION AVAILABLE   N.C. = NO CRACK   N.C.F. = NO CRACK FOUND   N.A. = NOT APPLICABLE   C.F. = CRACK FOUND   P.M. = PUNCH MARK INDISTINGUISHABLE FROM CRACK ON SPECIMEN

A.

TABLE XXIII
TEST DATA FOR 7075-T6511 ALUMINUM CYLINDERS

θ₁	θ₂	2c (LENGTH)	a (DEPTH)	l₁	l₂	θ₁	θ₂	X-RAY	PENETRANT	MAG PART	EDDY C	ACTUAL FAILURE LOAD KIPS	YIELD LOAD KIPS	ACTUAL FAILURE STRESS	K_IC(B)	90% CL K_IC	HOLE ANALYSIS	PENET K_IC	PENET K_C(B)	MAG PART K_IC	MAG PART K_C(B)	ULTRA K_IC	ULTRA K_C(B)	X-RAY K_IC	X-RAY K_C-B
		C	0.	18.04	-	6°	-	N.C.F.	N.C.F.		-	188.0	177.0	-	-	-	-	-	-			-	-	-	-
		0	0	16.11	-	181°	-	N.C.F.	N.C.F.		-	185.0	180.0	82.1	224.4	187.7	-	-	-			-	-	-	-
		0	0	0	0	0	0	N.C.F.	N.C.F.		C.F.	178.5	176.0	79.1	147.2	163.9	-	-	-			-	-	-	-
		2.935	-	16.69	16.69	100°	214°	C.F.	C.F.		C.F.	26.5	-	11.7	23.5	33.8	-	-	-			-	-	-	-
		0	0	0	0	0	0	N.C.F.	N.C.F.			189.0	181.0												
		.0785	.009	16.5	-	172°	174°	N.C.F.	N.C.F.		C.F.	182.5	173.0	82.1	196.9	177.0	-	279.0	212.8			228.0	189.2	-	-
		.1832	.11	15.85	15.9	105°	175°	C.F.	N.C.F.		C.F.	162.5	-	71.6	102.4	147.4	-	114.0	164.0			149.2	164.2	-	-
		.0785	-	15.13	-	65°	68°	N.C.F.	N.C.F.		C.F.	183.0	175.0	80.8	211.0	182.3	-		164.0			228.0	189.2	-	-
		-	.005	16.98	-	102°	-	N.C.F.	N.C.F.		N.C.F.	192.0	-	85.3	279.0	212.8	-	-	-			-	-	-	-
		0	0	0	0	0	0	N.C.F.	N.C.F.		N.C.F.	195.0	177.0	-	-	-									
		0	0	0	0	0	0	N.C.F.	N.C.F.			192.0	175.0	-	-	-									
		.1309	.005	14.33	-	78°	78°	N.C.F.	N.C.F.		N.C.F.	183.5	182.0	80.8	176.5	170.4		-	-			176.5	170.4	-	-
		-	-	-	-	-	-								-	-									
		0	0	0	0	0	0	N.C.F.	N.C.F.		N.C.F.	193.5	182.0	85.2	279.0	212.8	-	-	-			-	-	-	-
		.1309	.11	15.12	15.14	218°	223°	N.C.F.	N.C.F.		C.F.	165.0	-	73.3	118.7	163.2		119.0	163.2			176.5	170.4	-	-
		0	0	0	0	0	0	N.C.F.	N.C.F.		N.C.F.	194.5	182.0	-	-	-		-	-			-	-	-	-
		-	-	-	-	-	-	-	N.C.F.																
		0	0	0	0	0	0	N.C.F.	N.C.F.		C.F.	179.5	178.0	79.6	196.9	177.0	-	197.4	177.2			-	-	-	-
		-	-	-	-	-	-		N.C.F.																
		0	0	0	0	0	0	N.C.F.	N.C.F.		N.C.F.	195.5	179.0	85.5	176.3	170.4	-	-	-			-	-	-	-
		0	0	0	0	0	0	N.C.F.	N.C.F.		N.C.F.	197.5	182.0	88.0	224.4	187.7	-	-	-			-	-	-	-
		.1621	.07	17.03	17.04	105°	111°	N.C.F.	C.F.		-	177.4	-	80.1	130.4	162.6	-	122.7	162.9			158.6	165.9	-	-
		.2880	.09	16.12	-	197°	208°	N.C.F.	N.C.F.		C.F.	158.0	-	70.5	124.8	162.7		124.8	162.7			119.0	163.2	-	-
		.2094	.05	15.28	-	19°	27°	N.C.F.	N.C.F.		N.C.F.	170.0	168.0	76.1	148.2	164.1	-	161.2	166.5			139.6	163.1	-	-
		.3142	.15	16.36	-	245°	253°	C.F.	C.F.		C.F.	122.5	-	55.3	84.2	121.1	-	86.1				98.7	142.0	-	-
		.0524	.005	16.81	-	286°	288°	N.C.F.	N.C.F.		N.C.F.	183.5	180.0	81.7	241.8	195.2	-		124.0			279.0	212.8	-	-
		0	0	0	0	0	0	N.C.F.	N.C.F.		N.C.F.	192.5	176.0	-	-	-									
		.3665	.145	16.45	-	44°	54°	N.C.F.	C.F.		C.F.	159.5	-	71.2	108.9	156.7	-	105.5	151.8			105.5	151.8	-	-
		.2618	.014	18.23	-	43°	53°	N.C.F.	C.F.		C.F.	171.0	-	76.4	131.5	162.6		-	-			124.9	162.7	-	-
		-	-	-	-	-	-	-	-		-	-	-	-	-	-									
		0	0	0	0	0	0	N.C.F.	N.C.F.		N.C.F.	186.0	179.0	82.7	228.0	189.2	-	-	-			-	-	-	-
		.1309	.10	14.17	-	226°	231°	N.C.F.	N.C.F.		C.F.	182.0	-	80.7	160.5	166.3		-	-			176.5	170.4	-	-
		0	0	0	0	0	0	N.C.F.	N.C.F.		N.C.F.	190.0	182.0	85.2	276.7	211.6		-	-			-	-	-	-
		.0785	.07	14.81	-	253°	256°	N.C.F.	N.C.F.		N.C.F.	186.5	171.0	83.2	196.9	177.0		-	-			228.0	189.2	-	-
		0	0	0	0	0	0	N.C.F.	N.C.F.		C.F.	187.5	176.0	84.3	276.7	211.6						-	-	-	-
		.1571	.10	15.33	15.37	258°	264°	N.C.F.	N.C.F.		-	181.5	181.0	81.9	176.3	170.4						161.2	166.5	-	-
		0	0	0	0	0	0	N.C.F.	N.C.F.		-	195.5	182.0	-	-	-						-	-	-	-
		0	0	0	0	0	0	N.C.F.	N.C.F.		N.C.F.	181.5	179.0	80.8	176.3	170.4	-	-	-			-	-	-	-
		0	0	0	0	0	0	N.C.F.	N.C.F.		N.C.F.	174.0	170.0	78.5	160.5	166.3	-	-	-			-	-	-	-
		0	0	0	0	0	0	N.C.F.	N.C.F.		N.C.F.	186.5	178.0	-	-	-		-	-			-	-	-	-
		0	0	0	0	0	0	N.C.F.	N.C.F.		C.F.	185.0	182.0	82.4	148.2	164.1	-	-	-			-	-	-	-
		P.M.	.005	15.90	-	278°	-	N.C.F.	N.C.F.		N.C.F.	179.0	-	79.4	146.5	163.8	-	-	-			-	-	-	-
		P.M.	.008	15.95	-	267°	-	N.C.F.	N.C.F.		N.C.F.	186.5	182.0	81.5	176.5	170.4	-	-	-			-	-	-	-
		P.M.	.005	16.03	-	287°	-	N.C.F.	N.C.F.		N.C.F.	184.0	177.0	80.9	174.3	169.8	-	-	-			-	-	-	-
		P.M.	.005	16.05	-	265°	-	N.C.F.	N.C.F.		N.C.F.	184.0	180.0	80.9	175.5	170.2	-	-	-			-	-	-	-
		P.M.	.005	15.95	-	268°	-	N.C.F.	N.C.F.		N.C.F.	190.5	179.0	84.3	211.4	182.5	-	-	-			-	-	-	-
		P.M.	.005	15.93	-	264°	-	N.C.F.	N.C.F.		N.C.F.	115.0	-	51.9	196.9	177.0	53.7	-	-			-	-	-	-
		P.M.	.005	16.03	-	27°	-	N.C.F.	N.C.F.		N.C.F.	183.0	180.0	81.6	175.5	170.2	-	-	-			-	-	-	-
		P.M.	.006	15.96	-	292°	-	N.C.F.	N.C.F.		N.C.F.	124.5	-	56.3	175.5	170.2	50.7	-	-			-	-	-	-
		P.M.	.006	16.03	-	259°	-	N.C.F.	N.C.F.		N.C.F.	185.5	-	81.8	193.6	175.9	-	-	-			-	-	-	-
		P.M.	-	16.00	-	252°	-	N.C.F.	N.C.F.		N.C.F.	156.0	-	-	-	-	NC	-	-			-	-	-	-
		P.M.	.005	15.93	-	271°	-	N.C.F.	N.C.F.		N.C.F.	136.0	-	60.8	195.9	177.0	52.1	-	-			-	-	-	-
		P.M.	-	15.91	-	268°	-	N.C.F.	N.C.F.		N.C.F.	117.0	-	52.1	196.7	177.0	56.7	-	-			-	-	-	-
		P.M.	-	15.96	-	270°	-	N.C.F.	N.C.F.		N.C.F.	116.0	-	52.0	175.5	170.2	51.2	-	-			-	-	-	-
		P.M.	-	16.03	-	253°	-	N.C.F.	N.C.F.		N.C.F.	115.5	-	52.2	224.4	187.7	55.8	-	-			-	-	-	-

BENCH MARK INDISTINGUISHABLE FROM CRACK ON SPECIMEN

B.

TABLE XXIII (CONTINUE

SPEC#	NUMBER OF CYCLES IN FATIGUE	ACTUAL CRACK GEOMETRY FROM FRACTURE SURFACE LENGTH 2c	DEPTH a	l₁	l₂	θ₁	θ₂	HOLES DIST x₁	x₂	PENETRANT LENGTH 2c	l₁	l₂	θ₁	θ₂	MAG PART 2c	a	l₁	l₂	θ₁	θ₂	ULTRASONICS LENGTH 2c	DEPTH a	l₁	l₂
A56	4,170	.1584	.07	15.99	15.97	259°	265°	.17	.22	0	0	0	0	0							P.M.	.005	16.02	-
A57	3,340	.1584	.07	16.00	16.02	271°	277°	-	-	0	0	0	0	0							P.M.	-	16.02	-
A58	4,900	.1369	.09	16.02	16.06	261°	266°	-	-	0	0	0	0	0							0	0	16.10	-
A59	4,280	.1621	.08	15.99	15.95	276°	282°	.12	.28	0	0	0	0	0							.0785	.008	15.96	18.01
A60	21,000	.1833	.09	17.77	17.77	232°	239°	-	-	0	0	0	0	0							.1047	.008	17.81	17.84
A61	0	-	-	-	-	-	-	-	-	0	0	0	0	0							P.M.	.008	16.00	
A62	0	-	-	-	-	-	-	-	-	0	0	0	0	0							0	0	0	0
A63	0	-	-	-	-	-	-	-	-	0	0	0	0	0							0	0	0	0
A64	7,100	.1584	.04	16.07	16.05	295°	301°	-	-	0	0	0	0	0							0	0	16.04	-
A65	5,200	.1574	.05	15.89	15.90	230°	236°	-	-	0	0	0	0	0							.0785	.005	15.98	15.98
A66	7,500	.1584	.08	15.06	15.07	116°	122°	-	-	0	0	0	0	0							0	0	15.98	-
A67	7,500	.3269	.18	15.99	15.90	266°	278°	-	-	.3439	15.98	15.96	80°	85°							.1621	.172	15.98	16.02
A68	8,000	.1844	.09	15.90	15.92	83°	90°	-	-	.1309	0	0	0	0							.1071	.013	15.95	15.98
A69	7,500	.4232	.20	16.06	16.12	223°	235°	-	-	.5010	16.00	16.06	219°	230°							.3455	.192	16.00	16.06
A70	5,500	.3144	.14	16.05	16.06	359°	11°	.38	.50	.2132	16.04	16.08	359°	7°							.2738	.10	16.02	16.10
A71	7,500	.4610	.20	15.95	15.83	42°	59°	-	-	.4200	16.00	15.97	38°	54°							.3142	15	16.00	16.00
A72	8,100	.3475	.19	15.99	16.06	345°	358°	-	-	.4247	16.07	16.00	355°	11°							.4008	.132	16.02	16.10
A73	6,400	.2422	.12	15.91	15.93	272°	281°	-	-	.2390	15.94	15.98	270°	279°							2738	.08	15.92	16.00
A74	5,500	.2665	.13	16.05	16.00	169°	179°	-	-	.1574	16.01	16.02	168°	174°							.2242	.123	15.97	16.05
A75	8,700	.1578	.07	16.02	16.03	91°	97°	-	-	0	0	0	0	0							.1047	.006	16.02	16.02
A76	6,700	.2479	.12	16.06	15.98	336°	345°	-	-	.104	15.97	15.97	335°	339°							.1369	.08	15.97	16.01
A77	9,200	.42191	.18	16.06	16.01	190°	206°	-	-	.4200	16.00	16.04	186°	202°							.2356	.11	16.02	16.02
A78	8,500	.4284	.17	16.17	16.08	91°	107°	-	-	.3731	16.11	16.18	88°	102°							.3403	.145	16.10	16.10
A79	10,300	.4978	.20	15.85	15.87	179°	198°	-	-	.5251	15.96	15.92	175°	195°							.3455	.145	15.94	16.00
A80	7,900	.3621	.17	16.05	15.87	202°	214°	-	-	.2479	15.96	16.04	201°	210°							0	0	16.00	16.03
A81	8,500	.6042	.25	15.83	15.88	249°	272°	-	-	.5864	15.95	15.84	245°	267°							.4974	.18	15.99	15.99
A82	8,000	.4307	.19	15.91	16.01	84°	100°	-	-	.4008	16.04	15.96	80°	95°							.3927	.135	16.10	16.10
A83	7,400	.5768	.21	16.08	16.11	107°	129°	-	-	.5588	16.19	16.09	103°	124°							.2880	.156	15.97	15.97
A84	8,100	.3416	.15	15.87	15.90	111°	124°	-	-	.2096	15.99	16.00	112°	120°							.2618	.117	15.96	15.96
A85	8,000	.3297	.16	15.91	16.01	141°	153°	-	-	.2908	16.09	15.96	139°	150°							.2887	.122	16.00	16.02
A86	8,000	.1324	.09	16.04	16.02	133°	142°	.23	.41	.1574	16.07	16.06	129°	135°							.2432	.013	16.04	16.10
A87	8,000	.3577	.17	16.11	16.00	170°	183°	.23	.58	.3182	15.98	16.03	168°	180°							0	0	16.00	16.00
A88	8,300	.3142	.19	15.96	15.95	87°	99°	-		.3156	16.10	16.07	83°	95°							.3403	.145	16.06	16.06
A89	3,500	.0698	.03	18.05	18.05	179°	183°	-		P.M.	18.01	0	174°	0							0	0	18.08	-
A90	7,965	.1369	.04	15.95	15.99	177°	162°	-	-	P.M.	16.03	0	180°	0							0	0	16.02	-
A91	8,500	.2422	.13	16.01	15.95	36°	45°	.24	.48	.2895	16.01	16.04	29°	40°							.1401	.008	16.00	16.05
A92	8,400	.2895	.15	16.00	16.03	291°	302°	.24	.53	.2887	16.00	16.02	289°	300°							.1047	.006	16.00	16.00
A93	9,000	.2104	.10	15.96	15.98	110°	118°	.54	.75	.1857	16.00	15.97	105°	112°							0	.007	15.98	-
A94	2,500	.1574	.05	16.06	16.05	344°	350°	-	-	0	0	0	0	0							0	0	15.97	-
A95	2,000	.0913	.04	18.00	17.99	97°	100°	-	-	.1584	18.00	18.02	90°	96°							.0524	.005	17.97	17.97
A96	3,000	.1900	.09	18.06	18.11	47°	50°		-	.0810	18.08	18.10	48°	51°							0	0	18.10	-
A97	3,000	.1052	.03	18.01	18.00	300°	304°	-	-	P.M.	17.95	0	305°								0	0	0	0
A98	2,150	.1052	.04	18.03	18.06	289°	293°	-	-	.0791	18.06	18.05	289°	292°							0	0	18.05	-
A99	5,000	.1369	.06	17.45	17.99	273°	278°	-	-	P.M.	18.00	0	270°	0							0	0	18.00	-
A100	0	N.C.	0	0	0	0	0	-	-	0	0	0	0	0							0	0	0	0
A101	0	-	0	0	0	0	0	-	-	0	0	0	0	0							0	0	0	0
A102	7,300	.1844	.08	17.96	17.94	278°	285°	-	-	.2618	17.97	17.97	270°	280°							.1401	.008	17.95	18.00
A103	8,300	.1598	.07	17.88	17.91	322°	328°	-	-	.0840	17.94	17.91	327°	330°							0	0	17.95	-
A104	8,000	.1324	.04	17.92	17.94	351°	356°	-	-	P.M.	19.98	0	360°	0							0	0	0	0
A105	7,000	-	.05	18.08	18.02	225°	231°	-	-	.1857	18.07	18.10	220°	227°							0	0	18.10	-
A106	0	N.C.	0	0	0	0	0	-	-	0	0	0	0	0							0	0	0	0
A107	7,000	.3219	.14	15.93	16.00	358°	10°	-	-	.2648	17.94	17.98	349°	359°							.1571	.018	17.97	17.97
A108	8,050	.1962	.07	17.90	17.83	0°	7°	-	-	.1835	17.90	17.89	0°	7°							0	0	0	0
A109	8,200	.1598	.04	17.75	17.78	201°	207°	-	-	P.M.	17.85	0	215°	0							0	0	0	0
A110	8,300	.2116	.09	17.93	17.96	47°	55°	-	-	.1962	17.91	17.98	42°	50°							P.M.	.005	17.90	-

NOTES: - = NO INFORMATION AVAILABLE   N.C. = NO CRACK   N.C.F. = NO CRACK FOUND   N.A. = NOT APPLICABLE   C.F. = CRACK FOUND   P.M. = PUNCH MARK INDISTINGUISHABLE FROM CRACK ON SPECIMEN

A.

TABLE XXIII (CONTINUED)

θ1 (lab)	θ2	LENGTH 2a	DEPTH	l1	l2	θ1	θ2	X-RAY	PENETRANT	MAG PART	EDDY C	ACTUAL FAILURE LOAD KIPS	YIELD LOAD KIPS	ACTUAL FAILURE STRESS	Kc_iB	90% CL Kic	HOLE ANALYSIS	PENET Kic	PENET Kc/B	MAG PART Kic	MAG PART Kc/B	ULTRA Kic	ULTRA Kc/B	X-RAY Kic	X-RAY Kc/B
P.M.	.005	16.02	-	258°	-	N.C.F.	N.C.F.		N.C.F.	118.0	-	53.5	160.5	166.3	49.8	-	-			-	-	-	-		
P.M.	-	16.02	-	273°	-	N.C.F.	N.C.F.		-	173.0	172.0	77.7	160.5	166.3	-	-	-			-	-	-	-		
0	0	16.10	-	261°	-	N.C.F.	N.C.F.		-	183.5	-	80.5	172.6	169.3	-	-	-			-	-	-	-		
.0785	.008	15.96	18.01	272°	275°	N.C.F.	N.C.F.		-	108.5	-	49.0	155.6	165.9	50.8	-	-			228.0	189.2	-	-		
.1047	.008	17.81	17.84	230°	234°	N.C.F.	N.C.F.		-	174.5	170.0	78.1	149.2	164.2	-	-	-			197.4	177.2	-	-		
P.M.	.008	16.00	-	46°	-	N.C.F.	N.C.F.		-	191.0	179.0	-	-	-	-	-	-			-	-	-	-		
0	0	0	0	0	0	N.C.F.	N.C.F.		-	195.0	178.0	-	-	-	-	-	-			-	-	-	-		
0	0	0	0	0	0	N.C.F.	N.C.F.		-	194.5	-	-	-	-	-	-	-			-	-	-	-		
0	0	16.04	-	299°	-	N.C.F.	-		-	196.0	184.0	85.2	160.5	166.3	-	-	-			-	-	-	-		
.0785	.005	15.98	15.98	228°	231°	N.C.F.	-		-	183.0	-	81.7	161.0	166.5	-	-	-			223.0	189.2	-	-		
0	0	15.98	-	107°	-	N.C.F.	-		-	187.0	181.0	82.2	160.5	166.3	-	-	-			-	-	-	-		
.1621	.172	15.98	16.02	262°	276°	N.C.F.	-		-	157.0	-	70.3	111.7	160.8	-	103.9	156.7			158.6	165.9	-	-		
.1071	.013	15.95	15.98	81°	85°	N.C.F.	-		-	182.0	181.0	81.0	148.7	164.2	-	176.5	170.4			195.2	176.4	-	-		
.3455	.192	16.00	16.06	223°	236°	N.C.F.	-		-	146.5	-	65.2	98.2	141.3	-	90.2	130.0			108.7	156.4	-	-		
.2738	.10	16.02	16.10	359°	9°	N.C.F.	-		-	166.0	-	73.1	113.9	163.9	48.5	138.3	163.0			122.1	162.9	-	-		
.3142	.15	16.00	16.00	39°	51°	C.F.	-		-	144.0	-	63.0	94.1	135.4	-	98.6	141.8			114.0	164.0	102.3	147.2		
.4008	.132	16.02	16.10	354°	9°	N.C.F.	-		-	155.5	-	69.8	108.4	155.9	-	98.0	141.1			100.9	145.2	-	-		
.2738	.08	15.92	16.00	272°	282°	N.C.F.	-		-	177.0	-	78.7	129.8	162.6	-	130.7	162.6			122.1	162.9	-	-		
.2242	.123	15.97	16.05	168°	176°	N.C.F.	-		-	176.5	-	77.4	123.7	162.8	-	161.0	166.5			134.9	162.7	-	-		
.1047	.006	16.02	16.02	87°	91°	N.C.F.	-		-	184.0	180.0	82.1	161.0	166.5	-	-	-			197.4	177.2	-	-		
.1369	.08	15.97	16.01	335°	340°	N.C.F.	-		-	178.5	-	79.7	128.3	162.6	-	197.4	177.2			172.6	169.3	-	-		
.2356	.11	16.02	16.02	189°	198°	N.C.F.	-		-	151.5	-	67.2	98.3	141.5	-	98.5	141.7			131.6	162.6	-	-		
.3403	.145	16.10	16.10	90°	103°	N.C.F.	-		-	145.5	-	64.8	97.6	140.4	-	104.6	150.5			109.5	157.6	-	-		
.3455	.145	15.94	16.00	173°	192°	C.F.	-		-	139.5	-	61.7	90.5	130.3	-	88.1	126.9			108.7	156.4	99.8	143.6		
0	0	16.00	16.03	201°	212°	N.C.F.	-		-	163.0	-	71.8	106.1	152.8	-	120.3	162.6			118.7	163.2	-	-		
.4774	.18	15.99	15.99	247°	264°	N.C.F.	-		-	122.0	-	53.7	82.2	118.3	-	83.4	120.0			90.6	130.3	98.6	141.8		
.3727	.128	16.10	16.10	79°	94°	C.F.	-		-	147.0	-	65.2	97.3	140.1	-	100.9	145.2			101.9	146.7	114.6	163.5		
.2880	.156	15.97	15.97	109°	120°	C.F.	-		-	127.5	-	56.6	84.1	121.0	-	85.4	123.0			119.0	163.2	97.4	140.2		
.2618	.117	15.96	15.96	111°	121°	C.F.	-		-	160.0	-	71.3	109.3	157.3	-	139.5	163.1			124.8	162.7	-	-		
.2887	.122	16.00	16.02	138°	149°	N.C.F.	-		-	160.0	-	71.4	111.2	160.1	-	118.4	163.3			118.9	163.2	-	-		
.2432	.013	16.04	16.10	130°	139°	N.C.F.	-		-	114.0	-	51.3	175.5	170.2	49.5	161.0	166.5			129.5	162.6	-	135.5		
0	0	16.00	16.00	169°	178°	C.F.	-		-	89.5	-	40.4	106.8	153.7	44.5	113.2	163.0			131.5	162.6	-	-		
.3403	.145	16.06	16.06	82°	95°	N.C.F.	-		-	153.0	-	67.4	114.8	164.0	-	113.7	163.6			109.5	157.6	112.9	162.5		
0	0	18.08	-	175°	-	C.F.	N.C.F.		-	193.0	180.0	86.0	241.8	195.2	-	-	-			-	-	-	-		
0	0	16.02	-	173°	-	N.C.F.	C.F.		-	153.0	-	68.2	172.6	169.3	-	-	-			-	-	-	-		
.1401	.008	16.00	16.05	25°	40°	N.C.F.	C.F.		-	107.5	-	47.2	129.8	162.6	50.3	118.7	163.2			170.6	168.8	-	-		
.1047	.006	16.00	16.00	292°	296°	N.C.F.	C.F.		-	99.0	-	44.4	118.7	163.2	46.9	118.9	163.2			197.4	177.2	-	-		
0	.007	15.98	-	109°	-	N.C.F.	C.F.		-	130.1	-	58.4	139.3	163.0	45.7	148.2	164.1			-	-	-	-		
0	0	15.97	-	348°	-	N.C.F.	N.C.F.		-	192.5	180.0	86.8	161.0	166.5	-	-	-			-	-	-	-		
.0524	.005	17.97	17.97	93°	95°	N.C.F.	N.C.F.		-	186.0	173.0	83.9	211.4	182.5	-	160.5	166.3			279.0	212.8	-	-		
0	0	18.10	-	53°	-	N.C.F.	C.F.		-	191.5	180.0	85.8	146.5	163.8	-	71.0	102.1			-	-	-	-		
0	0	0	0	0	0	N.C.F.	N.C.F.		-	194.0	-	86.0	196.9	177.0	-	-	-			-	-	-	-		
0	0	18.05	-	289°	-	N.C.F.	N.C.F.		-	195.5	184.0	87.1	196.9	177.0	-	-	-			-	-	-	-		
0	0	18.00	-	273°	-	N.C.F.	C.F.		-	190.0	182.0	84.1	172.6	169.3	-	-	-			-	-	-	-		
0	0	0	0	0	0	N.C.F.	N.C.F.		-	197.0	-	-	-	-	-	-	-			-	-	-	-		
0	0	0	0	0	0	N.C.F.	C.F.		-	193.0	180.0	-	-	-	-	-	-			-	-	-	-		
.1401	.008	17.95	18.00	277°	282°	N.C.F.	C.F.		-	180.0	176.0	80.4	148.7	164.2	-	124.8	162.7			170.6	168.8	-	-		
0	0	17.95	-	331°	-	N.C.F.	C.F.		-	180.5	-	80.5	159.8	166.2	-	-	-			-	-	-	-		
0	0	0	0	0	0	N.C.F.	N.C.F.		-	189.5	176.0	83.9	175.5	170.2	-	-	-			-	-	-	-		
0	0	18.10	-	222°	-	N.C.F.	C.F.		-	184.5	176.5	-	-	-	-	-	-			-	-	-	-		
0	0	0	0	0	0	N.C.F.	N.C.F.		-	195.5	182.5	-	-	-	-	-	-			-	-	-	-		
.1571	.018	17.97	17.97	350°	356°	N.C.F.	C.F.		-	176.0	-	78.5	112.6	162.0	-	124.1	162.8			161.2	166.5	-	-		
0	0	0	0	0	0	N.C.F.	N.C.F.		-	183.0	176.0	81.7	144.2	163.5	-	-	-			-	-	-	-		
0	0	0	0	0	0	N.C.F.	C.F.		-	183.5	-	81.9	159.8	166.2	-	-	-			-	-	-	-		
P.M.	.005	17.90	-	46°	-	N.C.F.	C.F.		-	178.8	178.0	80.0	138.9	163.0	-	144.2	163.5			-	-	-	-		

H MARK INDISTINGUISHABLE FROM CRACK ON SPECIMEN

B.

TABLE XXIV

SUMMARY OF TEST DATA FOR 4330V M(

SPEC	NUMBER OF CYCLES IN FATIGUE	ACTUAL CRACK GEOMETRY FROM FRACTURE SURFACE LENGTH 2c	DEPTH a	l_1	l_2	θ_1	θ_2	SPECIMENS WITH HOLES DISTANCE FROM HOLE l_1	l_2	PENETRANT LENGTH 2c	l_1	l_2	θ_1	θ_2	MAGNETIC PARTICLE LENGTH 2c	DEPTH	l_1	l_2	θ_1	θ_2	ULTRASONICS LENGTH 2c	DEPTH	l_1	l_2
S1	100,003	N.C.	--	--	--	--	--	N.A.	N.A.	--	--	--	--	--	--	--	--	--	--	--	C	.005	15.53	15.53
S2	63,000	--	--	--	--	--	--	N.A.	N.A.	--	--	--	--	--	.1574		15.47	15.48	131°	137°		.005	15.53	15.53
S3	6,500	.2356	.10	16.08	16.06	28°	37°	N.A.	N.A.	.1844	15.09	16.10	23°	30°	.2358		16.10	16.11	27°	36°	.1071	.012	16.17	16.20
S4	9,000	.1309	.08	16.10	16.10	241°	246°	N.A.	N.A.	0	--	--	--	--	0		--	--	--	--	0	--	--	--
S5	2,700	--	--	--	--	--	--	N.A.	N.A.	.1875	15.32	15.86	167°	174°	.2178		15.82	15.86	165°	173°	.4708	.005	15.34	15.88
S6	2,130	.2358	.11	15.91	15.90	75°	85°	N.A.	N.A.	0	--	--	--	--	.2104		16.06	16.08	79°	87°	.1160	.021	15.88	15.93
S7	2,200	.3365	.12	16.03	16.03	218°	232°	N.A.	N.A.	.2495	16.10	16.12	217°	227°	.2882		16.10	16.16	219°	230°	.4052	.056	16.03	16.13
S8	12,800	.1052	.06	16.17	16.16	172°	176°	N.A.	N.A.	0	--	--	--	--	0		--	--	--	--	.0524	.005	16.03	16.05
S9	23,000	--	--	--	--	--	--	N.A.	N.A.	--	--	--	--	--	--		15.00	16.00	126°	129°	--	.005	16.00	16.00
S10	19,600	.1574	.07	16.15	16.14	146°	152°	N.A.	N.A.	.3142	16.00	16.02	148°	156°	.2104		16.04	16.06	146°	152°	.1047	.090	16.02	16.06
S11	27,900	.2355	.11	16.00	16.02	127°	136°	N.A.	N.A.	0	--	--	--	--	0		--	--	--	--	.1811	.007	15.85	15.94
S12	29,100	.1700	.08	16.00	15.05	167°	174°	N.A.	N.A.	0	--	--	--	--	.2358		16.03	16.04	165°	178°	.1271	.005	16.00	16.10
S13	49,100	.3148	.12	16.02	16.05	185°	197°	N.A.	N.A.	.2618	16.00	16.00	190°	200°	.3466		16.25	16.30	140°	145°	.1309	.018	16.00	16.00
S14	38,000	.2152	.10	15.97	16.02	189°	197°	N.A.	N.A.	.2096	16.00	16.00	196°	204°	.2095		15.98	16.03	184°	204°	.1720	.022	15.90	15.97
S15	57,000	.3440	.16	15.96	15.91	39°	52°	N.A.	N.A.	0	--	--	--	--	.2096		15.94	15.97	38°	49°	.3142	.007	15.90	15.90
S16	84,000	.5260	.20	16.13	16.08	309°	329°	N.A.	N.A.	.5236	16.00	16.00	313°	333°	.5792		16.07	16.13	307°	329°	.2218	.080	16.10	16.10
S17	35,000	.4729	.17	16.03	15.99	7°	25°	N.A.	N.A.	.7572	16.00	16.00	11°	40°	.4500		15.97	16.04	7°	24°	.3142	.005	15.76	15.96
S18	44,700	.3477	.17	16.03	16.06	58°	72°	N.A.	N.A.	.3727	16.03	16.75	63°	79°	.2624		16.02	16.04	183°	193°	.2096	.045	16.05	16.05
S19	30,000	--	--	--	--	--	--	N.A.	N.A.	0	--	--	--	--	.6785		15.96	15.96	115°	118°	.0524	.005	15.90	15.90
S20	45,000	.1324	.07	15.90	15.92	317°	322°	N.A.	N.A.	.2618	15.90	15.90	322°	330°	.1844		15.87	15.89	317°	324°	.1448	.005	15.82	15.92
S21	33,000	.2115	.10	16.01	15.98	213°	221°	N.A.	N.A.	0	--	--	--	--	.1571		16.02	16.02	213°	219°	.1448	.006	16.00	16.10
S22	62,000	.2923	.10	16.06	16.01	311°	322°	N.A.	N.A.	.2356	16.00	16.00	313°	322°	.2908		16.00	16.04	309°	320°	.1862	.030	16.00	16.10
S23	67,500	.3456	.12	16.01	16.02	114°	127°	N.A.	N.A.	0	--	--	--	--	.2096		16.00	16.03	116°	127°	0	--	--	--
S24	67,600	.4460	.20	15.92	15.96	0°	17°	N.A.	N.A.	.2096	16.00	16.00	10°	18°	.2880		16.00	16.00	5°	16°	.3400	.054	15.35	15.35
S25	55,400	.4200	.18	16.00	16.03	21°	27°	N.A.	N.A.	.5760	16.00	16.00	17°	42°	.3938		16.01	16.04	23°	38°	.2342	.012	16.06	16.12
S26	86,500	.2880	.13	15.78	15.98	124°	135°	N.A.	N.A.	.3400	16.00	16.00	125°	138°	0		--	--	--	--	.4712	.012	16.10	16.10
S27	28,900	--	--	--	--	--	--	N.A.	N.A.	0	--	--	--	--	.1309		16.00	16.00	236°	241°	.1402	.005	15.95	16.00
S28	49,400	--	--	--	--	--	--	N.A.	N.A.	0	--	--	--	--	0		--	--	--	--	0	--	--	--
S29	38,700	.1309	.06	16.03	16.03	16°	21°	N.A.	N.A.	0	--	--	--	--	.1047		15.97	15.97	20°	24°	.2221	.08	16.00	16.10
S30	NONE	--	--	--	--	--	--	N.A.	N.A.	0	--	--	--	--	0		--	--	--	--	0	--	--	--
S31	NONE	N.C.	--	--	--	--	--	N.A.	N.A.	0	--	--	--	--	0		--	--	--	--	0	--	--	--
S32	NONE	N.C.	--	--	--	--	--	N.A.	N.A.	C	--	--	--	--	0		--	--	--	--	0	--	--	--
S33	54,000	.3427	.15	15.98	15.96	300°	316°	N.A.	N.A.	0	--	--	--	--	.2132		15.95	15.99	308°	314°	.2720	.022	15.94	16.02
S34	62,000	N.C.	--	--	--	--	--	.06	.13	--	--	--	--	--	0		--	--	--	--	0	--	--	--
S35	50,000	.4722	.15	15.96	15.93	170°	188°	N.A.	N.A.	.5023	15.92	15.99	166°	189°	.3947		15.94	15.16	171°	188°	.1047	.005	16.00	16.00
S36	58,400	.2880	.10	15.97	15.97	134°	145°	N.A.	N.A.	.1844	15.95	15.97	137°	144°	.1400		15.95	15.98	134°	148°	.2096	.025	16.02	16.02
S37	60,000	--	--	--	--	--	--	N.A.	N.A.	0	--	--	--	--	0		--	--	--	--	0	--	--	--
S38	58,000	--	--	--	--	--	--	N.A.	N.A.	--	--	--	--	--	--		--	--	--	--	--	.005	15.95	15.95
S39	36,000	.3144	.14	16.02	16.0	265°	277°	N.A.	N.A.	.2104	16.00	16.02	267°	275°	.2418		16.00	16.00	265°	275°	.2356	.007	16.00	16.00
S40	49,680	.1584	.07	16.08	16.10	131°	137°	N.A.	N.A.	0	--	--	--	--	.1324		15.93	15.95	133°	138°	.0895	.005	15.98	15.98
S41	22,200	.1324	.07	16.01	16.03	268°	273°	N.A.	N.A.	.1584	15.95	15.97	270°	276°	.2375		15.95	15.98	268°	277°	.1309	.022	13.77	15.97
S42	37,000	.2618	.09	16.12	16.12	256°	268°	N.A.	N.A.	0	--	--	--	--	.1574		16.14	16.15	263°	269°	.2096	.040	16.16	16.16
S43	49,450	.1313	.06	16.07	16.06	1°	6°	N.A.	N.A.	0	--	--	--	--	.2356		16.00	16.00	359°	8°	.1571	.009	16.00	16.00
S44	12,000	--	--	--	--	--	--	N.A.	N.A.	--	--	--	--	--	--		15.92	15.92	54°	56°	--	.005	15.92	15.92
S45	35,000	.1584	.08	15.98	16.00	266°	272°	N.A.	N.A.	.2358	16.01	16.02	268°	277°	.1584		16.02	16.04	271°	277°	.0524	.005	16.00	16.00
S46	44,400	.1836	.09	16.01	16.00	84°	91°	N.A.	N.A.	.3406	15.97	15.98	83°	96°	.1032		15.98	15.98	83°	90°	.0931	.005	15.95	16.00
S47	44,000	.3417	.13	16.00	16.03	280°	293°	N.A.	N.A.	.2104	16.02	16.04	284°	290°	.3929		16.00	16.01	288°	295°	.1621	.012	16.00	16.04
S48	36,200	.3937	.17	16.00	16.02	101°	118°	N.A.	N.A.	.3405	15.99	16.00	96°	107°	.3932		15.98	16.00	93°	108°	.2768	.032	16.03	16.12
S49	50,000	.1400	.06	16.08	16.08	--	--	.21	.34	0	--	--	--	--	.2620		16.00	16.01	273°	283°	.1600	.012	15.97	16.00
S50	21,000	.1584	.07	16.01	16.02	111°	117°	N.A.	N.A.	0	--	--	--	--	.1322		16.07	16.07	107°	119°	.1584	.028	16.10	16.12
S51	27,900	.2358	.09	16.01	16.02	261°	270°	N.A.	N.A.	.2020	16.00	16.01	260°	273°	.1571		16.00	16.00	262°	268°	.1547	.005	16.03	16.03
S52	35,400	.2923	.12	16.05	16.00	339°	350°	N.A.	N.A.	0	--	--	--	--	.2375		16.05	16.08	342°	351°	.2479	.022	16.02	16.10
S53	5,000	.1047	.05	16.15	16.15	119°	123°	N.A.	N.A.	.1343	16.07	15.12	115°	120°	.2618		16.10	16.10	112°	122°	0	--	--	--
S54	10,000	--	--	--	--	--	--	N.A.	N.A.	0	--	--	--	--	0		--	--	--	--	.0524	.005	15.97	15.97
S55	32,500	.2819	.12	15.94	15.94	164°	178°	N.A.	N.A.	.2552	15.97	15.98	165°	180°	.3666		15.97	15.98	159°	173°	.2646	.045	16.00	16.05

TABLE XXIV
OF TEST DATA FOR 4330V MODIFIED STEEL CYLINDERS

θ₁	c₂	LENGTH 2ℓ	DEPTH a	ℓ₁	ℓ₂	θ₁	θ₂	X-RAY	PENETRANT	MAG PART	EDDY C	ACTUAL FAILURE LOAD PSI	YIELD LOAD KPS	ACTUAL FAILURE STRESS	K_IC (b)	K_IC	HOLE ANALYSIS	PENET K_IC	PENET K_IC(b)	MAG PART K_IC	MAG PART K_IC(b)	ULTRA K_IC	ULTRA K_IC(b)	X-RAY K_IC	X-RAY K_IC(b)
--	--	--	--	--	--	--	--	--	--	--	--	--	--	--	--	--	--	--	--	--	--	--	--	--	--
131°	137°	.0	.003	15.53	15.53	137°	137°	N.C.F.	--	--		440,000		--	--	--	--	--	--	391.8	486.5	--	--	--	--
27°	36°	.1071	.014	16.17	16.20	028°	032°	N.C.F.	--	--		416,000		185.2	427.4	320.1	--	362.0	461.1	320.1	427.4	475.0	561.2	--	--
--	--	0	--	--	--	--	--	--	--	--		475,000		210.3	519.9	429.7	--	--	--	--	--	--	--	--	--
165°	173°	.4208	.005	15.84	15.88	160°	171°	N.C.F.	--	--		420,500		--	--	--	--	359.0	458.6	333.1	437.6	239.6	372.9	--	--
79°	87°	.1160	.021	15.88	15.93	78°	82°	N.C.F.	--	--		450,000		202.9	427.4	320.1	--	--	--	338.9	442.2	456.4	544.1	--	--
219°	230°	.4052	.056	16.03	16.13	211°	226°	N.C.F.	--	--		422,500		189.2	390.0	263.0	--	311.2	420.6	289.6	404.7	244.2	375.4	--	--
--	--	.0524	.005	16.05	16.05	170°	172°	N.C.F.	--	--		487,500		219.7	565.2	479.3	--	--	--	--	--	679.1	758.0	--	--
126°	129°	--	.005	16.00	16.00	150°	152°	N.C.F.	--	--		490,000		--	--	--	--	--	--	--	--	--	--	--	--
146°	152°	.1047	.010	16.06	16.06	144°	148°	N.C.F.	--	--		480,000		213.7	486.5	391.8	--	277.3	396.2	338.9	442.2	480.4	566.3	--	--
--	--	.1811	.007	15.85	15.94	121°	127°	N.C.F.	--	--		433,000		196.8	427.6	320.3	--	--	--	--	--	365.3	463.9	--	--
169°	178°	.1271	.005	16.00	16.10	164°	167°	N.C.F.	--	--		459,500		206.5	456.7	356.6	--	--	--	320.1	427.4	436.1	525.6	--	--
140°	145°	.1309	.003	16.00	16.00	195°	199°	N.C.F.	--	--		420,000		190.1	396.1	277.1	--	303.8	415.1	256.8	382.9	429.7	519.9	--	--
184°	204°	.1720	.022	15.90	15.97	186°	194°	N.C.F.	--	--		420,000		183.6	439.2	335.1	--	339.6	442.7	339.6	442.8	374.8	471.9	--	--
38°	49°	.3142	.007	15.90	15.90	040°	052°	N.C.F.	--	--		407,000		188.7	388.1	265.1	--	--	--	288.9	404.2	277.3	396.2	--	--
307°	329°	.2618	.080	15.10	16.10	309°	319°	C.F.	--	--		351,000		154.7	360.4	214.3	--	214.6	360.6	204.3	356.4	303.8	415.1	255.6	382.2
2°	24°	.3142	.085	15.96	15.96	006°	018°	N.C.F.	--	--		358,000		162.8	365.8	226.1	--	178.4	349.7	231.6	368.6	277.3	396.2	--	--
183°	193°	.2091	.045	16.05	16.05	060°	068°	N.C.F.	--	--		365,000		166.3	382.6	256.4	--	248.1	377.7	303.4	414.7	339.7	442.9	--	--
115°	118°	.0524	.005	15.90	15.90	114°	116°	N.C.F.	--	--		495,000		--	--	--	--	--	--	554.9	636.6	679.1	758.0	--	--
317°	324°	.1461	.005	15.82	15.92	323°	327°	N.C.F.	--	--		435,000		213.8	517.7	427.2	--	303.8	415.1	362.0	461.1	408.5	501.1	--	--
213°	219°	.1418	.005	16.00	16.10	212°	216°	N.C.F.	--	--		448,000		202.9	441.5	338.0	--	--	--	392.2	486.8	408.5	501.1	--	--
309°	320°	.1842	.030	16.00	16.10	313°	319°	N.C.F.	--	--		406,500		184.7	403.3	287.5	--	320.3	427.5	288.3	403.8	360.3	459.7	--	--
116°	127°	0	--	--	--	--	--	N.C.F.	C.F.	C.F.		389,000		183.4	389.0	266.4	--	--	--	288.9	404.2	--	--	--	--
5°	16°	.3403	.054	15.35	15.35	003°	016°	N.C.F.	--	--		342,000		156.3	369.2	232.8	--	339.7	442.9	289.7	404.8	266.5	389.0	--	--
23°	30°	.2242	.012	16.04	16.12	020°	028°	N.C.F.	--	--		371,000		169.0	373.0	239.9	--	204.8	356.7	247.7	377.5	328.3	433.9	--	--
--	--	.4712	.012	16.10	16.10	121°	139°	N.C.F.	--	--		400,000		177.2	404.8	289.7	--	266.5	389.0	--	--	226.5	366.0	--	--
234°	241°	.1462	.005	15.95	16.00	336°	343°	N.C.F.	--	--		482,500		--	--	--	--	--	--	429.7	519.9	415.2	506.9	--	--
--	--	0	--	--	--	--	--	N.C.F.	--	--		495,000		--	--	--	--	--	--	--	--	--	--	--	--
20°	24°	.2121	.008	16.00	16.10	026°	034°	N.C.F.	--	--		492,000		219.8	519.9	429.7	--	--	--	480.4	566.3	322.7	429.4	--	--
--	--	.6	--	--	--	--	--	N.C.F.	--	--		488,000		--	--	--	--	--	--	--	--	--	--	--	--
--	--	0	--	--	--	--	--	N.C.F.	--	--		487,000		--	--	--	--	--	--	--	--	--	--	--	--
--	--	0	--	--	--	--	--	N.C.F.	--	--		488,500		--	--	--	--	--	--	--	--	--	--	--	--
306°	314°	.2738	.022	15.94	16.02	304°	314°	N.C.F.	--	C.F.		383,000		177.3	388.4	265.6	--	--	--	336.7	440.4	279.1	410.1	--	--
--	--	0	--	--	--	--	--	N.C.F.	--	N.C.F.		377,000		--	--	--	--	--	--	--	--	--	--	--	--
171°	186°	.1047	.009	16.00	16.00	176°	180°	C.F.	--	C.F.		364,000		166.4	365.9	226.2	--	219.3	362.6	247.4	377.3	480.4	566.3	--	--
134°	140°	.2091	.025	16.02	16.02	136°	144°	N.C.F.	--	C.F.		387,000		179.2	404.8	289.7	--	362.0	461.1	388.5	483.7	339.7	442.9	207.7	357.7
--	--	0	--	--	--	--	--	N.C.F.	--	N.C.F.		478,000		--	--	--	--	--	--	--	--	--	--	--	--
--	--	--	.005	15.95	15.95	111°	113°	N.C.F.	--	N.C.F.		464,000		--	--	--	--	--	--	--	--	--	--	--	--
265°	275°	.2306	.007	16.00	16.00	265°	274°	N.C.F.	--	C.F.		386,000		178.7	396.2	277.3	--	334.2	438.4	303.8	415.1	320.3	427.5	--	--
133°	138°	.0795	.005	15.98	15.98	131°	134°	N.C.F.	--	C.F.		458,000		208.5	485.4	390.6	--	--	--	427.2	517.7	554.9	636.6	--	--
268°	277°	.1	.022	15.97	15.97	268°	273°	N.C.F.	--	C.F.		472,000		213.6	517.7	427.2	--	390.6	485.4	319.0	426.5	429.7	519.9	--	--
263°	269°	.262	.040	16.16	16.16	259°	267°	N.C.F.	--	C.F.		408,000		188.2	415.1	303.8	--	--	--	391.8	486.5	339.7	442.9	--	--
359°	8°	.1521	.009	16.00	16.00	001°	007°	N.C.F.	--	C.F.		457,000		213.7	519.3	429.0	--	--	--	320.3	427.5	392.2	486.8	--	--
54°	56°	--	.005	15.92	15.92	051°	052°	N.C.F.	--	C.F.		464,000		--	--	--	--	--	--	--	--	--	--	--	--
277°	277°	.0524	.005	16.00	16.00	267°	265°	N.C.F.	--	C.F.		443,000		197.9	485.4	390.6	--	320.1	427.4	390.6	485.4	679.1	758.0	--	--
83°	90°	.0931	.005	15.95	16.00	088°	091°	N.C.F.	--	C.F.		437,000		203.3	431.8	362.8	--	266.4	389.0	363.2	462.1	509.5	593.5	--	--
260°	295°	.1671	.012	16.00	16.04	28°	289°	C.F.	--	C.F.		385,000		173.5	388.7	265.9	--	338.9	442.2	248.0	377.6	386.1	481.6	310.9	420.4
93°	108°	.2768	.032	16.03	16.12	094°	104°	N.C.F.	--	C.F.		360,000		165.2	377.5	247.8	--	266.4	389.0	247.9	377.6	295.5	409.0	--	--
273°	283°	.1600	.012	15.97	16.00	268°	274°	N.C.F.	--	C.F.		310,000		152.4	507.2	415.5	339.8	--	--	303.7	415.0	388.6	483.7	--	--
107°	119°	.1584	.028	16.10	16.12	109°	115°	N.C.F.	--	C.F.		290,000		135.3	485.4	390.6	--	--	--	363.2	462.1	390.6	485.4	--	--
262°	268°	.1147	.005	16.03	16.03	263°	267°	N.C.F.	--	N.C.F.		420,000		188.7	427.4	320.1	--	303.7	415.0	392.2	486.8	480.4	566.3	--	--
342°	351°	.2477	.022	16.02	16.10	343°	352°	N.C.F.	--	C.F.		389,000		179.3	403.3	287.5	--	--	--	319.0	426.5	312.2	421.1	--	--
112°	122°	.0	--	--	--	--	--	N.C.F.	--	C.F.		476,000		220.4	566.3	490.4	--	424.2	515.0	303.8	415.1	--	--	--	--
--	--	.0524	.005	15.97	15.97	259°	261°	N.C.F.	--	C.F.		475,000		--	--	--	--	--	--	--	--	679.1	758.0	--	--
159°	173°	.2666	.065	16.00	16.05	160°	170°	N.C.F.	--	C.F.		291,000		182.0	415.1	303.8	--	479.2	565.2	256.8	302.9	301.1	413.1	--	--

PUNCH MARK INDISTINGUISHABLE FROM CRACK ON SPECIMEN

259

B.

TABLE XXIV (CONTINUED)

SPEC#	NUMBER OF CYCLES IN FATIGUE	ACTUAL CRACK GEOMETRY FROM FRACTURE SURFACE						SPECIMENS WITH HOLES, DISTANCE FROM HOLE		CRACK GEOMETRY BY NDT INSPECTION IN LABORATORY															
		LENGTH 2c	DEPTH a	LOCATION MEASUREMENTS						PENETRANT					MAGNETIC PARTICLE						ULTRASONICS				
				l_1	l_2	θ_1	θ_2	x_1	x_2	LENGTH 2c	l_1	l_2	θ_1	θ_2	LENGTH 2c	DEPTH a	l_1	l_2	θ_1	θ_2	LENGTH 2c	DEPTH a	l_1	l_2	θ_1
S56	28,000	.1309	.08	16.08	16.08	155°	160°	N.A.	N.A.	0	--	--	--	--	.2096		16.08	16.09	149°	157°	.0785	.006	16.13	16.13	155°
S57	22,000	.2358	.08	16.03	16.04	161°	170°	N.A.	N.A.	.1047	16.07	16.07	164°	168°	.2648		16.04	16.08	159°	164°	.2094	.005	16.13	16.13	158°
S58	36,300	.2882	.14	15.81	15.80	224°	235°	N.A.	N.A.	.2882	15.82	15.83	224°	235°	.3670		15.83	15.85	220°	236°	.2964	.025	15.83	15.90	223°
S59	30,000	.1500	.06	16.07	16.05	--	--	.23	.38	0	--	--	--	--	.0840		16.00	16.03	333°	336°	.1309	.020	16.03	16.03	332°
S60	32,000	.2000	.09	15.95	15.95	129°	135°	.24	.44	0	--	--	--	--	.2625		15.96	15.98	124°	134°	.1207	.012	15.92	15.98	129°
S61	24,100	.1200	.07	16.16	16.14	--	--	.17	.28	0	--	--	--	--	.1857		16.12	16.15	218°	225°	.1928	.009	16.08	16.14	216°
S62	15,000	.1200	.06	16.01	15.99	--	--	.15	.28	0	--	--	--	--	.1309		15.94	15.94	180°	185°	0	--	--	--	--
S63	17,900	.1300	.07	16.08	16.10	--	--	.19	.32	.1857	16.04	16.07	124°	131°	.1832		16.07	16.07	123°	130°	.1571	.009	16.05	16.05	119°
S64	21,100	.1836	.08	15.99	15.98	291°	298°	.17	.36	0	--	--	--	--	.1571		16.00	16.00	293°	299°	.1621	.042	15.96	16.00	287°
S65	28,000	.2635	.11	16.00	15.97	151°	161°	.21	.47	.2618	16.00	16.00	155°	165°	.3142		16.00	16.00	150°	162°	.1763	.008	15.97	16.05	152°
S66	33,000	.1300	.07	16.02	16.03	--	--	.23	.36	.1309	15.97	15.97	263°	268°	.3365		15.96	15.96	272°	286°	.0808	.005	15.97	16.03	264°
S67	21,000	.1309	.07	16.03	16.03	268°	273°	.11	.24	.1047	16.00	16.00	267°	271°	.1309		16.00	16.00	265°	270°	.1047	.020	16.00	16.00	268°
S68	18,700	.1309	.06	--	--	279°	284°	N.A.	N.A.	0	--	--	--	--	.1324		16.16	16.18	275°	280°	0	--	16.15	16.1?	278°
S69	21,100	.0700	.03	--	--	--	--	N.A.	N.A.	0	--	--	--	--	.2096		15.95	15.96	216°	224°	.0816	.005	15.85	15.92	217°
S70	21,000	.2356	.10	15.94	15.94	148°	157°	.19	.39	.1574	15.94	15.95	153°	159°	.2104		15.94	15.96	148°	156°	.1571	.005	16.00	16.00	145°
S71	15,100	.1500	.07	16.01	16.03	186°	195°	.18	.34	0	--	--	--	--	.2882		15.96	15.97	186°	197°	.0785	.005	16.00	16.00	194°
S72	27,500	.1052	.06	15.98	15.97	304°	308°	.19	.28	.2104	15.95	15.97	301°	309°	.1835		15.96	15.97	304°	311°	0	.005	15.98	15.98	305°
S73	44,600	.3938	.17	16.06	16.09	192°	207°	.28	.68	.4461	16.11	15.14	188°	205°	.2096		16.14	16.15	192°	200°	.1832	.027	16.00	16.00	189°
S74	45,100	.2635	.14	--	--	293°	303°	.21	.49	.1835	16.19	16.20	294°	301°	.2887		16.19	16.21	291°	302°	.1928	.025	16.20	16.26	294°
S75	--	N.C.	--	--	--	--	--	N.A.	N.A.	0	--	--	--	--	0		--	--	--	--	0	--	--	--	--
S76	--	N.C.	--	--	--	--	--	N.A.	N.A.	0	--	--	--	--	0		--	--	--	--	0	--	--	--	--
S77	60,000	--	--	--	--	--	--	N.A.	N.A.	0	--	--	--	--	0		--	--	--	--	0	--	--	--	--
S78	41,500	.4990	.21	15.97	15.93	162°	181°	N.A.	N.A.	.5606	15.94	16.05	157°	178°	.3371		16.00	16.04	161°	175°	.3989	.022	15.93	16.00	164°
S79	60,000	--	--	--	--	--	--	N.A.	N.A.	--	--	--	--	--	--		--	--	--	--	--	--	--	--	--
S80	55,000	--	--	--	--	--	--	.06	.22	--	--	--	--	--	--		--	--	--	--	--	--	--	--	--
S81	59,200	.1700	.05	15.90	15.88	46°	50°	N.A.	N.A.	0	--	--	--	--	.1835		15.94	15.95	305°	312°	.0785	.005	15.97	15.97	047°
S82	45,000	.1574	.06	16.07	16.06	318°	324°	N.A.	N.A.	0	--	--	--	--	.1309		16.02	16.02	321°	326°	.1309	.005	16.07	16.07	321°
S83	30,500	.2356	.11	--	--	278°	287°	N.A.	N.A.	.2635	16.02	16.05	278°	288°	.3403		16.04	16.04	276°	289°	.2087	.005	16.00	16.10	278°
S84	60,000	N.C.	--	--	--	--	--	.19	.29	0	--	--	--	--	0		--	--	--	--	0	--	--	--	--
S85	44,500	.3144	.13	15.96	15.97	290°	302°	N.A.	N.A.	.3372	15.93	15.98	288°	302°	.4461		15.95	15.98	285°	302°	.1571	.029	16.00	16.00	293°
S86	49,000	N.C.	--	--	--	--	--	N.A.	N.A.	0	--	--	--	--	0		--	--	--	--	0	--	--	--	--
S87	55,000	N.C.	--	--	--	--	--	N.A.	N.A.	0	--	--	--	--	0		--	--	--	--	0	--	--	--	--
S88	45,000	N.C.	--	--	--	--	--	.29	.37	0	--	--	--	--	0		--	--	--	--	0	--	--	--	--
S89	56,000	--	--	--	--	--	--	N.A.	N.A.	--	--	--	--	--	--		--	--	--	--	--	--	--	--	--
S90	13,000	--	--	--	--	--	--	N.A.	N.A.	0	--	--	--	--	0		--	--	--	--	0	--	--	--	--
S91	27,000	.1000	.04	--	--	--	--	N.A.	N.A.	0	--	--	--	--	0		--	--	--	--	0	--	--	--	--
S92	--	--	--	--	--	--	--	N.A.	N.A.	0	--	--	--	--	0		--	--	--	--	0	--	--	--	--
S93	--	--	--	--	--	--	--	N.A.	N.A.	0	--	--	--	--	0		--	--	--	--	0	--	--	--	--
S94	23,500	--	--	--	--	--	--	N.A.	N.A.	--	--	--	--	--	--		--	--	--	--	--	--	--	--	--
S95	75,000	--	--	--	--	--	--	N.A.	N.A.	0	--	--	--	--	0		--	--	--	--	0	--	--	--	--
S96	29,000	.2000	.02	16.37	16.33	--	--	N.A.	N.A.	0	--	--	--	--	0		--	--	--	--	0	--	--	--	--
S97	35,500	N.C.	--	--	--	--	--	N.A.	N.A.	0	--	--	--	--	0		--	--	--	--	0	--	--	--	--
S98	20,100	--	--	--	--	--	--	N.A.	N.A.	--	--	--	--	--	--		--	--	--	--	--	--	--	--	--
S99	10,600	--	--	--	--	--	--	N.A.	N.A.	0	--	--	--	--	0		--	--	--	--	0	--	--	--	--
S100	28,500	--	--	--	--	--	--	N.A.	N.A.	0	--	--	--	--	0		--	--	--	--	0	--	--	--	--

NOTES -- = NO INFORMATION AVAILABLE   N.C. = NO CRACK   N.C.F. = NO CRACK FOUND   N.A. = NOT APPLICABLE   C.F. = CRACK FOUND   P.M. = PUNCH MARK INDISTINGUISHABLE FROM CRACK ON SPECIMEN

A.

TABLE XXIV (CONTINUED)

IN LAB $2\theta_1$	ULTRASONICS LENGTH 2c	DEPTH a	l_1	l_2	θ_1	θ_2	X-RAY	PENETRANT	MAG PART	EDDY C	ACTUAL FAILURE LOAD PSI	YIELD LOAD KIPS	ACTUAL FAILURE STRESS	K_{IC} (b)	90% CL K_{IC}	HOLE ANALYSIS	PENET K_{IC}	PENET $K_{C(b)}$	MAG PART K_{IC}	MAG PART $K_{C(b)}$	ULTRA K_K	ULTRA $K_{C(b)}$	X-RAY K_{IC}	X-RAY $K_{C(b)}$
157°	.0785	.006	16.13	16.13	155°	158°	N.C.F.	--	C.F.		448,000		203.1	519.9	429.7	--	--	--	339.6	442.7	175.5	349.3	--	--
164°	.2094	.005	16.13	16.13	158°	166°	N.C.F.	--	C.F.		415,000		187.1	427.4	320.1	--	480.4	566.3	302.1	413.8	339.7	442.9	--	--
234°	.2964	.025	15.83	15.90	223°	234°	N.C.F.	--	C.F.		389,000		174.2	404.7	289.6	--	289.6	404.7	256.6	382.8	285.5	401.9	--	--
336°	.1309	.020	16.03	16.03	332°	337°	N.C.F.	--	C.F.		339,000		154.7	494.8	401.4	343.5	--	--	536.4	619.0	429.7	519.9	--	--
134°	.1207	.012	15.92	15.98	129°	133°	N.C.F.	--	N.C.F.		271,000		122.2	449.3	347.6	305.9	--	--	303.4	414.7	447.5	535.9	--	--
225°	.1928	.009	16.08	16.14	216°	223°	N.C.F.	--	C.F.		334,000		154.6	537.1	448.8	289.9	--	--	360.8	460.1	354.0	454.5	--	--
185°	0	--	--	--	--	--	N.C.F.	--	C.F.		316,000		144.7	537.1	448.8	201.5	--	--	429.7	519.9	--	--	--	--
130°	.1571	.009	16.05	16.05	119°	125°	N.C.F.	--	N.C.F.		337,000		153.8	521.2	431.2	317.6	360.8	460.1	360.8	462.1	392.2	486.8	--	--
299°	.1621	.042	15.90	16.00	287°	293°	N.C.F.	--	C.F.		281,000		125.8	461.8	362.8	285.1	--	--	392.2	486.8	386.1	481.6	--	--
162°	.1763	.008	15.97	16.05	152°	158°	C.F.	--	C.F.		248,000		114.4	414.4	302.8	250.6	303.8	415.1	277.3	396.2	370.2	468.0	299.2	411.7
286°	.0808	.005	15.97	16.03	264°	267°	N.C.F.	--	C.F.		339,000		152.4	521.2	431.2	345.7	429.7	512.9	268.0	390.0	546.9	629.0	--	--
270°	.1047	.020	16.00	16.00	268°	272°	N.C.F.	--	N.C.F.		250,000		110.3	519.9	429.7	277.9	480.4	566.3	429.7	519.9	480.4	566.3	--	--
280°	0	--	16.15	16.15	278°	278°	N.C.F.	C.F.	N.C.F.		478,000		217.4	519.9	429.7	--	--	--	427.2	517.7	--	--	--	--
224°	.0816	.005	15.85	15.92	217°	220°	N.C.F.	C.F.	N.C.F.		474,000		220.4	668.2	587.6	--	--	--	339.6	442.7	544.2	626.4	--	--
156°	.1571	.005	16.00	16.00	145°	151°	N.C.F.	--	C.F.		225,000		100.5	427.5	320.3	264.5	391.8	486.5	338.9	442.2	392.2	486.8	--	--
197°	.0785	.005	16.00	16.00	194°	197°	N.C.F.	--	N.C.F.		314,000		141.8	494.8	401.4	317.0	--	--	289.6	404.7	554.9	636.6	--	--
311°	0	.005	15.98	15.98	305°	305°	N.C.F.	--	C.F.		360,000		162.6	565.2	479.3	336.4	338.9	442.2	362.9	461.9	--	--	--	--
200°	.1832	.027	16.00	16.00	189°	196°	N.C.F.	C.F.	C.F.		221,000		99.2	377.5	247.7	233.8	232.8	369.2	339.6	442.7	363.2	462.1	--	--
302°	.1928	.025	16.20	16.26	294°	301°	N.C.F.	C.F.	C.F.		239,000		151.2	414.4	302.8	240.0	362.9	461.9	289.3	404.6	354.0	454.5	--	--
--	0	--	--	--	--	--	N.C.F.	--	N.C.F.		386,000		--	--	--	--	--	--	--	--	--	--	--	--
--	0	--	--	--	--	--	N.C.F.	--	N.C.F.		377,000		--	--	--	--	--	--	--	--	--	--	--	--
--	0	--	--	--	--	--	N.C.F.	N.C.F.	N.C.F.		479,500		--	--	--	--	--	--	--	--	--	--	--	--
175°	.3989	.022	15.93	16.00	164°	179°	C.F.	C.F.	C.F.		339,000		152.8	363.0	220.1	--	207.6	357.7	267.8	389.9	246.1	376.5	266.8	366.1
--	--	--	--	--	--	--	N.C.F.	N.C.F.	N.C.F.		476,000		--	--	--	--	--	--	--	--	--	--	--	--
--	--	--	--	--	--	--	N.C.F.	N.C.F.	N.C.F.		476,000		--	--	--	217.7	--	--	--	--	--	--	--	--
312°	.0785	.005	15.97	15.97	047°	050°	N.C.F.	C.F.	C.F.		440,000		201.7	473.8	377.0	--	--	--	362.9	461.9	554.9	636.6	--	--
326°	.1309	.005	16.07	16.07	321°	326°	N.C.F.	C.F.	N.C.F.		472,000		213.3	486.5	391.8	--	--	--	429.7	519.9	429.7	519.9	--	--
289°	.2087	.005	16.00	16.10	278°	285°	N.C.F.	C.F.	C.F.		425,000		192.9	427.5	320.3	--	302.8	414.4	266.5	389.0	340.3	443.3	--	--
--	0	--	--	--	--	--	N.C.F.	N.C.F.	N.C.F.		377,000		--	--	--	--	--	--	--	--	--	--	--	--
302°	.1571	.029	16.00	16.00	293°	299°	N.C.F.	C.F.	C.F.		372,000		169.5	396.2	277.3	--	267.7	389.8	232.8	369.2	392.2	486.8	--	--
--	0	--	--	--	--	--	N.C.F.	N.C.F.	C.F.		387,000		--	--	--	--	--	--	--	--	--	--	--	--
--	0	--	--	--	--	--	N.C.F.	N.C.F.	N.C.F.		390,000		--	--	--	--	--	--	--	--	--	--	--	--
--	0	--	--	--	--	--	N.C.F.	N.C.F.	N.C.F.		384,000		--	--	--	--	--	--	--	--	--	--	--	--
--	--	--	--	--	--	--	N.C.F.	N.C.F.	C.F.		479,000		--	--	--	--	--	--	--	--	--	--	--	--
--	0	--	--	--	--	--	N.C.F.	N.C.F.	N.C.F.		476,000		--	--	--	--	--	--	--	--	--	--	--	--
--	0	--	--	--	--	--	N.C.F.	N.C.F.	N.C.F.		477,000		218.1	576.7	491.6	--	--	--	--	--	--	--	--	--
--	0	--	--	--	--	--	N.C.F.	N.C.F.	N.C.F.		482,000		--	--	--	--	--	--	--	--	--	--	--	--
--	0	--	--	--	--	--	N.C.F.	N.C.F.	N.C.F.		477,000		--	--	--	--	--	--	--	--	--	--	--	--
--	--	--	--	--	--	--	N.C.F.	N.C.F.	N.C.F.		479,000		--	--	--	--	--	--	--	--	--	--	--	--
--	0	--	--	--	--	--	N.C.F.	N.C.F.	N.C.F.		478,000		--	--	--	--	--	--	--	--	--	--	--	--
--	0	--	--	--	--	--	N.C.F.	N.C.F.	N.C.F.		476,000		216.0	449.3	347.6	--	--	--	--	--	--	--	--	--
--	0	--	--	--	--	--	N.C.F.	N.C.F.	N.C.F.		481,000		--	--	--	--	--	--	--	--	--	--	--	--
--	--	--	--	--	--	--	N.C.F.	N.C.F.	N.C.F.		478,000		--	--	--	--	--	--	--	--	--	--	--	--
--	0	--	--	--	--	--	N.C.F.	N.C.F.	N.C.F.		481,000		--	--	--	--	--	--	--	--	--	--	--	--
--	0	--	--	--	--	--	C.F.	N.C.F.	N.C.F.		479,000		--	--	--	--	--	--	--	--	--	--	219.9	362.9

MARK INDISTINGUISHABLE FROM CRACK ON SPECIMEN

B.

REFERENCES

1. I. Bouton, "Fundamental Aspects of Structural Reliability," Aerospace Engineering, June 1962.

2. "Fracture Toughness Testing and Its Applications," ASTM Special Technical Publication No. 381, April 1965.

3. W. F. Brown, Jr. and J. E. Srawley, "Plane Strain Crack Toughness Testing of High Strength Metallic Materials," ASTM Special Technical Publication No. 410, December 1967.

4. A. S. Tetelman and A. J. McEvily, Jr., Fracture of Structural Materials, John Wiley & Sons, Inc., 1967.

5. Fracture of Engineering Materials, American Society for Metals, 1964.

6. R. C. McMaster, Ed., Non-Destructive Testing Handbook, Vol. 1 and Vol. 2, Society for Non-Destructive Testing, Ronald Press, 1963.

7. E. H. Rodgers, C. P. Merhib, "A Report Guide to Liquid Penetrant Literature," AMRA MS 64-12, August 1964.

8. E. H. Rodgers, C. P. Merhib, "A Report Guide to Ultrasonic Test Literature," Vol. 1, AMRA, MTD, Vol. 1, March 1966.

9. E. H. Rodgers, C. P. Merhib, "A Report Guide to Magnetic Particle Test Literature," ARMA MS 65-04, 1965.

10. E. H. Rodgers, C. P. Merhib, "A Report Guide to Fluoroscopy Test Literature," AMRA 64-13, 1964.

11. S. A. Wenk, A. J. Schwarber, and R. R. Schowalter, "Survey to Determine the Air Force Research and Development Needs in the Field of Nondestructive Testing," WADC TR-56-607, June 1957.

12. Radiography in Modern Industry, Eastman Kodak Company, 1957.

13. H. Clauser, Practical Radiography for Industry, Reinhold Publ., 1952.

14. C. E. Betz, Principals of Penetrants, Magnaflux Corp., 1963.

15. Military Specifications, MIL I-25135 and MIL I 8916.

16. Magnaflux Data Sheets, Zy 6, Zy F, Zy 1, Zy.2 (1967).

17. W. E. Thomas, "An Analytical Approach to Penetrant Performance," Proc. Soc. Nondestructive Testing, Nov-Dec. 1963.

18. R. B. Houck, McCauley Unpublished paper, OSU 1965.

19. J. C. Harris, "Fluorescent Penetrant Inspection Materials Evaluation Method Development and Comparative Values," AFML-TR-65-64, July 1965.

20. R. B. McCauley and I. van Winkle, "Research to Develop Methods for Measuring the Properties of Penetrant Flaw Inspection Materials," WADD Summary Report (1960-1962) AF 33(615)-6420.

21. F. A. McClintock and G. R. Irwin, "Plasticity Aspects of Fracture Mechanics," in Fracture Toughness Testing & Its Applications, ASTM STP 381 (1964).

22. Magnetic Particle Testing, Magnaflux Corporation.

23. H. E. Duckworth, Electricity & Magnetism, Hold Rinehart & Winston (1961).

24. A. L. Phillips, Ed., Welding Handbook, American Welding Society, 1960, Sec. 828.

25. J. H. Lamble, Ed., Principles of Nondestructive Testing, J. Wiley, (1963).

26. F. P. Doane and C. E. Betz, Principles of Magnaflux, Magnaflux (1951).

27. W. A. Black, "Evaluation of Surface Defects by Nondestructive Testing," Blast. Furnace & Steel Plant, May 1960 (Vol. 48) p. 459.

28. H. Hansel, "The Defect Characteristics in the Magnetic-Nondestructive Test," Archiv. f. Eisenhuttenwesen, VII (1937) p. 497.

29. R. W. Buchanan, "Evaluation of Watertown Arsenal Ultrasonic Flaw Plotting Equipment," WA PR #2, Sept. 1954, USARMRA.

30. O. R. Gericke and J. J. Maguire, "Determination of Defect Geometry by Ultrasonic Pulse Analysis Testing, WAL. TR 8305/8, Jan. 1962, USARMRA.

31. B. Bans, G. E. Oldfield and H. Ravding, Ultrasonic Flaw Detection in Metals, Lliffe Books, 1962.

32. Ultrasonic Technology, R. Goodman, Reinhold, 1962.

33. Ultrasonic Inspection Process, Aerojet General, AGC-STD-4819, August 1953.

34. "Indication Limits, Recommended Ultrasonic Acceptance Standards for Airframe Aluminum Alloys," J. Soc. Nondestructive Testing, Vol. 20, No. 2 (1962), p. 60.

35. J. B. Morgan, "Ultrasonic Testing Standards for Steel Products," J. Soc. Non-destructive Testing, Vol. 20 (1962), p. 167.

36. D. A. Howe, "The Correlation of Defect Size and Reflected Ultrasonic Signal in Extruded Bar Stock," Ultrasonics (British) Oct-Dec. 1964 (p. 186).

37. P. Radislav, "Problems of Defectoscope Examination of Structural Metals for the Reactor of the First Czechoslovakian Atomic Power Station," Symposium in NDT on Nuclear Technology, Rumania, May 1965.

38. R. J. Botsco, "High Resolution Ultrasonics," Material Evaluation, April (1967) p. 76.

39. C. E. Feddersen and W. S. Hyler, "Compilation of Fracture Data for Aluminum Alloys," DMIC Technical Note, November 1, 1965.

40. R. E. Zinkhom, "Thickness Effects on 7075-T6 Material," Reynolds Metals Company, Richmond, Virginia, June 14, 1965.

41. "Fracture Toughness Data Summary of 2000 and 7000 Series Aluminum Alloys," The Boeing Company, Seattle, Washington, received from J. P. Butler, April 15, 1965.

42. W. E. Anderson, "Fracture Toughness Data Summary," Report D6-9068, The Boeing Company, Renton, Washington, June 1962.

43. A. J. McEvily, Jr., W. Illg, and H. F. Hardrath, "Static Strength of Aluminum Alloy Specimens Containing Fatigue Cracks," NACA TN 3816, Langley Aeronautical Laboratories, Langley Field, Virginia, October 1956.

44. T. W. Eichenberger, "Fracture Resistance Data Summary," Report DA-20947, The Boeing Airplane Company, Seattle, Washington, June 1962.

45. H. S. Pearson, "Tear Resistance Properties of Types 420 and 422 Corrosion Resistant Steel, 7075-T6 and 2024-T3 Aluminum Alloy," ER-2332, Lockheed Aircraft Corporation, Marietta, Georgia (1957).

46. Preliminary information, Aluminum Company of America, New Kensington, Pennsylvania, under an Air Force contract.

47. R. J. Urban, "Fracture Toughness and Crack Propagation of Aluminum Alloy," Report FGT 3087, General Dynamics/Fort Worth, Fort Worth, Texas, under Air Force Contract AF 33(657)-8260, July 14, 1964.

48. E. A. Steigerwald and G. L. Hanna, "Initiation of Slow Crack Propagation in High-Strength Materials," Proceedings, American Society for Testing Materials, Vol. 62, 1962, pp. 885-913.

49. L. R. Hall and A. S. Kobayashi, "On the Approximation of Maximum Stress Intensity Factors for Two Embedded Coplanar Cracks," Structural Development Research Memorandum No. 9, The Boeing Company, May 1964.

50. P. Van Dyke, "Stresses About a Circular Hole in a Cylindrical Shell," AIAA Journal, Vol. 3, No. 9 (1965), 1733.

51. A. I. Lurie, "Statics of Thin Walled Elastic Shells," Ozig, Moscow, 1947.

52. D. S. Houghton, "Stress Concentrations Around Cutouts in a Cylinder," Journal of Royal Aeronautical Society, Vol. 65 (1961), 202.

53. D. S. Houghton and A. Rothwell, "The Effect of Curvature on the Stress Concentrations around Holes in Shells," College of Aeronautics, Cranfield, England, Report 156, May 1962.

54. D. W. Houghton and A. Rothwell, "The Analysis of Reinforced Circular and Elliptical Cutouts under Various Loading Conditions," College of Aeronautics, Cranfield, England, Report 151, July 1961.

55. G. N. Savin, Stress Concentrations around Holes, Pergamon Press, New York, 1961.

56. R. E. Peterson, "The Interaction Effect of Neighboring Holes or Cavities, with Particular Reference to Pressure Vessels and Rocket Cases," ASME Journal of Basic Engineering, Vol. 65 (Dec. 1965), p. 879.

57. E. Wessel, W. G. Clark, and W. K. Wilson, "Engineering Methods for the Design and Selection of Materials Against Fracture," Final Report, Westinghouse Research Laboratories, June 1966, ATAC Contract DA-30-069-A76-602(T).

DOCUMENT CONTROL DATA - R&D

(Security classification of title, body of abstract and indexing annotation must be entered when the overall report is classified)

1. ORIGINATING ACTIVITY *(Corporate author)*	2a. REPORT SECURITY CLASSIFICATION
Lockheed-Georgia Company Materials Sciences Laboratory Marietta, Georgia 30060	Unclassified
	2b GROUP

3. REPORT TITLE

THE APPLICABILITY OF A FRACTURE MECHANICS-NONDESTRUCTIVE TESTING DESIGN CRITERION

4. DESCRIPTIVE NOTES *(Type of report and inclusive dates)*

Summary Technical Report   1 January 1967 to 31 December 1967

5. AUTHOR(S) *(Last name, first name, initial)*

Packman, Paul F.   Marchese, Gloria B.
Pearson, Hugh S.   Owens, John S.

6. REPORT DATE	7a. TOTAL NO. OF PAGES	7b. NO. OF REFS
		57

8a. CONTRACT OR GRANT NO. F33615-67-C-1180 b. PROJECT NO. 7381 c. Task No. 738102 d.	9a. ORIGINATOR'S REPORT NUMBER(S) AFML-TR-68-32 9b. OTHER REPORT NO(S) *(Any other numbers that may be assigned this report)*

10. AVAILABILITY/LIMITATION NOTICES

This document is subject to special export controls and each transmittal to foreign nationals may be made only with prior approval of the A. F. Materials Laboratory, MAMP, Wright-Patterson AFB, Ohio 45433.

11. SUPPLEMENTARY NOTES	12. SPONSORING MILITARY ACTIVITY AFML (MAAE) Wright-Patterson AFB, Ohio 45433

13. ABSTRACT

This report describes the work conducted on a program designed to investigate the potential applicability of a combined Fracture Mechanics-Nondestructive Inspection procedure as a design approach for aircraft structures. The program consisted of three phases, conducted simultaneously: (1) a literature survey to determine if sufficient fracture toughness information exists to determine a statistically valid value of K_{Ic}; (2) a test program to determine the minimum size of a crack that can be detected by each of four NDT methods: X-ray, magnetic-particle, penetrant, and ultrasonics; and (3) a test program to determine if fracture mechanics, when combined with flaw size as determined by NDT, can accurately predict the failure load of selected structures.

The results show that the sensitivity of the present NDT techniques needs improvement, particularly for small surface cracks. All NDT methods showed high accuracies in crack location, but not crack length. Ultrasonics and magnetic particle inspection appeared to be superior to penetrant and x-ray inspection.

The available test information on K_{Ic} for most materials is at best marginal for use in the design of critical components. The scatter in K_{Ic} is large and the 90% lower bound confidence values of K_{Ic} based on the standard deviation are so low as to render the design impractical.

The fracture mechanics-nondestructive testing failure load predictions generally agree with the actual failure loads to within 10%. Except for the small crack lengths the FM/NDT failure predictions were better than those predictions made using standard design.

Failure load predictions for test cylinders containing both one inch diameter bored hole and a small crack near the hole are in excellent agreement with the actual failure load.

DD ₁ FORM JAN 64 **1473**   267

| 14. | LINK A | | LINK B | | LINK C | |
KEY WORDS	ROLE	WT	ROLE	WT	ROLE	WT
Nondestructive Testing						
Fracture Mechanics						
Reliability						
Sensitivity						
Stress Concentration						
Flaw Detection						
Aluminum Alloy – 7075-T6511						
Steel – 4330V Modified						
Fatigue Crack						

INSTRUCTIONS

1. **ORIGINATING ACTIVITY:** Enter the name and address of the contractor, subcontractor, grantee, Department of Defense activity or other organization *(corporate author)* issuing the report.

2a. **REPORT SECURITY CLASSIFICATION:** Enter the overall security classification of the report. Indicate whether "Restricted Data" is included. Marking is to be in accordance with appropriate security regulations.

2b. **GROUP:** Automatic downgrading is specified in DoD Directive 5200.10 and Armed Forces Industrial Manual. Enter the group number. Also, when applicable, show that optional markings have been used for Group 3 and Group 4 as authorized.

3. **REPORT TITLE:** Enter the complete report title in all capital letters. Titles in all cases should be unclassified. If a meaningful title cannot be selected without classification, show title classification in all capitals in parenthesis immediately following the title.

4. **DESCRIPTIVE NOTES:** If appropriate, enter the type of report, e.g., interim, progress, summary, annual, or final. Give the inclusive dates when a specific reporting period is covered.

5. **AUTHOR(S):** Enter the name(s) of author(s) as shown on or in the report. Enter last name, first name, middle initial. If military, show rank and branch of service. The name of the principal author is an absolute minimum requirement.

6. **REPORT DATE:** Enter the date of the report as day, month, year; or month, year. If more than one date appears on the report, use date of publication.

7a. **TOTAL NUMBER OF PAGES:** The total page count should follow normal pagination procedures, i.e., enter the number of pages containing information.

7b. **NUMBER OF REFERENCES:** Enter the total number of references cited in the report.

8a. **CONTRACT OR GRANT NUMBER:** If appropriate, enter the applicable number of the contract or grant under which the report was written.

8b, 8c, & 8d. **PROJECT NUMBER:** Enter the appropriate military department identification, such as project number, subproject number, system numbers, task number, etc.

9a. **ORIGINATOR'S REPORT NUMBER(S):** Enter the official report number by which the document will be identified and controlled by the originating activity. This number must be unique to this report.

9b. **OTHER REPORT NUMBER(S):** If the report has been assigned any other report numbers *(either by the originator or by the sponsor)*, also enter this number(s).

10. **AVAILABILITY/LIMITATION NOTICES:** Enter any limitations on further dissemination of the report, other than those imposed by security classification, using standard statements such as:

(1) "Qualified requesters may obtain copies of this report from DDC."

(2) "Foreign announcement and dissemination of this report by DDC is not authorized."

(3) "U. S. Government agencies may obtain copies of this report directly from DDC. Other qualified DDC users shall request through
_____ ."

(4) "U. S. military agencies may obtain copies of this report directly from DDC. Other qualified users shall request through
_____ ."

(5) "All distribution of this report is controlled. Qualified DDC users shall request through
_____ ."

If the report has been furnished to the Office of Technical Services, Department of Commerce, for sale to the public, indicate this fact and enter the price, if known.

11. **SUPPLEMENTARY NOTES:** Use for additional explanatory notes.

12. **SPONSORING MILITARY ACTIVITY:** Enter the name of the departmental project office or laboratory sponsoring *(paying for)* the research and development. Include address.

13. **ABSTRACT:** Enter an abstract giving a brief and factual summary of the document indicative of the report, even though it may also appear elsewhere in the body of the technical report. If additional space is required, a continuation sheet shall be attached.

It is highly desirable that the abstract of classified reports be unclassified. Each paragraph of the abstract shall end with an indication of the military security classification of the information in the paragraph, represented as *(TS), (S), (C),* or *(U)*.

There is no limitation on the length of the abstract. However, the suggested length is from 150 to 225 words.

14. **KEY WORDS:** Key words are technically meaningful terms or short phrases that characterize a report and may be used as index entries for cataloging the report. Key words must be selected so that no security classification is required. Identifiers, such as equipment model designation, trade name, military project code name, geographic location, may be used as key words but will be followed by an indication of technical context. The assignment of links, rules, and weights is optional.